

**Aromatic Hydrogenation and Sulfur Removal
via the Water Gas Shift Reaction Using
Dispersed Catalysts**

By

Fatima Saleh Abusaido

A thesis
presented to the University of Waterloo
in fulfilment of the
thesis requirement for the degree of
Master of Applied Science
in
Chemical Engineering

Waterloo, Ontario, Canada, 1999

© Fatima Saleh Abusaido, 1999



National Library
of Canada

Acquisitions and
Bibliographic Services

395 Wellington Street
Ottawa ON K1A 0N4
Canada

Bibliothèque nationale
du Canada

Acquisitions et
services bibliographiques

395, rue Wellington
Ottawa ON K1A 0N4
Canada

Your file *Votre référence*

Our file *Notre référence*

The author has granted a non-exclusive licence allowing the National Library of Canada to reproduce, loan, distribute or sell copies of this thesis in microform, paper or electronic formats.

The author retains ownership of the copyright in this thesis. Neither the thesis nor substantial extracts from it may be printed or otherwise reproduced without the author's permission.

L'auteur a accordé une licence non exclusive permettant à la Bibliothèque nationale du Canada de reproduire, prêter, distribuer ou vendre des copies de cette thèse sous la forme de microfiche/film, de reproduction sur papier ou sur format électronique.

L'auteur conserve la propriété du droit d'auteur qui protège cette thèse. Ni la thèse ni des extraits substantiels de celle-ci ne doivent être imprimés ou autrement reproduits sans son autorisation.

0-612-51624-5

Canada

The University of Waterloo requires the signatures of all persons using or photocopying this thesis. Please sign below, and give address and date.

Aromatic Hydrogenation and Sulfur Removal via the Water Gas Shift Reaction Using Dispersed Catalysts

Abstract

The purpose of this thesis is to investigate the hydrogenation of aromatic compounds and sulfur removal present in diesel fuel through in situ hydrogenation via the water gas shift reaction (WGSR). Naphthalene (NAPH) and benzothiophene (BTH) are the model compounds to represent the aromatic and sulfur contents of diesel fuel, respectively. The H₂ generated in situ via the WGSR is utilized in the hydrogenation reaction by employing dispersed catalysts at the temperature of 340 °C. The activity of the in situ H₂ using an individual model compounds and binary mixtures of the model compounds will be compared. In addition, the activity differences among four types of Mo catalysts (phosphomolybdic acid, molybdic acid, ammonium-heptamolybdate-tetrahydrate and ammonium-tetrathio-molybdate), and four different catalyst concentrations based on Mo metals available in the phosphomolybdic acid catalyst (500, 1000, 1500 and 3000 ppm), will be addressed.

CO conversions in the presence of BTH or NAPH were found to be in the range of 92 – 94 % at 340 °C using phosphomolybdic acid as a dispersed catalyst with a concentration of 1500 ppm of the Mo metal. Under the same operating conditions, a slightly higher CO conversion for the binary mixture (BTH + NAPH) of 95.5% is

observed. The presence of benzothiophene and phosphomolybdic acid dispersed catalysts seems to be very effective in activating the water gas shift reaction.

Benzothiophene and naphthalene conversions were found to be 100% and 67.57% respectively in their mixture, under 600 psi CO/(2.5% H₂S) initial loading pressure, with NAPH: BTH ratio of 3.2 mol/mol at 340 °C and 1500 ppm Mo-metal concentration of the phosphomolybdic acid (PMA) catalyst. Variations of the CO loading pressure have more significant effects on NAPH conversions than the variation of water contents. Moreover, different Mo concentration produced even greater effects in the NAPH conversions. When the Mo concentration is 3000 ppm 82.3 % NAPH conversion is obtained. Different Mo catalysts at the same Mo concentration (1500 ppm) produce essentially the same conversions of CO, BTH and NAPH for reaction duration of 4 hours.

The measured kinetics, based on sampling from a batch autoclave, were found to follow a pseudo first order reaction. The rate constant calculated for CO, NAPH and BTH, is 4.88×10^{-4} , 7.33×10^{-5} , and 7.87×10^{-4} (s⁻¹), respectively. Ion chromatograph analyses of the aqueous solution indicated the presence of very small quantities of sulfate. This study demonstrates that the dispersed catalyst based on Mo and utilizing H₂ in situ is highly efficient for aromatic hydrogenation and hydrodesulfurization reactions.

Acknowledgments

The author would like to express her sincere thanks to Dr. F. Ng for her supervision and encouragement throughout the completion of this research study.

A special thanks goes to the readers of my thesis, Dr. G. L. Rempel and Dr. W. A. Anderson.

I wish also to thank B. Habicher, R. Singh, and R. Dickhout for their valuable technical assistance. Further, I would like to recognize all, in the Chemical Engineering Department at the University of Waterloo for their co-operations and support.

I would like to extend special and deepest thanks to the Kuwait Institute for Scientific Research for their financial support for my scholarship.

I wish to thank the National Sciences and Engineering Research Council for their financial support to this project.

Finally, a deep gratitude to my husband, Khalid, for his support, patience and encouragement.

To Khalid, Hani, Hanaa, Ebrahim, Najwa and my Mother with Love

Table of Contents

Subject	Page
Chapter 1	
Introduction and Objective	1
1.1 Petroleum Refining	1
1.1.1 Hydrocarbon Component	2
1.1.2 Nonhydrocarbon Components	4
1.2 Hydrotreating Processes	4
1.3 Hydrotreating Catalysis	6
1.4 Objectives	8
Chapter 2	
Literature Review	9
2.1 Aromatic Hydrogenation (AHYD)	9
2.1.1 Kinetics and Reaction Network	16
2.2 Hydrodesulfurization (HDS)	21
2.2.1 Kinetics and Reaction Network	23
2.3 Water Gas Shift Reaction (WGSR)	26
2.3.1 Kinetics and Mechanisms of WGSR	27
2.3.2 WGSR-Catalysts	30
Chapter 3	
Experimental Work	35
3.1 Experimental System Design	35
3.2 Experimental Procedure	41
3.2.1 Loading, Sealing and Leak testing the Reactor	41
3.3 Operating Conditions	41
3.4 Catalyst and Feed Preparation	42

3.4.1 Catalyst Preparation	42
3.4.2 Feed Preparation	42
3.5 Experimental Runs	44
3.6 Gas, Liquid and Solids Analyses	45
3.6.1 Gas Analysis	45
3.6.2 Liquid Analysis	49
3.6.3 Solid Analysis	49
3.6.4 Aqueous Layer Analysis	50
3.6.5 Reagents	50
3.7 Calculations	51
3.7.1 WGSR	51
3.7.1.1 WGSR Kinetics	53
3.7.2 The Hydrodesulfurization of BTH	55
3.7.2.1 Kinetics of The Hydrodesulfurization of BTH	57
3.7.3 The Hydrogenation of NAPH	58
3.7.3.1 Kinetics of The Hydrogenation of NAPH	61
3.7.4 Mass Balance	62
Chapter 4	
Results and Discussion	63
4.1 WGSR and HDS Reactivities	65
4.2 WGSR and AHYD Reactivities without BTH	73
4.3 Hydrogenation of Binary Mixture via the WGSR	83
4.3.1 Reproducibility	93
4.3.2 Effect of Changing H ₂ O/CO Ratio	95
4.3.2.1 Via the CO Loading Pressure	95
4.3.2.2 Via Water Content	99
4.3.3 Effects of Changing the Mo Concentration	103
4.3.4 Effects of Different Mo Catalyst	109

4.4 Aqueous Layer Analysis	117
4.5 Catalyst Characterization	119
4.5.1 Thermal Analyses (TGA/DTA)	119
4.5.2 X-Ray Diffraction (XRD)	127
Chapter 5	
Conclusions and Recommendations	135
5.1 Conclusions	135
5.2 Recommendations	137
Nomenclatures	138
Conversions	140
Bibliography	141
Appendices	
Appendix A Experimental Methods and Preparation Procedures	149
Appendix B Sample of Calculations for Individual Model Compounds	187
Appendix C Sample of Calculations for Binary Mixture	207
Appendix D Mass Balance	215
Appendix E Reproducibility	219
Appendix F Raw Data and Figures for Selected Runs	221
Appendix G Summary of Experimental Runs	263

List of Tables

Table	Page
2.1.1: Present and future specification of diesel	10
2.1.2: Aromatic type distribution in various distillates	11
3.3.1: Types of dispersed catalysts were used	43
4.1.1: Pseudo first order rate constant, and CO conversion for the WGSR at different [Mo] for BTH desulfurization, medium (CO/H ₂ S/H ₂ O)	68
4.1.2: Pseudo first order rate constant and conversion for HDS of BTH in different medium	72
4.2.1: Pseudo first order rate constant, and CO conversion for the WGSR at a different [Mo] for NAPH hydrogenation, medium (CO/H ₂ S/H ₂ O)	73
4.2.2: Mole fraction % of naphthalene reaction network for Run # 8	76
4.2.3: Pseudo first order rate constant, and conversion of NAPH hydrogenation in different medium	79
4.3.1: Pseudo first order rate constant and CO conversion for the WGSR for different model compound	84
4.3.2: Pseudo first order rate constants and conversions for BTH and NAPH in different medium	89
4.3.1.1: Reproducibility for the binary mixture (BTH+NAPH)	94
4.3.2.1.1: Results of changing the CO loading	96
4.3.2.1.2: H ₂ generated in the system at different CO loadings	96
4.3.2.2.1: Summary of the results for the changing water content	100
4.3.3.1: Effects of PMA concentration on the CO conversion and the rate constant, k_1 , for the WGSR in a mixture of NAPH and BTH	103

4.3.3.2: Effects of PMA concentration on the product yield for a mixture of NAPH and BTH	104
4.3.3.3: Effects of PMA concentration on TET selectivity, H ₂ S production, sulfur and aromatic removal for a mixture of NAPH and BTH	105
4.3.4.1: Effects of Mo catalysts on the reactivity of WGSR	110
4.3.4.2: Activity of different Mo catalysts	110
4.3.4.3: The amount of H ₂ generated in the system	117
4.4.1: The analysis of the aqueous layer analysis in final products for different Mo catalysts	118
4.5.1.1: The percent of weight loss for solids of different Mo concentration	121
4.5.1.2: The percent of weight loss for solids of different Mo catalysts	121

List of Figures

Figure	Page
2.1.1.1: Reaction network for naphthalene	18
2.2.1.1: Reaction network for benzothiophene proposed by Van Parijis et al. (1986a, b)	24
3.1: Work plan flow chart	36
3.1.1: Schematic diagram of the experimental system design	38
3.5.2: The filtration system used for solid and liquid separation under vacuum	47
4.1: Reaction scheme for the binary mixture of NAPH and BTH	64
4.1.1: A typical gas chromatogram at zero reaction time for WGSR, catalyzed by PMA at 340 °C and 600 psi CO/(2.5% H ₂ S), Run#10	66
4.1.2: Mole fraction of the WGSR components for the HDS of BTH catalyzed by PMA at 340 °C and 600 psi CO/(2.5% H ₂ S), Run # 10	67
4.1.3: Pseudo first order plot for the WGSR catalyzed by PMA at 340 °C and 600 psi CO/(2.5% H ₂ S), Run # 10	67
4.1.4: A typical liquid chromatogram for the HDS of BTH, catalyzed by PMA at 340 °C and 600 psi CO/(2.5% H ₂ S), Run # 10	70
4.1.5: Mole % of the BTH reaction network, catalyzed by PMA at 340 °C and 600 psi CO/(2.5% H ₂ S), Run # 10	71
4.1.6: Pseudo first order plot for BTH conversion, catalyzed by PMA at 340 °C and 600 psi CO/(2.5% H ₂ S), Run # 10	71
4.2.1: Mole fraction of the WGSR components for the NAPH hydrogenation catalyzed by PMA at 340 °C and 600 psi CO/(2.5% H ₂ S), Run # 8	74
4.2.2: Pseudo first order plot for WGSR, catalyzed by PMA at 340 °C and 600 psi CO/(2.5% H ₂ S), Run # 8	74
4.2.3: A typical liquid chromatogram for the HYD of NAPH, catalyzed by PMA at 340 °C and 600 psi CO/(2.5% H ₂ S), Run # 8	77

4.2.4: Mole fraction % of NAPH reaction network, catalyzed by PMA at 340 °C and 600 psi CO/(2.5% H ₂ S), Run#8	78
4.2.5: Pseudo first order constant for NAPH hydrogenation, catalyzed by PMA at 340 °C and 600 psi CO/(2.5% H ₂ S), Run#8	78
4.2.6: Mole fraction % for NAPH reaction network, catalyzed by PMA at 340 °C and 600 psi H ₂ /(2.5% H ₂ S), Run#14	81
4.2.7: Pseudo first order constant for NAPH conversion, catalyzed by PMA at 340 °C and 600 psi H ₂ /(2.5% H ₂ S), Run#14	81
4.2.8: Mole fraction % for tetralin dehydrogenation catalyzed by PMA at 340 °C and 600 psi CO/(2.5% H ₂ S), Run#19	82
4.3.1: Mole fraction % of the WGSR components for the HYD of(BTH+NAPH), catalyzed by PMA at 340 °C and 600 psi H ₂ /(2.5% H ₂ S), Run#23	85
4.3.2: Pseudo first order plot for WGSR in the binary mixture, catalyzed by PMA at 340 °C and 600 psi H ₂ /(2.5% H ₂ S) Run#23	85
4.3.3: A typical liquid chromatogram for the HYD of (BTH+NAPH), catalyzed by PMA at 340 °C and 600 psi H ₂ /(2.5% H ₂ S) Run # 23	86
4.3.4: Mole fraction for the BTH and NAPH reaction network, catalyzed by PMA at 340 °C and 600 psi H ₂ /(2.5% H ₂ S) Run#23	87
4.3.5: Pseudo first order plot for NAPH conversion in the binary mixture, catalyzed by PMA at 340 °C and 600 psi H ₂ /(2.5% H ₂ S), Run#23	87
4.3.6: Pseudo first order plot for BTH conversion in the binary mixture catalyzed by PMA at 340 °C and 600 psi H ₂ /(2.5% H ₂ S), Run#23	88
4.3.7: Mole fraction % of the binary mixture component, catalyzed by PMA at 340 °C and 600 psi H ₂ /(2.5% H ₂ S), Run#17	90
4.3.8: Pseudo first order plot for NAPH conversion in the binary mixture, catalyzed by PMA at 340 °C and 600 psi H ₂ /(2.5% H ₂ S), Run#17	90
4.3.9: Pseudo first order plot for BTH conversion in the binary mixture, catalyzed by PMA at 340 °C and 600 psi H ₂ /(2.5% H ₂ S), Run#17	91

4.3.2.1.1: Mole fraction for the binary mixture (BTH+NAPH), catalyzed by PMA at 340°C, 300 psi CO/(2.5% H ₂ S), Run#25	97
4.3.2.1.2: The yield of TET and ETHBZ from the binary mixture reaction for different CO loading, catalyzed by PMA catalyst (1500 ppm Mo) at 340 °C	97
4.3.2.1.3: Pseudo first order plot for NAPH hydrogenation in the binary mixture, catalyzed by PMA at 340°C, 300 psi CO/(2.5% H ₂ S), Run#25	98
4.3.2.1.4: Pseudo first order plot for the HDS of BTH in the binary mixture, catalyzed by PMA at 340°C, 300 psi CO/(2.5% H ₂ S), Run#25	98
4.3.2.2.1: Mole fraction % of WGSR components for the HYD of a mixture of BTH+NAPH catalyzed by PMA at 340 °C, 600 psi CO/(2.5% H ₂ S)/35 ml H ₂ O, Run#18	101
4.3.2.2.2: Pseudo first order plot for WGSR, catalyzed by PMA at 340 °C, 600 psi CO/(2.5% H ₂ S)/35 ml H ₂ O, Run#18	101
4.3.2.2.3: The yield of TET and ETHBZ from the binary mixture reaction at different amounts of H ₂ O, catalyzed by PMA catalyst (1500 ppm Mo), at 340°C	102
4.3.3.1: Effect of Mo concentration on CO conversion for a mixture of BTH+NAPH	106
4.3.3.2: Pseudo first order rates constant of CO conversion at different Mo concentrations for a mixture of BTH+NAPH	106
4.3.3.3: Pseudo first order rate constants for HDS of BTH at different Mo concentrations for a mixture of BTH+NAPH	108
4.3.3.4: Pseudo first order rate constants for HYD of NAPH at different Mo concentrations for a mixture of BTH+NAPH	108
4.3.4.1a: Mole % of the WGSR components for the binary mixture of BTH and NAPH catalyzed by MA at 340°C, Run#26	111
4.3.4.1b: Mole % of the WGSR components for the binary mixture of BTH and NAPH catalyzed by AMT at 340°C, Run#27	111

4.3.4.1c: Mole % of the WGS components for the binary mixture of BTH and NAPH catalyzed by ATTM at 340°C, Run#30	112
4.3.4.2: Mole % of the WGS components for the binary mixture of BTH and NAPH without catalyst at 340°C, Run#29	112
4.3.4.3: Pseudo first order rate constant for CO conversion with different Mo catalysts	113
4.3.4.4: Hydrogenation activity of NAPH product for different Mo catalysts	115
4.3.4.5: Effect of reaction time on the hydrogenation activity in a mixture of NAPH and BTH catalyzed by PMA at 340°C, Run#23	115
4.3.4.6: NAPH conversions during reaction time for different Mo catalysts	116
4.3.4.7: BTH conversion during reaction time for different Mo catalysts	116
4.5.1.1: Weight loss of PMA spent catalyst at different Mo concentrations. A=500 ppm, B=1000 ppm, C=1500 ppm. D=3000 ppm	122
4.5.1.2: Weight loss for the different Mo spent catalysts	122
4.5.1.3: Differential changes in weight with temperatures (DTG) for PMA spent catalyst at different Mo concentrations	124
4.5.1.4: Differential changes in weight with temperatures (DTG) for different Mo spent catalysts	124
4.5.1.5: Temperature difference for different Mo concentrations of PMA spent catalysts with increasing temperature	125
4.5.1.6: Temperature difference for different Mo spent catalysts with increasing temperatures	125
4.5.1.7: Weight loss and temperature differences for the commercial grade of MoS ₂ with changing temperatures	126
4.5.2.1: XRD spectra of fresh PMA and MA catalyst	129

4.5.2.2: XRD spectra of spent PMA and MA catalysts from the reactions in CO/H ₂ S/H ₂ O medium of the binary mixture BTH+NAPH	130
4.5.2.3: XRD spectra of commercial grade of MoO ₃ and MoS ₂	131
4.5.2.4: XRD spectra of spent PMA catalyst at different Mo concentration	132
4.5.2.5: XRD spectra of fresh AMT and ATTM catalysts	133
4.5.2.5: XRD spectra of spent AMT and ATTM catalysts from the reactions in CO/H ₂ S/H ₂ O medium of the binary mixture BTH+NAPH	134

List of Photographs

Figure	page
3.1.2: Front view of the 1 L batch reactor as located in Lab 1521 in the Chemical Engineering Department at the University of Waterloo	39
3.1.3: The view of the closure assembly	40
3.5.1: The collected liquid and solids before separation	46
3.5.3: The collected solids and liquid product after separation	48

Chapter 1

Introduction and Objectives

Petroleum (crude oil) consists of two main components: hydrocarbons and nonhydrocarbons. The hydrocarbons may be gaseous, liquid or solid at atmospheric conditions. There are very complex mixtures of many compounds, ranging from light gases such as methane and propane to heavier substances such as asphalts, which are solid when separated from oil.

Components in petroleum containing up to four carbon atoms are usually gaseous and those having 20 or more carbons in their structure are solids. Hydrocarbons between these two ranges are considered to be liquids (Shaheen, 1983).

1.1 Petroleum Refining

Petroleum refining necessitates the separation of the original crude oil complex mixture in to fractions with specifications required by the international market.

1.1.1 Hydrocarbon Component

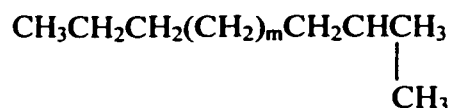
According to how the carbon atoms are connected, hydrocarbons are grouped in to paraffins, naphthenes, aromatics and asphaltics (Speight, 1991).

Paraffins consist of saturated hydrocarbons with straight or branched chains, but without any ring structure:

a- Straight chain paraffin



b- Branched chain paraffin

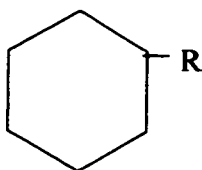


Saturated hydrocarbons contain one or more rings are called naphthenes, each ring may contain one or more paraffinic side chain(s).

a- Alkylcyclopentane



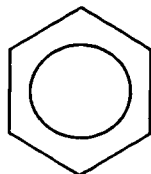
b- Alkylcyclohexane



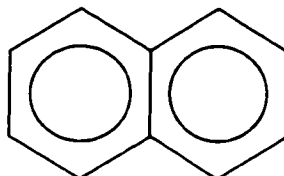
Aromatic compounds also exist in the crude oil and vary between 10% to 35% vol.

Hydrocarbons containing one or more aromatic nuclei are:

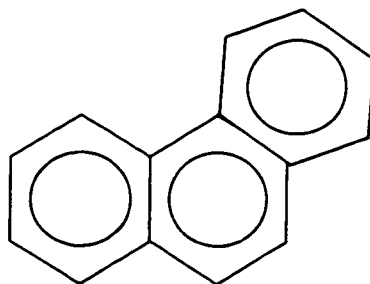
a. Benzene



b. Naphthalene



c. Phenanthrene



Beside hydrocarbons, crude oil consists of a number of organic nonhydrocarbons, which will be discussed in the next section.

1.1.2 Nonhydrocarbon Components

Nonhydrocarbon components consist of mainly sulfur, nitrogen and oxygen. Sulfur compounds are among the most important heteroatomic components of petroleum. There are many different sulfur compounds available in petroleum feedstock such as thiols, cyclic-sulfides, thiophene, benzothiophene, dibenzothiophene (Speight, 1991). It appears that the higher the sulfur contents the higher the density of crude oil. The total sulfur content in the crude may vary between 0.04% in light paraffin to 5% in heavy crude oil.

It is the presence of sulfur, aromatic and nitrogen compounds in finished petroleum cuts that often produces harmful effect on the environment issue. This will be introduced in the next section.

1.2 Hydrotreating Processes

Almost all petroleum cuts from the lightest to the heaviest undergo hydrotreatment. The primary purpose of hydrotreating is to saturate the olefins, and to reduce sulfur, and nitrogen content at mild operating conditions, without changing the boiling range of the feed. Moreover, hydrotreating is a process to stabilize petroleum products and remove objectionable elements from products or feedstock by reacting them with hydrogen gas in the presence of catalyst.

Normally, stabilization includes converting unsaturated hydrocarbons such as olefins, and unstable diolefins to paraffins. The objectionable elements removed by hydrotreating include sulfur, nitrogen, oxygen, halides and trace metals. (Gary and

Handwerk, 1994). When the process is devoted to sulfur removal, it is usually called hydrodesulfurization (HDS). Similarly, when the process is devoted to nitrogen removal, it is called hydrodenitrogenation (HDN). Finally, aromatic hydrogenation (AHYD) saturates aromatic rings and reduces the aromatic content by converting aromatics to paraffins.

Recently, the Clear Air Act (CAA) in the United States has tightened the specification of the middle distillate (e.g., diesel). In October 1993, the Environmental Protection Agency (EPA) and the California Air Resources Board (CARB) introduced the clean diesel program to reduce the emission of sulfur, particulates and nitrogen. In 1993 the EPA ruled that fuels must contain less than 0.05 wt % sulfur, greater than 40.0 for the cetane number and less than 35.0 vol. % aromatics, (Nikanjam, 1993).

In 1998 the standards of the EPA and the CARB have included that a very low sulfur fuel 0.005 wt % with aromatic content of only 10.0 vol. %. The cetane index, which specifies the ignition quality of diesel fuel, has been set at a minimum of 40 by EPA, and 48 by CARB. This quality specified for middle distillate fuels is similar with the octane number of gasoline. For the years 1998-2000, diesel engine manufacturers are requiring 55.0 cetane. Reduction of aromatic will reduce the emission of NO_x, CO, hydrocarbons, toxics, and possibly particulates. In addition, a higher cetane index improves fuel stability and reduces white smoke especially in cold climates. Sulfur reduction to less than 0.05 wt % leads to reduction of particulates, monoaromatic reduction had no effect but polyaromatics need further investigation in terms of No_x and particulate reduction (Khan and Reynolds, 1996).

Therefore, hydrodesulfurization (HDS) and aromatic hydrogenation are important factors in meeting emission requirements. This reduction is expected to influence the control of diesel fuel quality in North America.

1.3 Hydrotreating Catalysis

Hydrotreating catalysts are based on the transition metal sulfides. Catalysts such as sulfided $\text{CoO-MoO}_3/\gamma\text{-Al}_2\text{O}_3$ ($\text{Co-Mo/Al}_2\text{O}_3$) are commonly used for hydrodesulfurization (HDS) due to their high activity and selectivity for the HDS reactions. Although Girgis et al. (1991) have reported that sulfided $\text{NiO-MoO}_3/\text{Al}_2\text{O}_3$ ($\text{Ni-Mo/Al}_2\text{O}_3$) and $\text{NiO-WO}_3/\gamma\text{-Al}_2\text{O}_3$ ($\text{Ni-W/Al}_2\text{O}_3$) have higher activity for hydrogenation and they are applicable for hydrodenitrogenation (HDN). In addition, NiMo, or NiW, was considered to yield a higher degree of unwanted hydrogen consumption due to aromatic saturation, (Gary and Handwerk, 1994). However, these catalysts have low activity for aromatic saturation, even at high pressure (100 bars) and long residence time. They leave a high quantity of unconverted aromatics in the products. In addition, high temperatures are not helpful because of the highly exothermic and equilibrium limited hydrogenation reaction. (Lucien et al., 1993).

The conventional aromatic hydrogenation catalysts are metallic nickel or noble metals, supported on high surface area. These catalysts are very active, but problematic because of their sensitivity to sulfur poisoning, (Bergem et al., 1997). In addition, the sulfided $\text{Pt}/\gamma\text{-Al}_2\text{O}_3$ has shown an increased activity of 20 times for hydrogenation

compared to the conventional NiMo catalyst. Gültekin et al., 1984 have suggested that the inhibition of the aromatic hydrogenation is due to the presence of H_2S and NH_3 .

For the transition metals nitrides and carbides catalysts shows an excellent activity in HDN, but there is a lack of information for the carbides as a hydrogenation catalyst.

Recently some researchers have used the platinum (Pt), palladium (Pd), iridium (Ir) and ruthenium (Ru) supported on Y-zeolite catalysts in hydrogenation reactions, because these catalysts demonstrate an improvement in sulfur resistance and an increase in the hydrogenation activity, (Song et al., 1997 and Bergem et al., 1995).

Further unsupported dispersed catalysts, an alternative to conventional catalyst, are attracting attention for the hydrogenation processes particularly, in utilizing the hydrogen generated through the water gas shift reaction in the presence of dispersed catalyst (e.g., phosphomolybdic acid, PMA and molybdic acid, MA). Some of the advantages of using dispersed catalysts are: (1) they have low tendency to deactivate, (2) their microsize maximizes the surface area and (3) they minimize the coke formation. Information that is more detailed will be presented in Chapter 2.

1.4 Objectives

Many studies have investigated the removal of sulfur and aromatics from middle distillates (e.g., diesel) by using the conventional catalysts; CoMo and NiMo traditionally supported on γ -alumina, as discussed in Section 1.3. Currently, the development of a new generation of more effective hydrotreating catalysts is becoming increasingly more important for the production of clean fuel (i.e. low sulfur and aromatics), due to environmental concerns.

This research study is aimed to develop a single stage hydrotreating process to upgrade diesel fuel to meet the new low specifications with dispersed catalysts, by utilizing the H_2 generated in situ via the water gas shift reaction.

In this thesis, results are presented in which benzothiophene and naphthalene are used as the representative model compounds for the aromatic and sulfur components in diesel fuel. Four types of unsupported Mo dispersed catalyst were employed to evaluate their activities on the sulfur removal and aromatic hydrogenation. These results will be compared with externally supplied hydrogen. The effects of water content and the initial loading pressure of H_2 and CO for the hydrogenation reaction will also be explored. Lastly, this work will examine the kinetics of aromatic hydrogenation and sulfur removal in the reaction mixture of benzothiophene and naphthalene by using different molybdenum concentration and different molybdenum catalysts.

Chapter 2

Literature Review

2.1 Aromatic Hydrogenation (AHYD)

Because aromatic and sulfur emissions are toxic and carcinogenic, their removal from middle distillates has boosted interest in developing more active catalysts, especially for diesel and gas oils. Table 2.1.1 indicates the present and future specifications of required diesel fuels (adapted from Grange and Vanhaeren, 1997). In spite of efforts, there is no recognized alternative to the conventional Co (Ni) Mo/Al₂O₃. Although CoMo/Al₂O₃ catalysts have been greatly improved for hydrodesulfurization (HDS), they were still not able to satisfy the present drastic regulations for sulfur and aromatic removal (Leglise et al., 1998).

The main type and amount of aromatic in the middle distillates (MD) varies depending on the origin of the MD cut. Table 2.1.2 summarizes typical analysis data

was completed on a high performance liquid chromatography (HPLC) for the aromatics in distillates from different sources (adapted from Cooper and Donnis, 1996)

Table 2.1.1: Present and future specification of diesel

Location	Present			Future		
	S(ppm) ¹	A(wt%) ²	CN ³	S(ppm) ¹	A(wt%) ²	CN ³
European Union						
(Year-1996)	2000	no limit	47	500	25	47
(Year-2000)				350	11	51
(Year-2005)				50	11	51
Sweden						
Class1	10	5	50			
Class2	50	20	47			
Finland	50	20	47- 49			
USA	500	35	40			
California	500	10	48			
(Year-2000)				500	10	(55-59)
Japan	2000	no limit	40			

¹ Sulfur contents (ppm). ² Aromatic content (wt%). ³ Cetane number.

At present, the aromatic hydrogenation (AHYD) is considered to be more difficult than hydrodesulfurization (HDS) under the same operating conditions that are usually used for hydrotreating. Ali (1998) studied the AHYD over a conventional NiMo/Al₂O₃ hydrotreating catalyst. When hydrogen sulfide (H₂S) and ammonia (NH₃) were employed to investigate their influence on AHYD the aromatic heteroatom was slightly reduced to a certain extent. There was a severe inhibition of AHYD in the presence of H₂S and NH₃.

Therefore AHYD in real feeds (e.g. middle distillates) under industrial hydrotreating conditions was inhibited by the H₂S produced from HDS and NH₃ produced by hydrodenitrogenation (HDN). Because of this problem, it is more challenging to find a good sulfur tolerant catalyst to reduce the aromatic in diesel feed stocks.

To handle the aromatics present in a middle distillate (e.g., diesel) researchers must understand the effect of the catalyst types, operating conditions, and the chemistry of the reaction of each compound that exist in the diesel fuel. Several studies have focused on the HDS and AHYD by using conventional supported catalysts, or promoted supported catalysts. However, research data on unsupported dispersed catalysts was rather limited.

Table 2.1.2: Aromatic type distribution in various distillates

Property	Straight Run Kerosene	Heavy FCC Gasoline	Light Coker Gas oil	Light Atmospheric Gas oil	Light Cycle Oil	Heavy Atmospheric
Specific gravity (15 °C)	0.803	0.840	0.861	0.846	0.997	0.864
Aromatics (Vol%)						
mono	15.7	38.8	16.3	16.5	8.2	22.5
Di	1.7	5.5	16.4	7.0	69.8	8.5
Tri	0.1	0.5	8.0	0.1	4.0	0.7
Total	17.5	44.8	40.7	23.6	82.0	31.7

Naphthalene was chosen to establish the reaction conditions because it is present in relatively high concentrations in petroleum and coal liquids. In addition, the hydrogenation of naphthalene to tetralin and further slow hydrogenation to decalin (Sapre and Gates 1981).

Noble metal catalysts were found to be very effective for AHYD. Corma et al., (1997) have studied platinum (Pt) supported on MCM-41 materials. Platinum showed a very high surface area and MCM-41 has a uniform arrangement of mesopores. Consequently, they presented superior activity for the hydrogenation of naphthalene compared with conventional Pt- containing supports such as commercial amorphous silica alumina, silica, γ -alumina, and zeolite USY at moderate temperatures. When sulfur compound was added to the naphthalene, the Al-MCM-41 and USY supports showed a higher sulfur resistance among the other catalysts.

Lin and Song, (1996) observed the naphthalene hydrogenation in the presence and absence of benzothiophene using noble metal catalyst such as Pt/ Al_2O_3 , Pd/ Al_2O_3 and Pd/ TiO_2 . They demonstrated that Pt and Pd supported on Al_2O_3 or TiO_2 may be efficient for the hydrogenation of the polyaromatic hydrocarbons at temperature ranges of 200 to 280 °C. Naphthalene hydrogenation may proceed even in the presence of benzothiophene at a maximum concentration of 4200 ppm. The activity of noble metal catalysts decreased with the addition of sulfur. Pd displayed more sulfur tolerance than Pt when supported on Al_2O_3 . However, when a TiO_2 support was used, the sulfur resistance increased.

Kimbara and Charland (1996) carried out another study for the hydrogenation of aromatics in synthetic crude distillates using platinum supported on molecular sieves. They focused on reducing the distillate aromatic content to meet diesel emission control standards and the cetane number requirements. Efforts were made to improve the dispersion of Pt and its resistance to poisoning by sulfur compounds. Although, noble metals were vulnerable to the poison from the sulfur compounds in petroleum feedstocks, a first stage hydroreatment is usually required to reduce the heteroatom content to less than 10 ppm. So, two molecular sieves were compared, pillared, interlayered with clay and Y-Zeolite under an operating temperature 400 °C. The Pt. cluster supported in Y-Zeolite was found to have an acceptable hydrogenation activity. This enhancement in activity was due to the unique structure of the Y-Zeolite (e.g., super cage) that produced uniform dispersed electron deficient Pt metal clusters. The Pt/PILC-alumina catalyst showed no enhanced resistance to being poisoned by sulfur, because the unique structure of the pillared clay may have been selective to ring opening of naphthalene in middle distillate feed stocks.

Huang and Kang (1995) tested the hydrogenation of naphthalene with platinum/ γ -alumina (Pt/ γ -Al₂O₃), and platinum/alumina-aluminum phosphate (Pt/AAP) catalysts. Their experiments indicated that the Pt/AAP catalyst had better hydrogenation activity and lower cis-decalin selectivity than the Pt/ γ -Al₂O₃ catalyst due to the higher acidity of the AAP support than that of the γ -Al₂O₃ supports. The addition of phosphorous to Pt/Y-Al₂O₃ improved the hydrogenation activity but reduced selectivity of cis-decalin.

However, the high phosphorous content (ratio of Al/P < 20) of Pt/ γ -Al₂O₃ was poisonous to the hydrogenation activity and cis-decalin selectivity.

The studies of noble metal catalysts have attracted the researchers such as Song and Schmitz (1997). They observed the hydrogenation of naphthalene in tridecane at 200 °C with a zeolite- supported Pt and Pd catalysts were prepared using mordenite (HM38) and Y-zeolite (HY) as support materials compared with Al₂O₃- and TiO₂- supported Pt and Pd catalysts. The Pt/HM38 and Pt/HY catalysts have a higher activity than the Pt/Al₂O₃ catalyst. The addition of sulfur in the form of benzothiophene decreases the activity of all the catalysts tested. However, the Pd and Pt catalysts supported on zeolites demonstrated significant improvements in sulfur tolerance compared to Al₂O₃ or TiO₂ supports. Thus they suggested, the mordenite supported Pd catalysts are promising for practical application, but further studies are needed.

Alternative hydrogenation catalysts may include more active sulfides such as transition metal. Yumoto et al. (1994) investigated the effect of adding nickel (Ni, 2.0 wt %) and vanadium (V, 4.0 wt %) sulfides on the conventional catalyst NiMo/ γ -Al₂O₃ for the HDS and AHYD. Naphthalene (NAPH) and dibenzothiophene (DBT) were used as a model compounds. The addition of Ni led to slightly increased rate constants for the hydrogenation of NAPH and DBT. Conversely, the addition of V led to a decrease in the rate constants for NAPH hydrogenation and to an increase for the DBT hydrogenation network reactions. Therefore, Yumoto et al. (1994) have suggested that the deposit of nickel and vanadium sulfides in the hydroprocessing catalysts have significantly different effects on catalyst performance.

Halachev et al. (1996) have studied the effect of varying phosphorous concentration on NAPH hydrogenation in a batch reactor under 300 °C and 650 psi, with NiW/Al₂O₃ catalyst, for 8 hours reaction time. They have found the addition of phosphorous has a promoting effect on AHYD. However, during the reaction the number of active sites changed, and new active sites were possibly formed. Halchev et al. (1998) studied the same type of catalyst, but it was supported on mesoporous material Ti-HMS. The catalyst was presulfided with 15 vol. % H₂S/H₂; the naphthalene hydrogenation reaction was carried out in a batch reactor for 7 hours at 325 °C. Their results have shown that when the new mesoporous material Ti-HMS functioned as a support for the NiMo and NiW catalysts, they were highly active with better activity and selectivity in the reaction of naphthalene hydrogenation, than with the conventional alumina supports. The total conversion of naphthalene to decalins (cis and trans) using NiW/Ti-HMS was found to be 70 to 73 % compared to the conventional catalyst NiMo, which was approximately 20 %.

Nonaka et al. (1998) have used light cycle oil (LCO), which is produced from the fluid catalytic cracking process (FCC). The oil was used as a blending component in a wide range of fuels. Nonaka studied the effects of adding Re on NiW/Al₂O₃ catalyst for the HDS and AHYD of LCO. When 1% of Re was added to the NiW catalyst it increased HDS activity, but decreased AHYD activity. However, 2% of Re at mild reaction conditions was observed to increase the AHYD activity. And at severe reaction condition, the addition of Re seems to reduce the AHYD, because the reaction was controlled by equilibrium limitations.

As introduced previously, hydrogenation was usually carried out using a supported catalyst or active metals such as transition or noble metals. Zhan and Guin (1994) have studied the hydrogenation of naphthalene using a dispersed iron catalyst. They found the in situ pre-reduction of iron oxide with hydrogen produced a very active catalyst for AHYD. When the original iron oxide was employed without any pretreatment, an in situ reduction process appeared to occur before the hydrogenation reaction proceeded. Sulfur rapidly poisoned the hydrogenation function of the iron catalyst, because the iron sulfide phases had a much lower AHYD activity than the reduced iron. When the sulfur disappeared and concentration of naphthalene decreased, the pre-reduced iron catalyst was more active compared with the conventional NiMo/Al₂O₃ catalyst.

2.1.1 Kinetics and Reaction Network

The hydrogenation of aromatic hydrocarbons is an exothermic process. When the temperature was increased to give higher rate reactions it resulted in a lower conversion of aromatics due to equilibrium limitations. Aromatic saturation is a reversible reaction favoured at low temperatures as proposed by Girgis and Gates (1991).

Frye (1962) and Frye and Weitkamp (1969) showed the hydrogenation equilibrium constants for naphthalene to be less than unity at typical hydroprocessing temperatures. Consequently, operation at high hydrogen partial pressure was essential to hydrogenate aromatic hydrocarbons to achieve appreciable saturation. They found an

increase in H₂ pressure from 9.7 to 37 atm at 369 °C increases the equilibrium conversion of naphthalene from 17 % to 84 %.

Sapre and Gates (1981) carried out experiments using CoMo/Al₂O₃ catalyst at 325 °C in a batch reactor to establish the reaction networks for the hydrogenation of naphthalene. They demonstrated that the hydrogenation of naphthalene is sequential, with a rate of tetralin hydrogenation being an order of magnitude less than that of naphthalene hydrogenation as shown in Figure 2.1.1.1. Thus, tetralin was the primary product of naphthalene hydrogenation and it was further converted to cis- and trans- decalins, with the trans- isomer being predominant. Kim and Curtis (1990) have examined the reaction pathway of naphthalene in the presence of molybdenum naphthenate and excess sulfur. The most active catalytic species were those with a stoichiometry close to MoS₂. The MoS₂ produced was a solid black powder, with a particle size in the range of (500 – 2500 °A) in diameter. This removed the restriction of pore diffusion that has been shown to affect unfavorably the activity of the catalyst (Curtis et al. 1985). Tetralin was found to be the primary product with a conversion of 92 %, and small amount of cis- and trans-decalins. No dehydrogenation of naphthalene and decalin was observed at 380°C, but the dehydrogenation of tetralin to naphthalene possibly occurred at higher temperatures than 400° C.

Bouchy et al. (1992) studied the kinetic hydrogenation of methyle-naphthalene on sulfided NiMoP/Al₂O₃ at temperature range of 300-400 ° C. The substitution of the hydrogen atom by the methyl group did not change the thermodynamic properties much more than the use of naphthalene. They confirmed that the hydrogenation of the first ring

at the low temperature of 300 °C is slow. The hydrogenation of the second ring was slower than the first ring, and it can be completed for a contact of one-hour reaction time at 400 °C. The thermodynamic equilibrium for the hydrogenation of the second ring was reached only at temperature higher than 400 °C. With the increase of hydrogen pressure at the same temperature, the thermodynamic equilibrium was reached for the hydrogenation of both the first and the second ring in a contact time of one hour.

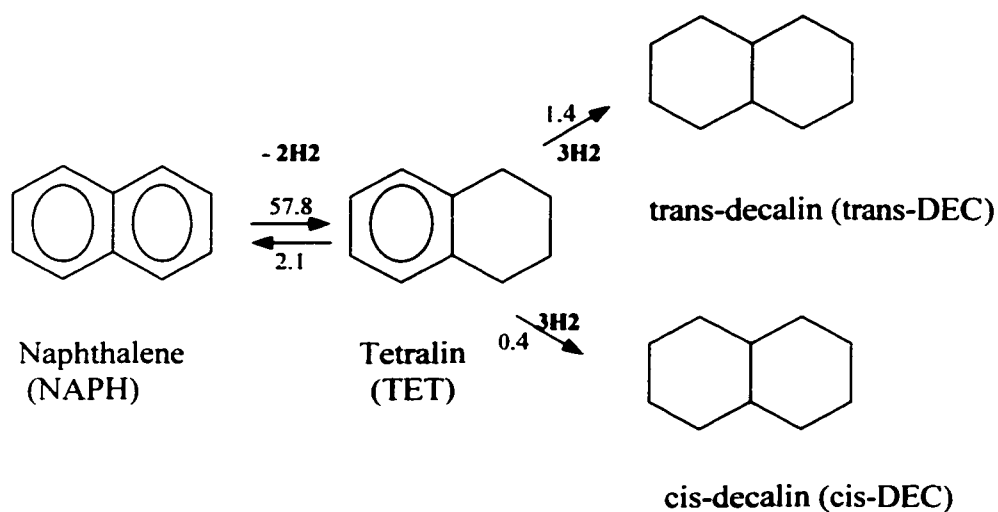


Figure 2.1.1.1: Reaction network for naphthalene. The numbers on the arrows are the first order rates constant in (L/g catalyst·s)

Huang and Kang (1995a,b) have studied the kinetics of the hydrogenation of naphthalene dissolved in n-hexadecane over Pt/Al₂O₃ with externally supplied hydrogen. The reaction was carried out in a flow trickle bed reactor system at temperatures between 200–260 °C. Naphthalene was found completely hydrogenated to tetralin in front of the catalyst bed under the specified operating condition. This experiment has proven that there was a well-correlated pseudo-first order reaction profile for the hydrogenation of tetralin and the isomerization of cis- decalin. The hydrogenation activity increased in correlation to the increased of temperature and pressure.

The commercial hydroprocessing catalyst NiMo/ γ -Al₂O₃ enriched in nickel and vanadium sulfides were tested for their effect on the hydrogenation of naphthalene and dibenzothiophene, (Yumoto et al., 1996). Results showed that the nickel sulfide deposits had little effect on the rate constants of the naphthalene and dibenzothiophene hydrogenation reactions. However, the vanadium sulfide deposits led to decreased rate constants for the naphthalene hydrogenation reaction, and an increase in the rate constant of the dibenzothiophene hydrogenation reaction.

In addition, group VIII transition metal supports were tested for their hydrogenation activity. Ru was loaded on three kinds of metallic oxide supports, Ru/Mn₂O₃-ZnO, Ru/Mn₂O₃-NiO and Ru/Mn₂O₃-La₂O₃, (Kotanigawa et al., 1997). Their study illustrated that the Ru/Mn₂O₃-NiO had the best performance for the hydrogenation reactions among the other catalysts, yielded 33.0 mol % of decalin from the naphthalene hydrogenation. The researchers concluded that Ru on a non-acidic support, of Mn₂O₃-NiO showed the best activity even with small quantities of Ru (e.g., 0.1wt %).

Zeolite-supported Pt and Pd catalysts were also tested for the hydrogenation of naphthalene. Schmitz et al. (1996) studied the hydrogenation of naphthalene at three different temperatures 25, 100, and 200 °C with reaction times from 6 minutes to 24 hours. Pt and Pd catalysts were supported on four zeolites, three hydrogen-mordenites (HM) with different ratios of ($\text{SiO}_2/\text{Al}_2\text{O}_3$), and one zeolite (HY). Schmitz et al. have found that catalytic selectivity depends on both the metal and the zeolite. The Pt/HY showed a high selectivity for cis-decalin (80 %) compared to the other catalysts, which did not promote the isomerization of cis-decalin. Overall, Pd catalysts showed a higher selectivity for trans-decalin than the Pt catalysts; also the isomerization of cis-decalin to trans-decalin was more rapid on the Pd catalysts.

For some time molybdenum has been a focus of research in the catalytic hydrogenation processes. Since the catalytic active form of MoS_2 is insoluble, the dispersion of molybdenum into hydrocarbon particles have often been carried out using catalyst precursors. Such precursors are soluble compounds of molybdenum that may have had little or no catalytic activity themselves, but have been presumed to convert to a catalytically active form at temperatures greater than 300 °C.

Dutta and Schobert (1996) have examined the hydrogenation of naphthalene using ammonium tetrathiomolybdate (ATTM) as a catalyst precursor. The experiment was carried out at 350 °C to 450 °C up to equilibrium conditions. The results revealed that tetralin was the only hydrogenation product observed at 350 °C and cracking or isomerization products of tetralin were seen at 450° C. The reaction did not reach

equilibrium, and as the temperature increased the forward rate constant reaction increased.

2.2 Hydrodesulfurization (HDS)

One of the most important catalytic processes used to remove sulfur from petroleum fractions is hydrodesulfurization (HDS). An increasing commercial demand to convert sulfur rich feed stocks and the environmental demand to further reduce the sulfur content of oil products has led to a need for more efficient processes and more active catalysts. Most of the organosulfur compounds in middle distillates are present in the form of heterocyclic compounds as introduced in section 1.1.2. The least reactive organosulfur compounds in petroleum are thiophenic compounds, (Gates et al., 1979). The following discussion summarizes the new catalytic hydrodesulfurization processes.

Reyes et al. (1994) studied the effect of adding different amount of phosphorus (P_2O_5) on W/Al_2O_3 catalyst for the HDS activity. They found that the addition of phosphorous has increased the HDS activity of the middle distillate significantly.

Walters et al. (1994) discovered that the thiophene hydrodesulfurization activity, and product selectivity on zeolite-supported metal sulfide catalysts were dependent not only on the type of metal sulfide and the pore structure of the zeolite, but also on the acidity. As the acidity increased the HDS of thiophene increased. The acidity effect was due to small metal sulfide particles and the acidic support working together, not the increase in metal sulfides dispersion.

Ramanathan and Oyama (1995) evaluated a new class of hydrotreating catalyst. They were the transition metal carbides and nitrides that have different structure and properties than the conventional sulfided hydrotreating catalyst as $\text{CoMo/Al}_2\text{O}_3$ and $\text{NiMo/Al}_2\text{O}_3$. The commercial $\text{NiMo/Al}_2\text{O}_3$ catalyst showed better activity than the transition metal carbides and nitrides for the HDS of dibenzothiophene in the presence of quinoline. The reason for the lower activity could be due to the competitive adsorption of the more basic quinoline compounds on the available sites. Therefore, these kinds of catalyst have not been very promising for HDS reactions and further investigation is needed.

Yue et al. (1997) investigated the HDS activity using the new family of amorphous mesoporous catalyst, such as MCM-41 and KIT-1. The KIT-1 was a disordered mesoporous molecular sieve and it was similar to MCM-41 because of high surface area and uniform mesoporous channels. When MoO_3 and NiO were supported on KIT-1, exhibited higher catalytic activities for thiophene HDS than the similar MCM-41 and NaY zeolite supported catalysts. This occurred because of the three dimensional disordered network of short channels in KIT-1, that decreases the possibility of blockage in the catalysts, and assisted the transport of reactant and product molecules.

Farag et al. (1998) have examined different ways of preparing sulfided Co and Mo supported on carbon, and its influence on the HDS activity. They have found that carbon was an effective support for HDS catalyst. Sulfidation of the Mo precursor before the addition of the Co promoter greatly enhanced the activity of the HDS reaction. The enhancement in activity was due to a more efficient production of the Co-Mo-S active

species from the MoS_2 on the carbon surface. Farag et al. (1998) study has confirmed that the activity of HDS depends on the metal loading, as well as the order of the metal addition during preparation.

2.2.1 Kinetics and Reaction Network

Sulfur removal is considered to be exothermic and irreversible under the reaction conditions employed in industry (Gates et al., 1979; Vrinat, 1983). Speight (1981) has shown that sulfur removal occurs with or without prior hydrogenation of the hetrocyclic rings. Desulfurization involved C-S scission (hydrogenolysis) to produce H_2S and the corresponding hydrocarbon. Van Parijs et al. (1986a,b) have discovered that sulfur removal from thiophene was substantially slower than benzothiophene at the pressure ranges 5.0-30.0 atm. Rollmann (1977) have found benzothiophene (BTH) and dibenzothiophene (DBTH) have similar reactivities in trickle bed experiments at the pressure of 59.0 atm.

Girgis and Gates (1991) and Vrinat (1983) come to the same agreement, i.e., the differences in the patterns of reactivities in the HDS indicated that sulfur removal was sensitive to the reaction conditions. This included the way in which the catalyst was activated; the type of the reactor (pulsed, continuous flow, or batch); the concentration of organic reactants and H_2S ; and finally, the hydrogen pressure and catalyst size.

Benzothiophene (BTH) is one of the organosulfur compounds usually found in the middle distillates. Van Parijs et al. (1986a) have reported on reaction network for BTH in n-heptane solvent at 2.30 atm and 240-300 ° C on $\text{CoMo}/\text{Al}_2\text{O}_3$ catalysts as

shown in Figure 2.2.1.1. Styrene was not detected and was assumed to have hydrogenated rapidly to give ethylbenzene (ETHBZ) after being formed from BTH. The same authors Van Parijs et al. (1986b) reported that two different types of catalytic sites were assumed: one for hydrogenolysis of benzothiophene and 1,2 dihydrobenzothiophene (DHBTH), and one for the hydrogenation of BTH.

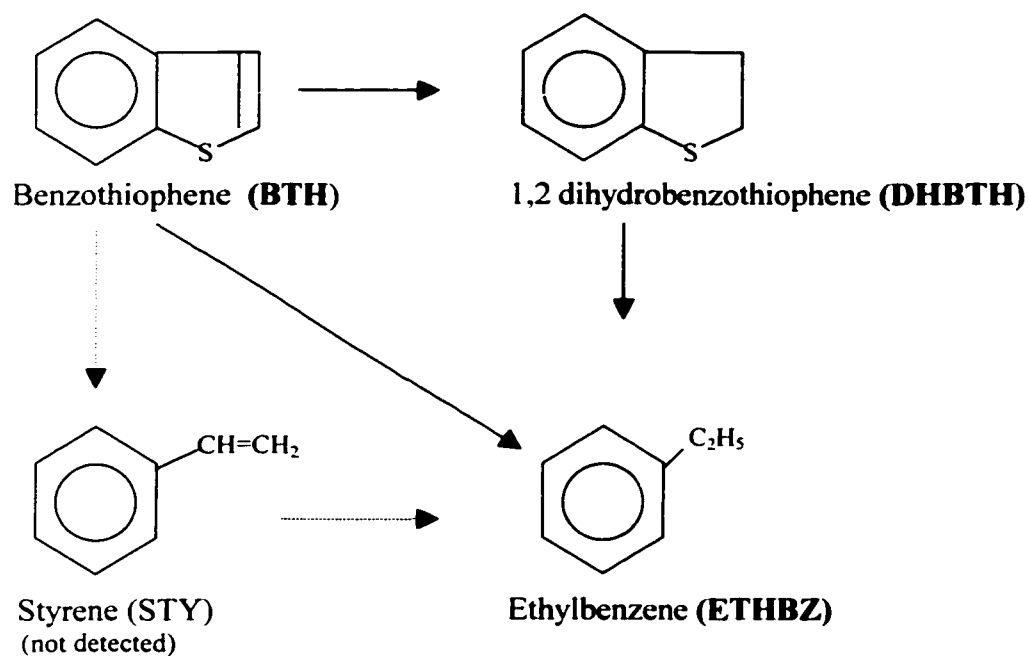


Figure 2.2.1.1: Reaction network for benzothiophene proposed by Van Parijs et al. (1986a, b)

Shi et al. (1996) have observed the kinetics and mechanisms of benzothiophene HDS reaction over a sulfided NiO-MoO/ γ -Al₂O₃ commercial catalyst. The catalyst contained 15.5 % MoO₃ and 4.5 % NiO. They found that styrene was not detected, the DHBTH was an intermediate, and that ETHBZ was the primary product. The conversion of BTH and the concentration of ETHBZ increased as temperatures increased to the range of 180-260°C.

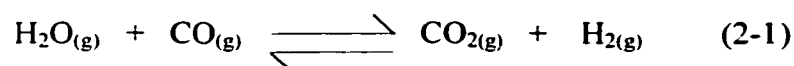
Recently, Li and Lee (1998) have observed the HDS of benzothiophene over molybdenum nitride (Mo₂N), which was prepared by a temperature programmed reaction method, from MoO₃, 12-molybdophosphoric acid (H₃PMo₁₂O₄₀26H₂O, denoted as HPA), a mixture of MoO₃+P₂O₅ and a stream of NH₃ was passed through the reaction. They found that the Mo₂N was an effective catalyst for the HDS of BTH. The ETHBZ was the primary product for most of the temperature ranges used. The addition of P₂O₅ to the precursor, MoO₃, improved the activity of the Mo₂N catalysts in HDS of BTH; it also increased their resistance against catalyst deactivation. However, the reaction pathway for BTH was not changed by the addition of phosphorous.

The high consumption of hydrogen during the AHYD and HDS processes require a cheap source of hydrogen. The in situ generation of hydrogen via the water gas shift reaction would be helpful to the petroleum refining processes.

2.3 Water Gas Shift Reaction (WGSR)

The demand for hydrogen usage in the hydrotreating processes is increasing due to the requirement for substantial quantities of hydrogen for upgrading petroleum products. Catalytic reformers are recovering part of the needed hydrogen. Usually, the external hydrogen is manufactured either by steam methane reforming or by partial oxidation processes. (Speight, 1991).

Keiski et al. (1996) reported that the WGSR is a reversible and exothermic reaction. Usually the reactions have occurred in the presence of catalyst carbon monoxide and water (or steam) to produce carbon dioxide and hydrogen gas:



$$\Delta H_{298} = -41.09 \text{ kJ/mol}$$

$$\Delta S_{298} = -42.39 \text{ J/Kmol}$$

Some researchers have used the produced hydrogen in the HDS reaction as a one step reaction. Hook and Akgerman (1986) used hydrogen generated in situ via the WGSR to study the HDS of dibenzothiophene (DBTH). They observed that the rate constants of HDS for DBTH with in situ H_2 were of a magnitude greater than those obtained from externally supplied H_2 . Massoth et al. (1990), Hou et al. (1983), Takemura et al. (1981) and Newsome (1980) have reported that sulfided forms of the supported transition metal

oxide were found to be more active in the hydrotreatment processes catalyzing the WGSR as well as the HDS reaction.

Few researchers have examined the efficiency of the dispersed catalyst. Ng and Rintjema (1992) have developed a one stage process for catalytic emulsion breaking, and upgrading via the activation of water using dispersed molybdcic acid catalyst. They have reported that the hydrogen generated in situ was showing more activity than the externally supplied H_2 . They achieved up to 96% sulfur removal, whereas, only 30% sulfur removal was achieved under the same operating condition by supplying external hydrogen to the reactor.

Ng and Tsakiri (1992) have reported similar results for the HDS of BTH in an emulsion using phosphomolybdcic acid as the catalytic precursor.

Recently, Siewe and Ng (1998) observed the reactivity of using two kinds of dispersed catalyst, ammonium tetrathiomolybdate and phosphomolybdcic acid, for the HDS of cold lake diesel via the WGSR. They proposed that partial oxidation flue gases containing a mixture of H_2 , CO, CO_2 and H_2O could be used to achieve reasonable levels of sulfur removal from an industrial type feed.

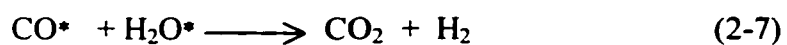
2.3.1 Kinetics and Mechanisms of WGSR

To further understanding of the reaction mechanism of the shift reaction, Shchibrya et al. (1965) proposed that the reaction might proceed through a redox mechanism, where the catalyst was reduced by CO through the formation of CO_2 and reoxidized by H_2O through the formation of H_2 .

This was in agreement with Newsome (1980) who suggested an oxidation-reduction mechanism for the WGSR as the follows:



While, Oki (1973) suggested another possible mechanism for the shift reaction:



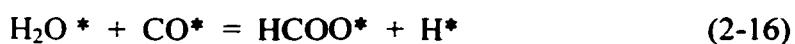
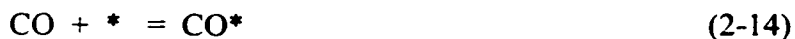
Two mechanisms were proposed by Grenoble et al. (1981); Kuijpers et al. (1986); Nakamura et al. (1990) and Fujita et al. (1992).

(1) Surface redox mechanism:



In this mechanism, water dissociatively adsorbs to produce oxygen adatoms O* and hydrogen, followed by the well-known reaction of CO with O* to produce CO₂.

(2) Langmuir-Hinshelwood mechanism:



Xue et al. (1996) have found that the conversion of the CO decreased, as the reaction temperature increased. When a low ratio of H₂O to CO was employed, side reactions occurred producing undesired products such as carbon and methane, as the ratio decreased, the risk of carbon formation increased due to the oxide reactions.

Using CO₂/H₂ cycles, Gines et al. (1997) have examined the kinetics of the reverse water-gas shift reaction over CuO/ZnO/Al₂O₃ catalysts. They found that different reagents become rate-limiting depending on the pressure, whereas in H₂-rich regions the rate increased strongly with CO₂ partial pressure and was zero order in hydrogen. The reaction was less active under low pressures ratio of H₂/CO₂ and was of a strong positive high order in hydrogen and low order in carbon dioxide. Both the dissociation and water formation determine the rate of the overall reaction.

2.3.2 WGSR Catalysts

Many materials are capable of catalyzing the WGSR. Moe (1962) and Bohloro (1969) have initiated discussion of a potential shift reaction. Two classes of materials are used in industry as shift catalysts: the iron-based catalyst and copper-base catalyst. The iron-based catalysts were known as the high temperature shift catalysts and operate in the temperature range of 320 - 450 °C and the iron oxide catalysts tolerate small quantities of sulfur. Recently, copper-based shift catalysts were accepted in the industry and they were known as the low temperature shift catalysts, and operate in the temperature range of 200-250 °C. They have good activity, favorable equilibrium at lower temperatures, and have better selectivity, which resulted in fewer side reactions at elevated pressures. In addition they were considered to be a completely sulfur intolerant.

Other factors in addition to metal catalysts which affect the WGSR conversion, are solvent polarity, and whether or not the reaction medium is acidic, basic, or neutral. Laine et al. (1988) have described that the main catalytic mechanisms occurred through the activation of CO followed by its reaction with water. The free CO coordinated with unsaturated metal. When the metal is neutral and supports several good electron donor ligands, OH acts as a strong nucleophile capable of reacting with the activated CO. In contrast, when the metal has little electron density to donate to the coordinated CO, the positive metal complex may react with water to produce a metallocarboxylic acid.

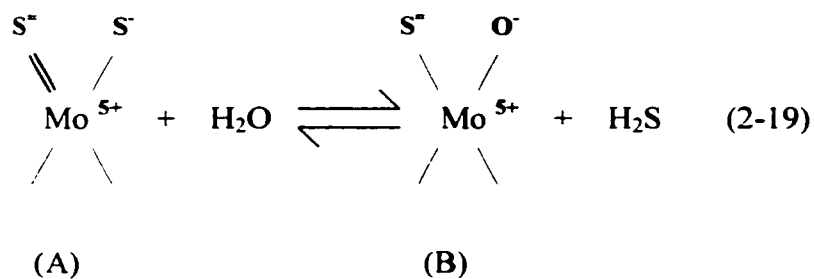
When the reaction condition occurs under an acidic medium, the entire complex can be protonated. This reduces the electron density available for back bonding with CO, making it sufficiently electron deficient that it can then react with water. An alternate

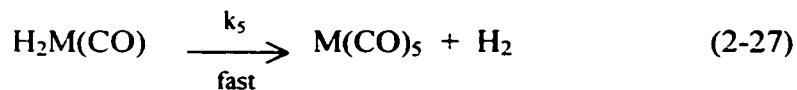
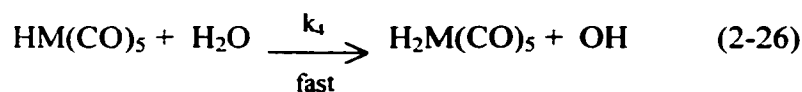
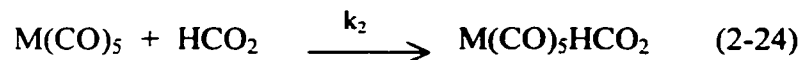
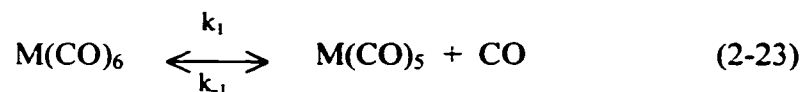
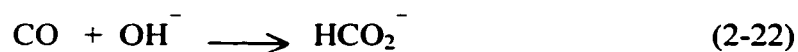
reaction pathway was available through CO activation rather than through a coordinatively unsaturated metal. This reaction begins with CO and OH⁻ to produce formate, which decomposes to formic acid with excess water.

Kang et al. (1977) and King et al. (1978) have reported on the Fe (CO)₅ catalysis of WGS in basic media using tetrahydrofuran and alcohols as solvents. Marnot et al. (1981) have shown that Rh or Ir metals catalyze the WGS under acidic conditions.

Hydrogen sulfide has been used to presulfide the Mo/Al₂O₃ catalyst to promote the WGS. Hou et al. (1983) have studied the WGS over molybdenum sulfide-based catalysts in the presents of hydrogen sulfide. They proposed the following WGS mechanisms:

Step 1:





Were $\text{M} = \text{Cr}, \text{Mo}, \text{W}$.

In conclusion, catalyst textures and structure, and feed mixture compositions may strongly affect the kinetics and mechanism of the WGSR.

From this point of view, this thesis investigates the reactivity of different kinds of Mo dispersed catalysts with aromatic hydrogenation and sulfur removal together via WGSR. The advantage of the dispersed catalyst is that it eliminates the conventional poisoning problem associated with heterogeneous catalysis.

Little work has been carried out on the hydrogenation of aromatics using a dispersed catalyst with the advantage of using the hydrogen produced via the WGSR. This thesis examines the hydrogenation of a mixture of naphthalene and bezothiophene as representative model compounds in diesel fuel utilizing the hydrogen produced via the WGSR. Different operating conditions were investigated, and it will be discussed in detail in the next chapter.

Chapter 3

Experimental Work

Chapter 3 details the design of the experiment, the types of samples and the analysis of the results. The flow sheet, shown in Figure 3.1, indicates the work plan that was followed for the hydrogenation process.

3.1 Experimental System Design

The experiments were carried out in a 1000 cm³ 316 stainless steel, Autoclave Engineers (AE) batch reactor. A schematic of the apparatus is shown in Figure 3.1.1. The system consisted of a main body of 316 stainless steel and a closure assembly with eight screws, a main nut, a bearing washer, and a seal ring shown in Figure 3.1.2.

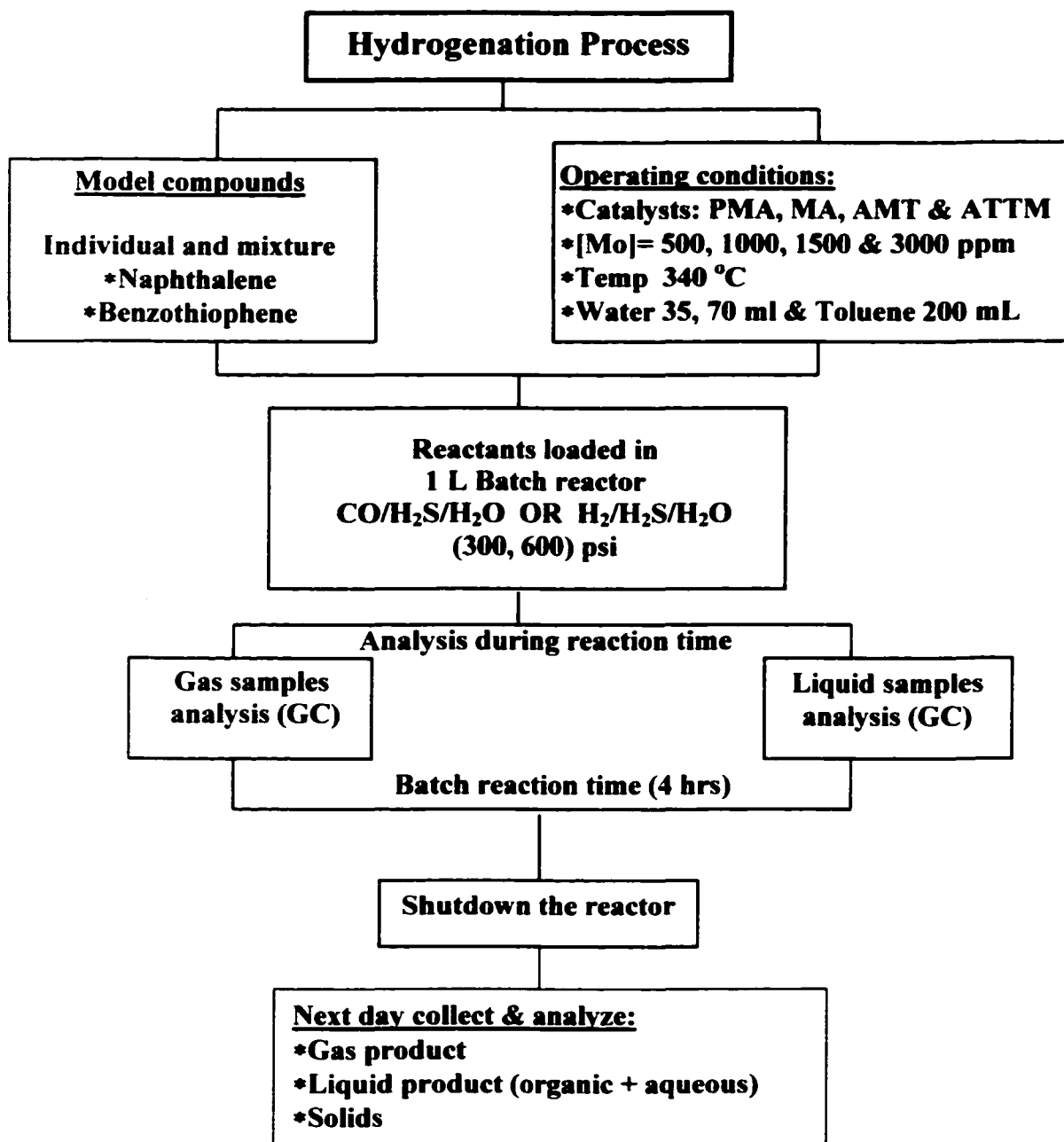


Figure 3.1: Work plan flow chart

Figure 3.1.3 illustrates how the magnetic drive impeller speed was attached to the middle of the closure assembly. A specific mixing speed, up to 3000 rpm was maintained by a tachometer. An insulated electric furnace sleeve type of 3 KW in total heated the reactor. The furnace was controlled by a OMEGA automatic temperature controller (model-2011) equipped with a type K thermocouple input, and the furnace temperature should not exceed 760 °C.

A type K thermocouple contained in a thermowell with a diameter of 0.270 cm measured the temperature at the bottom of the reactor. The pressure inside the system was monitored by using OMEGA pressure transducer (type P1021-0005), with a pressure gauge of dial (0-10000) psi as seen in Figure 3.1.2. The maximum allowable pressure in the system was 9000 psi @ 450 °C.

As a safety precaution, the system was constructed with two rupture disks (see Figure 3.1.1). The one for the reactor was designed to fail at 10,450 psi at 22 ° C and the other one for the sampling system was designed to fail at 1027 psi at 22 ° C. The reactor system was designed to collect only gas samples but was modified to enable the collecting of liquid and gas samples during the reaction time, in order to determine the kinetics of the catalytic reactions.

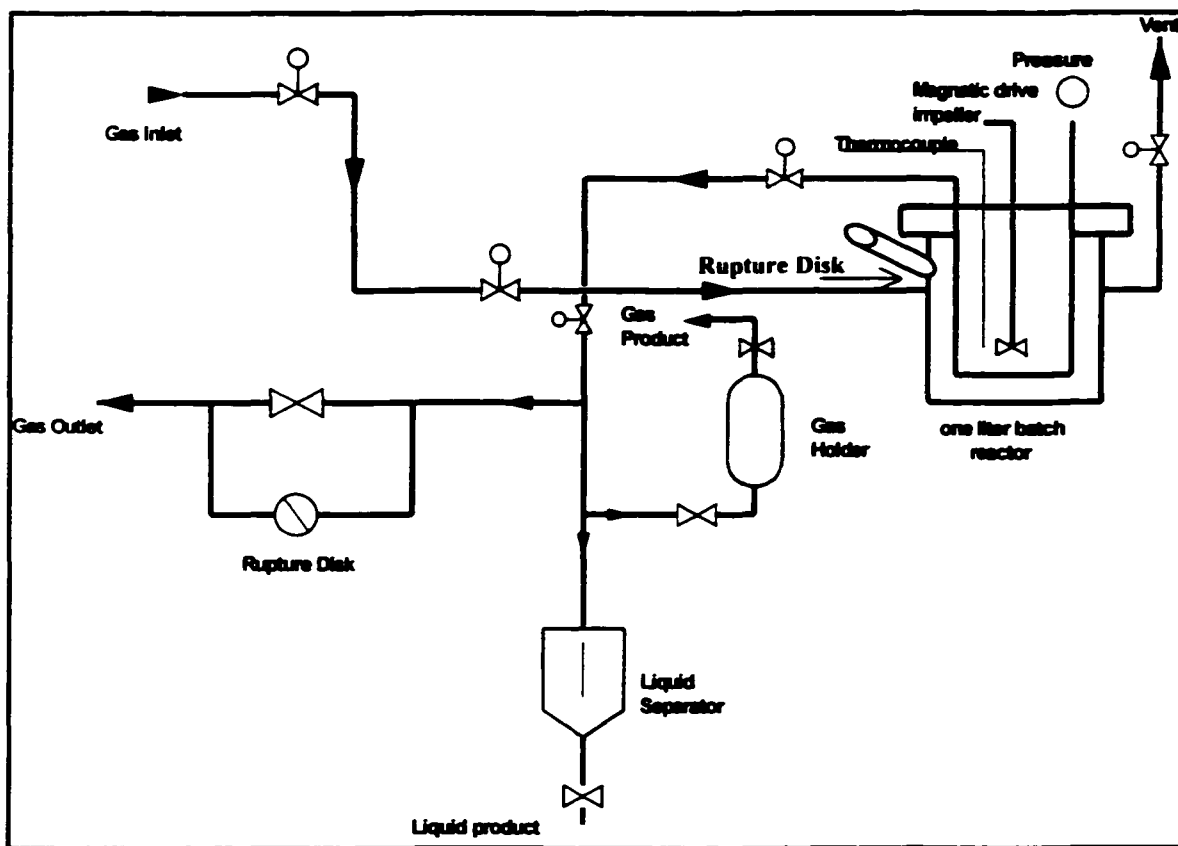


Figure 3.1.1 Schematic diagram of the experimental system design

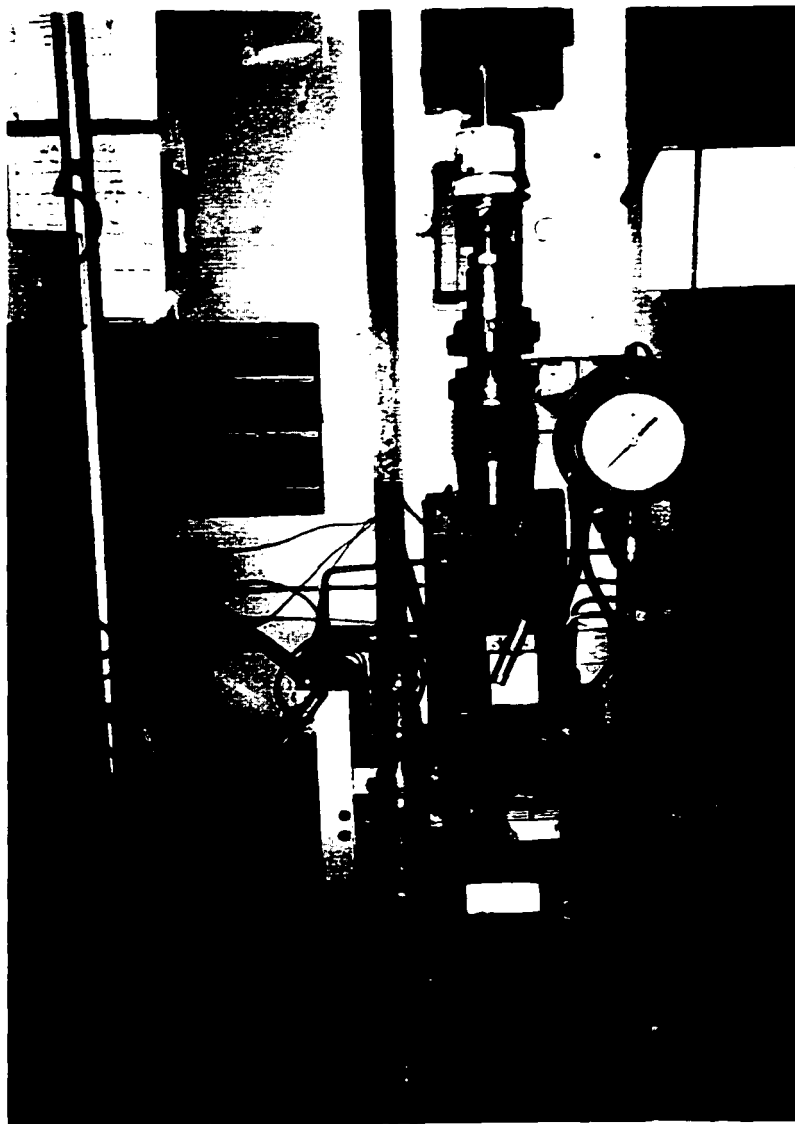


Figure 3.1.2: Front view of the 1 L batch reactor as located in Lab-1521 in Chemical Engineering Department at the University of Waterloo

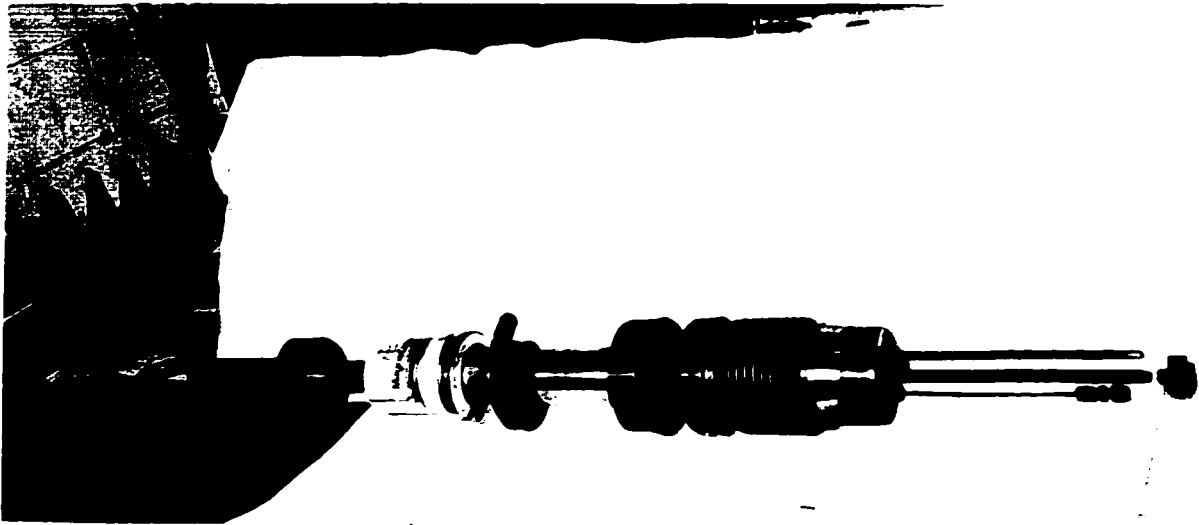


Figure 3.1.3: The view of the closure assembly.

3.2 Experimental Procedure

3.2.1 Loading, Sealing and Leak testing the Reactor

Loading, sealing and leak testing the reactor was carried out by following a specific procedure to ensure that the system performed well during the course of the experiment. These steps are detailed in Appendix (A.1).

3.3 Operating Conditions

The experiment was carried out in the 1 L reactor system at 340 °C with a gas loading of 600 psi (CO or H₂ mixed with 15 psi H₂S). For materials consisting of model compounds naphthalene and benzothiophene, the experiments were carried out with CO/H₂S and H₂/H₂S gases at initial loading pressures of 300 and 600 psi. The water content was changed to 35 and 70 ml, to observe the effect of changing the H₂O/CO ratio on the WGSR and the hydrogenation process.

In addition, the molybdenum concentration in the phosphomolybdic acid catalyst (PMA) was varied in the range of 500 - 3000 ppm. Table 3.3.1 illustrates the four types of Mo dispersed catalysts that were used for the hydrogenation of the binary mixture of BTH and NAPH. The Mo concentration in each catalyst solution was fixed at 1500 ppm.

3.4 Catalyst and Feed Preparation

3.4.1 Catalyst Preparation

The catalyst was introduced in to the system in the solution form (e.g., PMA, MA and ATM). However, the ATTM catalyst was in the powder form, because it is insoluble in water. To prepare the stock solution of each catalyst, specific amount of catalyst powder was measured and dissolved in the deionized water to insure uniform dispersity. The weight of catalyst solution calculated was dependent on the Mo concentration; it was 1500 ppm Mo for all the types of catalyst. The calculated amount of catalyst solution was added to the deionized water to measure 70 ml in total, for calculation see Appendix A.2.

The pH for the formed aqueous layer was measured using a pH meter (Model-320-CORNING) before and after the reaction. The Mo concentration was quantified using a calibration curve on the Direct Current Plasma Emission Spectrometer (model Fisons/ARL Spectraspan 7), DCP machine. The standard solutions for calibration were prepared from a 10,000 ppm Mo standard solution purchased from BDH Inc. The calibration curve is displayed in Appendix A.3.

3.4.2 Feed Preparation

Naphthalene (99.9% pure, BDH) and bezothiophene (95% pure, Aldrich) were the model compounds chosen for this investigation for the aromatic hydrogenation and sulfur

removal, respectively. The weights of these model compounds were calculated to be similar to those in diesel fuel, (20 wt % aromatic and 1.8 wt % sulfur).

The weight ratio of NAPH:BTH (3.20:1.0 mol/mol) was constant for all the experimental runs. A technical grade of toluene was used as the dissolving reagent (200 ml). A sample of the calculation may be found in Appendix A.4.

Table 3.3.1: Types of Mo dispersed catalyst were used

Catalyst type	Molecular formula	Purity (%)	Supplier Company
Phosphomolybdic acid Hydrate A.C.S reagent (PMA)	$12\text{MoO}_3 \cdot \text{H}_3\text{PO}_4 \cdot x\text{H}_2\text{O}$	---	Aldrich
Molybdic Acid A.C.S reagent (MA)	Contains 85% MoO_3	85	Fluka
Ammoniumheptamolybdate- Tetrahydrate A.C.S reagent (ATM)	$(\text{NH}_4)_6\text{Mo}_7\text{O}_{24} \cdot 4\text{H}_2\text{O}$	---	Aldrich
Ammoniumtetrathiomolybdate (ATTM)	$(\text{NH}_4)_2\text{MoS}_4$	99.97	Aldrich

3.5 Experimental Run

Each experimental run required approximately six hours, 2 hours for heating up the reactor and 4 hours for the reaction batch time. Before each run, the top of the reactor was wrapped with an insulation material (K wool) to minimize heat loss. Then the reactor was purged with the same loaded gas (e.g., CO or H₂) at approximately 100-200 psi to insure that the system was free of air and nitrogen gas. The required gases were introduced to the reactor at 600 psi for all the runs. The furnace temperature controller was at 500 °C to achieve reactor temperature with a warming rate of 3 °C/min. After the furnace was turned on, the magnetic drive stirrer was switched on so that its speed increased gradually to reach the required setting, which was 1300 rpm for this study.

Then the computer was turned on for monitoring and data collection. When the reaction temperature reached 340 °C, liquid and gas samples were collected in intervals of 30 min for the 4 hrs reaction batch time. Flushing between samples insured accuracy of GC/GLC analysis for each sample. The temperature was maintained constant during the reaction time through a bottom thermocouple inside the reactor. At the end of the experimental run, the reactor furnace and the magnetic drive stirrer were turned off to allow the reactor to cool to ambient temperature. Usually, the reactor temperature and pressure were recorded at the next day. The gas product was collected by evacuating it into a gasbag of size 40 L and subjected to GC analysis.

The reactor was then disassembled and liquid and solids collected. The liquid volume was measured as shown in Figure 3.5.1. The solids were separated under vacuum, (see Figure 3.5.2). Further, the solids were subjected to thermogravimetric

(TGA/DTA) and X-ray diffraction (XRD) analyses. The organic liquid product was collected, (see Figure 3.5.4) for GC-liquid analysis, and the aqueous layer was separated from the organic layer for pH measurement and ion chromatography (IC) analysis for sulfate ions.

3.6 Gas, Liquid, and Solids Analyses

3.6.1 Gas Analysis

A Perkin–Elmer model 8500 Gas/Liquid Chromatograph (GC) was equipped with injectors and detectors. One detector analyzed both the gases sampled during the reaction batch time, and the gas products collected in the sampling bag at the end of reaction. The Thermal Conductivity Detector (TCD) analyzed non-hydrocarbon gases. Gas samples were injected into a 10 port gas-sampling valve, equipped with a 0.1 ml sampling loop.

The He carrier gas contained 8.60 % H₂. The inlet system was composed of two columns in series: the first column was 1.52m x 3.12mm O.D. packed with 80/100 mesh Hayesep C, and the second column was 2m x 3mm O.D packed with an 80/100 mesh 5A molecular sieve. The gases, H₂, O₂, N₂ and CO, were separated on the 10 port sampling valve on the molecular sieve, whereas CO₂ and H₂S gases were separated on the HayesepC column, because CO₂ and H₂S poison the molecular sieve. The established method used for the gas analysis on GC can be found in Appendix A.5.

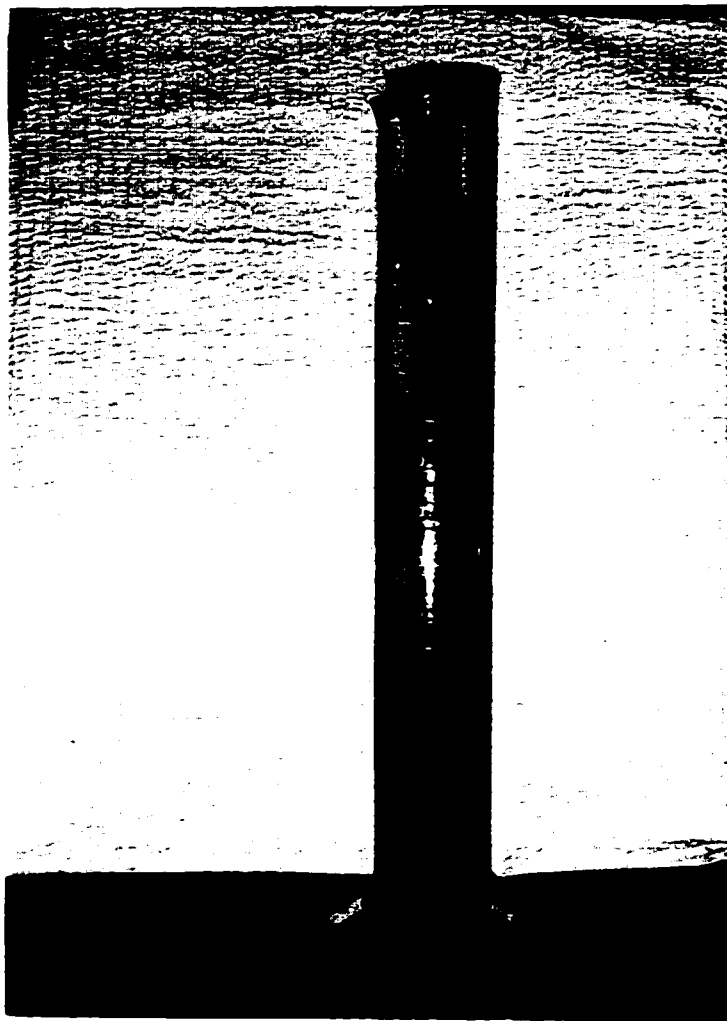


Figure 3.5.1: The collected liquid and solids before separation

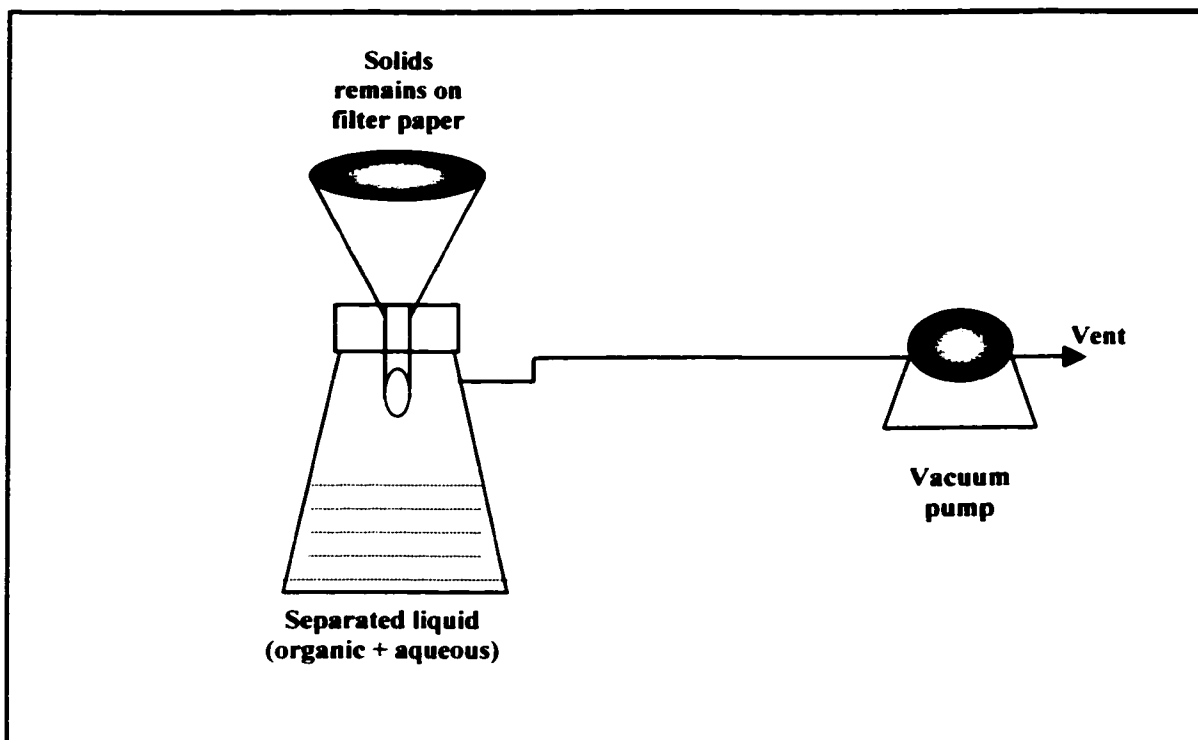


Figure 3.5.2: The filtration system used for solid and liquid separation under vacuum

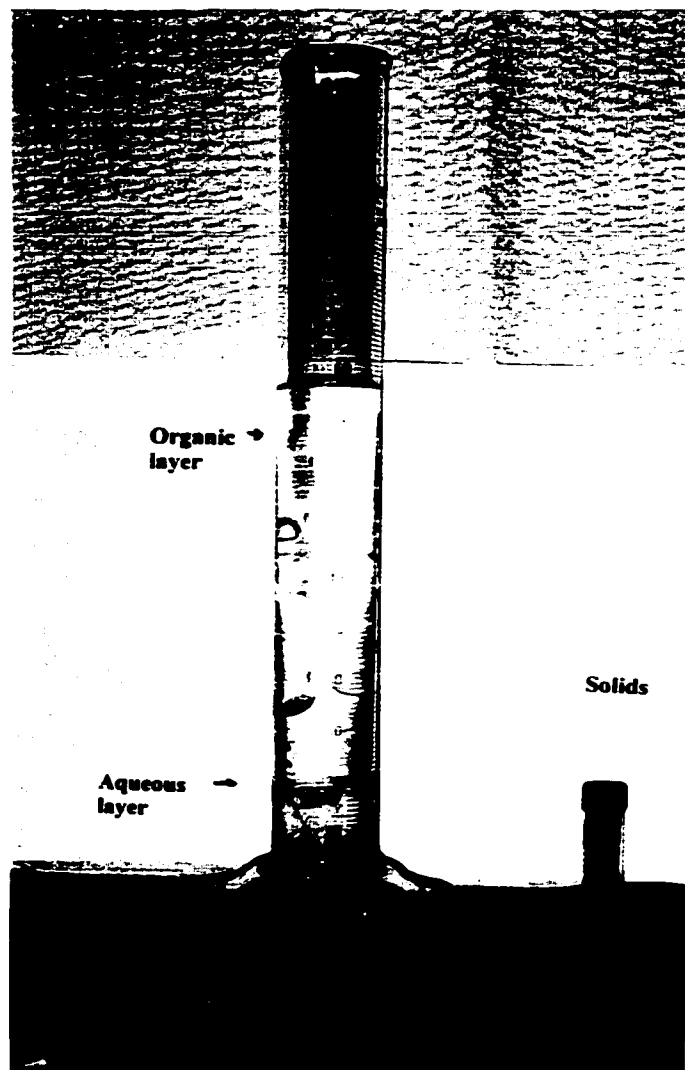


Figure 3.5.3: The collected solids and liquid product after separation

3.6.2 Liquid Analysis

The Perkin Elmer model 8500, was equipped with a 30m x 0.25mm O.D., DB-1701 fused silica column coated with 0.25 μm 7% cyanopropylphenyl silicone. The flame ionization detector (FID) was used to analyze the liquid samples. The system consisted of a split injector maintained at 250 °C and split of 160:1. According to the types of network reactions of the model compounds was used, three calibrations were established for BTH, NAPH, and the mixture of NAPH+BTH. Details of the established methods can be found in Appendix A.6.

3.6.3 Solid Analysis

The solid layer was composed of the spent catalyst together with some carbon deposits. Solids were subjected to two different types of tests. Firstly, the X-ray Diffraction (XRD) with a rotating angle of 2θ , by using (Siemens D500 X-ray diffractometer with the $\text{CuK}\alpha$ radiation ($\lambda=1.543\ 24$) as the X-ray source, operating at 1.2 kW (40 kV x 30 mA). This was compared with commercial grade samples of MoS_2 and MoO_3 , because these phases were most likely present in the spent catalysts, the experimental method is listed on Appendix A.7.

Secondly, the thermogravimetric/differential thermal analysis (TGA/DTA) was applied to measure the amount, and the rate of weight changes in the material, either as a function of increasing temperature, or isothermally, as a function of time. The temperature for each sample was carried out in the range of 50 - 600 °C by using the (TA

Instruments 2100 thermal analysis, TGA/DTA, 1500 °C). The program setting for the TGA/DTA method is shown in Appendix A.8.

3.6.4 Aqueous Layer Analysis

After the aqueous layer was separated completely from the organic layer under vacuum filtration system (refer to Figure 3.5.2), the pH was measured. Also, the Ion chromatography system (IC), the Dionex DX 500 Chromatograph, was used to detect the presence of sulfate ions (SO_4^{2-}). The calibration was established by preparing a standard solution using sodium sulfate (Na_2SO_4), and selected samples of different runs were analyzed (see Appendix A.9).

3.6.5 Reagents

The current experimental work required several reagents. A technical grade of toluene was obtained from the Department of Chemistry at the University of Waterloo. Naphthalene of 99.9 % pure was obtained from the BDH Inc. Tetralin of 99 % pure, cis/trans decalins of 99 % pure, benzothiophene of 95 % pure, and ethylbenzene of 99 % pure were obtained from Aldrich.

Carbon monoxide of 99.5% pure, prepurified nitrogen, 99.99 % pure hydrogen, H_2/He with 8.5 % hydrogen, and prepurified He were obtained from PRAXAIR.

3.7 Calculations

3.7.1 WGSR

A. CO Conversion

The CO conversion for the WGSR was calculated from the measurement of the total moles for CO before and after the reaction as follows:

$$X_{CO} (\%) = \left[\frac{(N_{CO})_i - (N_{CO})_f}{(N_{CO})_i} \right] \times 100 \quad (3-1)$$

where,

$N_{CO,i}$ = initial moles of CO

$N_{CO,f}$ = final moles of CO

N refers to, number of moles calculated based on the ideal gas law:

$$N = \frac{PV}{RT} \quad (3-2)$$

where.

P = pressure (atm)

V = total working reactor volume (L)

T = temperature (K)

R = gas constant (0.08206 atm L/ mol K)

B. H₂ Consumed and Generated



The hydrogen gas consumed was calculated according to the stoichiometry of the WGSR as follows:

$$(N_{\text{H}_2})_{\text{Consumed}} = (N_{\text{CO}_2})_f - (N_{\text{H}_2})_f \quad (3-4)$$

$$(N_{\text{H}_2})_{\text{Generated}} = (N_{\text{CO}})_i - (N_{\text{CO}})_f \quad (3-5)$$

where.

$N_{\text{CO}_2 f}$ = final moles of CO₂

$N_{\text{H}_2 f}$ = final moles of H₂

C. H₂S Generated

The number of moles of hydrogen sulfide generated in the system during the reaction time was calculated as follows:

$$(N_{H_2S})_{Generated} = (N_{H_2S})_i - (N_{H_2S})_f \quad (3-6)$$

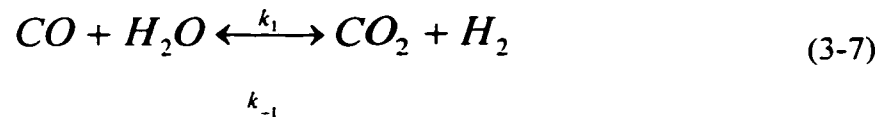
where,

$(N_{H_2S})_i$ = initial moles of H₂S

$(N_{H_2S})_f$ = final moles of H₂S

A sample of the calculation is shown in Appendix B.1.

3.7.1.1 WGS Kinetics



To determine the kinetics of the WGS, gas samples were taken during the course of the reaction to monitor the CO concentration over a period time. Since H₂ was consumed during the reaction, the reaction was considered to be irreversible and followed pseudo first order kinetics since H₂O was in excess:

$$\text{rate} = -\frac{d[\text{CO}]}{dt} = k'_1 [\text{H}_2\text{O}][\text{CO}] \quad (3-8)$$

$$= k_1 [\text{CO}] \quad (3-9)$$

where, $k_1 = k'_1 [\text{H}_2\text{O}]$ is the pseudo first order rate constant.

$$r = -\frac{d[\text{CO}]_t}{dt} = k_1 [\text{CO}]_0 \quad (3-10)$$

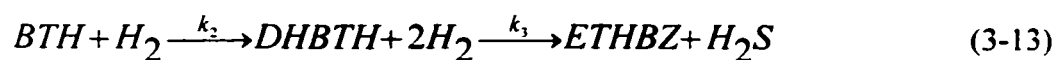
$$r = -\frac{d[\text{CO}]_t}{[\text{CO}]_0} = k_1 dt \quad (3-11)$$

Integration gives:

$$-\ln \frac{[\text{CO}]_t}{[\text{CO}]_0} = k_1 t \quad (3-12)$$

Plotting the left side of equation (3-12) versus the reaction time t , results in a straight line passing through the origin with a slope equal to the rate constant (k_1). A sample of calculation and data are shown in Appendix B.2.

3.7.2 The Hydrodesulfurization of BTH



Ethylbenzene (ETHBZ) was the primary product detected from the HDS of BTH. The DHBTH was found as an intermediate product in small quantities. From the GC analysis, the mol fraction % of each component was calculated by normalization as follows:

$$N_{TOT} = \sum (N_{BTH} + N_{EB} + N_{DHBTH})_t \quad (3-14)$$

$$mol \% BTH = \frac{(N_{BTH})_t}{N_{TOT}} \times 100 \quad (3-15)$$

$$\text{mol \% ETHBZ} = \frac{(N_{\text{ETHBZ}})_t}{N_{\text{TOT}}} \times 100 \quad (3-16)$$

$$\text{mol \% DHBTH} = \frac{(N_{\text{DHBTH}})_t}{N_{\text{TOT}}} \times 100 \quad (3-17)$$

Where, N_{BTH} , N_{ETHBZ} , and N_{DHBTH} were the mole fraction of benzothiophene, ethylbenzene and dihydrobenzothiophene, respectively, at reaction time, t . After the determination of the mole fraction of each species, the following was calculated:

(1) The BTH conversion (X_{BTH}) is as follows:

$$X_{\text{BTH}} (\%) = \frac{(N_{\text{BTH}})_i - (N_{\text{BTH}})_f}{(N_{\text{BTH}})_i} \times 100 \quad (3-18)$$

where.

$(N_{\text{BTH}})_i$ = initial number of moles of BTH

$(N_{\text{BTH}})_f$ = final number of moles of BTH

(2) Sulfur removal is calculated as follows:

$$\% S_{rem} = \frac{(N_{ETHBZ})_f}{(N_{ETHBZ} + N_{DHBTH} + N_{BTH})_f} \times 100 \quad (3-19)$$

(3) ETHBZ yield is calculated as follows:

$$\% yield = \frac{(N_{ETHBZ})_f}{(N_{BTH})_i} \times 100 \quad (3-20)$$

(4) ETHBZ selectivity is calculated as follows:

$$(ETHBZ)_{selectivity} = \frac{(N_{ETHBZ})_f}{(N_{ETHBZ} + N_{DHBTH})_f} \quad (3-21)$$

Where, N_{ETHBZ} and N_{DHBTH} are the number of moles in the final product for ethylbenzene and dihydrobenzothiophene respectively. A sample of calculation can be found in Appendix B.3

3.7.2.1 Kinetics of The Hydrodesulfurization of BTH

The rate constant of the HDS of BTH is calculated by assuming pseudo first order reaction and by plotting $\ln(N_0/N_t)_{BTH}$ versus the reaction time, t . A straight line of slope

equal to the rate constant (k_2) was obtained. From, the network reaction equation (3-13), the rate equation is as follows:

$$-r_{BTH} = \frac{d[N_{BTH}]_t}{dt} = k_2 [N_{BTH}]_0 \quad (3-22)$$

Since the reaction was started with BTH only and ETHBZ is the primary product, therefore, integrating equation 3-22 gives:

$$-\ln \left(\frac{N_t}{N_0} \right)_{BTH} = k_2 t \quad (3-23)$$

A detailed sample of calculation can be found in Appendix B.4. The availability of H_2 was calculated. (see Appendix B.5).

3.7.3 The Hydrogenation of NAPH

For this study, naphthalene was selected as the model compound for the hydrogenation activity measurement. As introduced previously in Section 2.1.1, NAPH hydrogenation is a consecutive reaction to produce tetralin (TET) followed by cis and trans decalins. TET was the primary product, whereas, cis and trans decalins were found

in small quantities from the GC- liquid analysis. The GC-liquid analysis enabled the calculation of the mol fraction % of each species of the products, and the following was calculated:

(1)The NAPH conversion (X_{NAPH}) is defined as follows:

$$X_{NAPH} (\%) = \frac{(N_{NAPH})_i - (N_{NAPH})_f}{(N_{NAPH})_i} \times 100 \quad (3-24)$$

where,

$(N_{NAPH})_i$ = The initial moles of NAPH

$(N_{NAPH})_f$ = The final moles of NAPH

(2) The % of aromatic removal was defined as follows:

$$\% A_{rem} = \frac{\sum (N_{TET}, N_{cis-DEC}, N_{trans-DEC})_f}{\sum (N_{NAPH}, N_{TET}, N_{cis-DEC}, N_{trans-DEC})_f} \times 100 \quad (3-25)$$

(3) Tetralin yield was defined as the following:

$$\% yield = \frac{(N_{TET})_f}{(N_{NAPH})_i} \times 100 \quad (3-26)$$

(4) Tetralin selectivity was defined as the following:

$$(TET) \text{ selectivity} = \frac{(N_{TET})_f}{(N_{TET} + N_{DECS})_f} \quad (3-27)$$

The hydrogenation activity of naphthalene can be measured according to the following equation:

$$A_H = \frac{2 N_{TET} + 5 N_{DECS}}{5 (N_{NAPH} + N_{TET} + N_{DECS})} \quad (3-28)$$

where, N_{NAPH} , N_{TET} , and N_{DECS} were moles of naphthalene, tetralin and cis, trans-decalins present in the final product, respectively. The A_H value depends on the stoichiometry of the NAPH reaction, and it corresponds to the H_2 moles reacted divided by the maximum H_2 used to convert all the naphthalene to decalins. The hydrogenation activity (A_H) ranged from 0 to 1, as the product varied from the total aromatic to complete saturation (100 % HYD). Equation (3-28), was previously used by Guin et al., (1994) and Joo et al., (1996). A sample calculation is shown in Appendix B.6.

3.7.3.1 Kinetics of The Hydrogenation of NAPH

According to the reaction temperature used in the current study (340 °C), the equilibrium concentration of naphthalene was negligible, (Frye and Weitkamp, 1969). The formation of tetralin may be considered as an irreversible reaction, in the determination of the kinetic rate constant for the NAPH hydrogenation. The pseudo first order kinetic model is shown as follows:



$$-r_{NAPH} = -\frac{dN_{NAPH}}{dt} = k_4 N_{NAPH} \quad (3-30)$$

Integration gives:

$$-\int_{N_0}^{N_t} \frac{dN_{NAPH}}{N_{NAPH}} = k_4 \int_0^t dt \quad (3-31)$$

Therefore,

$$-\ln \left(\frac{N_t}{N_0} \right)_{NAPH} = k_4 t \quad (3-32)$$

Plotting the left side of the equation (3-32) versus the reaction time, t , resulted in a straight line of slope equal to the naphthalene rate constant k_4 . A sample of calculation can be found in Appendix B.7. The availability of H_2 was calculated for NAPH hydrogenation and a sample calculation is shown in Appendix B.8.

3.7.4 Mass Balance

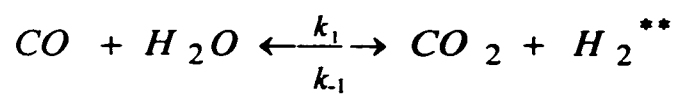
Due to the collection of gas/liquid samples, and flushing between the samples during reaction batch time, a complete mass balance could not be carried out. Appendix D.1 gives the overall mass balance. However, component mol balances for the BTH and NAPH were carried out and worked very well (see Appendix D.2).

Chapter 4

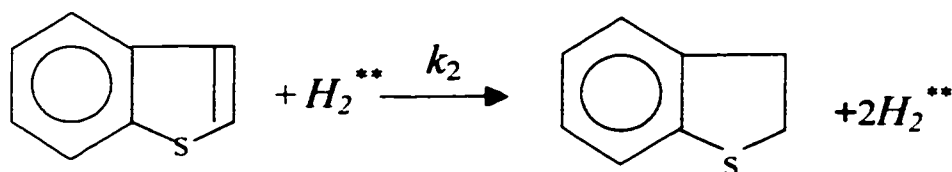
Results and Discussion

Chapter 4 represents details of the results derived from this research study. The effects of different process parameters on the utilization of hydrogen generated in situ from CO and H₂O via the water gas shift reaction for the hydrogenation of naphthalene, benzothiophene and their mixtures were investigated.

The reaction scheme for the mixture of naphthalene and benzothiophene hydrogenation via the H₂ in situ is shown in Figure 4.1.

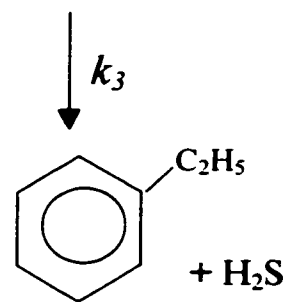


**Active
Hydrogen**

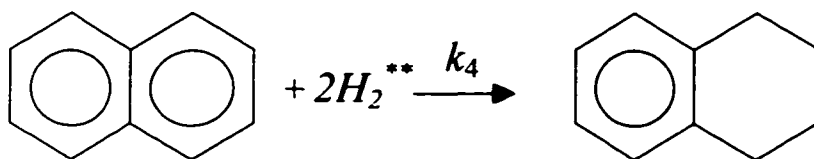


(BTH)

(DHBTH)



(ETHBZ)



(NAPH)

(TET)

Figure 4.1: Reaction scheme for the binary mixture of NAPH and BTH

4.1 WGSR and HDS Reactivities

BTH was selected as the representative model compound for sulfur removal, because it is one of the more refractory sulfur compounds. The WGSR was carried out at 340 °C and 600 psi CO/(2.5% H₂S) initial loading using a PMA catalyst with concentrations of 500 and 1500 ppm Mo. The main products of the WGSR are CO₂, H₂, and a significant appearance of H₂S was detected from the HDS of BTH. A typical gas chromatogram is shown in Figure 4.1.1

The mole % for each component of the gas sample collected during the four hour reaction time is calculated (see Figure 4.1.2, and Appendix B.1). The CO conversion was calculated to be 93.86% in this study as listed in Table 4.1.1. The rate constant was determined to be $4.25 \times 10^{-4} \text{ s}^{-1}$, by using the irreversible pseudo first order plot resulted with an excellent linear relationship and good fit of equation (3-12) of a Pearson correlation, $R^2 = 0.99$ as shown in Figure 4.1.3, (refer to Appendix B.2 for calculations). A comparison of the rate constants at two different metal (Mo) concentrations indicates that the rate constant of CO conversion increases with an increase in the Mo concentration, (see Table 4.1.1). In a previous study in our laboratory, Ng and Rintjema (1992) demonstrated that the rate constant for CO conversion was $1.4 \times 10^{-4} \text{ s}^{-1}$, at 340 °C and 600 psi CO loading with the MA catalyst (equivalent to 6000 ppm Mo metal). The rate constant for the present study is higher; due most likely to the H₂S initial loading (2.5%). It has been reported by Houalla et al. (1978) that a presulfided Co-Mo/ γ -Al₂O₃ catalyst increased the activity of the catalyst.

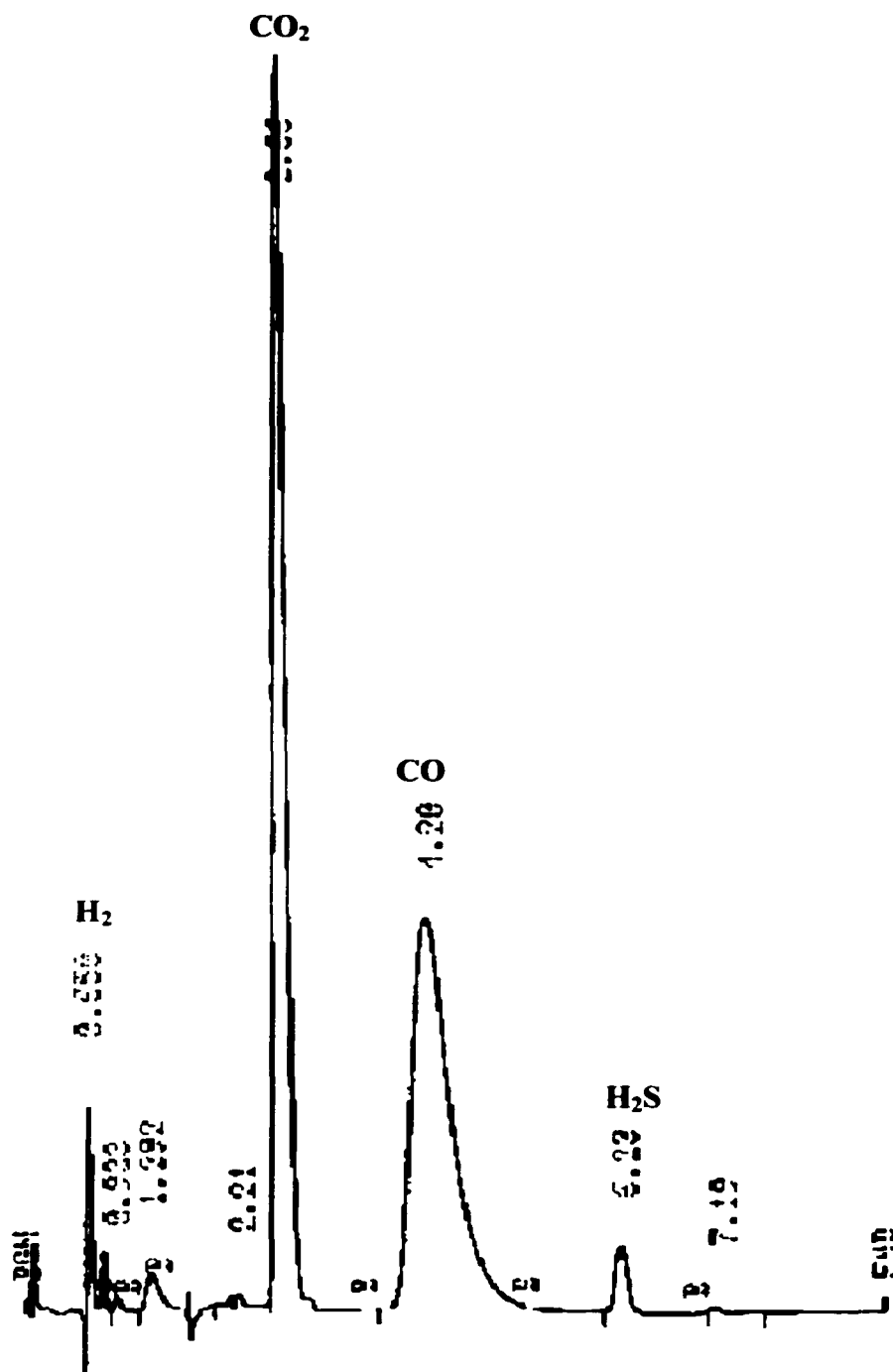


Figure 4.1.1: A typical gas chromatogram at zero reaction time for WGSR, catalyzed by PMA at 340 °C and 600 psi CO/(2.5% H₂S), Run#10

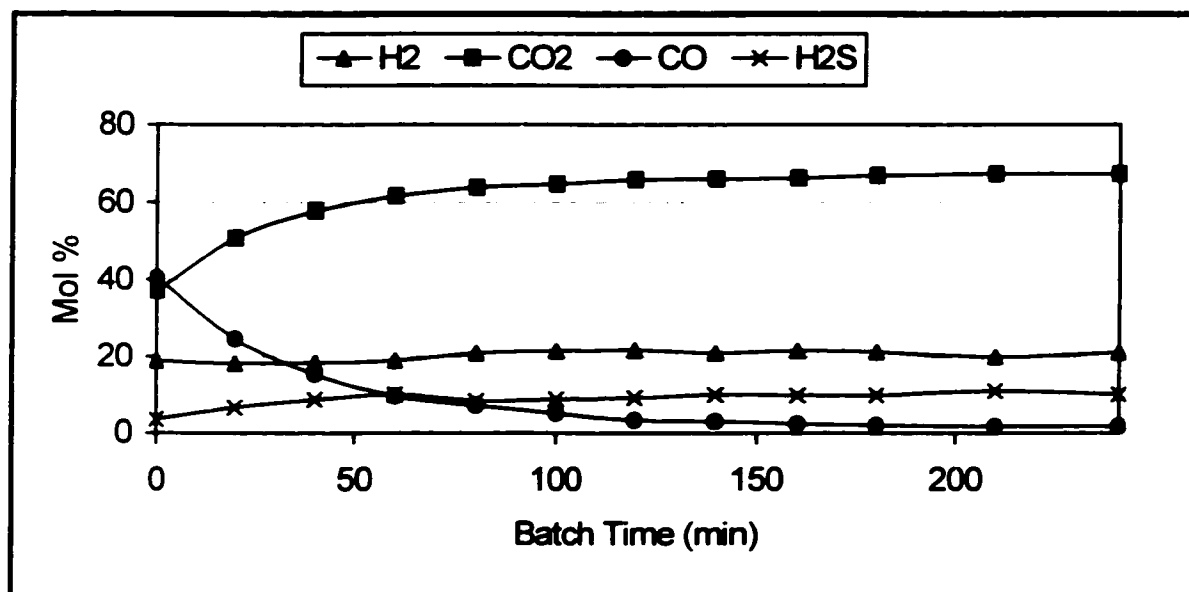


Figure 4.1.2: Mole fraction of the WGS components for the HDS of BTH, catalyzed by PMA at 340 °C and 600 psi CO/(2.5% H₂S), Run # 10

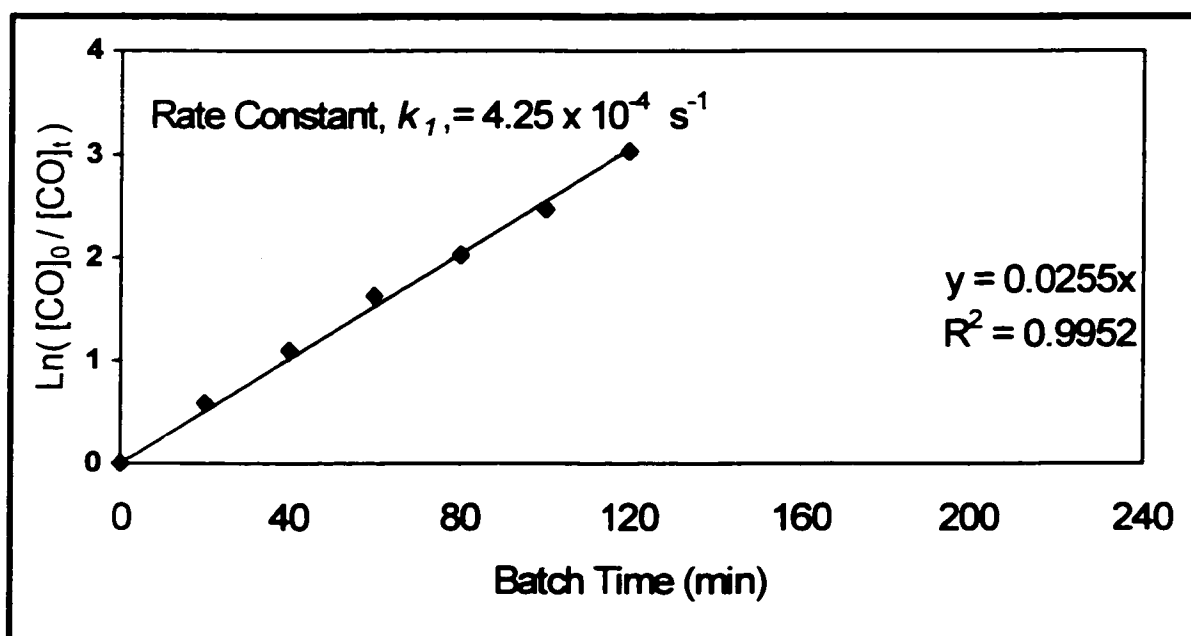


Figure 4.1.3: Pseudo first order plot for the WGS, catalyzed by PMA at 340 °C and 600 psi CO/(2.5% H₂S), Run # 10

Table 4.1.1: Pseudo first order rate constant and CO conversion for the WGSR at different Mo concentrations for BTH desulfurization, medium (CO/H₂S/H₂O)^{*}

Run #	Mo (ppm)	X _{CO} (%)	CO, k_1 (s ⁻¹)	X _{BTH} (%)
6	500	80.96	2.20×10^{-4}	97.72
10	1500	93.86	4.25×10^{-4}	99.27

^{*} 600 psi CO/(2.5%H₂S), at 340 °C, PMA catalyst, 14.1 gm BTH in 200 ml Tol, 70 ml water, stirrer speed 1300 rpm, Reaction time = 4 hrs

As introduced in Section 2.2.1, the HDS reaction of BTH shows that ethylbenzene is the main product and the DHBTH is an intermediate product. Figure 4.1.4 shows a typical chromatogram of the liquid analysis. The mol % of each component are calculated (refer to Appendix B.3) and plotted versus reaction batch time as shown in Figure 4.1.5. The rate constant (k_2) for the HDS of BTH to ETHBZ is determined through a pseudo first order plot, (see Figure 4.1.6 and Appendix B.4). As reported by Lee and Butt (1977) the HDS of BTH is following a first order reaction.

Two different media are compared, and the BTH conversion for H₂ in situ is slightly higher than that obtained using externally supplied H₂, over a reaction carried for 4 hours, where almost complete BTH conversion and sulfur removal are obtained, see Table 4.1.2. The rate constant for in situ H₂ is two times higher than that obtained using externally supplied H₂. Previous work by Rintjema (1992) demonstrated that the CO conversion for WGSR at the same reaction conditions in the absence of BTH was 80%. However, in the current study, the CO conversion in the presence of BTH is 93.86 %.

This suggests that the initial loading of H₂S and the presence of BTH cause a shift to the right of the WGSR because of H₂ consumption for the HDS. These results seem to agree with Stenberg et al. (1982), who found that the H₂S could also promote the WGSR since H₂S catalyzes the reaction.

In addition, Gissy et al. (1980) reported that presulfiding with a H₂S/H₂ mixture was the best technique for activating a CoO-MoO₃/γ-Al₂O₃ catalyst for the HDS reactions. Further, Kumar et al. (1984) reported that presulfiding the commercial catalyst NiO-MoO₃/γ-Al₂O₃ for the HDS of BTH via the WGSR, was found to be very effective for desulfurization of BTH under 68 atm over a temperature range of 310-370 °C. Kumar found that the rate constant for the HDS of BTH at an average temperature of 350 °C to be $1.42 \times 10^{-5} \text{ s}^{-1}$. A comparison of Kumar's results to the present study supports that hydrogen in situ using a dispersed catalyst is as active as the commercial supported catalyst. Nag et al. (1979) studied the desulfurization of BTH using a Co-Mo/ Al₂O₃ catalyst at lower temperature of 300 °C and 71 atm, they found that the rate constant of BTH was $8.11 \times 10^{-4} \text{ s}^{-1}$. Although there is a difference in reaction temperatures, compared to the value found in present research work, which is $10.78 \times 10^{-4} \text{ s}^{-1}$, it seems that the HDS of BTH via the WGSR using dispersed Mo catalyst is as efficient as the externally supplied hydrogen with a commercial catalyst.

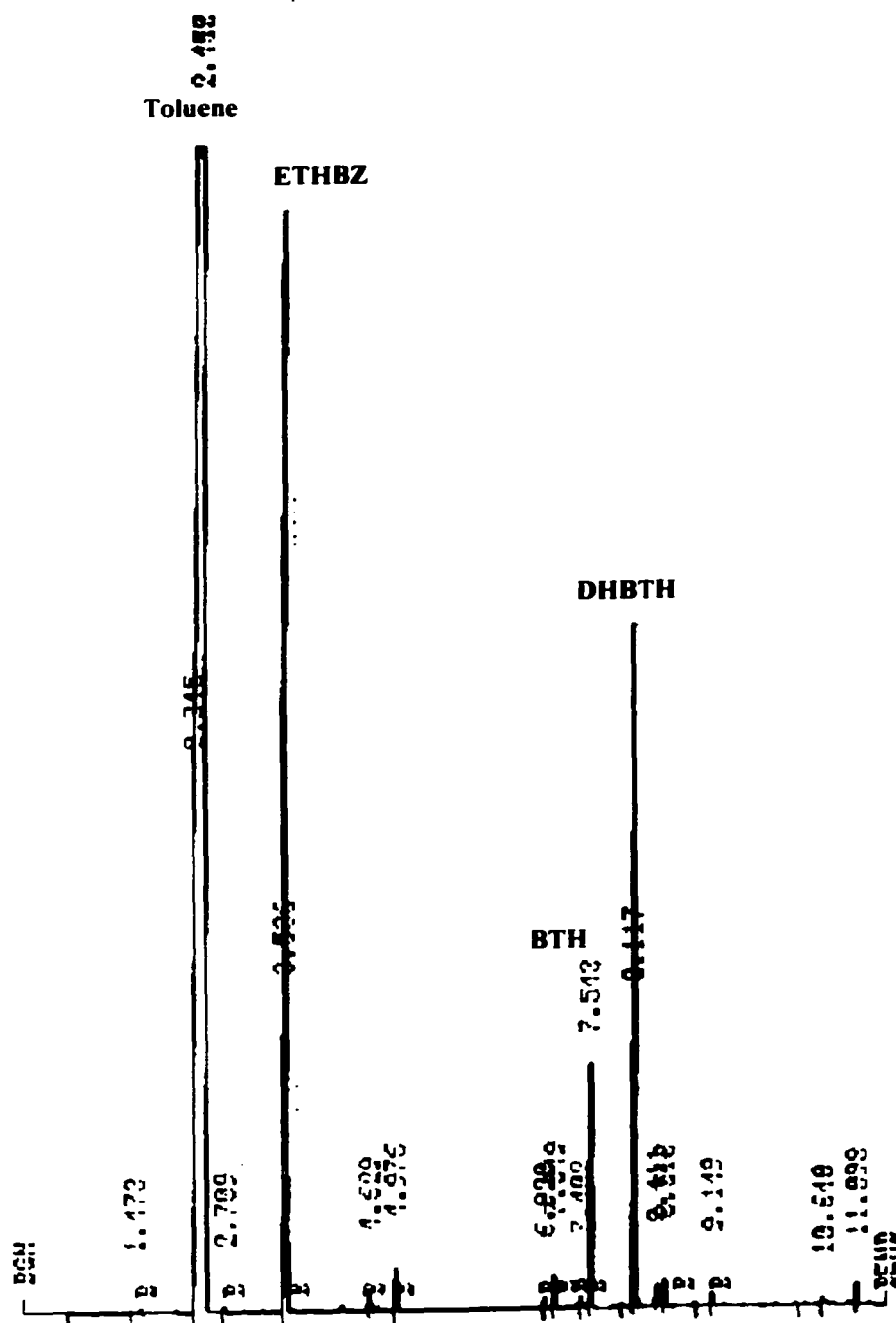


Figure 4.1.4: A typical liquid chromatogram for the HDS of BTH, catalyzed by PMA at 340 °C and 600 psi CO/(2.5% H₂S), Run#10

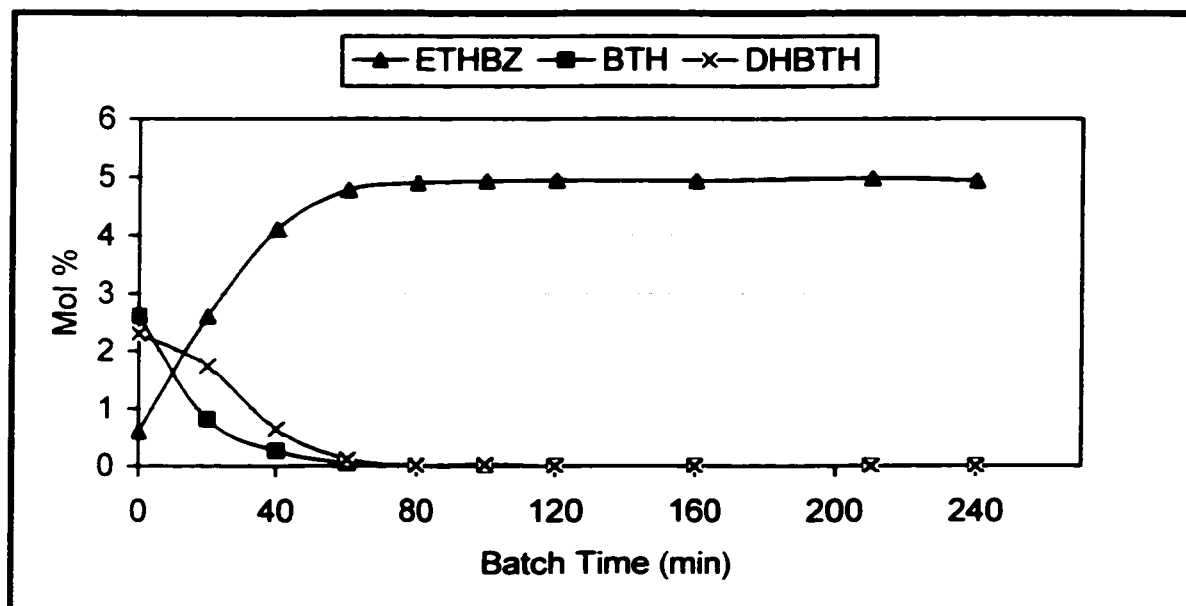


Figure 4.1.5: Mole % of the BTH reaction network, catalyzed by PMA at 340 °C and 600 psi CO/(2.5% H₂S), Run # 10

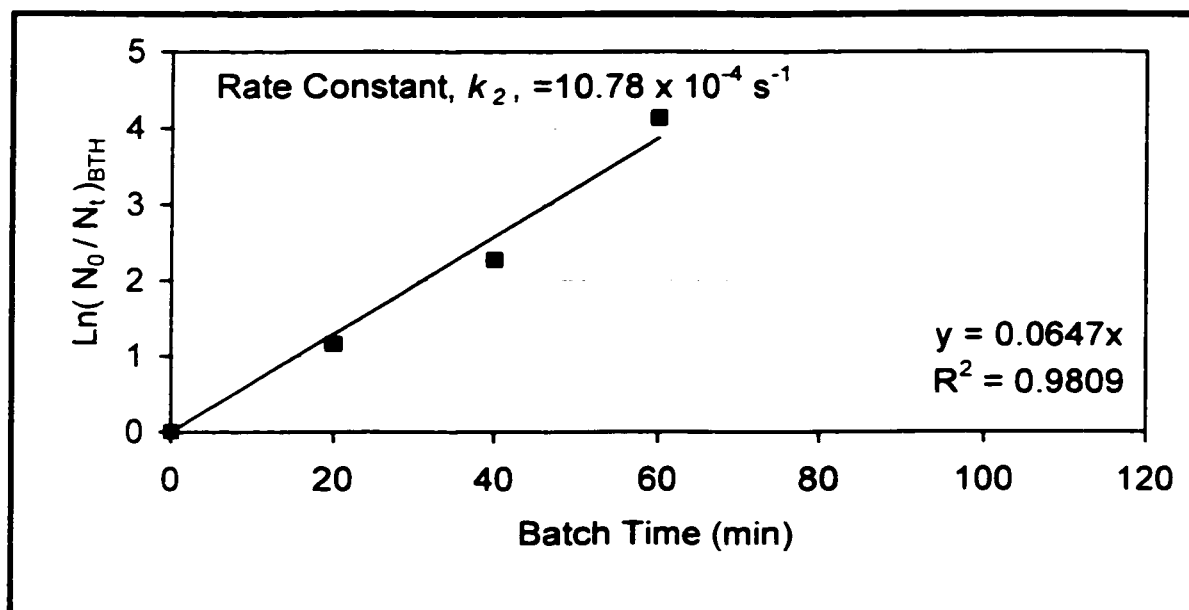


Figure 4.1.6: Pseudo first order plot for BTH conversion, catalyzed by PMA at 340 °C and 600 psi CO/(2.5% H₂S), Run#10

Table 4.1.2: Pseudo first order rate constant and conversion for HDS of BTH in different medium.

Run #	Medium	BTH, k_2 , (s^{-1})	X_{BTH} (%)	S rem [*] (%)
10	CO/H ₂ S/H ₂ O ¹	10.78×10^{-4}	99.27	99.16
15	H ₂ /H ₂ S/H ₂ O ²	6.00×10^{-4}	98.86	96.87

¹ 600 psi CO/(2.5%H₂S), at 340 °C, 1500 ppm Mo of PMA catalyst 14.1 gm BTH in 200 ml Tol, 70 ml water, stirrer speed 1300 rpm

² 600 psi H₂/(2.5%H₂S), at 340 °C, 1500 ppm Mo of PMA catalyst, 14.1 gm BTH in 200 ml Tol, 70 ml water, stirrer speed 1300 rpm.

Reaction time= 4hrs

*S rem= Sulfur removal

The experimental data for Run # 10 shows that the H₂ generated in the system is 1091 mmol of H₂. According to the stoichiometry and the amount of BTH in the reaction mixture, 315.2 mmol of H₂ is needed to achieve 100 % desulfurization of BTH and for BTH to be completely converted to ETHBZ. Therefore, an excess of 776 mmol of H₂ is available theoretically. Experimentally, the gas product GC-analysis shows that only 233.29 mmol of H₂ are available after the reaction is completed. Apparently, this indicates that a loss of H₂ occurred because of the gas/liquid sampling during the reaction. In addition, this discrepancy may also be partly a result of the solubility of H₂ in the liquid phase (refer to Appendix B.5 for calculations).

4.2 WGSR and AHYD Reactivities without BTH

Naphthalene was selected as a model compound for the aromatic hydrogenation (AHYD). The hydrogenation reaction was carried out via the WGSR at two different Mo concentrations of PMA catalyst at 340 °C and 600 psi CO/(2.5% H₂S) initial loading, as listed in Table 4.2.1. In addition, the WGSR produced CO₂, H₂ and a small amount of H₂S, as shown in Figure 4.2.1. The irreversible pseudo first order rate constant for CO conversion is determined (see Figure 4.2.2). By increasing the Mo concentration, the CO conversion and the rate constant are increased.

Table 4.2.1: Pseudo first order rate constant and CO conversion for the WGSR at different Mo concentrations for NAPH hydrogenation, medium (CO/H₂S/H₂O)^o

Run #	Mo (ppm)	X _{CO} (%)	CO, k_f (s ⁻¹)	X _{NAPH} (%)
7	500	84.21	1.60×10^{-4} (2.21×10^{-4}) ¹	28.76
8	1500	91.73	3.03×10^{-4} (3.60×10^{-4}) ¹	66.42

^o600 psi CO/(2.5 % H₂S), at 340 °C, PMA catalyst, 43.25 gm NAPH in 200 ml Tol, 70 ml water, stirrer 1300 rpm, 4 hrs reaction time
¹ k_f value calculated from a reversible first order kinetics, refer to Rintjema (1992), for data and figure refer to Appendix F

The observed pseudo first order rate constant for CO conversion in the presence of NAPH is 1.4 times slower than in the presence of BTH. This is possibly due to the faster BTH hydrogenation compared with NAPH hydrogenation and the lower sulfur content in the reaction medium. If the value of k_f is calculated according to a reversible first order reaction, (Frost and Pearson, 1963), the k_f value is $3.6 \times 10^{-4} \text{ s}^{-1}$ at 1500 ppm Mo, which is 1.18 times slower.

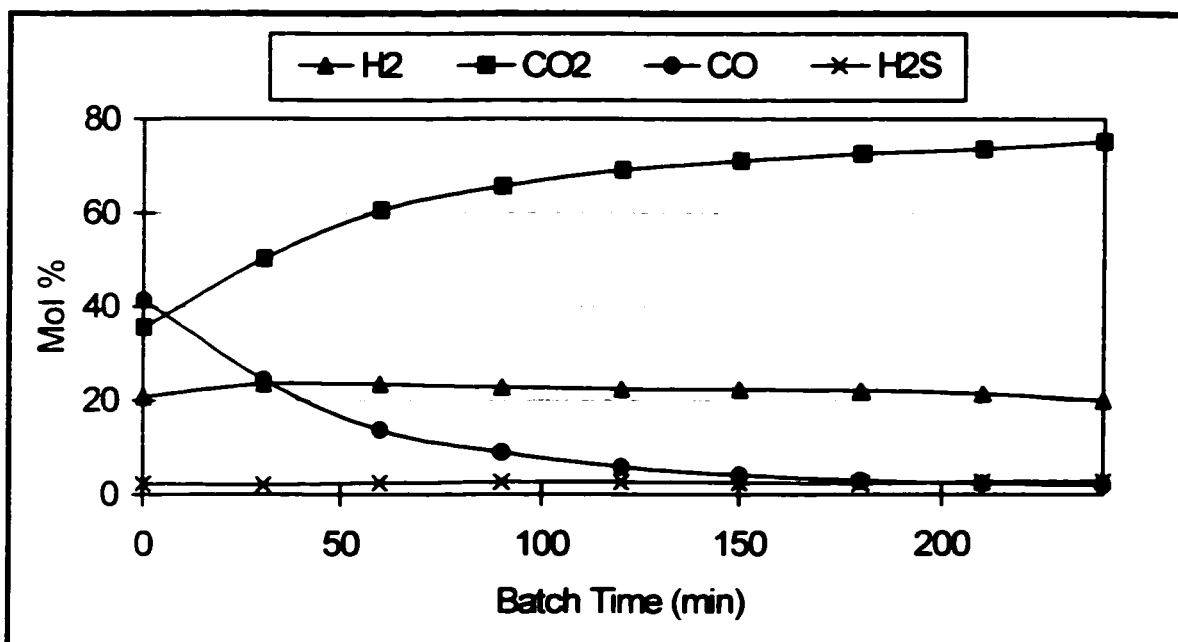


Figure 4.2.1: Mole fraction of the WGSR components for NAPH hydrogenation, catalyzed by PMA at 340 °C and 600 psi CO/(2.5% H₂S), Run # 8

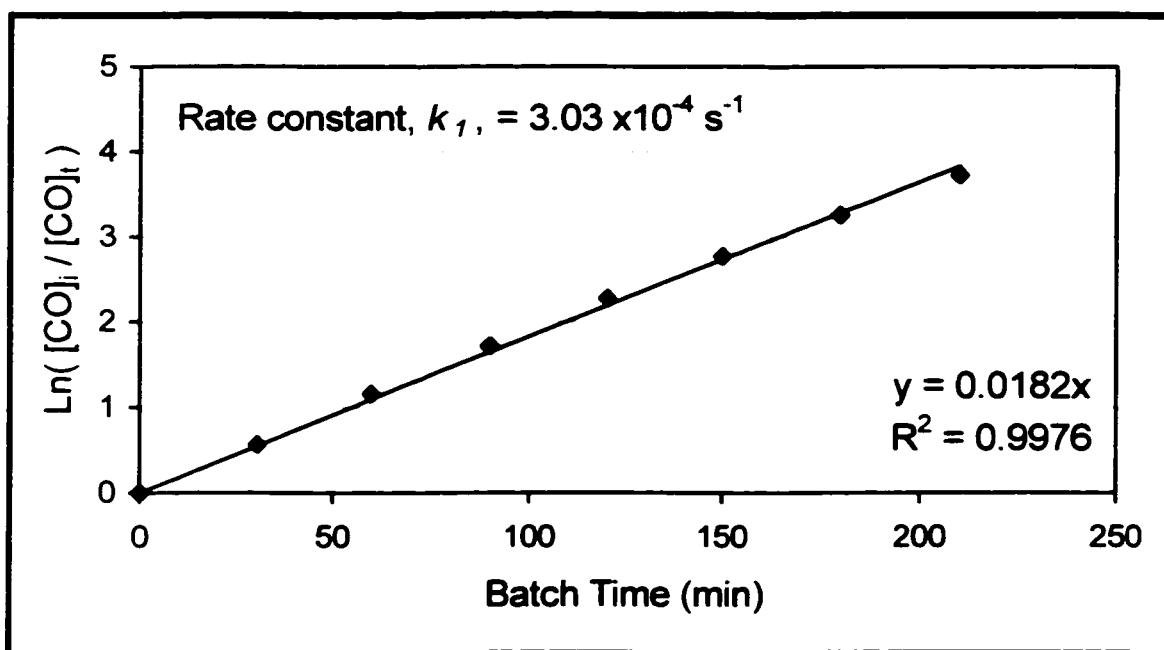


Figure 4.2.2: Pseudo first order plot for WGSR, catalyzed by PMA at 340 °C and 600 psi CO/(2.5% H₂S), Run # 8

These results suggest that the presence of BTH itself and/or the H_2S generated from the HDS of BTH, may also promote the formation of the active molybdenum sulfide and resulting in a faster rate for the WGSR. The CO and NAPH conversions increased at a higher Mo concentration because more active catalytic species of the PMA catalyst are available.

Naphthalene is being hydrogenated by utilizing the H_2 in situ generated from the WGSR, and tetralin (TET) is found in large quantities as a main product, (refer to Figure 4.1). Decalins are present in small amounts. This result is consistent with that reported in literature by Bordwell (1963), and Brewster (1953), that hydrogenation of NAPH to tetralin was relatively easy and further hydrogenation to decalin was much more difficult.

Figure 4.2.3 shows the chromatogram of one of the liquid samples that is analyzed on the GC. Since trans and cis decalins are present in very low concentrations: the tetralin formation reaction is considered as the major pathway for the NAPH hydrogenation reaction. Toluene was used as a dissolving reagent and it is observed that the hydrogenation of toluene is not occurring at $340^\circ C$, hence the mole fraction remains almost constant during the four hours reaction time. A sample of liquid analysis is shown in Table 4.2.2. Figure 4.2.4 represents a plot of the mole fraction % of each component versus the reaction time and a naphthalene conversion to tetralin of 66.42 % was obtained (see Appendix B.6), using PMA catalyst of 1500 ppm Mo after a reaction time of four hours. The pseudo first order rate constant for the hydrogenation of NAPH is determined from the slope of a good straight line as shown in Figure 4.2.5, (refer to Appendix B.7).

Table 4.2.2: Mole fraction % of naphthalene reaction network for Run # 8*

Batch time (min)	Toluene	trans-DEC	cis-DEC	TET	NAPH
0	80.235	0.000	0.000	0.024	19.527
30	83.507	0.000	0.000	1.303	15.190
60	83.506	0.000	0.000	2.518	13.976
90	84.499	0.000	0.000	3.809	11.691
120	84.992	0.025	0.000	4.995	9.987
150	84.434	0.000	0.000	6.369	9.196
180	85.393	0.024	0.082	6.908	7.592
210	85.434	0.021	0.000	7.707	6.837
240	85.745	0.054	0.028	8.145	6.027

* 600 psi CO/(2.5% H_2S), at 340 °C, 1500 ppm Mo of PMA catalyst, 43.25 gm NAPH in 200 ml Toluene, 70ml H_2O , stirrer 1300 rpm, Reaction time = 4 hrs.

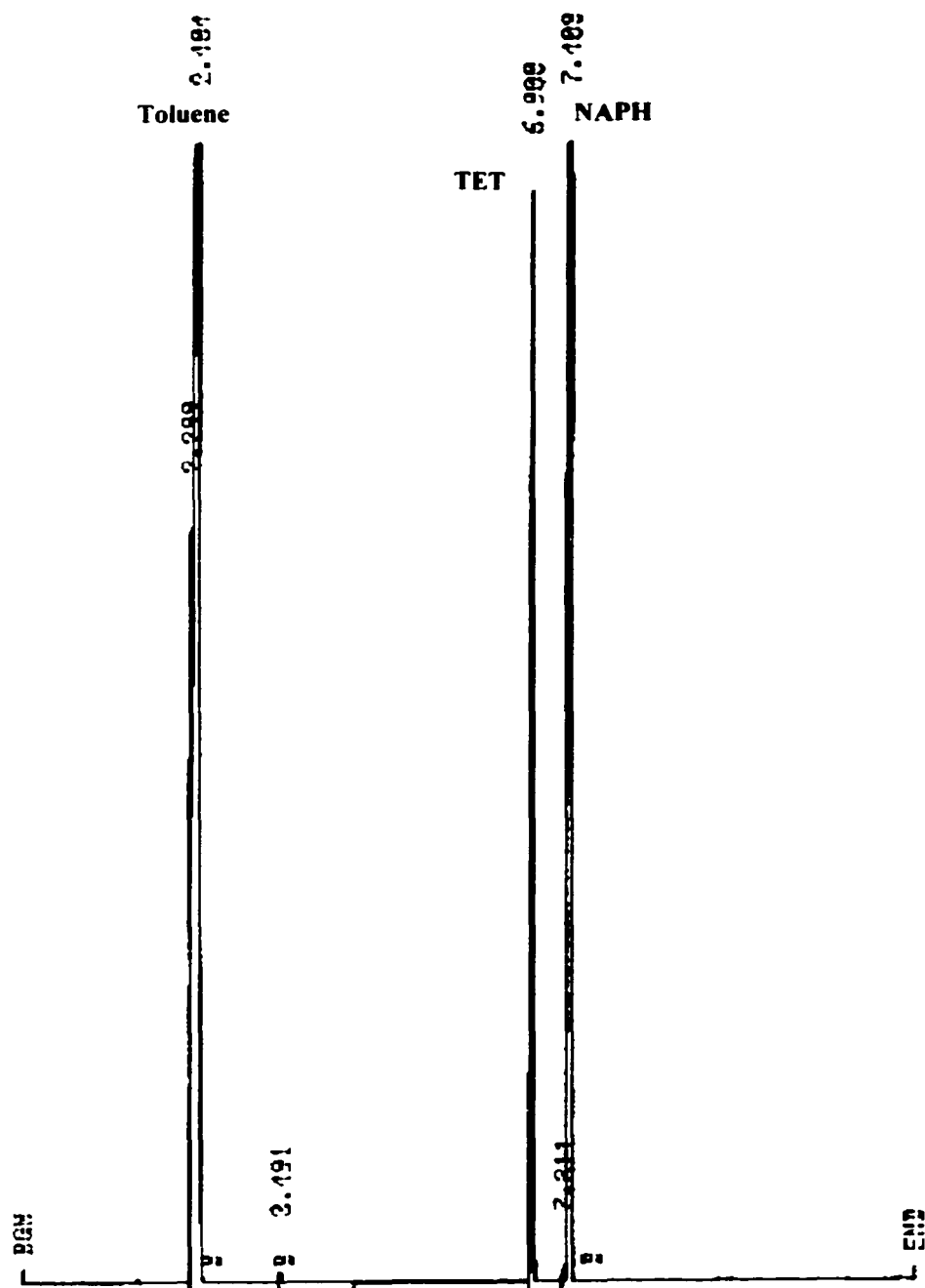


Figure 4.2.3: A typical liquid chromatogram for the HYD of NAPH, catalyzed by PMA at 340 °C and 600 psi CO/(2.5% H₂S), Run#8

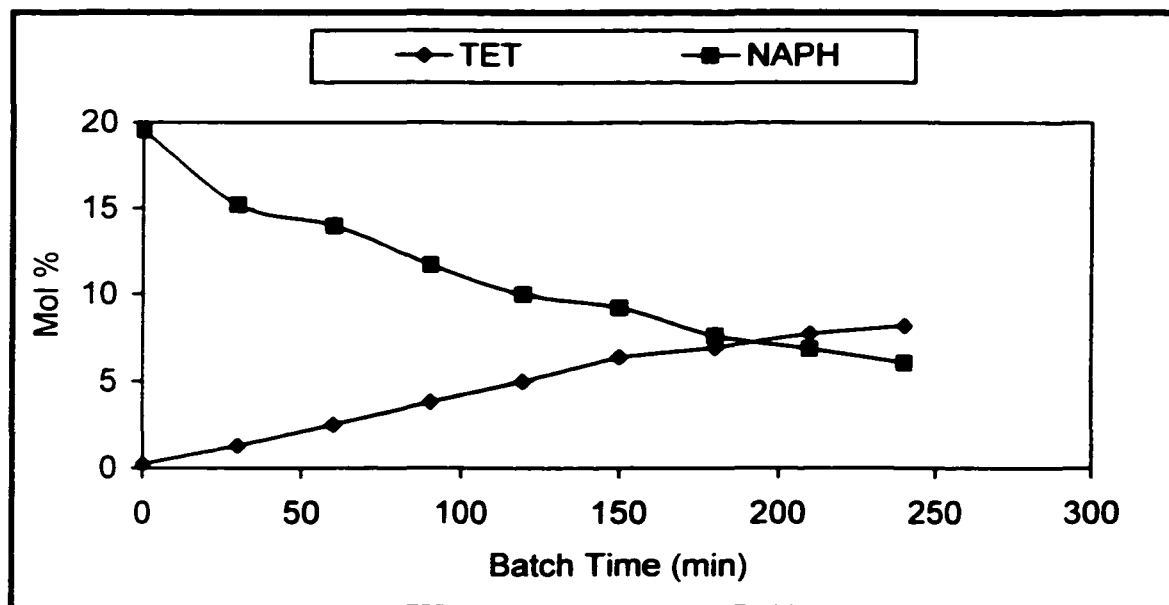


Figure 4.2.4: Mole fraction % of NAPH reaction network, catalyzed by PMA at 340 °C and 600 psi CO/(2.5% H₂S), Run#8

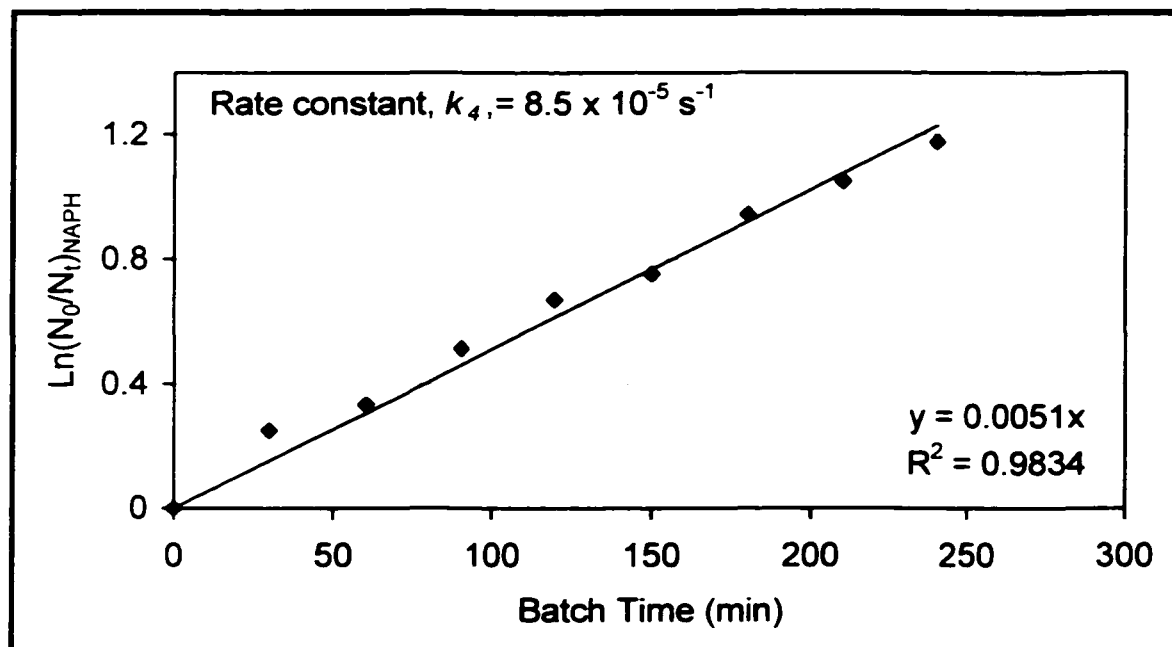


Figure 4.2.5: Pseudo first order constant for NAPH hydrogenation, catalyzed by PMA at 340 °C and 600 psi CO/(2.5% H₂S), Run#8

The rate constant for the in situ hydrogenation of NAPH is compared with the externally supplied H₂ under the same operating conditions (see Figure 4.2.6 and Figure 4.2.7). Based on these results, the rate constant for the hydrogenation of NAPH to TET, k_4 , using H₂ in situ is approximately two times faster than that for the externally supplied hydrogen (see Table 4.2.3). These findings are compared to Sapre and Gates (1981), where, they found the rate constant of NAPH hydrogenation to be 5.78×10^{-5} L/g of catalyst•s, when a sulfided commercial CoO-MoO₃/Al₂O₃ catalyst at 325°C and 75 atm was used. In addition, Yumoto et al. (1996) studied the NAPH hydrogenation over the commercial catalyst Ni-Mo/Al₂O₃ in a batch reactor at 350 °C, and concluded that the pseudo first order rate constant for NAPH was 6.9×10^{-5} L/g of catalyst•s. Therefore, it appears that the in situ hydrogen in our system is slightly more effective than the externally supplied hydrogen, and the in situ hydrogenation of NAPH using a dispersed catalyst shows slightly higher activity compared with the commercial catalyst.

Table 4.2.3: Pseudo first order rate constant and conversion of NAPH hydrogenation in different medium

Run #	Medium	NAPH, k_4 (s ⁻¹)	X _{NAPH} (%)	TET yield (%)	A rem* (%)
8	CO/H ₂ S/H ₂ O ¹	8.50×10^{-5}	66.42	57.02	63.28
14	H ₂ /H ₂ S/H ₂ O ²	4.67×10^{-5}	52.96	36.00	43.36

¹ 600 psi CO/(2 5%H₂S), at 340 °C, 1500 ppm Mo of PMA catalyst, 43.25 gm NAPH, 200 ml Tol, 70 ml water, stirrer speed 1300 rpm

² 600 psi H₂/(2 5%H₂S), at 340 °C, 1500 ppm Mo of PMA catalyst, 43.25 gm NAPH, 200 ml Tol, 70 ml water, stirrer speed 1300 rpm

Reaction time= 4 hrs

*A rem = Aromatic removal

The availability of in situ H_2 to complete a 100 % NAPH conversion is calculated (refer to Appendix B.8). To hydrogenate the first ring and produce tetralin, 675 mmol of H_2 are needed to hydrogenate the 337.44 mmol of NAPH in the feed. The H_2 in situ generated in the system according to the calculation for Run # 8 is 1067.3 mmol of H_2 . Theoretically, 392.4 mmol of H_2 is present in excess, whereas, from the GC analysis, only 257.94 mmol of H_2 is found in the gas product, based on the analysis of gas phase during reaction. In spite of the H_2 losses, the H_2 in situ is available in excess during the course of the reaction.

The naphthalene hydrogenation was considered as an irreversible reaction at 340 °C. This was confirmed by running an experiment using tetralin as the reactant feed in the presence of PMA (1500 ppm Mo) under the same operating conditions, at temperature of 340°C and pressure of 600psi CO/(2.5% H_2S)/(70 ml H_2O) for four hours reaction time. Results shows that only 4.80 % of tetralin is hydrogenated to decalins, and the reverse dehydrogenation to naphthalene is not detected at this temperature (340 °C), as shown in Figure 4.2.8. This result is in agreement with that of Dutta and Schobert (1996) who found that the dehydrogenation of tetralin to naphthalene occurs only at temperatures greater than 450 °C. In addition, data derived by Hooper et al. (1979) showed that formation of naphthalene from tetralin occurred only at temperatures greater than 435 °C.

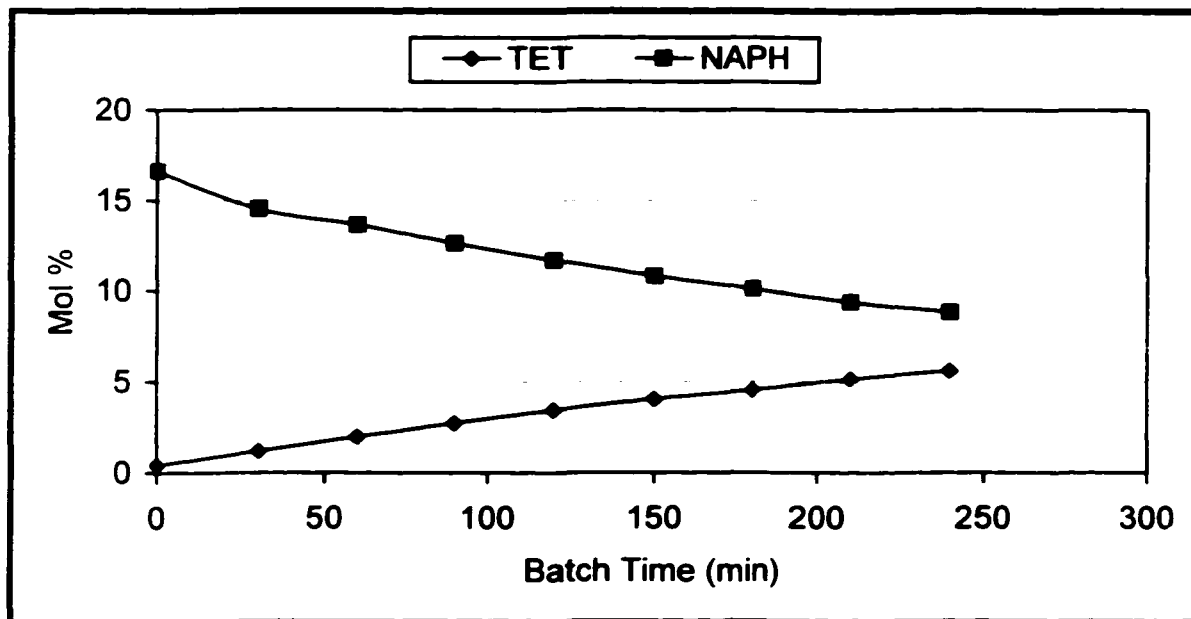


Figure 4.2.6: Mole fraction % for NAPH reaction network, catalyzed by PMA at 340 °C and 600 psi H₂/(2.5% H₂S), Run#14

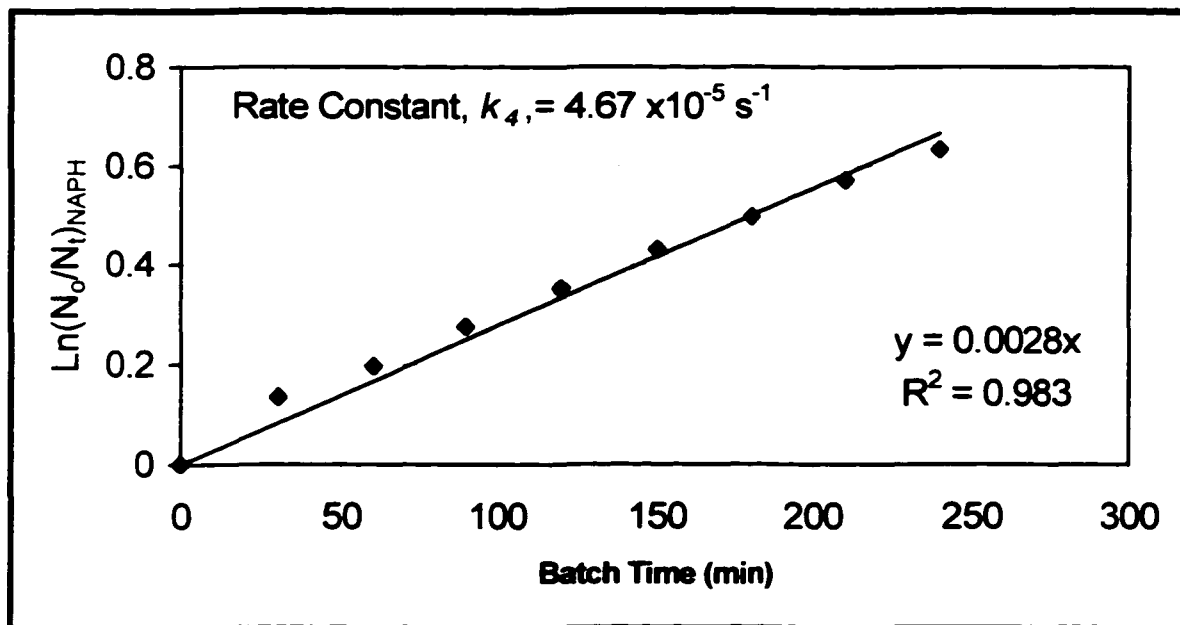


Figure 4.2.7: Pseudo first order constant for NAPH conversion, catalyzed by PMA at 340 °C and 600 psi H₂/(2.5% H₂S), Run#14

The concentration of the reactant and the product at equilibrium is not measured in the present work; therefore, the equilibrium constant K_p could not be determined. Gully and Balard (1963), reported that the hydrogen pressure has a strong effect on the equilibrium aromatic concentration for the reaction of naphthalene to tetralin, and as the pressure increased the equilibrium concentration of NAPH decreased.

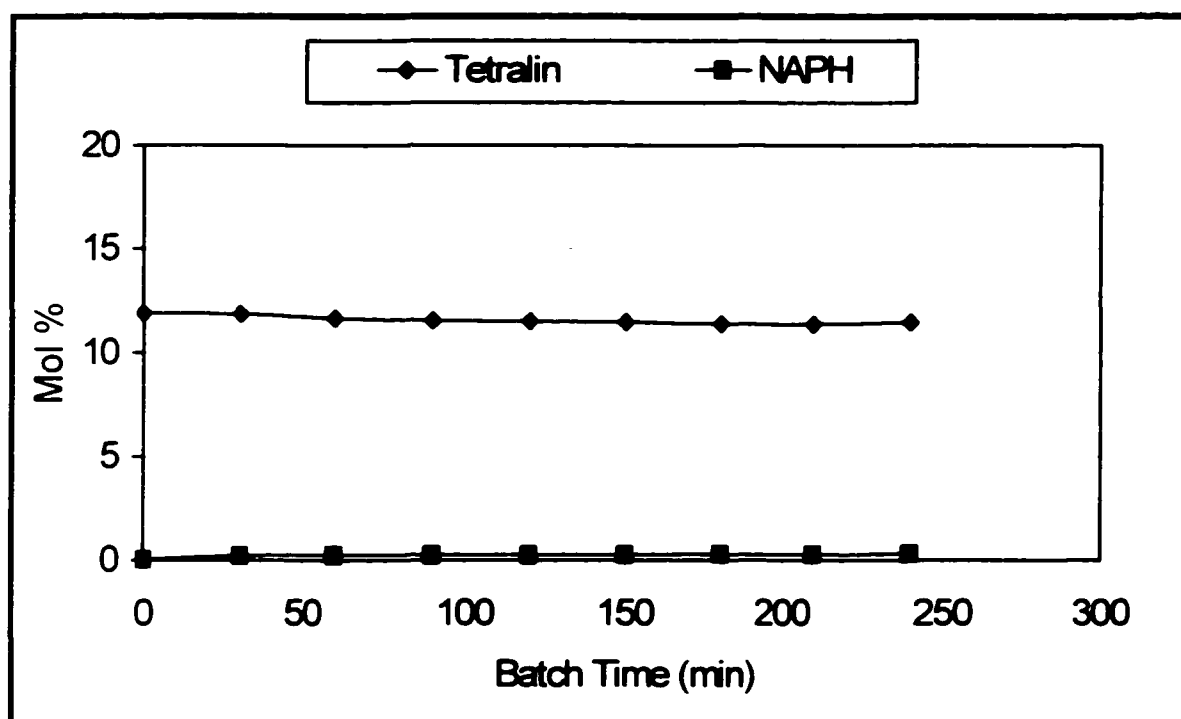


Figure 4.2.8: Mole fraction % for tetralin dehydrogenation catalyzed by PMA at 340 °C and 600 psi CO/(2.5% H₂S), Run#19

4.3 Hydrogenation of Binary Mixture via the WGSR

The hydrogenation of a binary mixture of BTH and NAPH is investigated to observe their reactivities via the WGSR, and any possible inhibition on the hydrogenation of NAPH due to the presence of sulfur. Results are limited to comparisons of either the rate constants or the reactant conversions for both the organosulfur (BTH) and aromatic hydrocarbons (NAPH). The reaction was carried out at 340 °C and 600 psi CO/H₂S/H₂O with a PMA catalyst concentration of 1500 ppm Mo. The mole fraction (%) of each component of the WGSR is presented in Figure 4.3.1 and the pseudo first order plot for CO conversion is shown in Figure 4.3.2. The CO rate constant for the binary mixture (BTH+NAPH) is ~ 1.5 times higher than using only the NAPH and 1.15 times higher than using only BTH, as summarized in Table 4.3.1. The difference in rate constant most likely is due to the presence of sulfur content in the reaction system, (see Appendix C.1 for calculations).

H₂S is known as a good promoter for the WGSR because it catalyzed the formation of MoS₂ from the catalyst precursor and increases the density of the Brønsted acid sites (Yoshida et al., 1979). Eventually, both hydrogen sulfide and hydrogen are required to maintain the catalysts in the form of sulfides rather than oxides (Broderick et al., 1982). Similarly, Hou et al. (1983) noticed that metal sulfides were more active than metal oxides using Mo/Al₂O₃. When the catalyst is exposed to H₂S prior to the reaction, the rapid uptake of sulfur formed an efficient active species of MoS₂, which increases the reactivity of the WGSR and the conversion of reactants significantly.

Table 4.3.1: Pseudo first order rate constant and CO conversion for the WGSR for different model compounds*

Run #	Model compound	CO, k_1 (s^{-1})	X_{CO} (%)
10	BTH	4.25×10^{-4}	93.86
8	NAPH	3.03×10^{-4} (3.6×10^{-4}) ¹	91.73
23	BTH+NAPH	4.88×10^{-4}	94.50

*600 psi CO/(2.5%)H₂S at 340 oC, 1500 ppm Mo of PMA catalyst, 14.1 gm BTH, 43.25gm NAPH, 200 ml Tol, 70 ml H₂O, stirrer speed 1300 rpm. Reaction time= 4hrs.

¹ k_1 value calculated from a reversible first order kinetics, refer to Rintjema (1992), for data and figure refer to Appendix F

The liquid samples are collected during the reaction of the binary mixtures (BTH+NAPH). The data analysis based on results of GC analysis is shown in Appendix C.2. A typical chromatogram for the binary mixture sample is presented in Figure 4.3.3. The mole fractions of products are normalized based only on the total liquid products but without gaseous products and solid deposits. This enables the calculation of the composition of each species. Figure 4.3.4 shows the mole fraction of each component versus the changes in the reaction batch time. The pseudo first order rate constants and conversions for both NAPH and BTH with their conversions are listed in Table 4.3.2, and shown in Figure 4.3.5 and Figure 4.3.6. It is interesting to note that in Figure 4.3.4 there appears to be a strong initial inhibition of NAPH hydrogenation due to the presence of BTH and essentially NAPH hydrogenation starts after almost complete sulfur removal. The inhibition effect of the naphthalene hydrogenation by dibenzothiophene has been reported by Lo (1981).

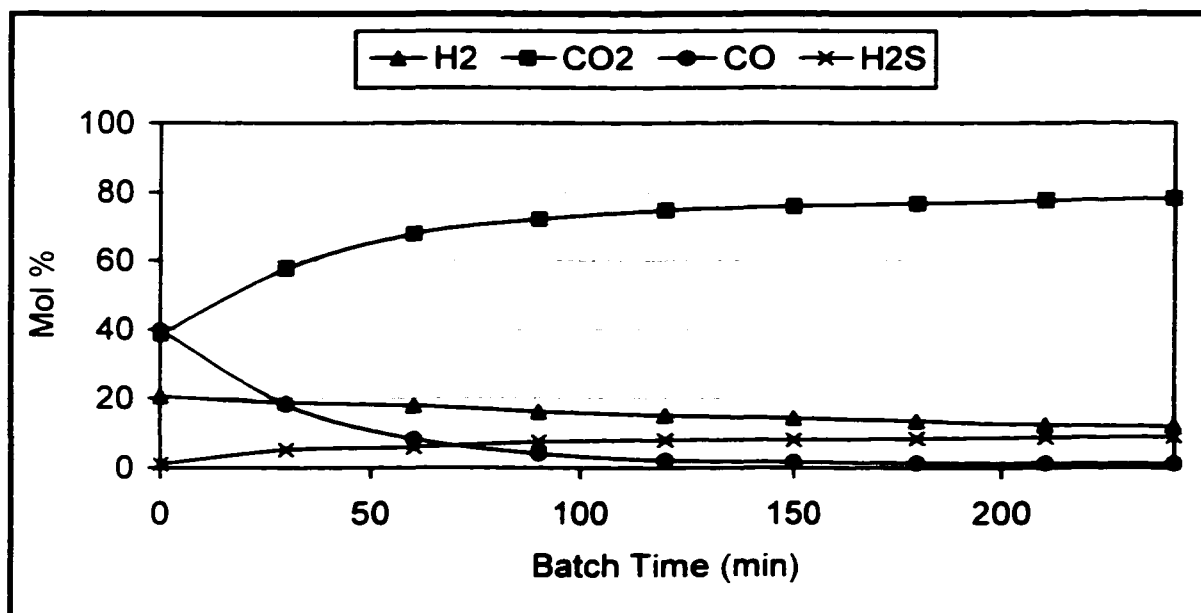


Figure 4.3.1: Mole fraction % of the WGSR components for the HYD of (BTH+NAPH). catalyzed by PMA at 340 °C and 600 psi H₂/(2.5% H₂S), Run#23

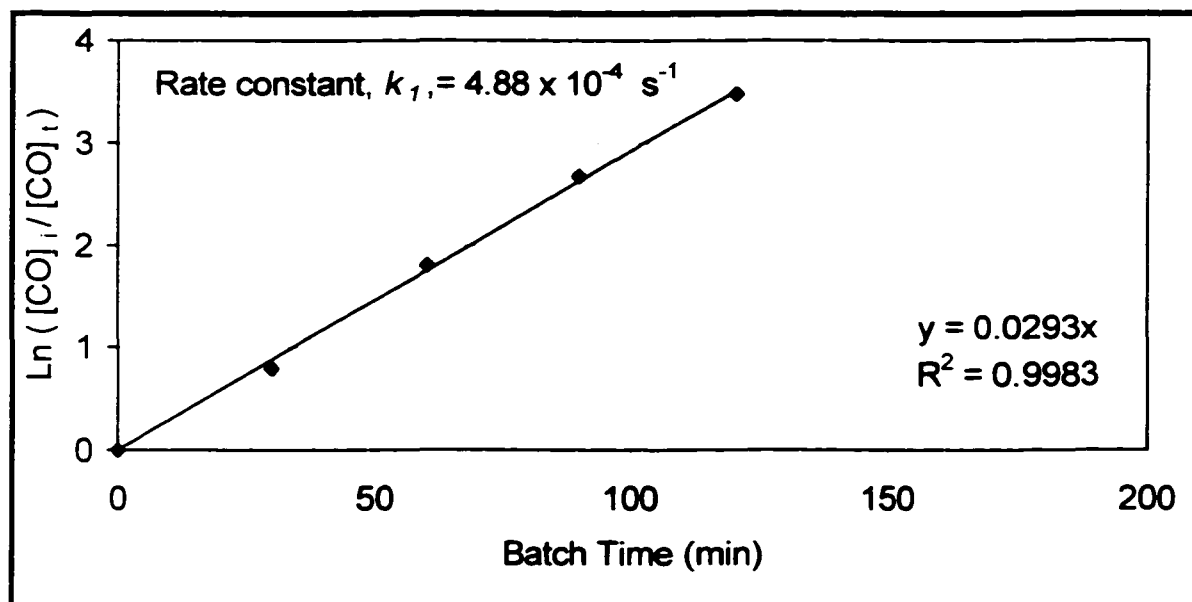


Figure 4.3.2: Pseudo first order plot for WGSR in the binary mixture, catalyzed by PMA at 340 °C and 600 psi H₂/(2.5% H₂S), Run#23

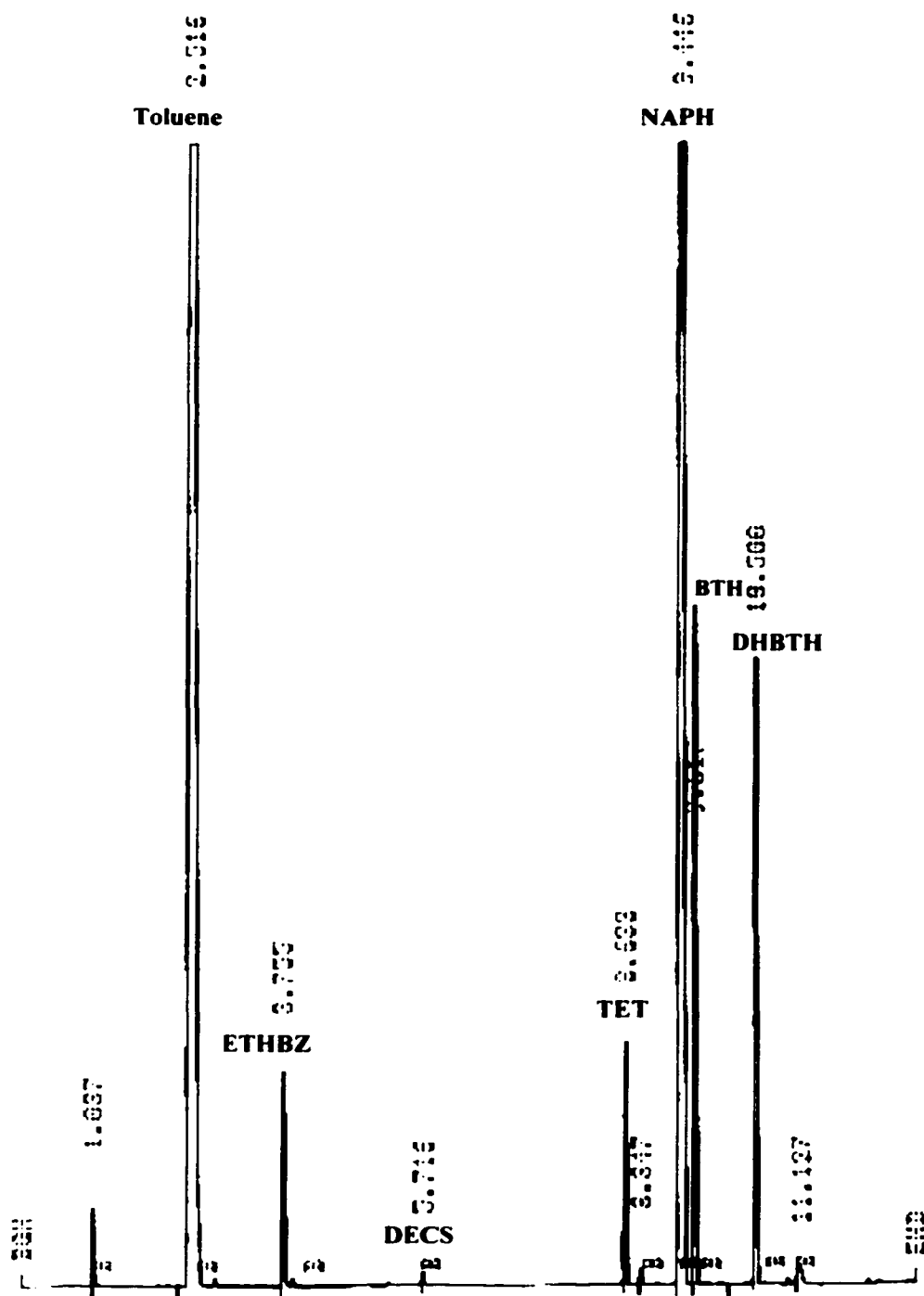


Figure 4.3.3: A typical liquid chromatogram for the HYD of (BTH+NAPH), catalyzed by PMA at 340 °C and 600 psi H₂/(2.5% H₂S), Run # 23

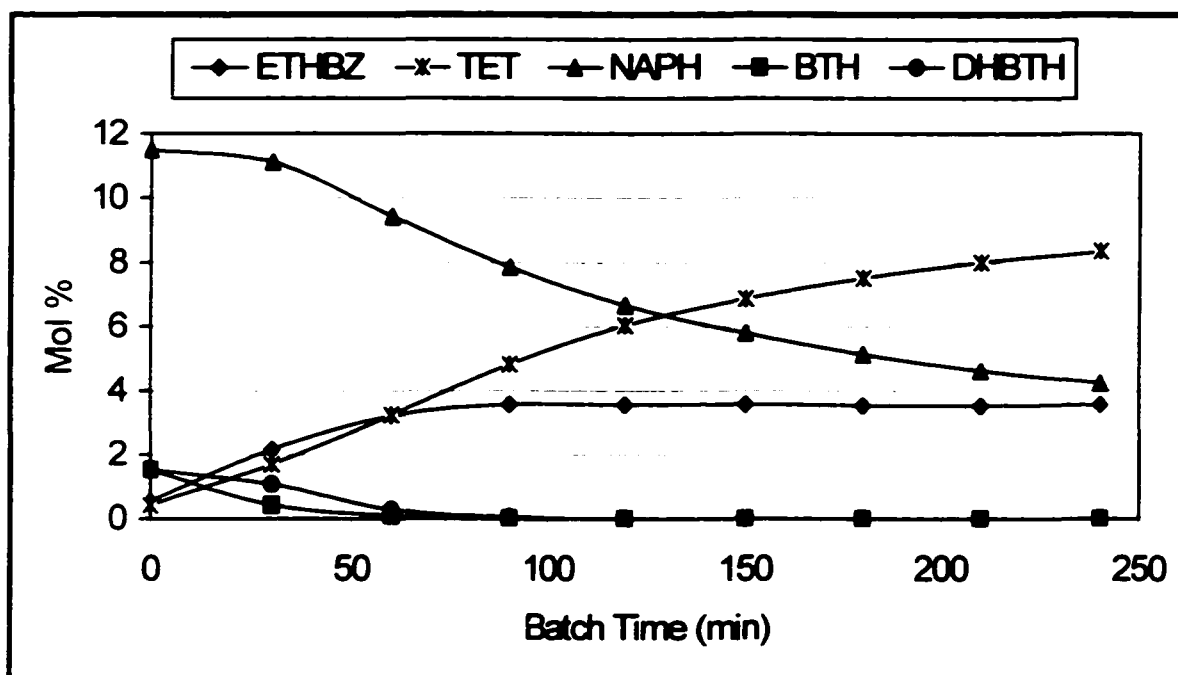


Figure 4.3.4: Mole fraction for the BTH and NAPH reaction network, catalyzed by PMA at 340 °C and 600 psi H₂/(2.5% H₂S), Run#23

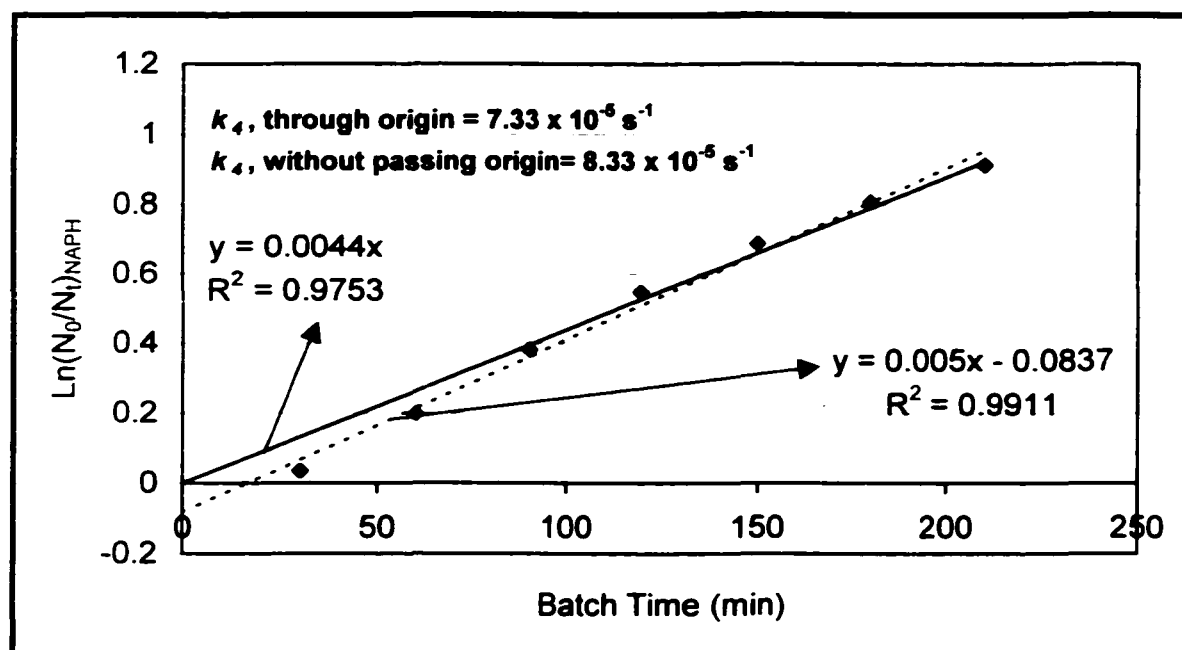


Figure 4.3.5: Pseudo first order plot for NAPH conversion in the binary mixture, catalyzed by PMA at 340 °C and 600 psi H₂/(2.5% H₂S), Run#23

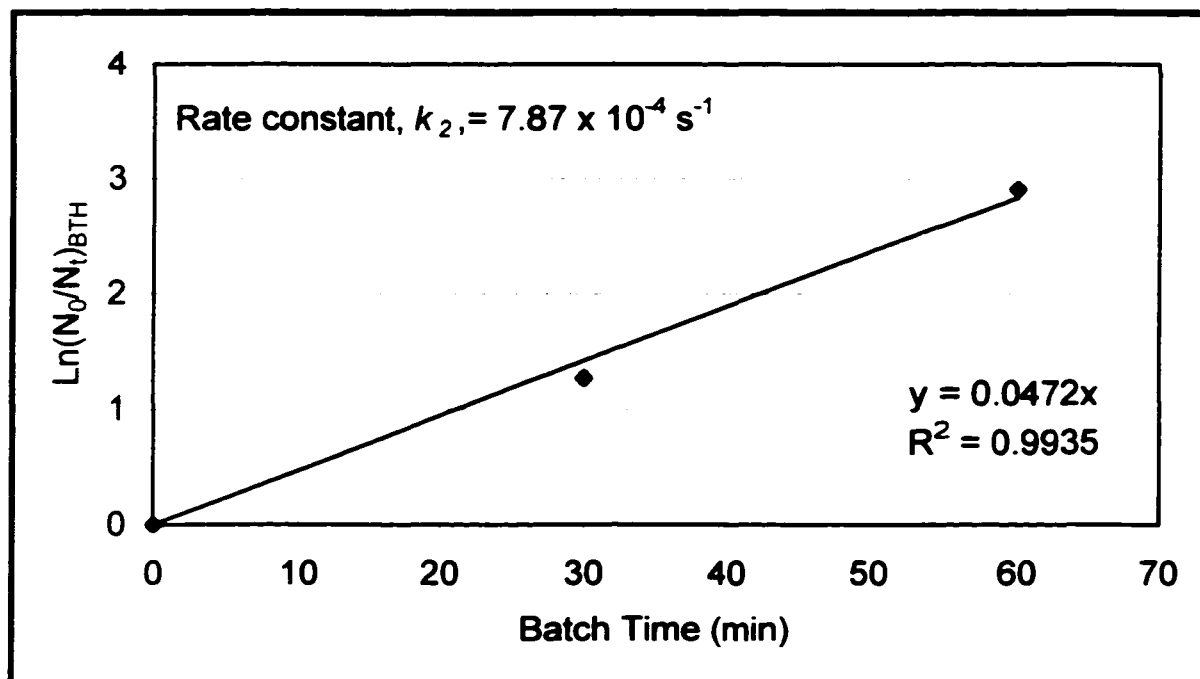


Figure 4.3.6: Pseudo first order plot for BTH conversion in the binary mixture, catalyzed by PMA at 340 °C and 600 psi $\text{H}_2/(2.5\% \text{H}_2\text{S})$, Run#23

As shown in Figure 4.3.5 the pseudo first order rate constant for NAPH hydrogenation was calculated by two different methods. The first method, use all the points and calculates the slope by linear regression of intercept = 0.0 giving a value for $k_r = 7.33 \times 10^{-5} \text{ s}^{-1}$. The second method, using linear regression of intercept $\neq 0.0$ gave a higher value of $k_r = 8.33 \times 10^{-5} \text{ s}^{-1}$. This result confirmed that, there is an initial inhibition of NAPH by BTH at the initial reaction time as was shown in Figure 4.3.4. Therefore, by neglecting the zero reaction time a higher NAPH rate constant (k_r) is obtained, this calculation was applied for NAPH hydrogenation in all mixture reaction experimental runs of (NAPH and BTH).

These results are compared with the externally supplied H₂ under the same operating conditions (see Figure 4.3.7). Similar behavior as for in situ H₂ was observed however, a lower NAPH conversion and rate constants for both BTH and NAPH hydrogenation are observed as listed in Table 4.3.2 and shown in Figures 4.3.8 and 4.3.9. Therefore, not only is the in situ H₂ considerably more reactive than the externally supplied H₂ for a single model compound, but also for the binary mixture of the model compounds.

Table 4.3.2: Pseudo first order rate constants and conversions for BTH and NAPH in different medium*

Run #	X _{NAPH} (%)	NAPH, k_1 Intercept = 0, (s ⁻¹)	NAPH, k_1 Intercept ≠ 0, (s ⁻¹)	X _{BTH} , (%)	BTH, k_2 (s ⁻¹)
23 ¹	67.57	7.33×10^{-5}	8.33×10^{-5}	100	7.87×10^{-4}
17 ²	59.57	5.00×10^{-5}	5.33×10^{-5}	100	4.57×10^{-4}

*600 psi (CO¹ or H₂²)/(2.5% H₂S) at 340°C. 1500 ppm of PMA catalyst, 14.1 g BTH, 43.25 g NAPH, 200 ml Tol, 70 ml H₂O, stirrer speed 1300 rpm. Reaction time = 4 hrs

Figure 4.3.7 shows the pseudo first order plots for the NAPH hydrogenation with externally supplied H₂. Apparently, an initial inhibition of the NAPH hydrogenation in the presence of BTH was also observed (compared with Figure 4.2.6).

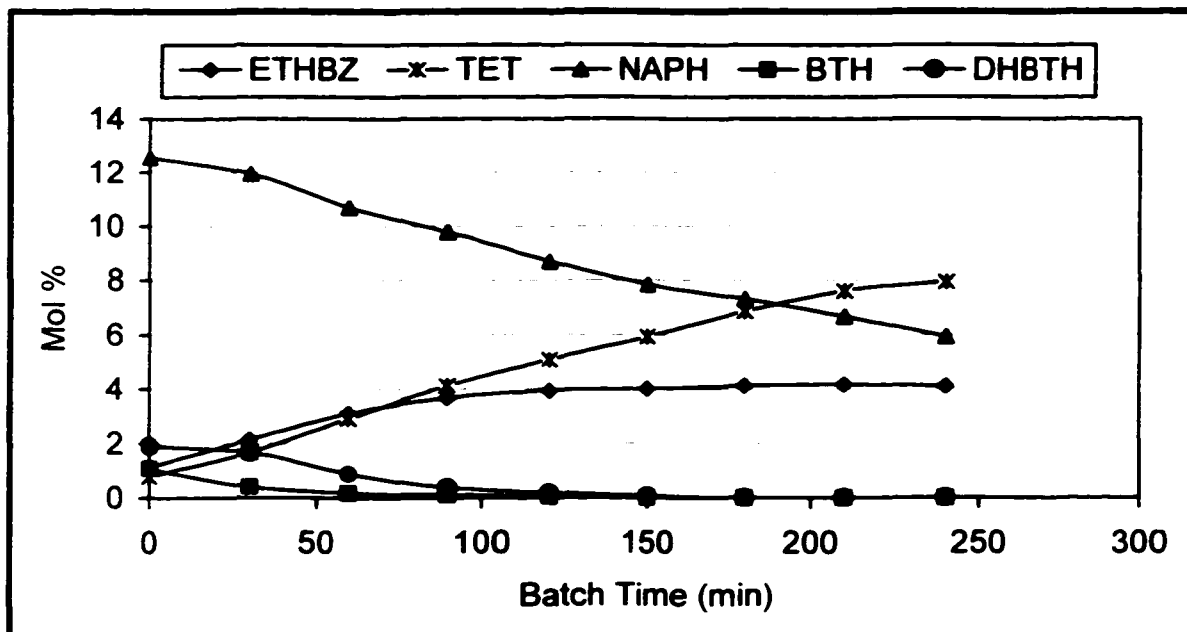


Figure 4.3.7: Mole fraction % of the binary mixture component, catalyzed by PMA at 340 °C and 600 psi H₂/(2.5% H₂S), Run#17

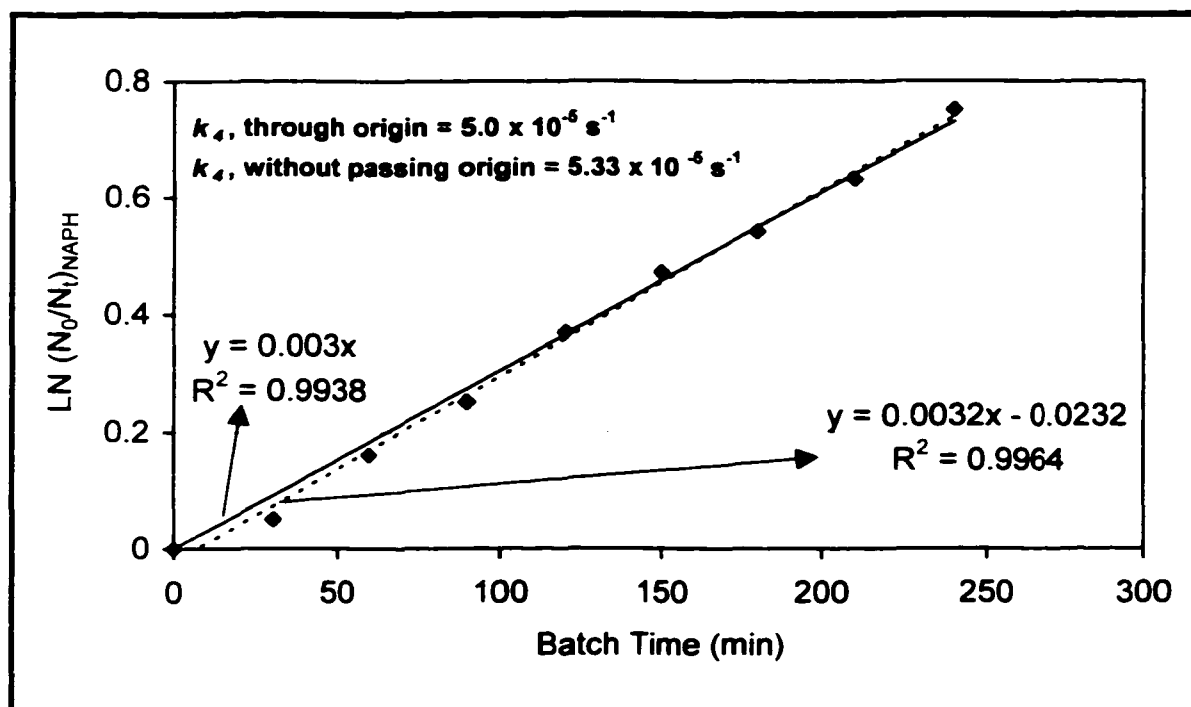


Figure 4.3.8 : Pseudo first order plot for NAPH conversion in the binary mixture, catalyzed by PMA at 340 °C and 600 psi H₂/(2.5% H₂S), Run # 17

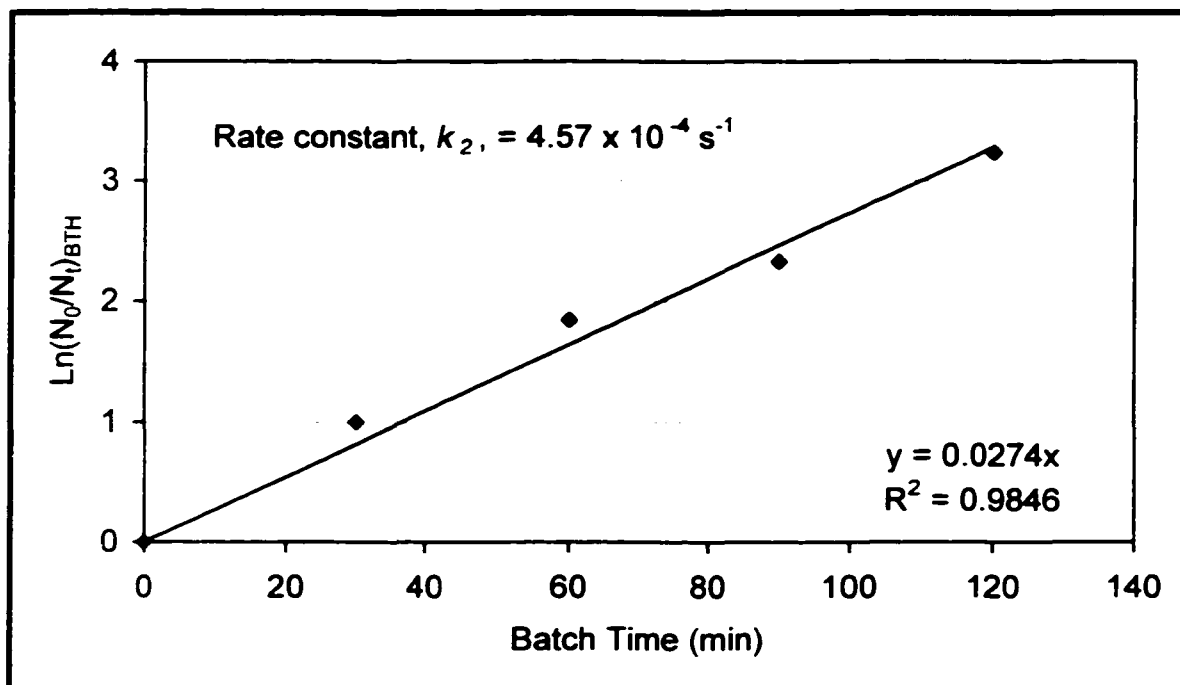


Figure 4.3.9: Pseudo first order plot for BTH conversion in the binary mixture. catalyzed by PMA at 340 °C and 600 psi H_2 /(2.5% H_2S), Run#17

In the present study, it is observed that the presence of sulfur compounds may inhibit the complete conversion of NAPH to TET. By contrast, NAPH does not inhibit the complete conversion of BTH to ETHBZ (see Table 4.3.2). Song and Schmitz (1997) also found the addition of sulfur in the form of BTH decreased the activity of all catalysts tested at 200°C for the hydrogenation of naphthalene. However, these results contradict with the work of Farag et al. (1999), who found a high concentration in the initial feedstock of NAPH (10 wt %), was inhibiting the HDS of 4,6- dimethyldibenzothiophene (4,6-DMDBT), and only 15% conversion was obtained. This reaction was carried out with a commercial CoMo catalyst supported on carbon at 340 °C and 2.9 MPa H₂ for a 20 minutes reaction time. In the present study with 20 wt % of NAPH in the initial feed a 100 % conversion of the HDS of BTH is obtained. Therefore, NAPH apparently is not inhibiting the desulfurization of BTH.

However, Sapre and Gates (1982) have reported that the inhibition by H₂S was milder compared to the organosulfur compounds. Gates et al., 1979 suggested that hydrogenation and hydrogenolysis occur on two different kinds of sites, since hydrogen sulfide affects the rates of thiophene hydrogenolysis and aromatic hydrogenation differently. Accordingly, the C-S bond cleavage may occur by direct desulfurization because it is considered a weak bond, and hydrogenolyzes easily to form H₂S. When aromatics are saturated, Π bonds are destroyed and σ C-C bonds become available to consume the hydrogen (Jafee, 1974). Moreover, Gissy et al. (1980) suggested that the catalyst sulfidation and the presence of hydrogen sulfide in the reaction system might

protect the catalyst against coke poisoning as well as promote the HDS activity. Further clarification of catalyst characterization will be discussed in Section 4.5.

The amount of H₂ needed to complete the hydrodesulfurization of BTH to ETHBZ, and to complete the hydrogenation of NAPH to TET is calculated to be 990.1 mmol of H₂ (see Appendix C.3). The calculation was based on Run # 23, theoretically, there should be 115.24 mmol of H₂ in excess, but GC analysis only shows 96.9 mmol of H₂ in excess in the gas product.

The 16% error is due, as stated before in Section 4.1, to the gas/liquid sampling during the reaction time. In addition, the flushing between each sample, and the lower density of the H₂ gas, facilitates the loss of the gas.

4.3.1 Reproducibility

For the experiments in this thesis, the reproducibility is based on the comparison of results obtained under two sets of replicate operating reaction conditions. Table 4.3.1.1 shows the two pairs of experimental runs (# 12 and # 23). The standard error is less than 2.5 %, which indicates that a good reproducibility is attained for the binary mixture of BTH and NAPH in the 1 L Autoclave Engineers batch reactor.

The small discrepancies among the results obtained are due to the fluctuation of the pressure in the system because of gas/liquid sampling and may be the inaccuracy in weighing the initial loading liquid feed. In addition, there are slight changes in yield and conversions, due to the small quantities of carbonaceous material that are formed during the four hours reaction time.

The reproducibility data for experiments # 13 and # 17, experiments # 20 and # 25 are shown in Appendix E. These experiments are reproducible within ± 2.5 % standard error.

Table 4.3.1.1: Reproducibility for the binary mixture (BTH+NAPH)

Run #	12	23		
Medium	CO/H ₂ S/H ₂ O	CO/H ₂ S/ H ₂ O	S	S _E
Pressure (psi)	600	600		
Temperature (°C)	340	340		
GC Liquid analysis				
BTH _{Initial} (mol%)	3.70	3.90	0.1414	0.10
NAPH _{Initial} (mol%)	11.53	12.33	0.5657	0.40
X _{CO} (%)	95.47	94.50	0.6859	0.48
X _{BTH} (%)	99.56	100.00	0.3111	0.22
ETHBZ yield (%)	94.35	92.54	1.2798	0.91
S removal (%)	99.53	100.00	0.3323	0.23
X _{NAPH} (%)	63.23	67.57	3.0688	2.17
TET yield (%) [*]	71.49	70.47	0.7212	0.51
A removal (%)	65.56	68.81	2.2981	1.63

S= Standard deviation, S_E= Standard Error, ^{*}Based on NAPH conversion

4.3.2 Effects of Changing H₂O/CO Ratio

4.3.2.1 Via the CO Loading Pressure

The water content in the system was kept constant (3888.9 mmol) by using PMA catalyst of (1500 ppm Mo) at 340 °C. The CO loading is examined for the two different loading pressures of 300 and 600 psi for the binary mixture (BTH+NAPH).

The hydrogenation of NAPH is severely affected when 300 psi CO loading is used (6.79 mol/mol of H₂O:CO ratio), Figure 4.3.2.1.1 shows the mole fraction % during reaction time. Thus only 24.65 % conversion is achieved, and it is almost three times less than using 600 psi (3.33 mol/mol, H₂O: CO ratio). For the BTH, the conversion was only negligibly affected by changing the CO loading, as shown in Table 4.3.2.1.1. The yields of ETHBZ and TET are shown in Figure 4.3.2.1.2. When the pseudo first order plot is considered for the hydrogenation of NAPH at 300 psi, apparently the rate constant, k_1 , is almost four times less than using 600 psi as shown in Figure 4.3.2.1.3 and the same observation is noticed by using the two methods of calculation as discussed in Section 4.3. The higher rate constant of NAPH conversion is obtained when using a linear regression of intercept $\neq 0.0$, due to the reasons stated previously in Section 4.3.

Further for the HDS of BTH the pseudo first order rate constant, k_2 , decreases five times as shown in Figure 4.3.2.1.4.

Table 4.3.2.1.1: Results of changing the CO loading*

Run #	H ₂ O:CO	X _{BTH}	X _{NAPH}	BTH, k_2	NAPH, k_4	NAPH, k_4
	Ratio	(%)	(%)	(s ⁻¹)	Intercept = 0.0 (s ⁻¹)	Intercept ≠ 0.0 (s ⁻¹)
25 ¹	6.798	96.74	24.65	1.70x 10 ⁻⁴	2.00 x 10 ⁻⁵	2.17 x 10 ⁻⁵
23 ²	3.330	100.00	67.57	7.87 x 10 ⁻⁴	7.33 x 10 ⁻⁵	8.33 x 10 ⁻⁵

*(300¹ or 600²) psi CO/(2.5%H₂S) at 340°C. 1500 ppm of PMA catalyst, 14.1 g BTH, 43.25 g NAPH, 200 ml Tol, 70 ml H₂O, stirrer speed 1300 rpm Reaction Time= 4 hrs

The H₂ generated in the system for both CO loadings is listed in Table 4.3.2.1.2. Clearly there is insufficient hydrogen at 300 psi CO loading as compared to the 600 psi (refer to Appendix F for data and figure). This implies that at 300 psi CO loading there is not sufficient H₂ to hydrogenate the BTH and the NAPH at the same time, this leads to hydrogen starvation in the system, (see Appendix C.4.1 for calculations).

Table 4.3.2.1.2: H₂ generated in the system at different CO loading

Loading CO/(2.5H ₂ S) psi	Initial CO (mmol)	H ₂ generated (mmol)	H ₂ needed* (mmol)	H ₂ excess (mmol)
300	572	531.53	990.8	-458.55
600	1169	1105.32	990.8	+115.25

* H₂ needed for complete conversion of BTH to ETHBZ and complete conversion of NAPH to TET

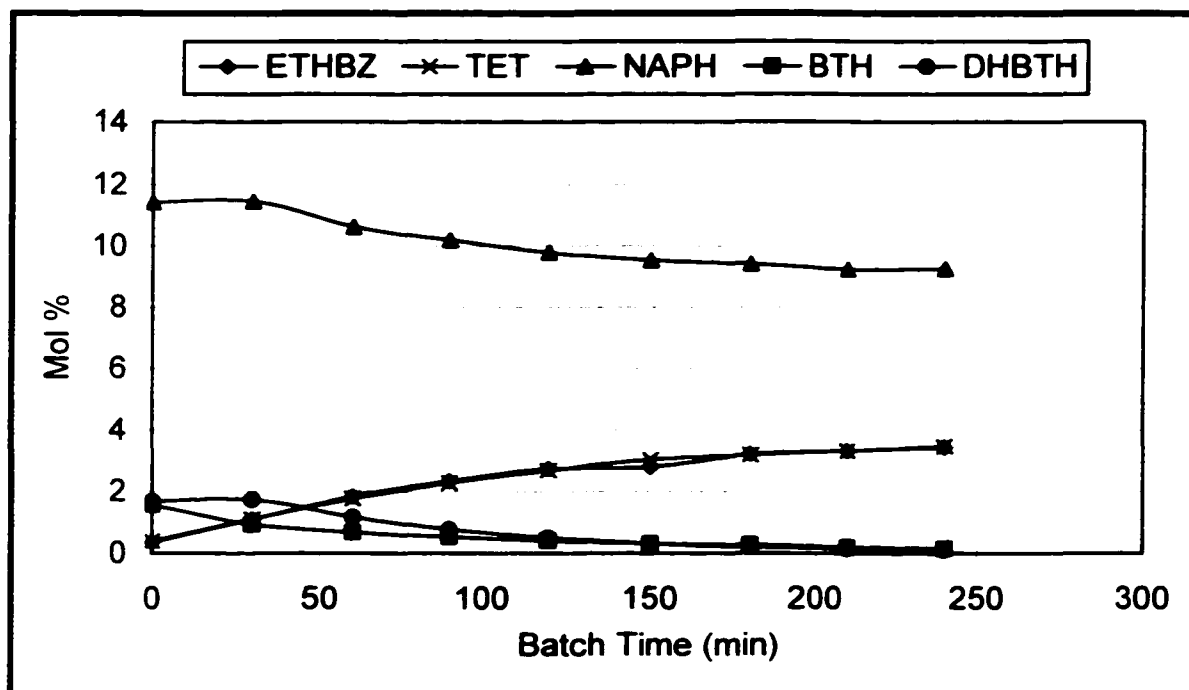


Figure 4.3.2.1.1: Mole fraction for the binary mixture (BTH+NAPH), catalyzed by PMA at 340°C, 300 psi CO/(2.5% H₂S), Run#25

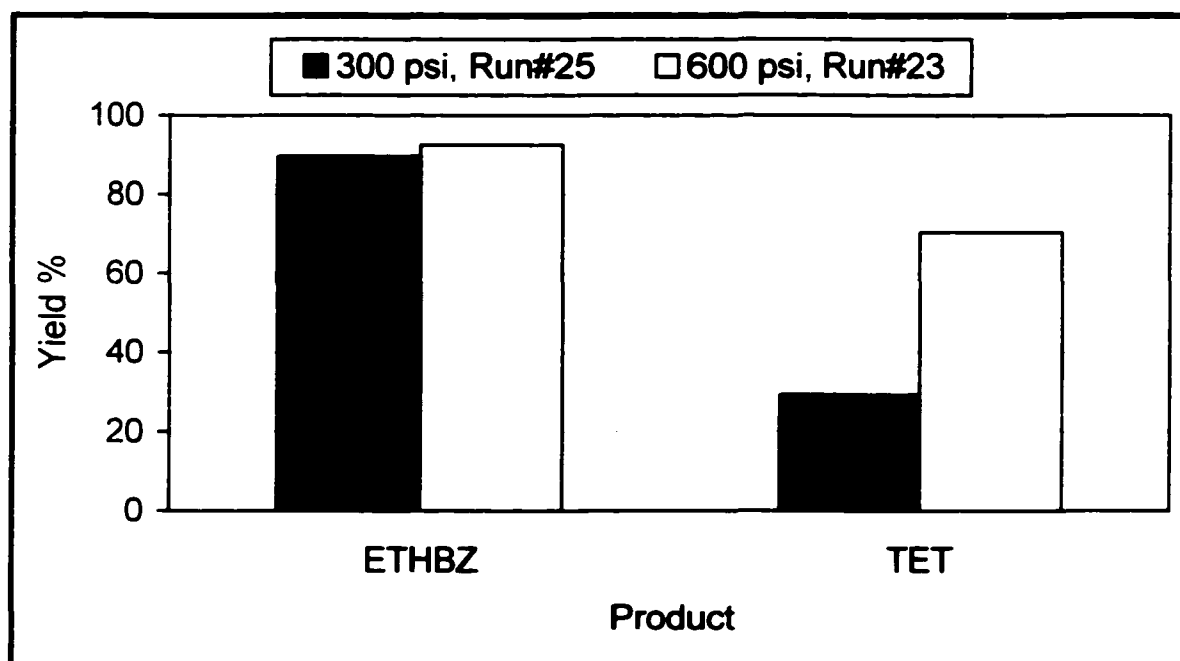


Figure 4.3.2.1.2: The yield of TET and ETHBZ from the binary mixture reaction for different CO loading, catalyzed by PMA catalyst (1500 ppm Mo) at 340 °C

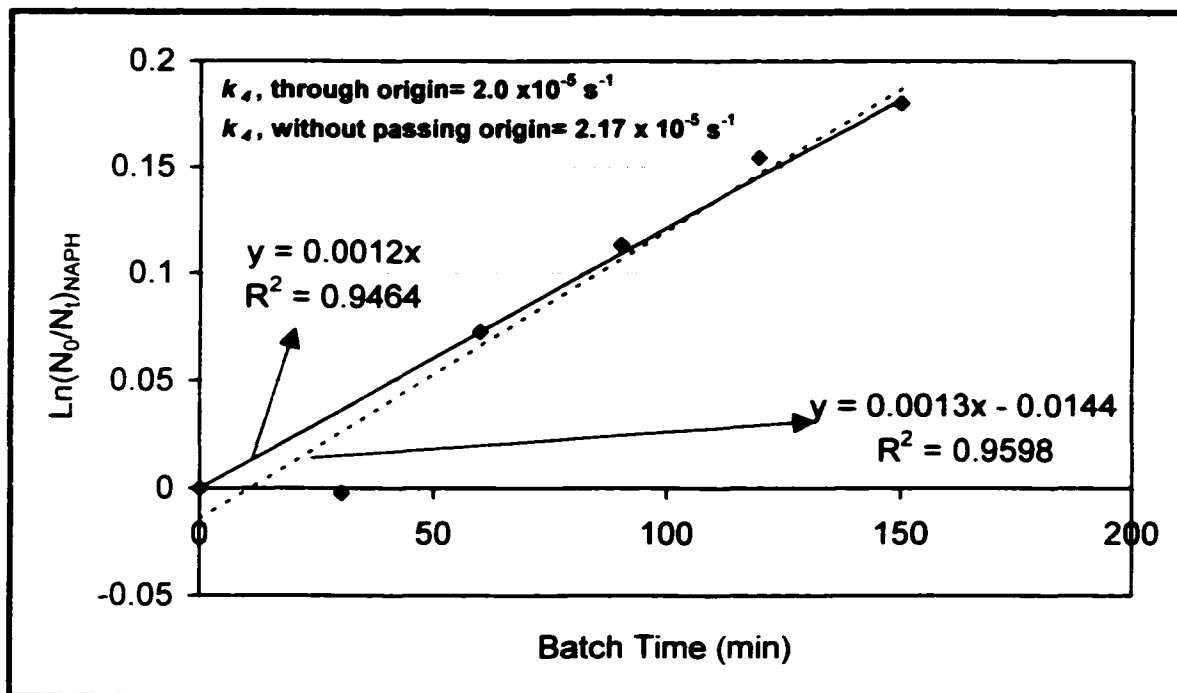


Figure 4.3.2.1.3: Pseudo first order plot for NAPH hydrogenation in the binary mixture, catalyzed by PMA at 340°C, 300 psi CO/(2.5% H₂S), Run#25

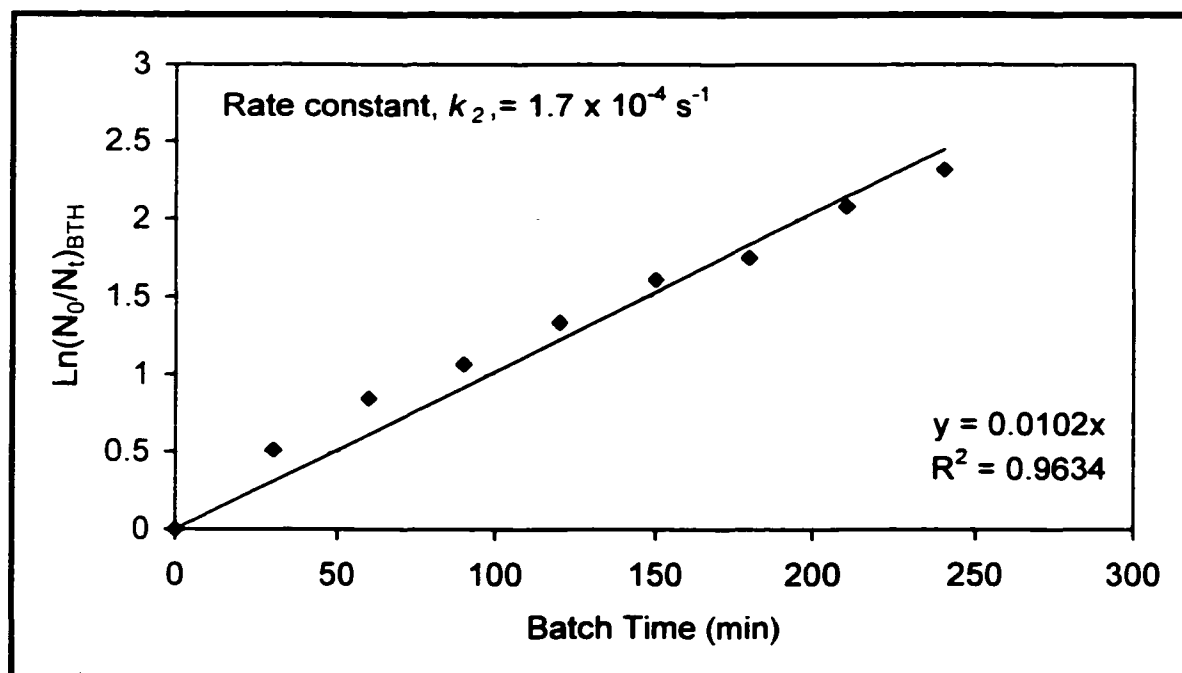


Figure 4.3.2.1.4: Pseudo first order plot for the HDS of BTH in the binary mixture, catalyzed by PMA at 340°C, 300 psi CO/(2.5% H₂S), Run#25

4.3.2.2 Via Water Content

The H₂O:CO ratio is changed by the use of two different amounts of water (35, 70 ml) under the same operating conditions of 600 psi CO loading pressure at 340 °C. The results are listed in Table 4.3.2.2.1. NAPH and BTH conversions are not affected by decreasing the amount of water. However, the pseudo first order rate constants for the conversions of BTH and NAPH decrease almost 50 % for the lower mole ratio of H₂O:CO because the WGSR is considerably slower, as illustrated in Figure 4.3.2.2.1. For a lower mole ratio of H₂O:CO, the WGSR takes twice the time to consume the CO compared to the higher mole ratio as introduced previously in Figure 4.3.1. Moreover, the pseudo first order rate constant for CO conversion at the higher H₂O:CO mole ratio is almost three times faster than at the lower mole ratio of H₂O:CO, see Figure 4.3.2.2.2.

However, if there is a further increase in the mole ratio of H₂O:CO, e.g., 6:1, it causes a drop in the CO conversion as well as a decrease in the amount of H₂ produced, this was observed in a previous study by Rintjema (1992). However, in the present study whether 35 ml or 70 ml of H₂O was used, the hydrogen production in the system is not being affected, see Table 4.3.2.2.1

Accordingly, the WGSR is affected more by the changing of the CO loading than the H₂O amounts (raw data for Run#18 is available in Appendix F). Figure 4.3.2.2.3, shows that the ETHBZ and TET yield is not significantly affected by changing water amounts. The calculations for the different mole ratio of H₂O:CO are shown in Appendix C.4.2.

These results agree very well with the observation of Keiski et al. (1996) on the WGSR using a commercial iron oxide-chromium oxide catalyst, ($\text{Fe}_3\text{O}_4\text{-Cr}_2\text{O}_3$), at a temperature range of 350-400°C. They found that the reaction rates are strongly dependent on the CO concentrations, but very little on the H_2O concentrations. The same observations were made by Milad (1994) for the WGSR using PMA catalyst (4467 ppm Mo) at 340°C. This result is expected since H_2O is in excess and the reaction kinetics are pseudo first order. Further, decrease in H_2O amount (e.g. 18 ml) a decrease in k_1 , k_2 and k_d rate constants is expected according to the obtained results as shown in Table 4.3.2.2.1, to verify this more experimental runs are needed.

Table 4.3.2.2.1: Summary of the results for the changing water content*

Run #	18	23
Water Content	35 ml	70 ml
$\text{H}_2\text{O}:\text{CO}$ Ratio (mol:mol)	1.66:1	3.33:1
X_{CO} , (%)	92.38	94.50
CO, k_1 , (s^{-1})	1.82×10^{-4}	4.88×10^{-4}
Initial CO (mmol)	1169.64	1169.00
H_2 generated (mmol)	1080.50	1105.32
H_2 needed** (mmol)	990.8	990.8
H_2 excess (mmol)	89.70	115.25
X_{NAPH} , (%)	63.66	67.57
NAPH, k_d , (s^{-1}) ¹	5.67×10^{-5}	7.33×10^{-5}
NAPH, k_d , (s^{-1}) ²	6.33×10^{-5}	8.33×10^{-5}
X_{BTH} , (%)	100	100
BTH, k_2 , (s^{-1})	5.2×10^{-4}	7.87×10^{-4}

*600psi (2.5% H_2S), at 340 °C, 1500 ppm Mo of PAM catalyst, 43.25 g NAPH, 14.1g BTH, 200 ml Toluene, stirrer speed 1300 rpm

** H_2 needed for complete conversion of BTH to ETHBZ and complete conversion of NAPH to TET

¹ Intercept = 0.0 ² Intercept \neq 0.0

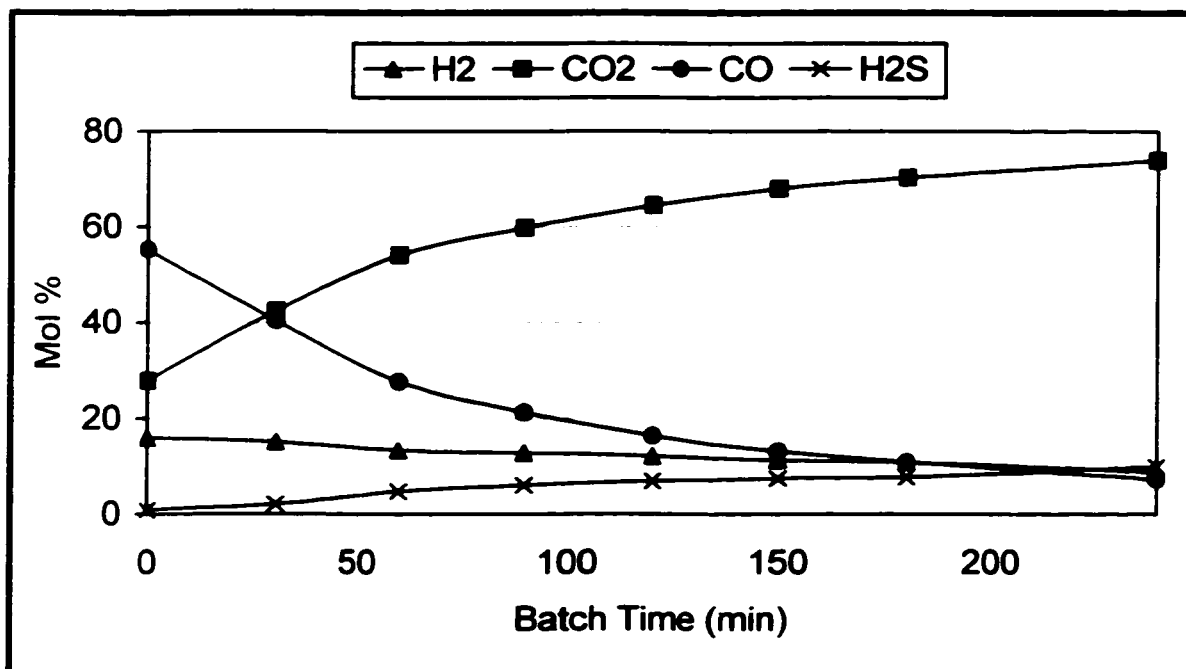


Figure 4.3.2.2.1: Mole fraction % of WGS components for the HYD of a mixture of BTH+NAPH catalyzed by PMA at 340 °C, 600 psi CO/(2.5% H₂S)/35 ml H₂O, Run#18

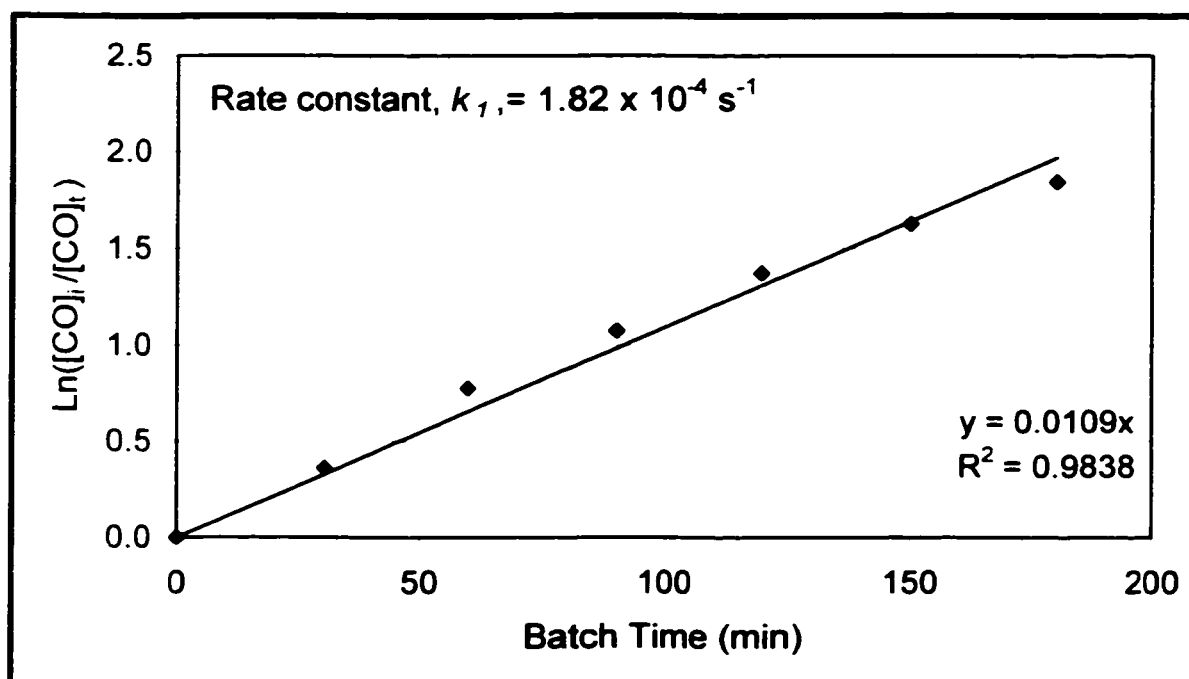


Figure 4.3.2.2.2: Pseudo first order plot for WGS, catalyzed by PMA at 340 °C, 600 psi CO/(2.5% H₂S)/35 ml H₂O, Run#18

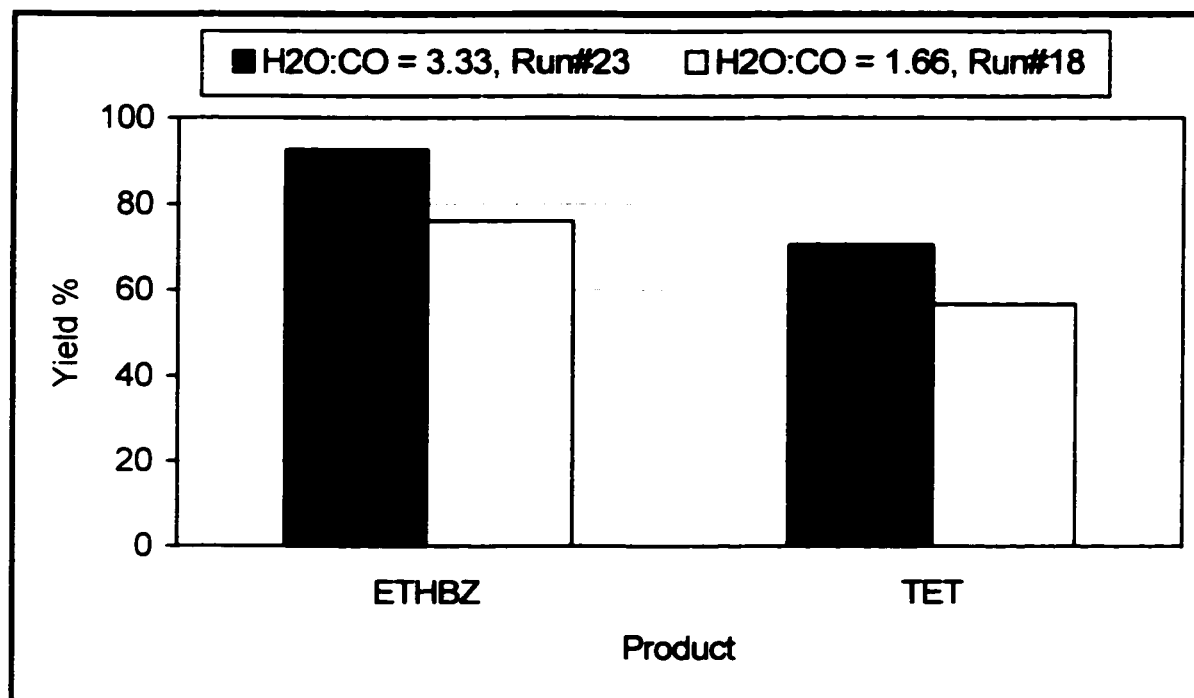


Figure 4.3.2.2.3: The yield of TET and ETHBZ from the binary mixture reaction at different amounts of H₂O, catalyzed by PMA catalyst (1500 ppm Mo), at 340°C.

4.3.3 Effects of Changing the Mo Concentration

The effect of different Mo concentrations on the hydrogenation of the binary mixture of (BTH+NAPH) and on the reactivity of WGSR is investigated at 340 °C and 600 psi initial loading of CO with 2.5% H₂S. PMA is used as a source of Mo metal, the results shows as the Mo concentration increases, the CO conversion increases slightly as illustrated in Figure 4.3.3.1 and Table 4.3.3.1. The pseudo first order rate constant of CO is determined for the blank run (without a catalyst, refer to Appendix F), and for each PMA concentration. The CO rate constant increases when the catalyst concentration increases as shown in Figure 4.3.3.2, and a first order dependence on Mo concentration is observed with a pseudo second order rate constant of 2.0×10^{-7} (s ppm Mo)⁻¹. Even, in the absence of catalyst a noticeable amount of CO conversion is observed. This is due to the catalytic effect of the reactor wall, which previously has been documented by Ng et al. (1992), and Wilson et al. (1982). Therefore, the WGSR is enhanced almost four times by using a PMA dispersed catalyst at 1500 ppm Mo.

Table 4.3.3.1: Effects of PMA concentration on the CO conversion and the rate constant, k_f , for the WGSR in a mixture of NAPH and BTH

Run #	[Mo] (ppm)	X _{CO} (%)	CO, k_f (s ⁻¹) × 10 ⁴
29	0 ¹	74.03	1.10
28	500	92.06	2.42
22	1000	93.98	2.88
23	1500	94.50	4.88
24	3000	95.46	6.55

* 600 psi CO/(2.5% H₂S), at 340 °C, PMA catalyst, 70ml H₂O, NAPH/BTH=3.2 mol/mol, Toluene=200 ml, stirrer speed 1300 rpm, Reaction Time = 4hrs
¹Run without catalyst (Blank)

The conversion of BTH after a total reaction time of 4 hours was not affected by increasing the PMA catalyst concentrations, and yielded almost the same amount of ETHBZ, see Table 4.3.3.2. However, the pseudo first order constant for BTH conversion (see Figure 4.3.3.3 and Table 4.3.3.2), increases with Mo concentration and reaches a maximum value at 1500 ppm Mo and decreases almost 25% at 3000 ppm Mo. Assuming a first order dependence on Mo concentration for ≤ 1500 ppm Mo, a straight line with a pseudo second order rate constant of $5.0 \times 10^{-7} (\text{s ppm Mo})^{-1}$ as shown in Figure 4.3.3.3 was obtained. This result may be due to the inhibition effect of HDS at higher concentrations of Mo or more H_2S is needed to sulfide the PMA catalyst as shown in Table 4.3.3.3 since the H_2S production was found to decrease at higher Mo concentrations (refer to Appendix B.1).

Table 4.3.3.2: Effects of PMA concentration on the product yield for a mixture of NAPH and BTH*

[Mo] (ppm)	X_{NAPH} (%)	TET yield (%)	NAPH, k_1 ($\text{s}^{-1} \times 10^5$) Intercept = 0.0	NAPH, k_2 ($\text{s}^{-1} \times 10^5$) Intercept \neq 0.0	X_{BTH} (%)	ETHBZ yield (%)	BTH, k_2 ($\text{s}^{-1} \times 10^5$)
0 ¹	7.19	7.36	0.00	0.00	75.56	52.48	0.58
500	34.72	35.92	2.17	2.50	100	94.69	5.20
1000	49.31	53.99	3.17	3.83	100	92.50	6.00
1500	67.57	70.48	7.33	8.33	100	92.56	7.87
3000	78.67	82.33	15.00	13.83	100	91.49	5.73

* 600 psi $\text{CO}/(2.5\% \text{H}_2\text{S})$, at 340 °C, PMA catalyst, 70ml H_2O , NAPH/BTH=3.2 mol/mol, Toluene=200 ml, stirrer speed 1300 rpm, Reaction Time = 4hrs
¹Run without catalyst (Blank)

The blank run (without the catalyst) shows a 54.68 % sulfur removal (see table 4.3.3.3). This occurred because the reactor wall is made of 316 SS containing chromium or nickel and occasionally in the presence of H₂S the reactor walls has been sulfided prior to reaction and enhances the WGSR. In addition, it took almost 2 hours to heat up the reactor to the required reaction temperature of 340°C and some hydrodesulfurization of BTH could occur prior to the reaction temperature of 340°C.

Table 4.3.3.3: Effects of PMA concentration on TET selectivity, H₂S production sulfur and aromatic removal for a mixture of NAPH and BTH*

Run #	Mo concentration (ppm)	S removal (%)	A removal (%)	H ₂ S produced (mmol)	TET selectivity
29	0 ¹	54.68	7.35	23.35	1.00
28	500	100.00	35.41	51.17	1.00
22	1000	100.00	47.98	47.67	0.98
23	1500	100.00	68.81	47.42	0.98
24	3000	100.00	79.58	39.88	0.98

* 600 psi CO/(2.5%H₂S), at 340 °C, PMA catalyst, 70ml H₂O, NAPH/BTH=3.2 mol/mol, Toluene=200 ml, stirrer speed 1300 rpm. Reaction Time = 4hrs

¹Run without catalyst (Blank)

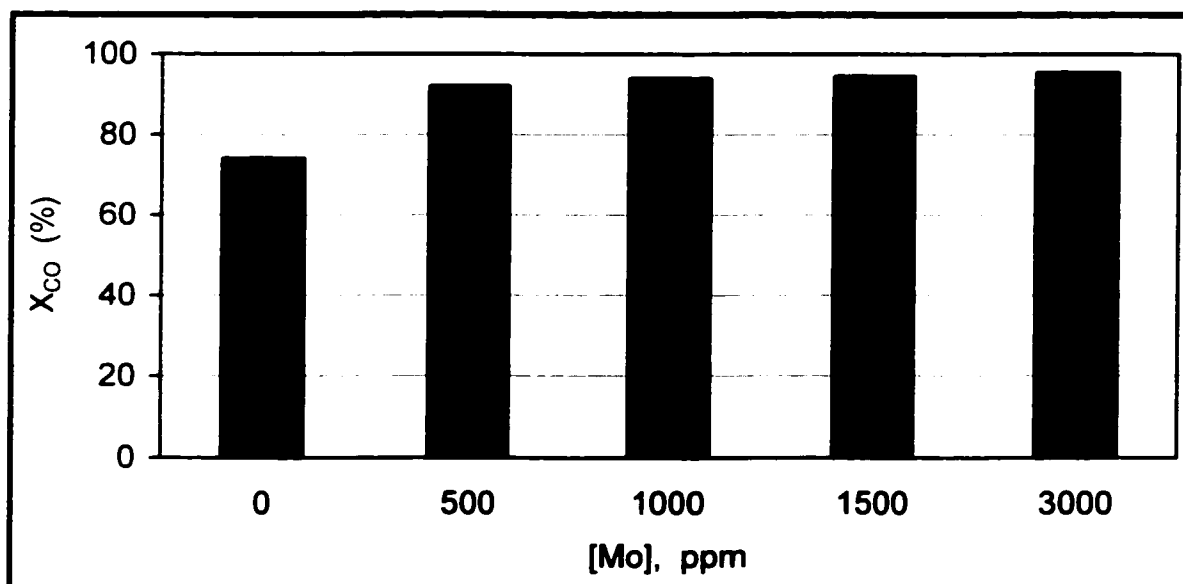


Figure 4.3.3.1: Effect of Mo concentration on CO conversion for a mixture of BTH+NAPH

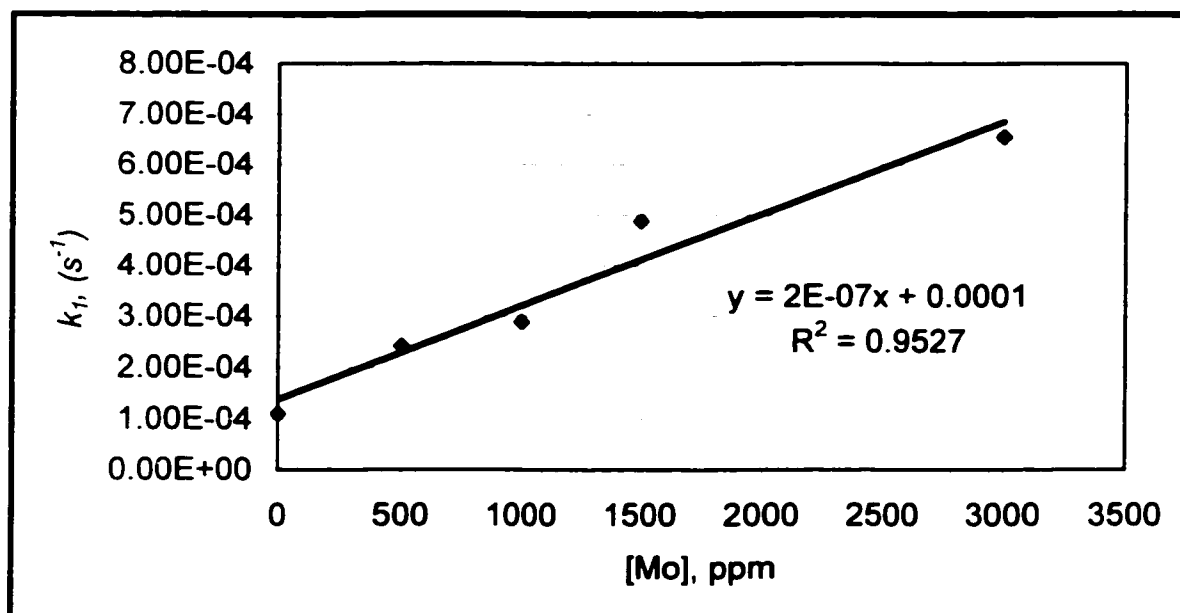


Figure 4.3.3.2: Pseudo first order rate constants of CO conversion at different Mo concentrations for a mixture of BTH+NAPH

By contrast, the NAPH hydrogenation shows a stronger dependence on the Mo concentration. Table 4.3.3.2 shows that TET yield and NAPH conversions increased significantly as the Mo concentration increases. This result is in agreement with Curtis et al. (1990) who used molybdenum naphthenate of (3000 ppm Mo) for the hydrogenation of NAPH and BTH, at 380 °C for 30 min reaction time, and almost a complete desulfurization of BTH to ethylbenzene as the main product (90%) was observed. In addition, NAPH hydrogenation yielded tetralin as a primary product (92%), and cis and trans decalins were present in small amounts. It is interesting to note that the 78.67 % NAPH conversion, (obtained from this current research) is better than the conversion of 60%, obtained from the HYD of NAPH over a supported catalyst, (P-Ni-W/Al₂O₃), at 300 °C and a pressure of 44 atm for a reaction time of 8 hours, as reported by Halachev et al. (1996). Moreover, in the present study TET selectivity is determined to be between 0.98 - 1.0 as shown in Table 4.3.3.3 and thus TET is favored to be the primary product at 340°C (refer to Appendix C.2 for calculation). Therefore, the dispersed catalyst compares favorably with the commercial catalysts.

Furthermore the pseudo first order constant of NAPH conversion shows a first order dependence on Mo concentration as shown in Figure 4.3.3.4 and Table 4.3.3.2, by using both methods of calculating the rate constant, k_d , when (intercept = 0.0, and intercept \neq 0.0). The pseudo second order rate was found to be $5.0 \times 10^{-8} \text{ (s ppm Mo)}^{-1}$ for both methods.

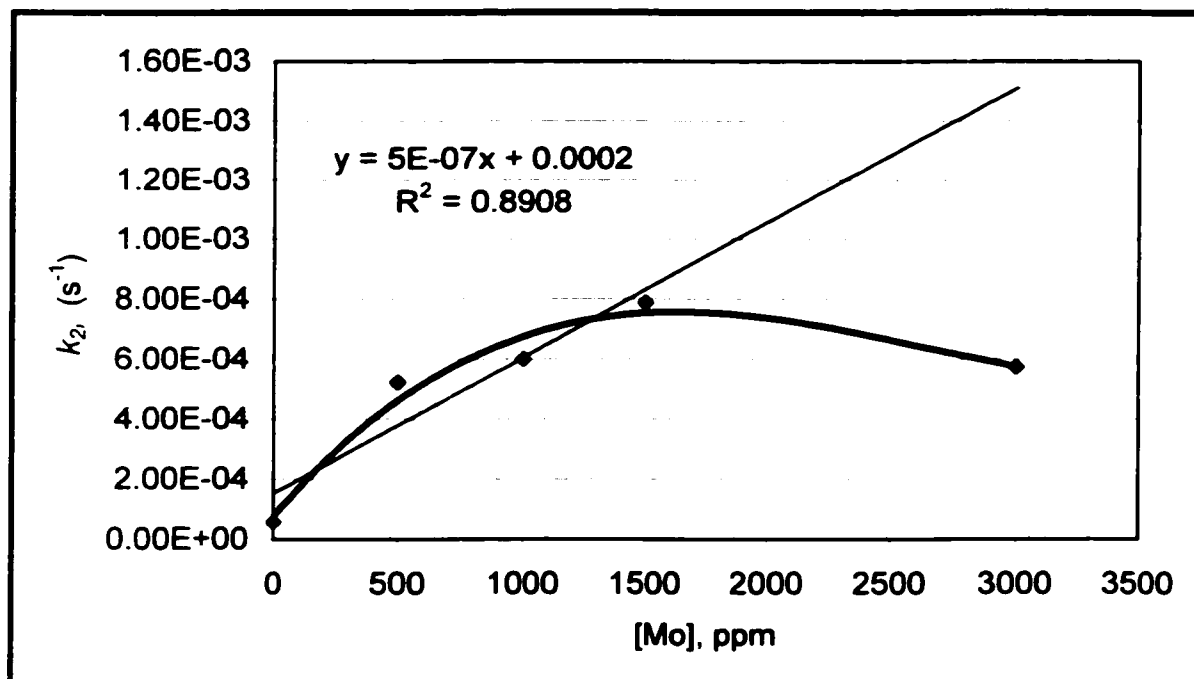


Figure 4.3.3.3: Pseudo first order rate constants for HDS of BTH at different Mo concentrations for a mixture of BTH+NAPH

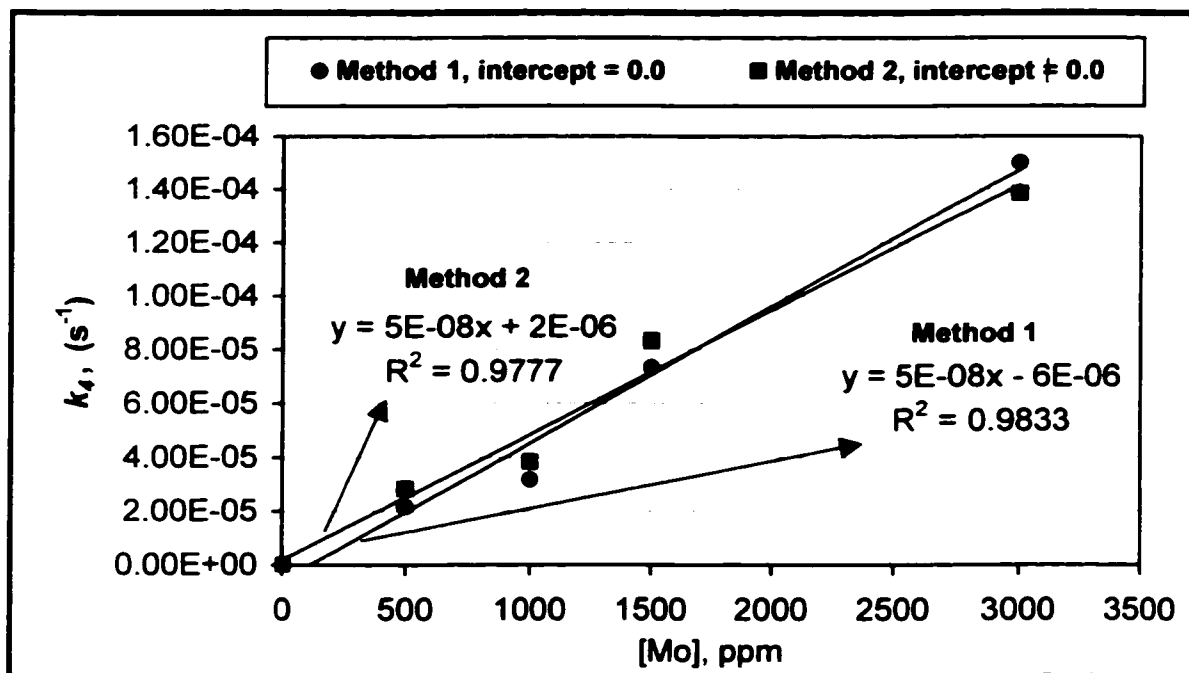


Figure 4.3.3.4: Pseudo first order rate constants for HYD of NAPH at different Mo concentrations for a mixture of BTH+NAPH

4.3.4 Effects of Different Mo Catalyst

Three additional sources of Mo at a concentration of 1500 ppm (MA, AMT and ATTM) are examined at 340°C and 600 psi CO initial loading with 2.5 % H₂S, to compare their reactivities on the hydrogenation process while utilizing the H₂ produced from the WGSR. The experimental run for the ATTM catalyst was carried out without the initial loading of 2.5 % H₂S due to the greater presence of sulfide species (MoS₄). Table 4.3.4.1 shows that the four catalysts significantly promote the WGSR compared to the blank reaction (without the catalyst). The mol % for each component of gas samples collected during reaction time for PMA (refer to Figure 4.3.1), and for MA, AMT and ATTM catalysts are shown in Figure 4.3.4.1a,b,c respectively. Comparing the four catalysts, MA and AMT are considered to be more active in promoting CO consumption than PMA and ATTM. Based on the fact that the WGSR starts prior to reaction temperature (340°C) in the presence of catalyst and almost 75 mol % of CO is converted at zero reaction time. While without any catalyst Figure 4.3.4.2 shows that only 18.0 mol % of CO is converted at zero reaction time.

Consistently the CO conversion is in the range of 94 % for the four types of catalysts at 1500 ppm Mo, and the pseudo first order rate constant decreases in the following order: PMA > ATTM > AMT > MA, (see Figure 4.3.4.3, for raw data refer to Appendix F).

The pH measurements were made before and after the reaction, as shown in Table 4.3.4.1. It is also interesting to note that PMA being the most acidic catalyst, is also the most active for the hydrogenation of NAPH. According to the NAPH hydrogenation rate

constant, k_d , obtained for the four catalysts using both method of intercept = 0.0 and intercept \neq 0.0, (see Table 4.3.4.2, for raw data and liquid analysis figures refer to Appendix F), the catalyst reactivity for the HYD of NAPH via the WGSR decreases in the following manner: PMA > AMT > ATTM \geq MA.

Table 4.3.4.1: Effects of Mo catalysts on the reactivity of WGSR*

Run #	Catalyst	X _{CO} (%)	CO, k_t (s ⁻¹ × 10 ⁴)	Pearson correlation R ²	pH before	pH after
29	Blank	74.03	1.10	0.99	5.65	3.36
23	PMA	94.50	4.88	0.99	1.94	4.56
26	MA	94.63	3.67	0.99	5.36	6.56
27	AMT	94.77	4.22	0.99	5.11	7.99
30	ATTM ¹	94.00	4.37	0.98	9.80	7.60

* 600 psi CO/(2.5%H₂S), at 340 °C, catalyst of 1500 ppm Mo, 70ml H₂O, NAPH/BTH=3.2 mol/mol, Toluene=200 ml, stirrer speed 1300 rpm, Reaction Time = 4 hrs

¹ This run is carried out without the initial loading of 2.5 % H₂S

Table 4.3.4.2: Activity of different Mo catalysts*

Run #	Catalyst	X _{BTH} (%)	BTH, k_2 (s ⁻¹ × 10 ⁴)	X _{NAPH} (%)	NAPH, k_d Intercept =0.0 (s ⁻¹ × 10 ⁵)	NAPH, k_d Intercept \neq 0.0 (s ⁻¹ × 10 ⁵)
29	Blank	75.56	0.58	7.19	NA ²	NA ²
23	PMA	100.00	7.87	67.57	7.33	8.33
26	MA	100.00	6.32	61.47	4.83	5.50
27	AMT	100.00	6.63	63.22	5.33	6.00
30	ATTM ¹	100.00	8.73	60.11	4.83	5.50

* 600 psi CO/(2.5%H₂S), at 340 °C, catalyst of 1500 ppm Mo, 70ml H₂O, NAPH/BTH=3.2 mol/mol, Toluene=200 ml, stirrer speed 1300 rpm, Reaction Time = 4 hrs

¹ This run is carried out without the initial loading of 2.5 % H₂S

² NA= Not available

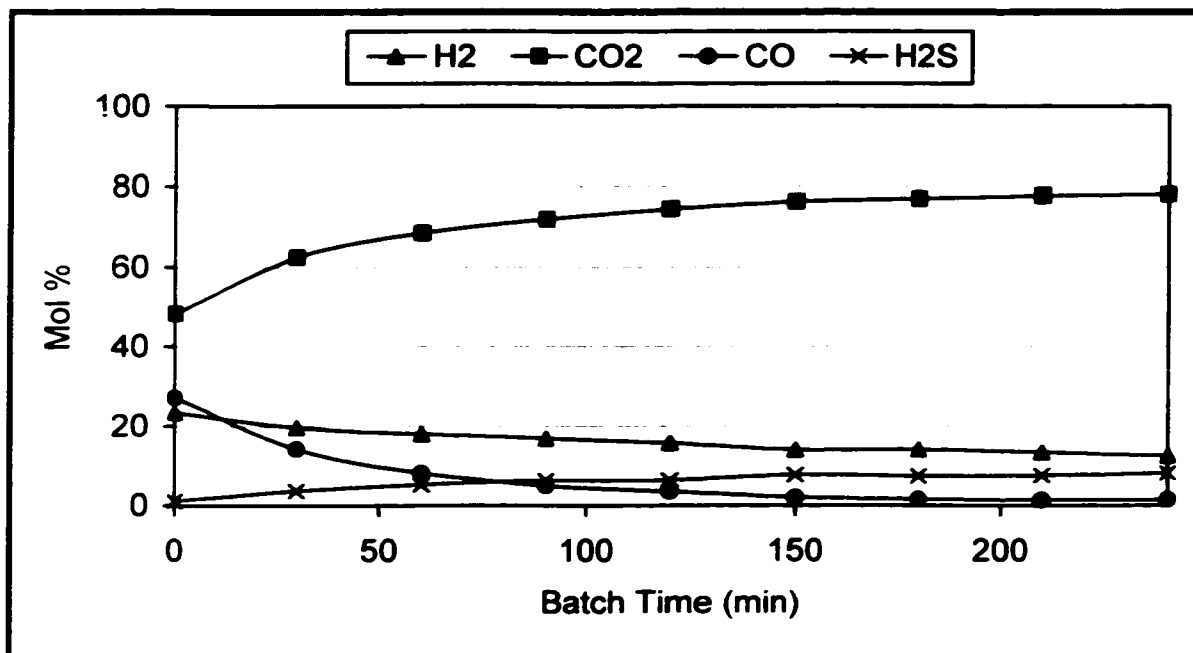


Figure 4.3.4.1a: Mole % of the WGS components for the binary mixture of BTH and NAPH catalyzed by MA at 340°C, Run#26

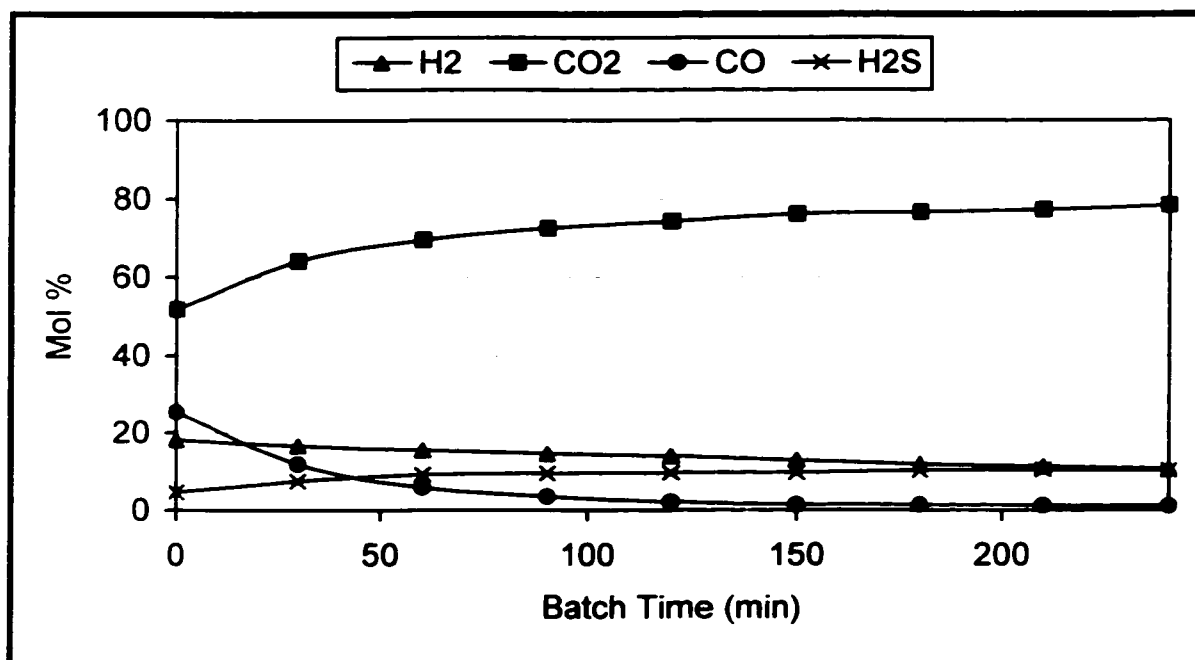


Figure 4.3.4.1b: Mole % of the WGS components for the binary mixture of BTH and NAPH catalyzed by AMT at 340°C, Run#27

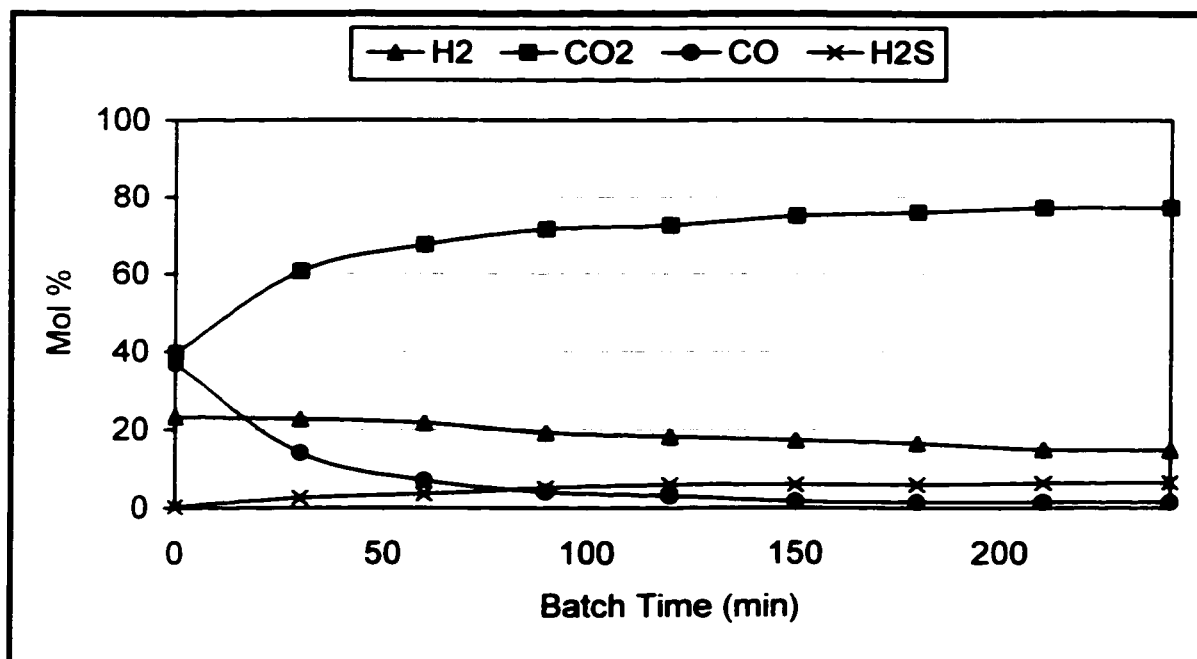


Figure 4.3.4.1c: Mole % of the WGSR components for the binary mixture of BTH and NAPH catalyzed by ATTm at 340°C, Run#30

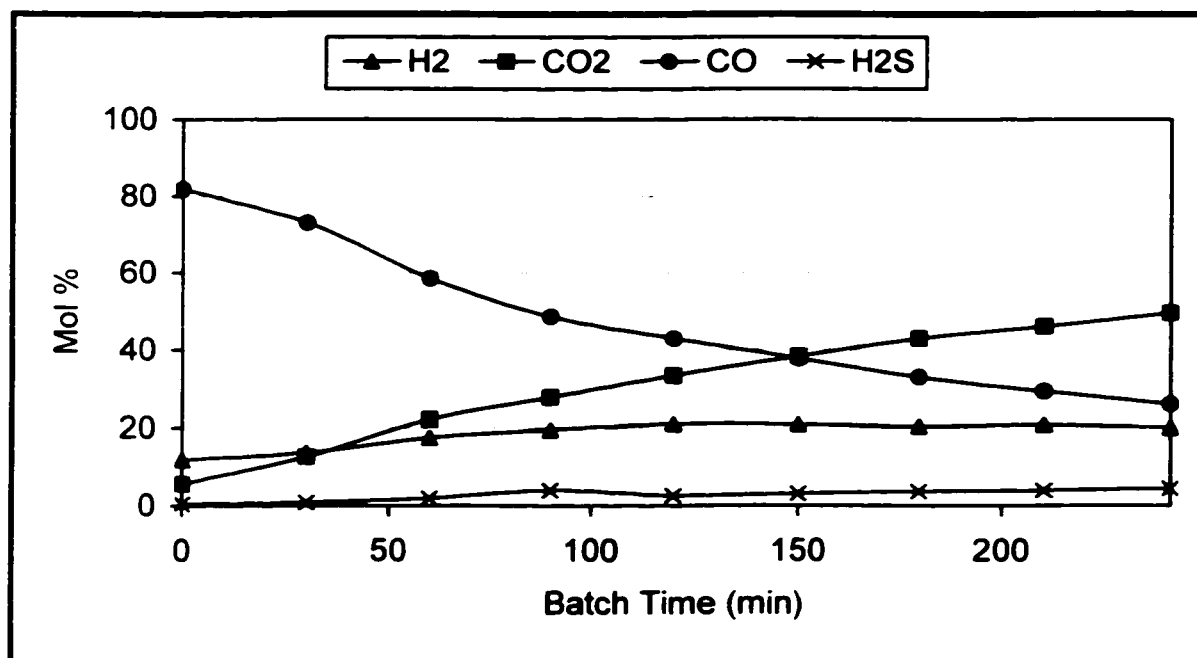


Figure 4.3.4.2: Mole % of the WGSR components for the binary mixture of BTH and NAPH without catalyst at 340°C, Run#29

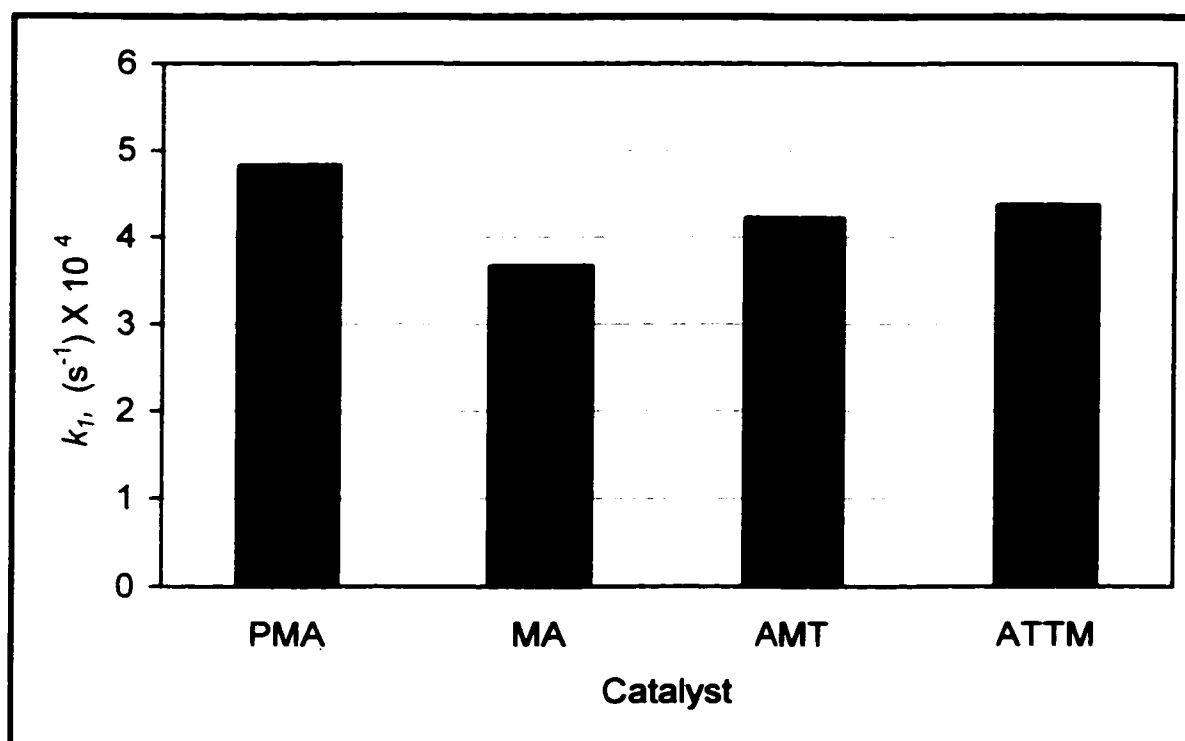


Figure 4.3.4.3: Pseudo first order rate constant for CO conversion with different Mo catalysts

In order to calculate the hydrogenation activity A_H of naphthalene, a simple equation (3-28) is used, (see Appendix B.6). The A_H is calculated from the product obtained at the end of the reaction period of 4 hours for each catalyst, as illustrated in Figure 4.3.4.4. The PMA catalyst shows a slightly higher A_H among the other catalysts. In the blank reaction, a negligible amount of A_H is noticed. The hydrogenation activity in the present study is affected by the reaction time as shown in Figure 4.3.4.5. This result is in agreement with Zhan and Guin (1994) who found that A_H was affected by the reaction time. When the unsupported iron oxide powder catalyst (Fe_2O_3) was used, within the first four hours A_H of 0.34 at 300 °C was obtained, and their A_H value is almost consistent with the present results which gives A_H of 0.28 at the 4th hour of reaction time at 340 °C (see Figure 4.3.4.5). Furthermore, the four catalysts showed almost the same activity during the four hours reaction time except for the PMA catalyst which showed a slightly higher activity for the NAPH hydrogenation, (refer to Appendix F). More studies are required to confirm this observation.

The NAPH and BTH conversions are determined and plotted versus the reaction batch time, as shown in Figure 4.3.4.6 and Figure 4.3.4.7 respectively. The PMA catalyst shows the best reactivity since the highest conversion of NAPH in the presence of BTH obtained within 4 hours reaction batch time. At zero reaction time only 10 to 15% of the NAPH was converted, whereas for BTH 65 to 78 % of BTH was converted. It seems that the presence of BTH is slightly inhibiting the NAPH hydrogenation as discussed previously in Section 4.3. This is consistent with the literature reported by Song and Schmitz (1997).

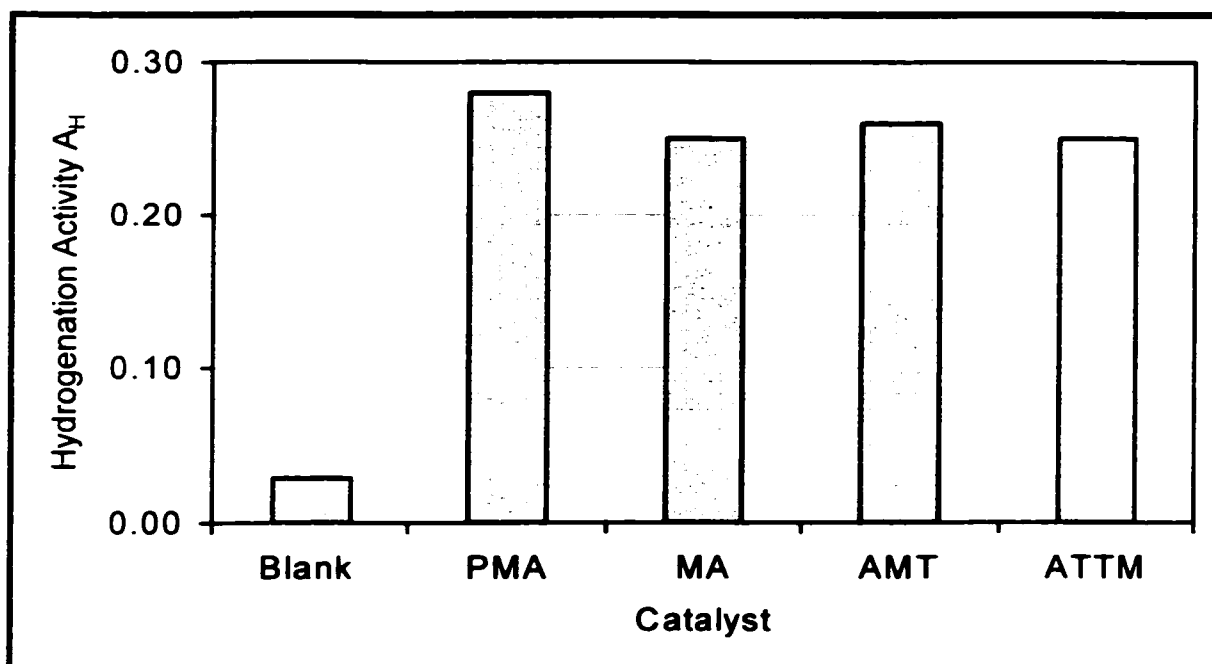


Figure 4.3.4.4: Hydrogenation activity of NAPH product for different Mo catalysts

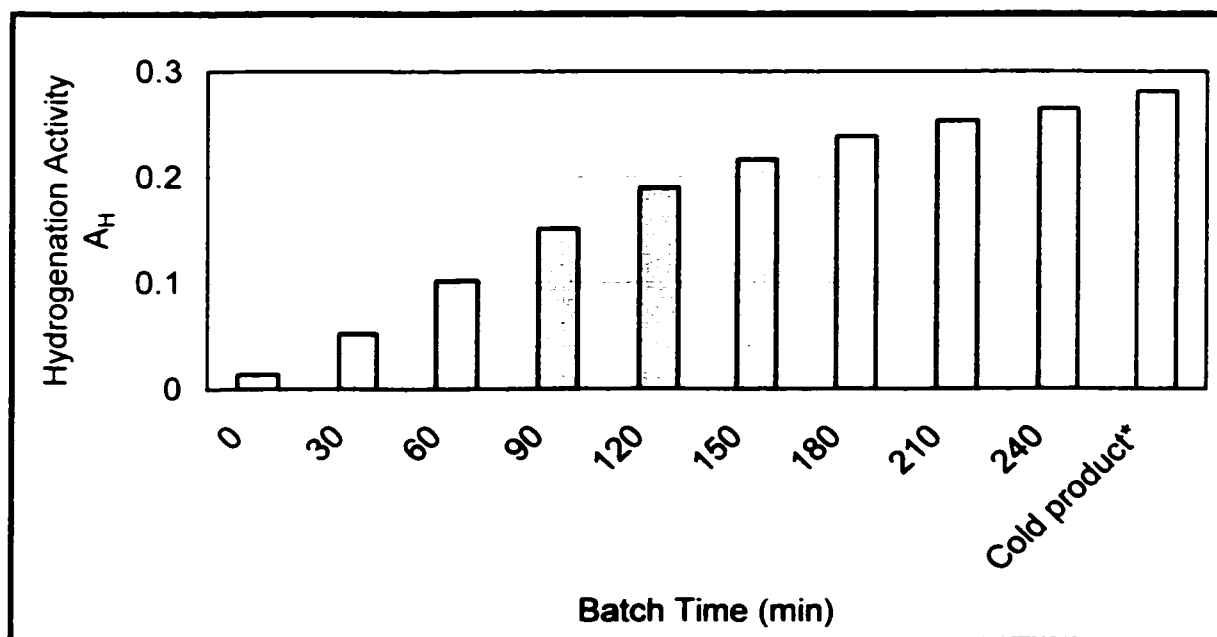


Figure 4.3.4.5: Effect of reaction time on the hydrogenation activity in a mixture of NAPH and BTH catalyzed by PMA at 340°C, Run#23

* Product collected at the end of reaction after the reactor has cooled down

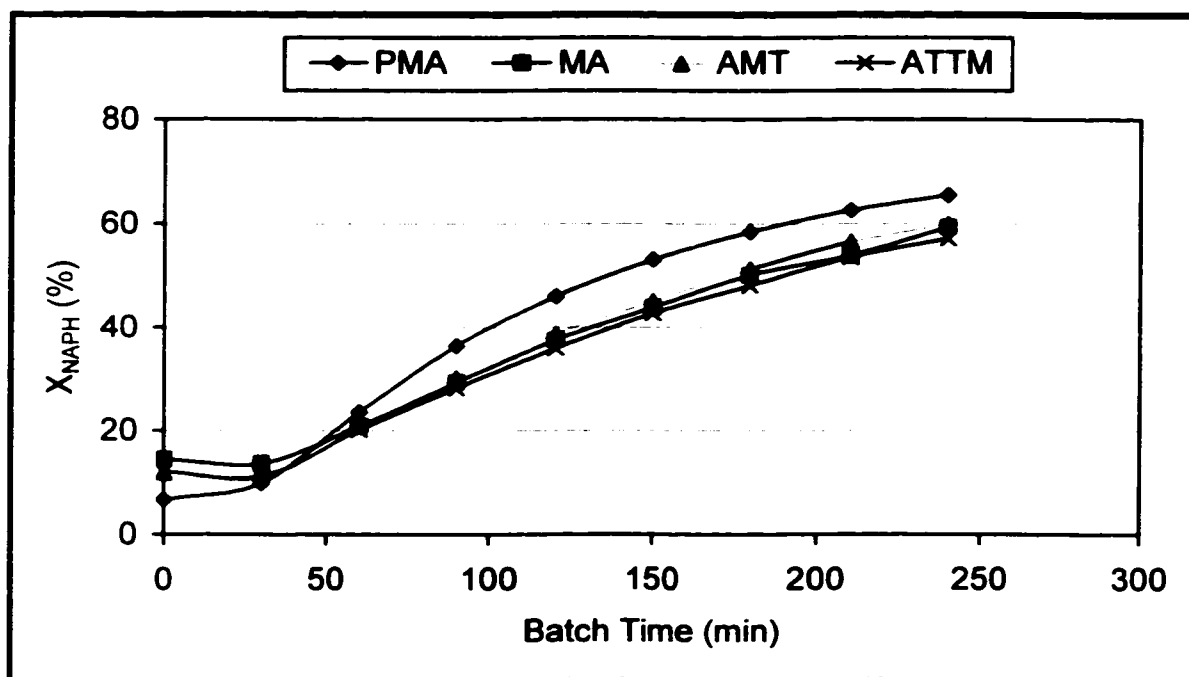


Figure 4.3.4.6: NAPH conversions during reaction time for different Mo catalysts

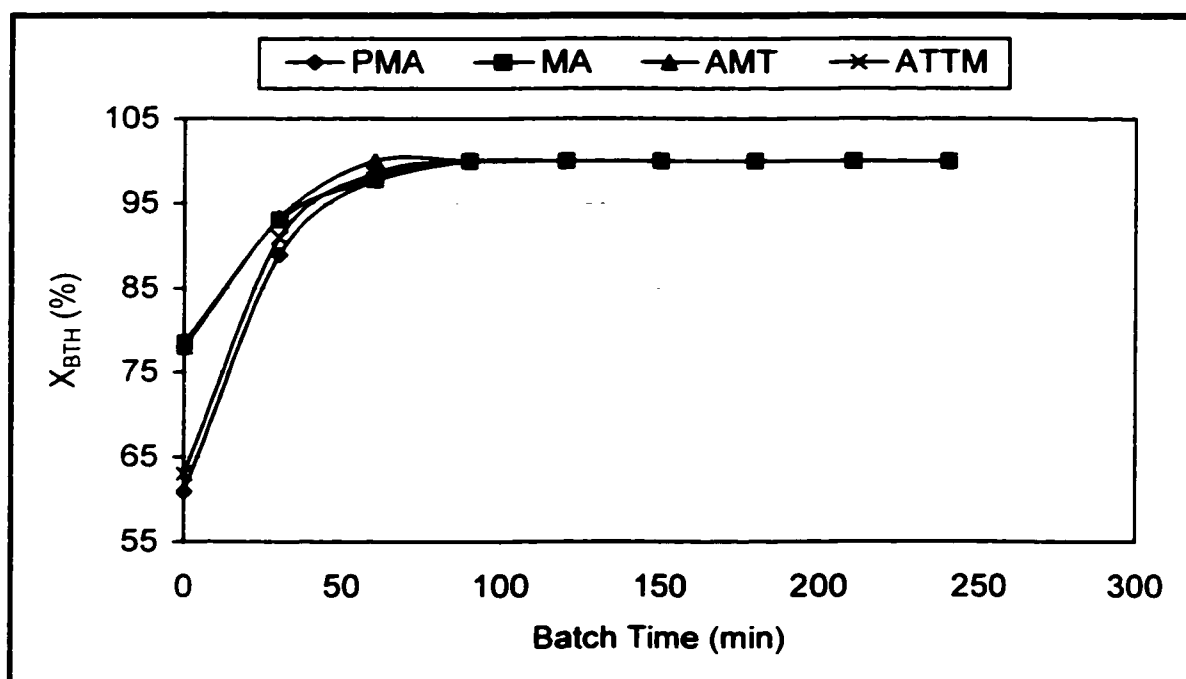


Figure 4.3.4.7: BTH conversion during reaction time for different Mo catalysts

The amount of H₂ generated in the system using the four catalysts individually, are enough to hydrogenate the BTH to ETHBZ, and the NAPH to TET. Table 4.3.4.3 indicates the excess amount of H₂ in the system.

Table 4.3.4.3: The amount of H₂ generated in the system

Catalyst	H ₂ generated (mmol)	H ₂ excess (mmol)
PMA	1105.32	115.24
MA	1106.85	116.77
AMT	1110.66	120.58
ATTM ¹	1136.42	146.34

¹ This run is carried out without the initial loading of 2.5 % H₂S

4.4 Aqueous Layer Analysis

Throughout the investigation of these experiments, BTH and NAPH are adopted as the model compounds for the HDS and AHYD via the WGS. Since H₂O and toluene are used in the reaction, this results in two phases, the organic and the aqueous phases, separated by a black solid layer which is the spent catalyst (refer to Figure 3.5.1). After the solids are separated under vacuum filtration system, (see section 3.5 and Figure 3.5.2). the aqueous layer is separated from the organic layer, and the aqueous layer is subjected to ion chromatograph (IC) analysis to detect the presence of the sulfate ions

(SO₄²⁻) that may be produced due to the presence of water. This is to confirm if the HDS of BTH via the WGSR is totally carried out through the hydrogenolysis of BTH to produce H₂S and not through oxidation of thiophene ring to produce SO₄²⁻ ions. Selected experiments are subjected to IC analyses. Table 4.4.1 lists the initial and final amounts of sulfur present in the experiments with different Mo catalysts. Interestingly, only a negligible quantity of sulfur is found in the aqueous layer of the final product. The calculations and chromatograms for each test are listed in Appendix A.9. These results show that the hydrolytic oxidation of benzothiophene to SO₄²⁻ is essentially negligible.

Table 4.4.1: The analysis of the aqueous layer in final products for different Mo catalysts*

Run#	Catalyst type	Initial amount of S in feed (mg)	Sulfate ions SO ₄ ²⁻ IC results (mg/l)	Amount of S from SO ₄ ²⁻ (mg)
29	Blank	4355.87	630.67	21.05
23	PMA	4355.87	92.60	3.09
26	MA	4355.87	67.65	2.26
27	AMT	4355.87	101.92	3.40
30	ATTM ¹	3974.97	42.45	1.42

*600 psi CO/(2.5%)H₂S, at 340 °C, [Mo] = 1500 ppm, NAPH/BTH= 3.2 mol/mol, Toluene=200 ml, stirrer speed 1300 rpm Reaction time = 4 hrs

¹ This run is carried out without the initial loading of 2.5 % H₂S

4.5 Catalyst Characterization

The experimental Section 3.6.3 of this thesis has described the X-ray diffraction (XRD) and thermal analyses, the thermogravimetric analysis (TGA) and the differential thermal analysis (DTA), which are performed on the fresh and spent catalysts to obtain qualitative information about the catalysts composition before and after each reaction.

The most likely phases present in the spent catalysts are MoS_2 , MoO_3 and the hydrocarbon deposits. These hydrocarbon deposits may be precursors for coke formation or coke itself. The fresh catalyst, MoS_2 , is also examined to obtain a comparison among components of the spent catalysts.

4.5.1 Thermal Analyses (TGA/DTA)

Usually, thermal analysis has been used to study the thermal behavior of solid materials, while they are undergoing the temperature programmed heating. Because of the reaction condition used in the current reaction study, it is assumed that a small amount of hydrocarbon and coke deposits is being formed. The TGA/DTA test enables the measurement of the amount of these deposits by oxidizing them in a (5 % O_2 mixed in He) atmosphere over the temperature range of 50 to 600 °C.

Figure 4.5.1.1 shows the weight % loss for the solids obtained from runs using different PMA concentrations. As the catalyst concentration increases the weight % loss increases, for concentration C and D the weight % loss is occurred in two temperature ranges of (50-180) °C and (200-450) °C, while, for concentration A and B it occurred

between the other two temperature ranges of (180-400) °C and (420-500) °C. The weight loss for concentration C and D is more than for A and B, this may reflect the incremental amount of hydrocarbon and coke deposits on the catalyst during the hydrogenation reaction of the binary mixture BTH+NAPH. This result is consistent with Mhaouer et al., 1996 who studied the hydrogenation of tetralin at 300°C under 50 atm on a Ru/KY zeolite catalyst in the presence of H₂S. They found that a significant amount of carbon remains on the catalyst. This carbon was insoluble coke composed of highly condensed polyaromatics. These condensed aromatics could block the catalyst and cause catalyst deactivation. In the present study, Table 4.5.1.1 shows the percent of weight loss for the solids of different spent catalyst concentrations, based on weight changed during the temperature program (TGA/DTA) analysis. Therefore, the weight loss increases as the concentration increases.

Consequently, Figure 4.5.1.2 shows the weight % loss for the different Mo catalysts used in the current study. There is a weight loss for the (PMA, AMT, AM, ATTM) catalysts in the range of (150-450) °C. Except for the PMA catalyst there is another region of weight loss, which is between (50-180) °C due to H₂O evaporation desorbed during the WGSR, since PMA is hygroscopic. Table 4.5.1.2 shows the percent of weight loss for the solids of different Mo spent catalysts based on weight changed during the thermal analysis (TGA/DTA). The weight loss would suggest predominantly due to the burning of coke formation under reaction conditions and the oxidation of the sulfidic species MoS₂ to MoO₃ accompanied by SO₂ evolution:



Table 4.5.1.1: The percent of weight loss for solids of different Mo concentrations*

[Mo] (ppm)	W ₁ (mg) T ₁ = 50 °C Time = 0 min	W ₂ (mg) T ₂ = 600 °C Time = 32 min	ΔW weight loss (mg)	weight loss (%)
500	12.01	9.15	2.86	23.81
1000	16.63	12.03	4.60	27.66
1500	19.29	12.70	6.59	34.16
3000	19.68	12.21	7.47	37.96

* For calculation, refer to Appendix A.8.1

Table 4.5.1.2: The percent of weight loss for solids of different Mo catalysts*

Catalyst	W ₁ (mg) T ₁ = 50 °C Time = 0 min	W ₂ (mg) T ₂ = 600 °C Time = 32 min	ΔW weight loss (mg)	weight loss (%)
PMA	19.29	12.70	6.59	34.16
MA	17.98	13.98	4.00	22.25
AMT	20.43	16.23	4.20	20.56
ATTM	19.22	15.13	4.09	21.28

* For calculation, refer to Appendix A.8.1

The PMA catalyst is showing the highest weight loss among the catalysts, because PMA catalyst is more acidic, and it may promote coke formation. Generally, there is an overall loss in weight for the different concentrations in the following sequence: 500 < 1000 < 1500 < 3000 and for different Mo catalysts, in following sequence: AMT < ATTM < MA < PMA.

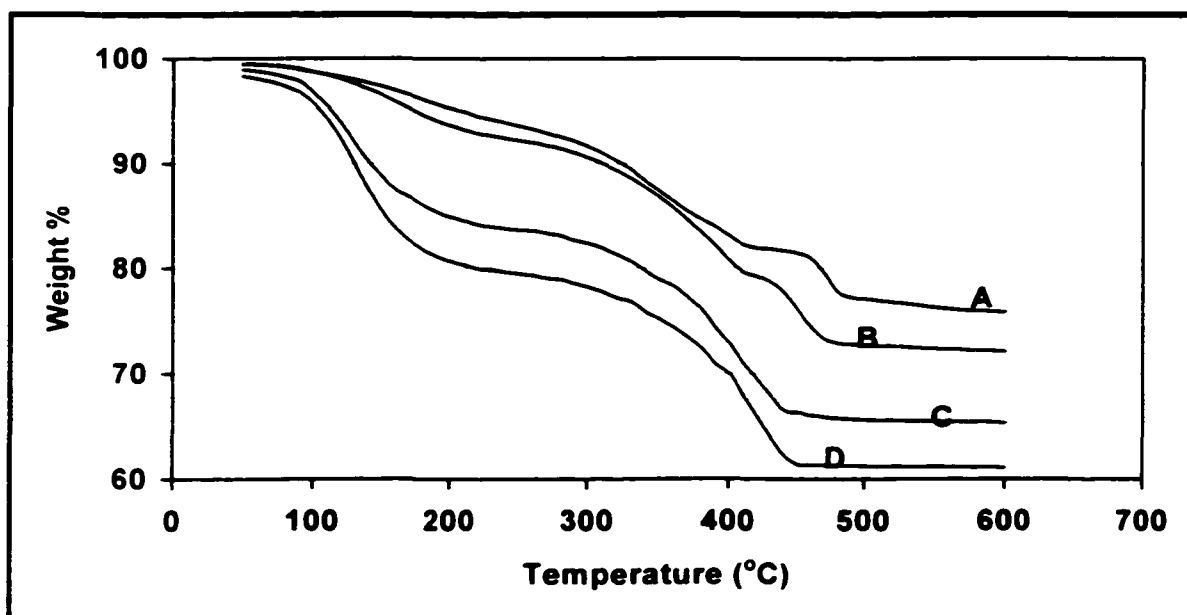


Figure 4.5.1.1: Weight loss of PMA spent catalyst at different Mo concentrations, A=500 ppm, B=1000 ppm, C=1500 ppm, D=3000 ppm

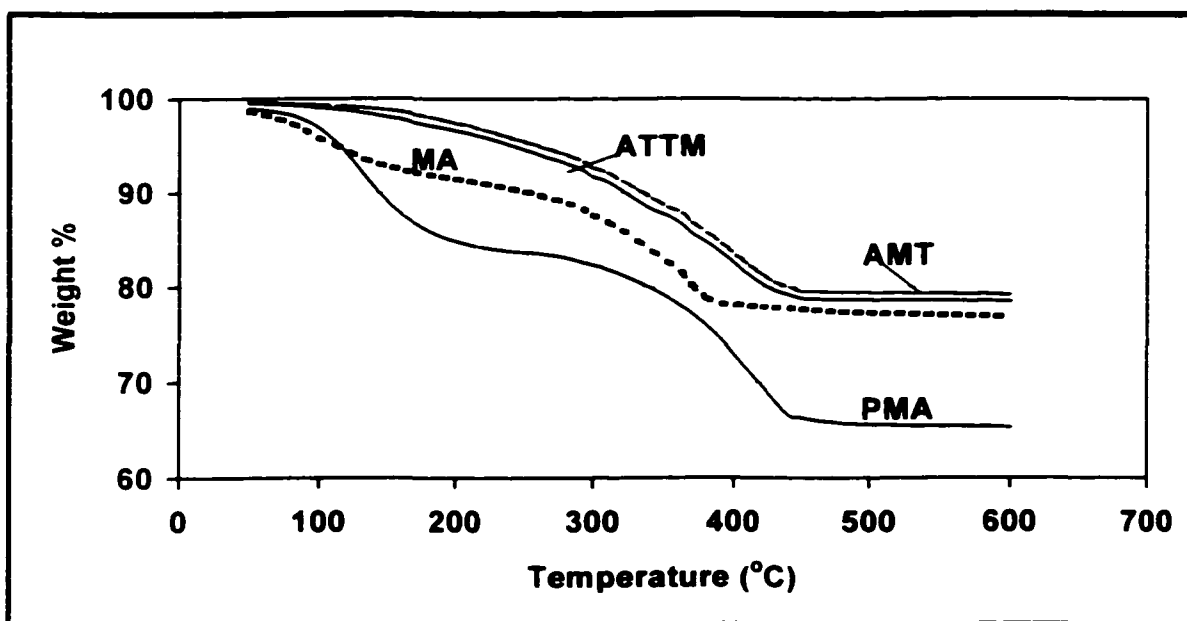


Figure 4.5.1.2: Weight loss for the different Mo spent catalysts

The differential thermogravimetric, (DTG), defined as a unit change in weight per unit temperature $d(\text{wt}\%)/d(^{\circ}\text{C})$, is plotted against increasing temperature. The DTG for solids determined from different concentrations of Mo, and for the different Mo catalysts are presented in Figure 4.5.1.3 and Figure 4.5.1.4 respectively. The DTG plot for the different concentrations show a significant initial weight loss in the range of 100-200 °C and a final weight loss in the range of 400-500°C for concentration C and D. with a maximum weight loss around 170 °C. For concentrations A and B a small weight loss is noticed. For the different types of catalysts, the DTG plot shows significant weight loss in the range of 100-250 °C for the PMA and the MA catalysts, but not for the ATTM and AMT. However, the temperature difference plots for the solids determined from runs with different concentrations and different Mo catalysts (see Figure 4.5.1.5 and Figure 4.5.1.6 respectively) indicate exothermic peaks in the range of 300-500 °C. This suggests most likely these losses are due to the CO₂ and MoS₂ oxidation, or burning off the traces of the model compounds used in the reaction system (BTH and NAPH).

The exothermic peaks are observed for concentration A and B in the range of 400-500 °C but less noticeable for concentration C and D in the same temperature range (see Figure 4.5.1.5). The exothermic peaks probably represent the oxidation of sulfur from MoS_x. The possible oxidation process occurring on the catalyst surface is the oxidation of MoS₂ to MoO₃, (see equation 4-1). A commercial grade MoS₂ is subjected to thermal analyses (TGA/DTA) to validate this decrease in weight, Figure 4.5.1.7 shows that the loss in weight occurs mainly at ~530 °C. Similar results have been observed by Siewe and Ng (1998).

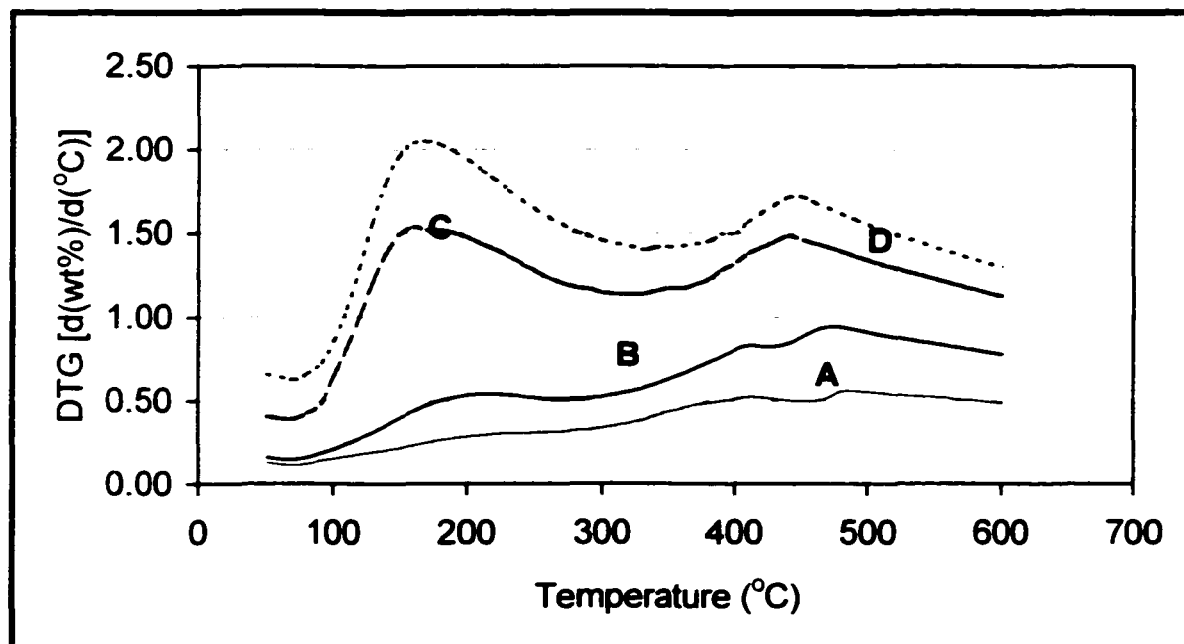


Figure 4.5.1.3: Differential changes in weight with temperatures (DTG) for PMA spent catalyst at different Mo concentrations, (A=500, B=1000, C=1500, D=3000)

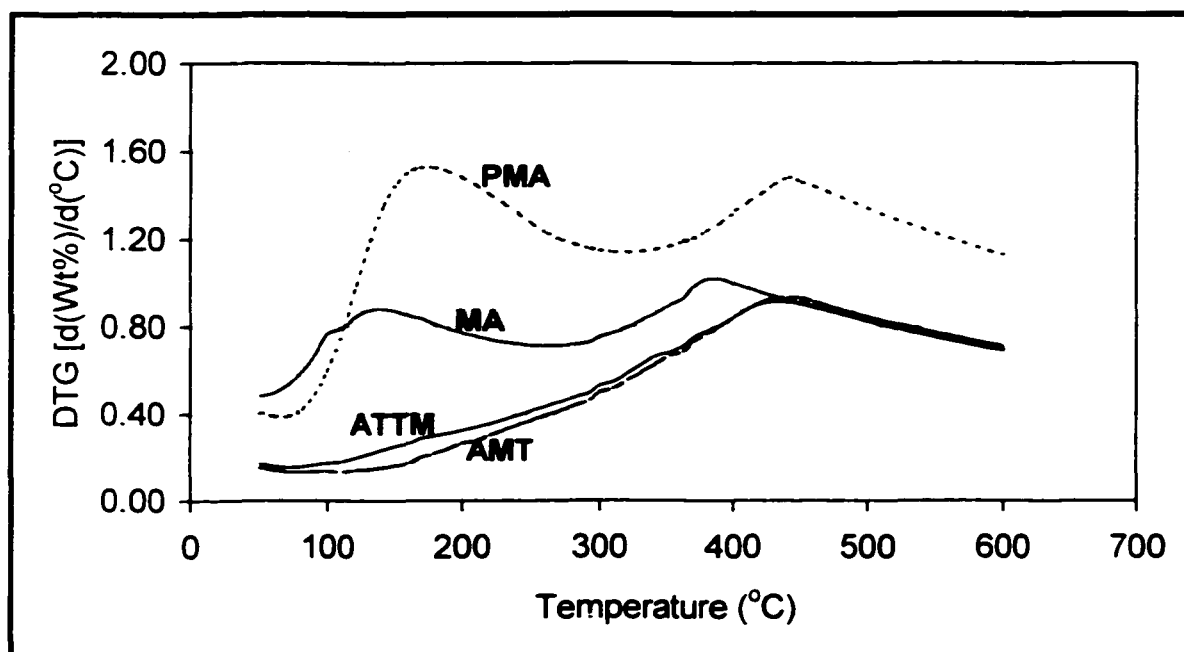


Figure 4.5.1.4: Differential changes in weight with temperatures (DTG) for different Mo spent catalysts

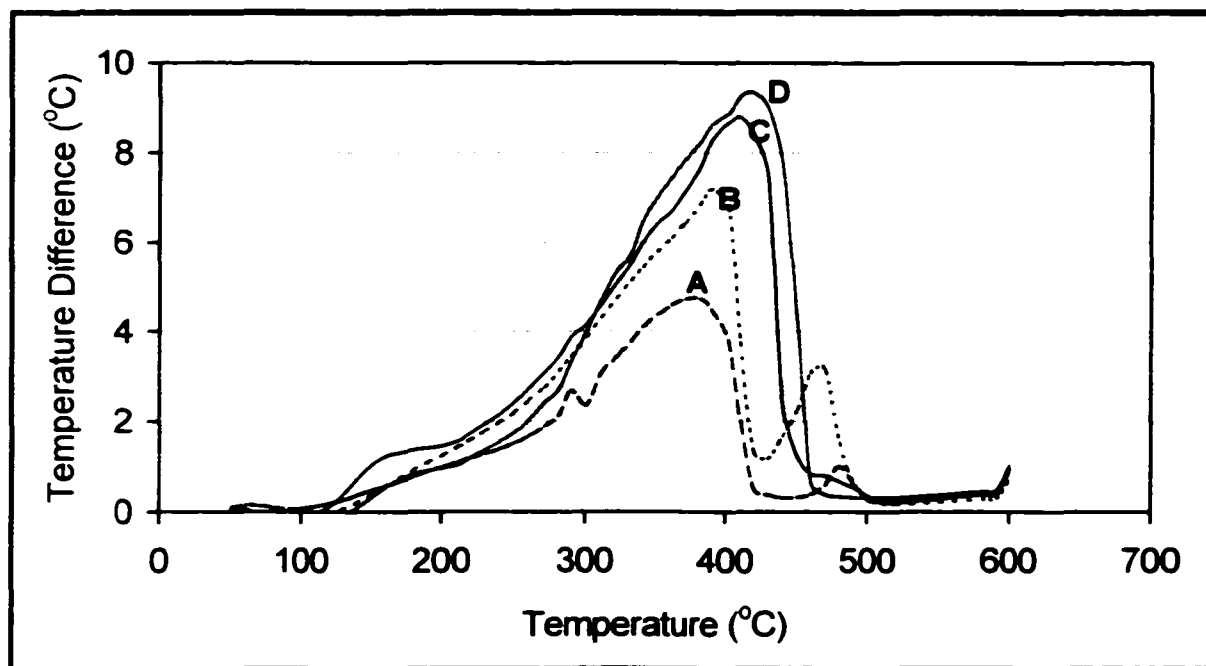


Figure 4.5.1.5: Temperature difference for different Mo concentrations of PMA spent catalysts with increasing temperature, (A=500,B=1000,C=1500.D=3000)

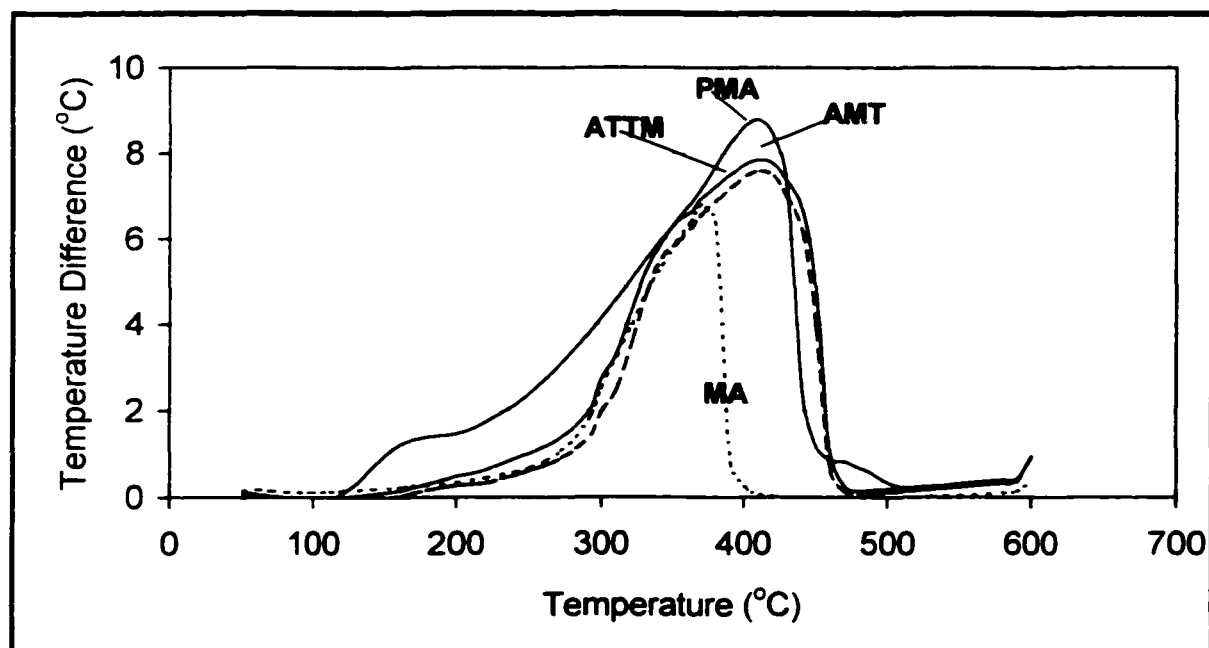


Figure 4.5.1.6: Temperature difference for different Mo spent catalysts with increasing temperatures

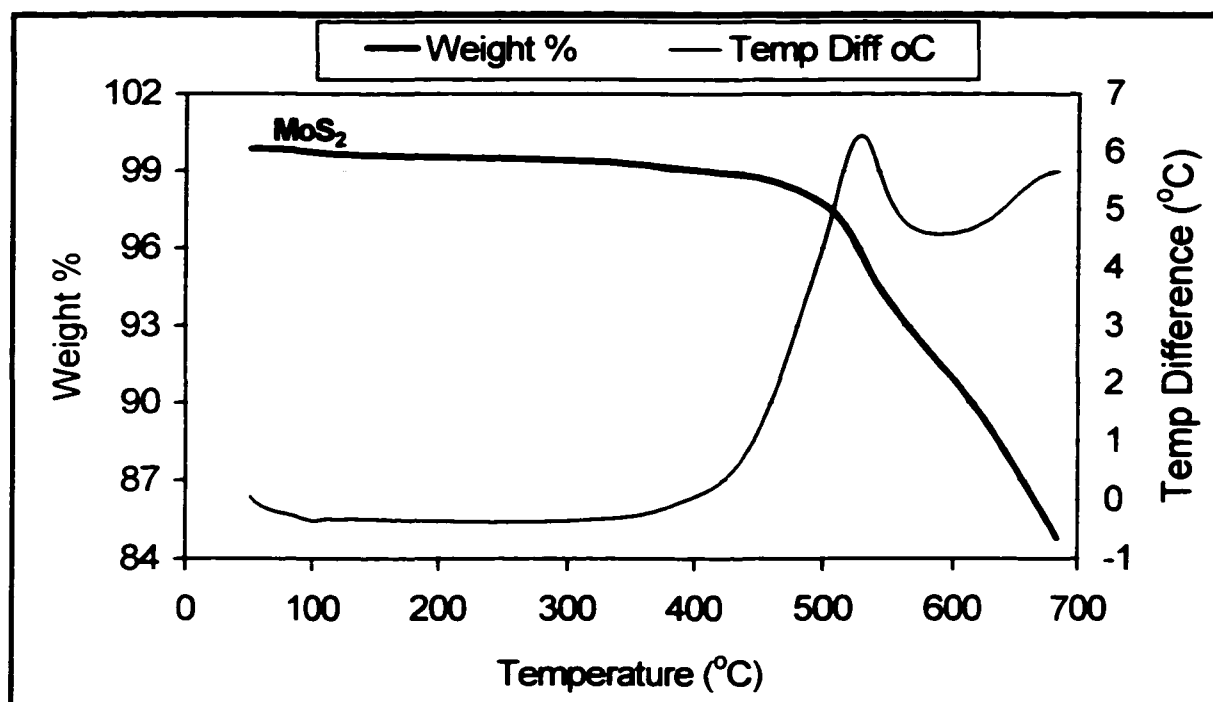


Figure 4.5.1.7: Weight loss and temperature differences for the commercial grade of MoS₂ with changing temperatures

4.5.2 X-Ray Diffraction Analysis (XRD)

The x-ray technique is used to identify the crystallographic phases that are present in the catalyst sample. As the x-ray beam strikes the sample surface at an angle (θ) and a wavelength of (λ) to satisfy the Bragg equation: (Niemantsverdriet, 1993)

$$\sin \theta = n\lambda / 2d \quad (4-2)$$

where, θ is the angle between the incoming x-ray and normal to the reflecting lattice plane, n is the integer called order of the reflection, λ is the wavelength of the x-ray beam, d is the distance between the two lattice planes.

X-ray diffraction spectra were obtained with a Siemens D500 diffractometer, and the test was performed in the range $2 - 80^\circ(2\theta)$. The XRD spectra for the fresh and spent (PMA, MA) catalysts are shown in Figure 4.5.2.1 and Figure 4.5.2.2 respectively. The fresh PMA and MA catalyst are showing amorphous crystallite phase predominantly MoO_3 , when compared to a commercial grade of MoO_3 as a reference, see Figure 4.5.2.3a. The spent PMA and MA dispersed catalyst are showing amorphous and undefined crystal structure with a disappearance for all peaks except for a distinctive peak which appear at an angle of $38.5^\circ (2\theta)$ for both PMA and MA. This may reflect the presence of MoO_3 . However, the possibility of existence of crystalline MoS_2 is very little compared to Figure 4.5.2.3b, except for a small peak appears at an angle of $14.7^\circ (2\theta)$ for

the spent PMA catalyst. It is interesting to note that the peak at an angle 14.7° (2θ) decreases as PMA concentration increases, suggesting that there is more crystalline MoS_2 formed at lower PMA concentration (Figure 4.5.2.4).

The XRD spectra of the fresh and spent (AMT, ATTM) dispersed catalysts are illustrated in Figure 4.5.2.5 and Figure 4.5.2.6 respectively. The fresh AMT is more amorphous than the ATTM. ATTM has the characteristic MoS_4^{2-} peak at an angle of $\sim 18^\circ$ (2θ), while AMT has the characteristic MoO_3 peak at an angle of 12.5° (2θ). The spent AMT and ATTM are very similar to the spent PMA and MA catalysts. The spent ATTM shows the disappearance of MoS_4^{2-} peak at an angle of 17° (2θ) and the appearance of MoS_2 peak at an angle of 14.7° (2θ), indicating the formation of the active MoS_2 species. Similarly, AMT showed the disappearance of MoO_3 peak at an angle of 12.7° (2θ) and the appearance of MoS_2 peak at an angle of 14.7° (2θ). This result is consistent with the results reported by Siewe and Ng (1998).

All the spent catalysts show similar XRD data. According to the HDS of BTH, all four catalysts provided 100% conversion of BTH while the PMA catalyst is slightly more active than the other catalysts for the hydrogenation of NAPH. This may be due to the presence of phosphorous (P) in PMA. More catalyst characterization is required to identify the active species involved in the reaction.

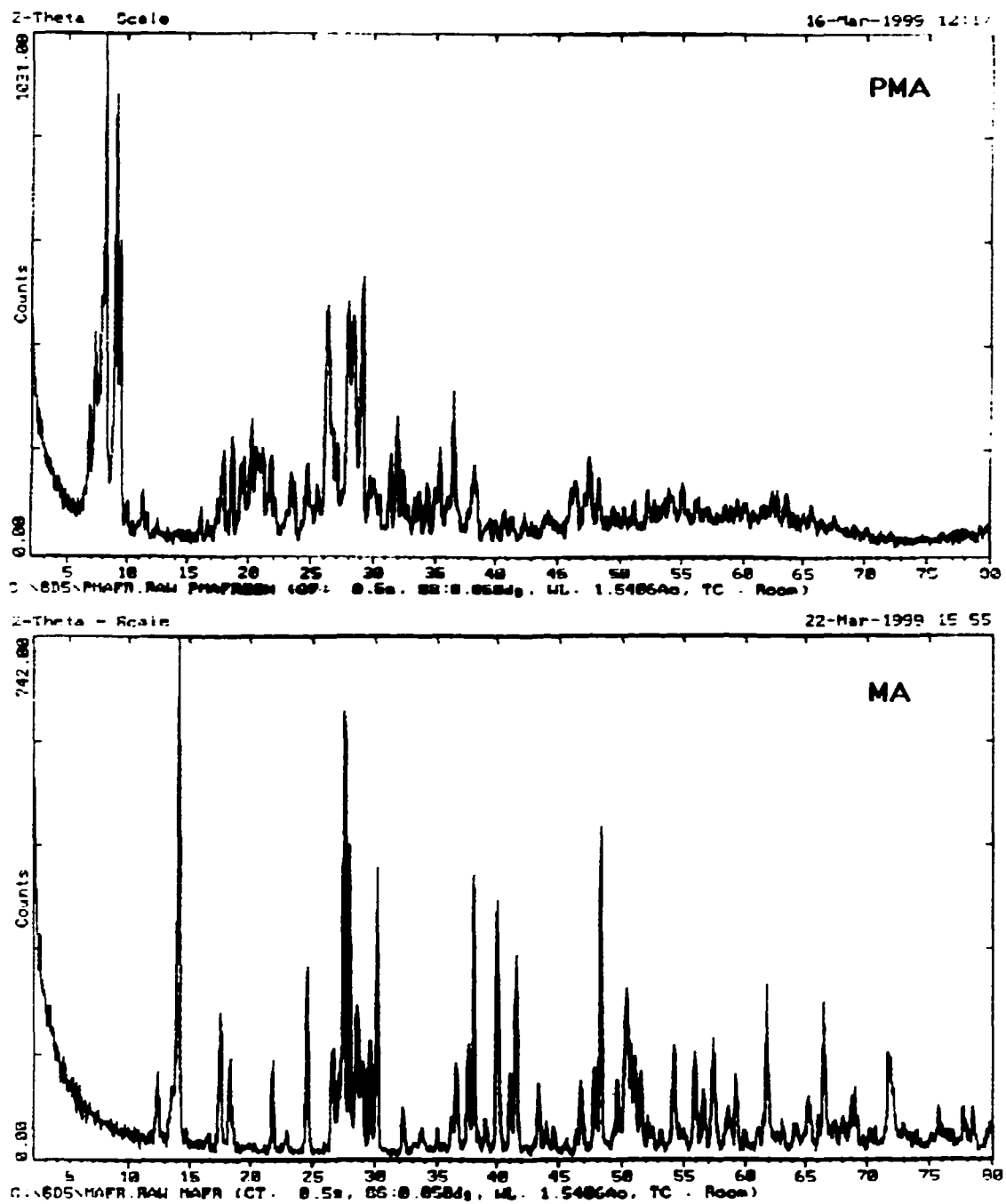


Figure 4.5.2.1: XRD spectra of fresh PMA and MA catalysts

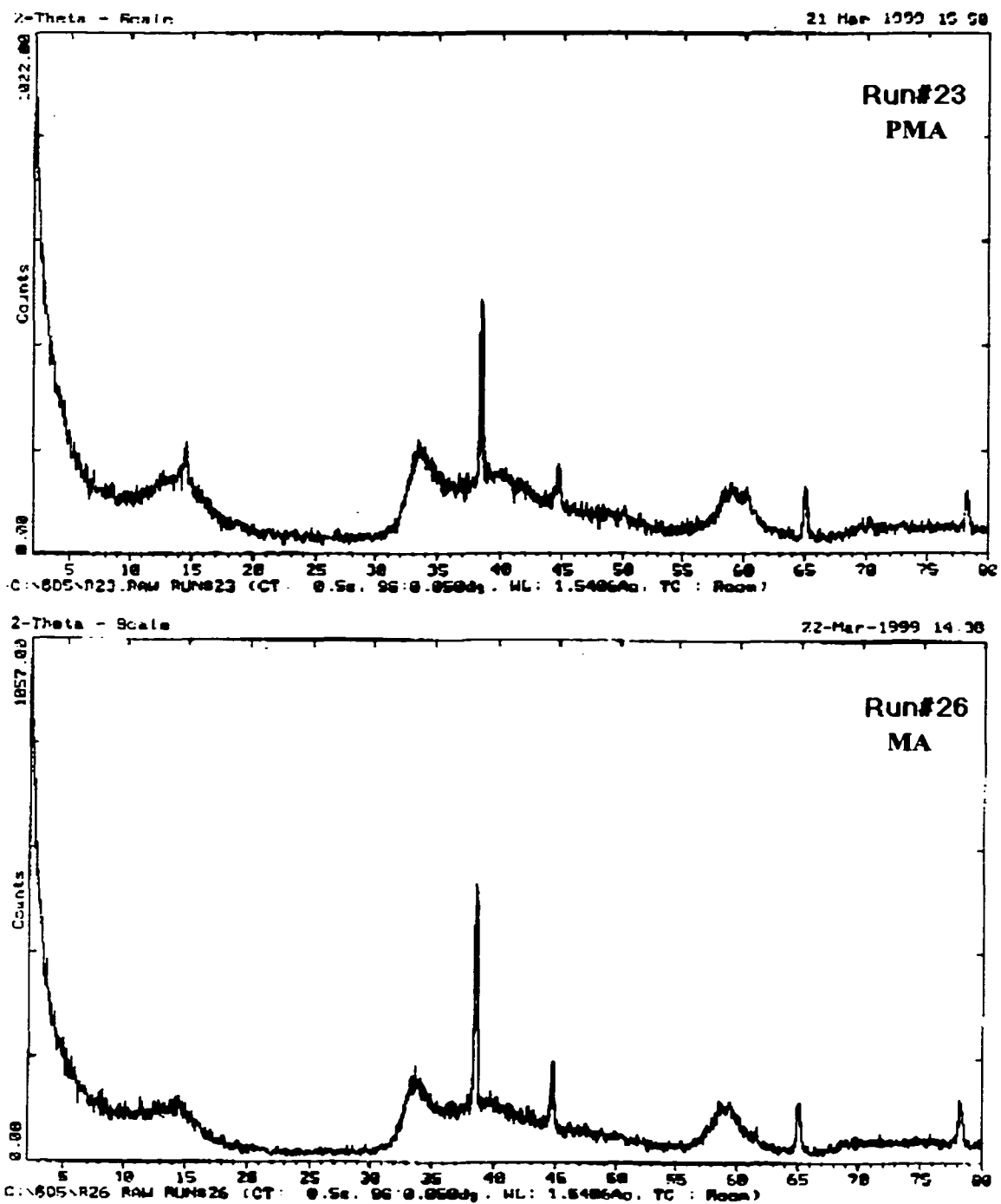


Figure 4.5.2: XRD spectra of spent PMA and MA catalysts from the reactions in CO/H₂S/H₂O medium of the binary mixture BTH+NAPH

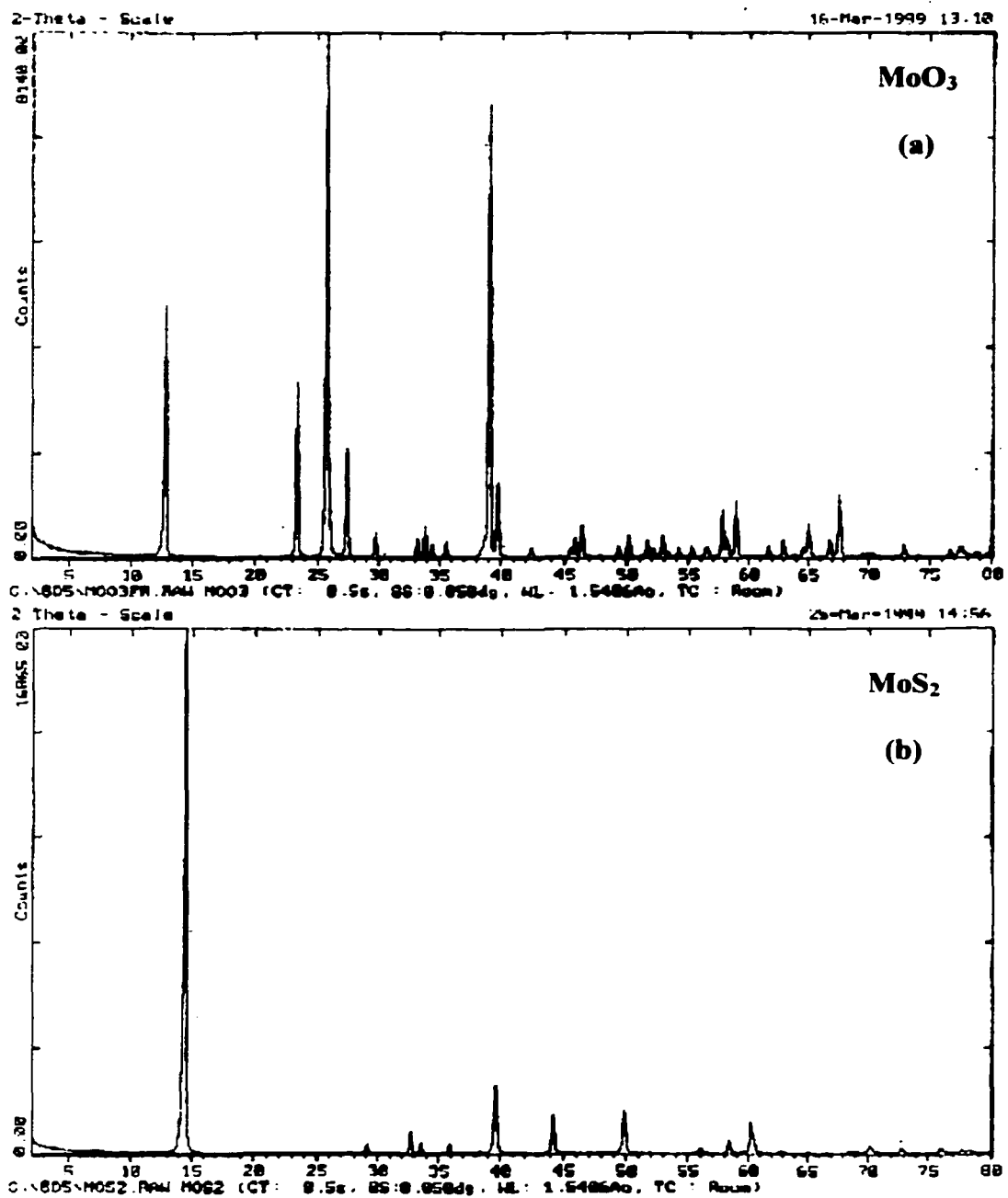


Figure 4.5.2.3: XRD spectra of commercial grade of MoO_3 and MoS_2

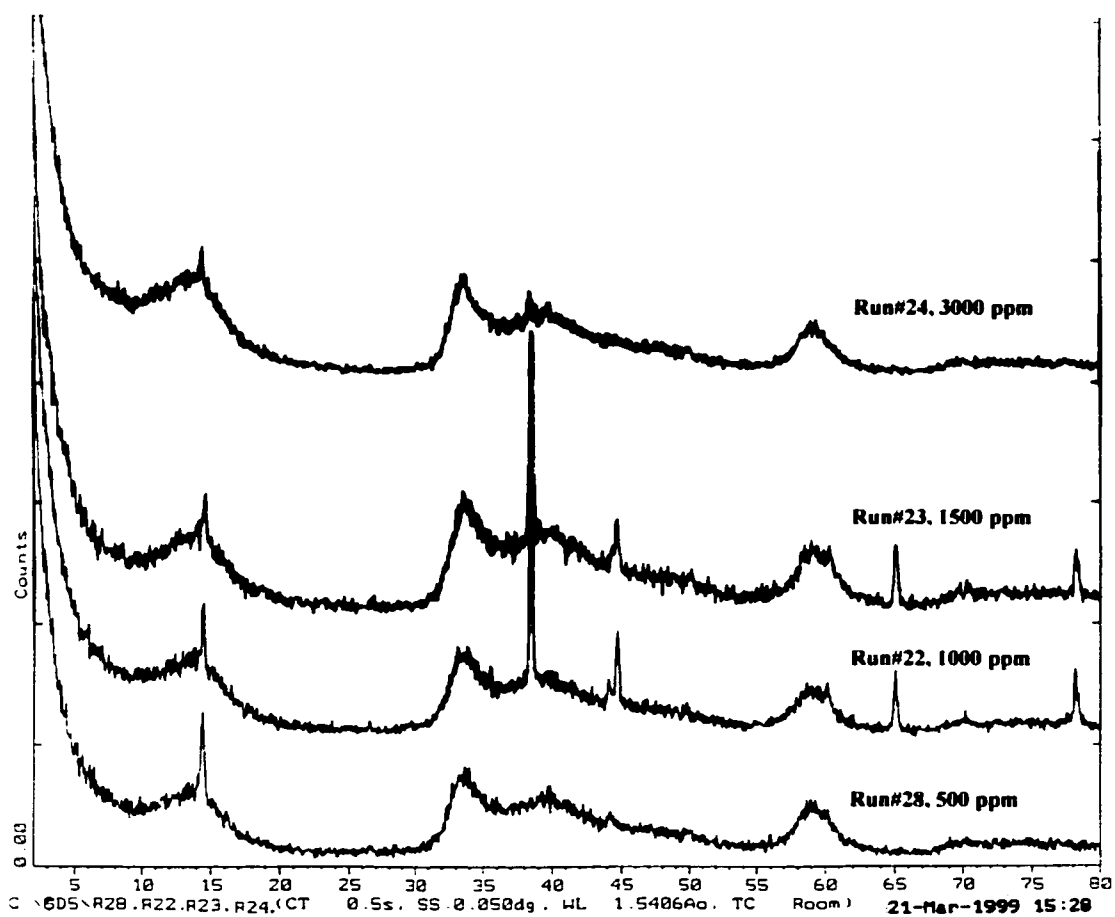


Figure 4.5.2.4: XRD spectra of spent PMA catalyst at different Mo concentration

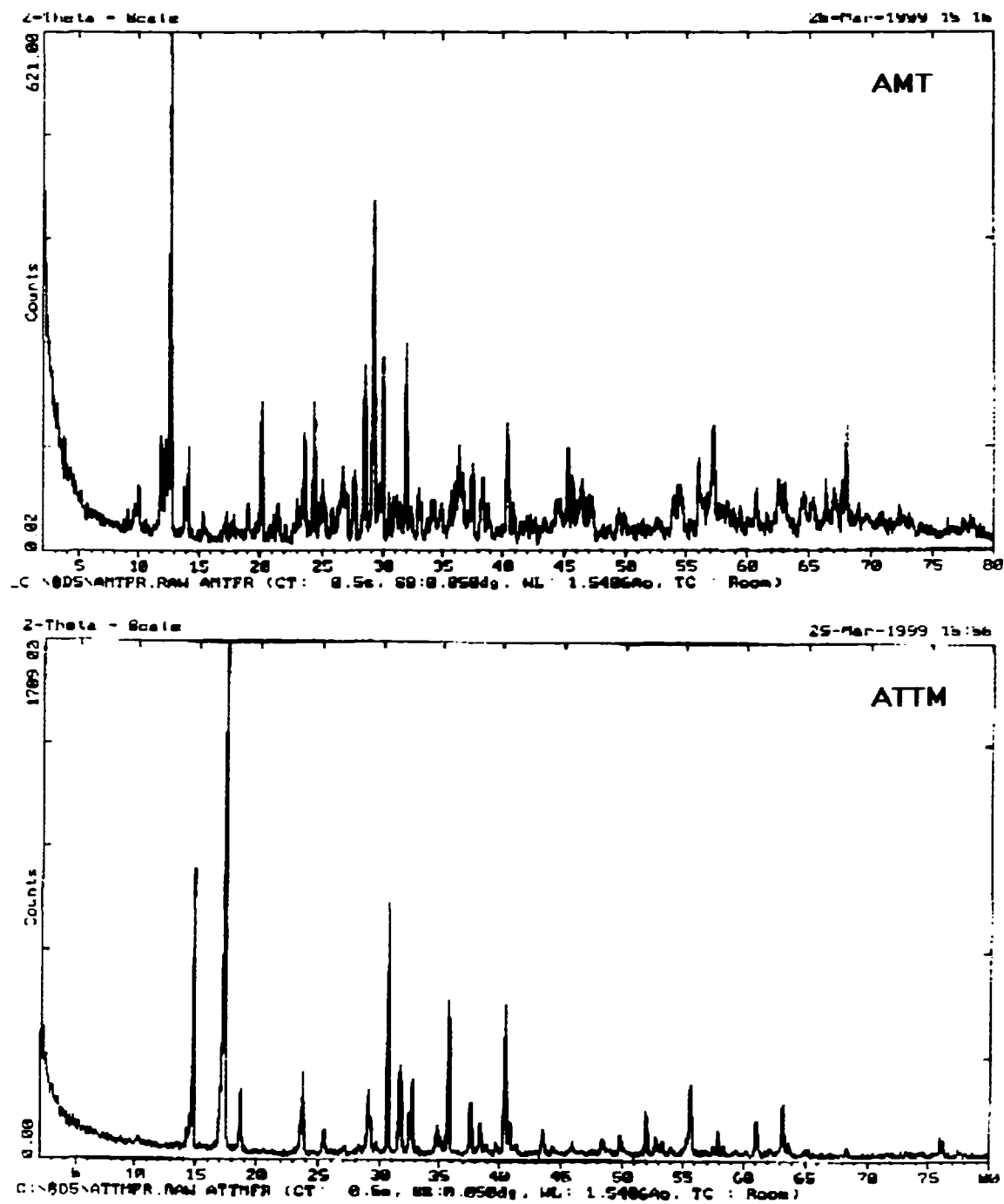


Figure 4.5.2.5: XRD spectra of fresh AMT and ATTM catalysts

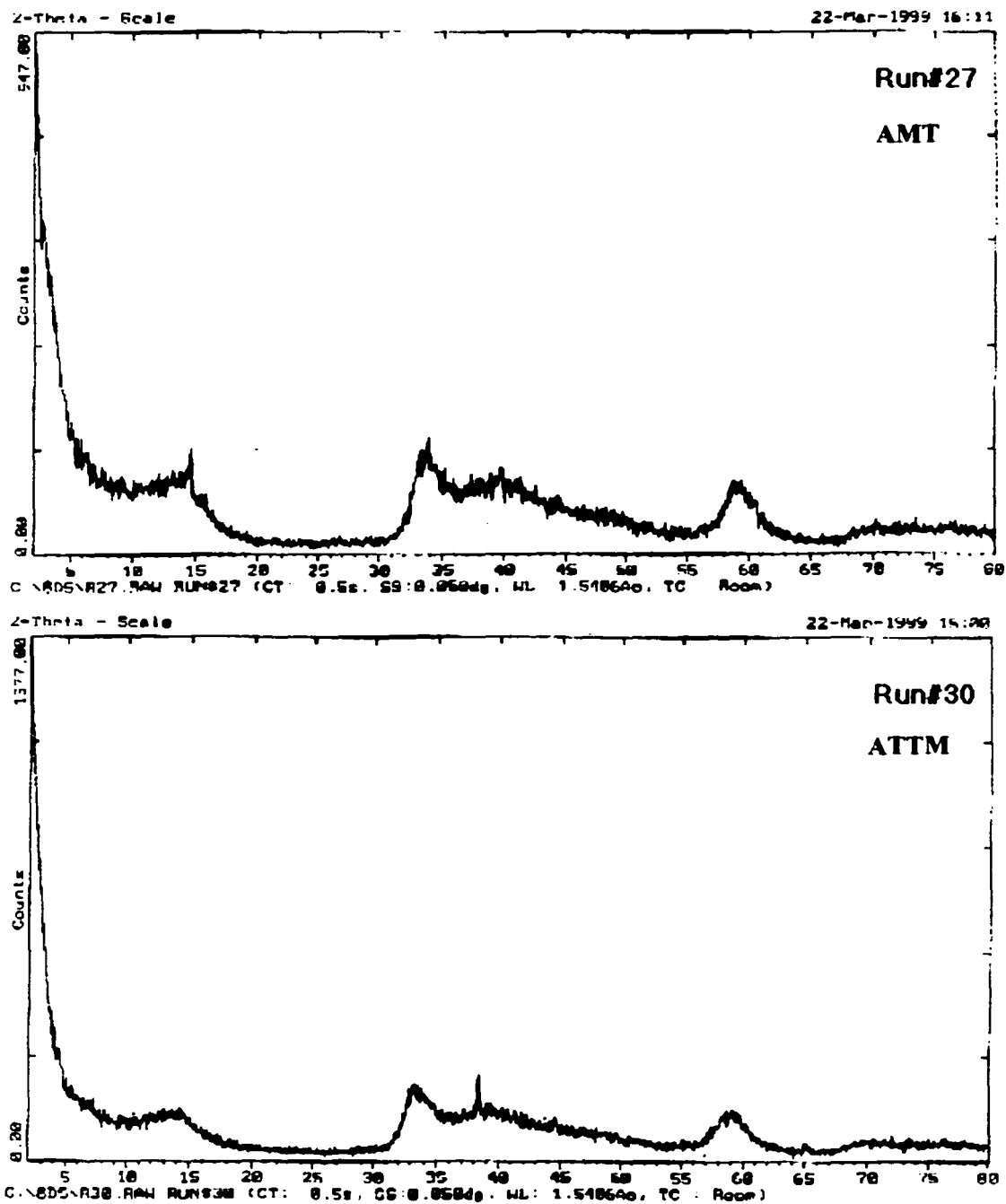


Figure 4.5.2.6: XRD spectra of spent AMT and ATTM catalysts from the reactions in CO/H₂S/H₂O medium of the binary mixture BTH+NAPH

Chapter 5

Conclusions and Recommendations

5.1 Conclusions

According to the objectives stated in Chapter 1, the results obtained in this study show that CO conversion is significantly affected by the initial loading of CO and the concentration of Mo. However, the CO conversion is not affected by changing the amounts of water due to the similar production of H₂. The hydrogen in situ generated via the WGSR is more effective than the externally supplied hydrogen at 600 psi initial loading.

The amount of H₂ generated in the system is in excess of that required for the complete desulfurization of BTH to ETHBZ, and to hydrogenate the NAPH to TET. CO conversions obtained for individual model compounds and for the binary

mixture in this study are essentially the same (92 - 94 %). This shows that the WGSR is not affected by whether one or two model compounds are used during the reaction.

For individual model compounds, BTH was completely desulfurized to ETHBZ through the DHBTH path way reaction with a 99.27 % conversion, and with a first order rate constant of $10.78 \times 10^{-4} \text{ s}^{-1}$. For the NAPH hydrogenation, TET is the primary product at 340°C with a NAPH conversion of 66.4 %, and a first order rate constant of $8.5 \times 10^{-5} \text{ s}^{-1}$.

However, when the binary mixture of (BTH + NAPH) is used under the same operating conditions, 100 % and 67.57 % conversions of the BTH and NAPH are obtained, respectively. It seems that NAPH and BTH are not inhibiting each other during the hydrogenation process, although at the initial part of the reaction there might be inhibition of the hydrogenation of NAPH by BTH.

Varying the Mo concentrations significantly affects the TET yield. Thus for the concentration of 3000 ppm Mo, an 82.33 % yield of TET is obtained, although it does not have an effect on the ETHBZ yield. In addition, the first order rate constant for BTH conversion is slightly lowered. The Mo dispersed catalysts (PMA, MA, AMT and ATTM) are effective for the WGSR but the pseudo first order constants for CO conversion are very similar. The reactivity of catalysts decreases as follows $\text{PMA} > \text{AMT} > \text{ATTM} \geq \text{MA}$ for the NAPH hydrogenation reaction. The PMA catalyst is more acidic according to the pH measurements and this probably accounts for the high activity of the Mo catalysts. Therefore the PMA catalyst is showing the highest hydrogenation activity (A_H) among the four catalysts.

Analysis of the aqueous layer for sulfate ions using ion chromatography reveals that a negligible amount of SO_4^{2-} is present. This confirms that the HDS reaction occurs through the hydrogenolysis of thiophene ring and not through the oxidation.

The analysis of the spent catalysts via thermogravimetric (TGA/DTA) and X-ray diffraction (XRD) confirms that the catalyst (ATTM, AMT, MA, and PMA) precursors are converted to a mixture of MoO_x and MoS_x species which are active for the WGSR, hydrodesulfurization and aromatic hydrogenation.

5.2 Recommendations

In order to achieve a higher degree of NAPH hydrogenation a study of the reaction of the binary mixture (BTH+NAPH) at a higher temperature and longer reaction time should be considered.

In addition a detailed study of the effect of adding the nitrogen model compound (e.g. quinoline) to the binary mixture would provide a good representative study of the hydrodesulfurization (HDS), aromatic hydrogenation (AHYD), and hydrodenitrogenation (HDN) reactions via the water gas shift reaction.

Optimizing new methods to increase catalyst activity like using a mixture of two catalysts are recommended. Further, more detailed characterization of the spent catalyst by studying particle and surface properties would provide useful information on the nature of the catalyst generated in situ during reaction.

Nomenclatures

AHYD	Aromatic hydrogenation
ATM	Ammoniumheptamolybdate tetrahydrate
ATTM	Ammoniumtetrathiomolybdate
BTH	Benzothiophene
CAA	Clear Air Act
CARB	California Air Resources Board
DCP	Direct Current Plasma
DEC	Decalin (cis,trans)
DHBTH	1,2 Dihydrobenzothiophene
DTA	Differential thermal analysis
DTG	Differential thermogravimetric
EPA	Environmental Protection Agency
ETHBZ	Ethylbenzene
FCC	Fluid catalytic cracking
GC	Gas chromatograph
HDN	Hydrodenitrogenation
HDS	Hydrodesulfurization
HPLC	High performance liquid chromatograph
IC	Ion chromatograph

MA	Molybdic acid
MD	Middle distillate
NAPH	Naphthalene
PMA	Phosphomolybdic acid
TET	Tetralin
TGA	Thermogravimetric analysis
TOL	Toluene
WGSR	Water gas shift reaction
XRD	X-ray diffraction

Conversions

Moles:	1000 mmol = 1 mol
Pressure:	psi = .06805 atm
	1 atm = 101,325 Pa (N/M ²)
	1 bar = 14.504 psi
Temperature:	T(°K) = T (°C) + 273.15
Time:	1 h = 60 min = 3600 s
Volume:	1000 ml = 1 L
Weight:	1000 mg = 1 g

BIBLIOGRAPHY

- Ali, S. A., Influence of Heteroatom Removal on Aromatic Hydrogenation, *Fuel Proc. Technol.*, 1998, **55**, 93
- Bergem, H., Blekken, E. A. and Holman, A., in Proceeding of the 1st International Symposium/6th European Workshop on Hydrotreating and Hydrocracking of Oil, 1997, Fractions, Oostende, Belgium, February 17-19, 391
- Bergem, H., Gitlesen, A., Holmen, A., Blekkan, E. A., Centi, G., Perathoner, S., Christiani, E., and Forzatti, P. (Ed), Environmental Catalysis. Proceedings of the 1st World Congress, Pisa (Italy), May 1-5 1995, 411
- Bohlbro, H., in An Investigation on the Kinetics of the Conversion of Carbon Monoxide with Water Vapor over Iron Oxide Based Catalysts, Gjellerup., Copenhagen. 1969
- Bordwell, F. G., Organic Chemistry, 1963, Macmillan, New York, Chap.15
- Bouchy, M., Dufresne, P. and Kasztelan, S., Hydrogenation and Hydrocracking of a Model Light Cycle Oil Feed . 1 Properties of Sulfided NiMo Hydrotreating Catalyst, *Ind. Eng. Chem. Res.*, 1992, **31**(12), 2661
- Brewster, R. Q., Organic Chemistry, 1953, Prentice-Hall, Engle-Wood Cliffs, NJ, Chap.31
- Broderick, D. H., Sapre, A. V., Gate, B. C. and Kwart, H., Hydrogenation of Aromatic Compounds Catalyzed by Sulfided CoO-MoO₃/γ-Al₂O₃ *J. Catal.*, 1982, **73**, 45
- Copper, B. H. and Donnis, B. B. L., Aromatic Saturation of Distillates: as overview *Appl. Catal.*, 1996, **137**, 203
- Corma, A., Martínez, A. and Martínez-Soria, V., Hydrogenation of Aromatics in diesel Fuels on Pt/MCM-41 Catalysts *J. Catal.*, 1997, **169**, 480
- Corma, A., Iglesias, M. and Sánchez, F., Hydrogenation of Aromatics under Mild Conditions on Transition Metal Complexes in Zeolites. A cooperative effect of molecular sieves, *Catal. Letters*, 1995, **32**, 313
- Curtis, C. W., Tsai, K. J. and Guin, J. A., Evaluation of Process Parameters for Combined Processing of Coal with Heavy Crudes and Residua, *Ind. Eng. Chem. Res.*, 1985, **24**, 1259

- Dutta, R. P. and Schobert, H. H., Hydrogenation / Dehydrogenation of Polycyclic Aromatic Hydrocarbons using Ammonium Tetrathiomolybdate as Catalyst Precursor, *Catal. Today*, 1996, **31**, 65
- Farag, H., Whitehurst, D. D. and Mochida, I., Synthesis of Active Hydrodesulfurization Carbon-Supported Co-Mo Catalysts. Relationships between Preparation Methods and Activity/Selectivity, *Ind. Eng. Chem. Res.*, 1998, **37**, 3533
- Farag, H., Sakanishi, K., Mochida, I., and Whitehurst, D. D., Kinetic Analyses and Inhibition by Naphthalene and H₂S in Hydrodesulfurization of 4,6-Dimethyldibenzothiophene (4,6-DMDBT) over CoMo-Based Carbon Catalyst, *Energy&Fuels*, 1999, **13**, 449
- Frost, A. A. and Pearson, R. G., Kinetics and Mechanism, 2nd edn, 1963, John Wiley Inc., United States of America. Ch.8, 185-189
- Frye, C. G., Equilibrium Hydrogenation of Polycyclic Aromatics, *Chem. Eng. Data*, 1962, **7**, 592
- Frye, C. G. and Weitkamp, A.W., Equilibrium Hydrogenations of Multi-Ring Aromatics, *Chem. Eng. Data*, 1969, **14**(3), 372
- Fujita, S. I., Usui, M. and Takezawa, N., Mechanism of the reverse Water-Gas Shift Reaction over Cu/ZnO Catalyst, *J. Catal.*, **134**, 220, 1992
- Gary, j. H., and Handwerk, G. E., Petroleum Refining Technology and Economics, 3rd edn, 1994, Marcel Dekker Inc., New York, 187
- Gates, B. C., Katzer, J. R. and Schuit, G. C. A., Chemistry of Catalysis Processes, 1979, McGraw-Hill, New York
- Ginés, M. J. L., Marchi, A. J. and Apesteguía, C. R., Kinetic Study of the Reverse Water-Gas Shift Reaction over CuO/ZnO/Al₂O₃ Catalysts, *Appl. Cata.*, 1997, **154**, 155
- Girgis, M. J., Gates, B. C., Reactivities, Reaction Networks, and Kinetics in High-Pressure Catalytic Hydroprocessing, *Ind. Eng. Chem. Res.*, 1991, **30**, 2021
- Gissy, H., Bartsch, R. and Tanielian, C., The Effect of the Feed Components on CoMo/Al₂O₃ Catalyst Activation, *J. Catal.*, 1980, **65**, 158
- Grange, P. and Vanhaeren, X., Hydrotreating Catalysts, an Old Story with New Challenges, *Catal. Today*, 1997, **36**, 375

- Grenoble D. C., Estadt, M. M. and Ollis, D. F., The Chemistry and Catalysis of the WGSR. 1. Kinetics over Supported Metal Catalysts, *J. Catal.*, 1981, **67**, 90
- Gully, A. J. and Balard, W. P., in Advances in Petroleum Chemistry and Refining, *J. J. McKetta, Jr.*, ed, Interscience Publishers, London, 1963, **7**, 241
- Gültekin, S., Ali, S. A. and Satterfield, C.N., Effect of Hydrogen Sulfide and Ammonia on Catalytic Hydrogenation of Propylbenzene, *Ind. Eng. Chem. Process Des. Dev.*, 1984, **23**, 179
- Halachev, T., Atanasova, P., Lopez Agudo, A., Arias, M. G. and Ramirez, J., Activity of P-Ni-W/Al₂O₃ Catalysts with Varying Phosphorous content in the Hydrogenation of Naphthalene, *Appl. Catal.*, 1996, **136**, 161
- Halachev, T., Nava, R. and Dimitrov, L., Catalytic activity of (P)NiMo/Ti-HMS and (P)NiW/Ti-HMS Catalysts in the Hydrogenation of Naphthalene *Appl. Catal.*, **169**, 1998, 111
- Hook, B. D. and Akgerman, A., Desulfurization of Dibenzothiophene by in Situ Hydrogen Generation through a Water Gas Shift Reaction, *Ind. Eng. Chem. Process Des. Dev.*, 1986, **25**, 278
- Hooper, R. J., Battaerd, H. A. J. and Evans, D. G., Thermal Dissociation of Tetralin Between 300 and 450 °C, *FUEL*, 1979, **58**, 132
- Hou, P., Meeker, D. and Wise, H., Kinetics Studies With a Sulfur-Tolerant Water Gas Shift Catalyst, *J. Catal.*, 1983, **80**, 280
- Houalla, M., Nag, N. K., Sapre, A. V., Broderick, D. H. and Gates, B. C., Hydrodesulfurization of Dibenzothiophene Catalyzed by Sulfided CoO-MoO₃/γ-Al₂O₃: The Reaction Network, *AIChE. J.*, 1978, **24**, 1015
- Huang, T. and Kang, B., The hydrogenation of Naphthalene with Platinum/Alumina-Aluminum Phosphate Catalysts, *Ind. Eng. Chem. Res.*, 1995, **34**, 2955
- Huang, T. and Kang, B., Kinetic study of Naphthalene Hydrogenation over Pt/Al₂O₃ Catalyst, *Ind. Eng. Chem. Res.*, 1995a, **34**, 1140
- Huang, T. and Kang, B., Naphthalene Hydrogenation over Pt/Al₂O₃ Catalyst in a Trickle Bed Reactor, *Ind. Eng. Chem. Res.*, 1995b, **34**, 2349
- Jaffe, S. B., Kinetics of Heat Release in Petroleum Hydrogenation, *Ind. Eng. Chem. Proc. Res. Dev.*, 1974, **13**(1), 34

- Joo, H. S. and Guin, J. A., Activity of Noble Metal-Promoted Hydroprocessing Catalysts for Pyridine HDN and Naphthalene Hydrogenation, *Fuel Proc. Technol.*, 1996, **49**, 137
- Kang, H. C., Mauldon, C. H., Cole, T., Slegeir, W., Cann, K. and Pettit, R., Reduction with Carbon Monoxide and Water in place of Hydrogen, *J. Am. Chem. Soc.*, 1977, **99**, 8323
- Keiski, R. L., Salmi, T., Niemistö, P., Ainassaari, J. and Pohjola, V. J., Stationary and Transition Kinetics of the High Temperature Water-Gas Shift reaction, *Appl. Catal.* 1996, **137**, 349
- Khan, M. R., and Reynolds, J. G., Formulating a Response to the Clear Air Act, *ACS CHEMTECH*, 1996, June, 56
- Kim, H. and Curtis, C. W., Reaction Pathways of Model Coprocessing Systems Using Molybdenum Naphthenate and Excess Sulfur, *Energy & Fuels*, 1990a, **4**, 206
- Kim, H. and Curtis, C. W., Interactive Chemistry of Coal-Oil Reactions Using Model Systems, *Energy & Fuels*, 1990b, **4**, 214
- Kimbara, N. and Charland, J., Hydrogenation of Aromatics in Synthetic Crude Distillates Catalyzed by Platinum Supported in Molecular Sieves *Ind. Eng. Chem. Res.*, 1996, **35**, 3874
- King, A. D., King, R. B. and Yong, D. B., Homogenous Catalysis of the Water Gas Shift Reaction with the use of Group 6 Transition Metal Carbonyls, *J. Am. Chem. Soc.*, 1981, **103**, 2699
- King, R. B., Frazier, C. C., Haines, R. M. and King, A. D., Active Homogeneous Catalysts for the WGS derived from the Simple Mononuclear Carbonyls of Iron, Chromium, Molybdenum and Tungsten, *J. Am. Chem. Soc.*, 1978, **100**, 2925
- Kotanigawa, T., Yamamoto, M. and Yoshida, T., Selective Nuclear Hydrogenation of Naphthalene, Anthracene and Coal-derived Oil over Ru Supported on Mixed Oxide, *Appl. Catal.*, 1997, **64**, 323
- Kuijpers, E. G. M., Tjepkema, R. B. and Van der wal, W. j. j., Structure-Sensitivity of the Water-Gas Shift Reaction over Highly Active Cu/SiO₂ Catalysts, *Appl. Catal.*, 1986, **25**, 139

- Kumar, M., Akgerman, A., and Anthony, R. G., Desulfurization by in Situ Hydrogen Generation through Water Gas Shift Reaction . *Ind. Eng. Chem. Process Des. Dev.*, 1994, **23**, 88
- Laine, R. M. and Crawford, E. J., Homogeneous Catalysis of the Water-Gas Shift Reaction, *J. Molecular Catal.*, 1988, **44**, 357
- Lee, H. C. and Butt, J. B., Kinetics of the Desulfurization of Thiophene: Reaction of Thiophene and Butene, *J. Catal.*, 1977, **49**, 320
- Leglise, J., Gestel, J. N., Finot, L., Duchet, J. C., and Dubois, J. L., Kinetics of Sulfur Model Molecules Competing with H₂S as a tool for Evaluating the HDS Activities of Commercial CoMo/Al₂O₃, *Catal. Today*, 1998, **45**, 347
- Li, S. and Lee, J. S., Molybdenum Nitride and Carbide Prepared from Heteropolyacid.III-Hydrodesulfurization of Benzothiophene, *J Catal.*, 1998, **178**, 119
- Lin, S. D. and Song, C., Noble Metal Catalysts for Low-Temperature Naphthalene Hydrogenation in the presence of Benzothiophene *Catal. Today*, 1996, **31**, 93
- Lo, H. S., Kinetic Modeling of Hydrotreating, *PhD. Dissertation*, University of Delaware, Newark, 1981
- Lucien, J. P., Van den Berg, J. P., Germaine, G., Van Hooijdonk, H.M.J.H., Gjers, M., and Thielemans, G.L.B., in M.C. Oballa and S.S. Shih (ed), Catalytic Hydroprocessing of Petroleum and Distillates: Proceedings of the AIChE Spring National Meeting, Houston, Texas, March28-April 1, 1993, Marcel Dekker, Inc., NewYork, 291
- Marnot, P.A., Ruppert, R. R., and Sauvage, J. P., Catalysis of the WGSR by Complexes of Rhodium and Iridium with 2,2-Bipyridine and Similar Ligands, *Nouv. J. Chem.*, 1981, **5**, 543.
- Massoth, F. E., Kim, C. S. and Cui, J-W., Studies of Molybdena-Alumina Catalysts, XVII. Sulfided Catalysts Exposed to Air, *Appl. Catal.*, 1990, **58**, 199
- Mhaouer, M., Lemberton, J.L., and Pérot, G., Hydrogenation of Tetralin on Sulfided Ruthenium on KY Zeolite Catalyst. Effect of Sulfidation Method, *Catal. Today*, 1996, **29**, 241
- Milad, I. K., Kinetic Study of Catalytic Desulfurization in an Emulsion Via in Situ H₂ Generation, *MASc. Thesis*, 1994, University of Waterloo

- Moe, J. M., Low Temperature CO Conversion, *Chem. Eng. Prog.*, 1962, **58**, 33
- Nag, N. K., Sapre, A. V., Broderick, D. H. and Gates, B. C., Hydrodesulfurization of Polycyclic Aromatics Catalyzed by Sulfided CoO-MoO₃/γ-Al₂O₃: The Relative Reactivities, *J. Catal.*, 1979, **57**, 509
- Nakamura, J., Campbell, J. M. and Campbell, C. T., Kinetics and Mechanism of the Water Gas Shift Reaction Catalyzed by the Clean and Cs-Promoted Cu(110) Surface: A Comparison with Cu(111), *J. Chem. Soc. Faraday Trans.*, 1990, **86**(15), 2725
- Nanaka, O., Tanaka, Y., Kodama, S. and Hagiwara, T., in Proceeding of the 216th National meeting of Symposium on Chemistry of Diesel Fuels, 1998, ACS, Boston, MA, August 23-27, 531
- Newsome, D. S., The Water Gas Shift Reaction *Catal. Rev. Sci. Eng.*, 1980, **21**(2), 275
- Ng, F. T. and Rintjema, R. T., Catalytic Desulfurization of Heavy Oil Emulsions, *Stud. Surf. Sci. Catal.*, Elsevier, 1992, Amsterdam, Ed. Delmon, B., 51
- Ng, F. T. and Tsakiri, S. K., Activation of Water in Emulsion for Catalytic Desulfurization of Benzothiophene, *FUEL*, 1992, **71**, 1309
- Niemantsverdriet, J. W., Spectroscopy in Catalysis an Introduction, 1993, VCH, NY, 6, 138
- Nikanjam, M., Development of the first CARB Certified Alternative Diesel Fuel, Society of Automotive engineers, 1993, paper No. H930728, Warrendale, PA
- Oki, S., Happel, j., Hnatow, M. and Kaneko, Y., Proceedings of the 5th International Congress on Catalysis, 1973, 1, Hightower, J. ed, 173
- Ramanathan, S. and Oyama, S.T., New Catalysts for Hydroprocessing: Transition Metal Carbides and Nitrides, *J. Phys. Chem.*, 1995, **99**, 16365
- Reid, R. C., Prausnitz, J. M. and Poling, B. E., The properties of Gases & Liquids, 4th. 1987, McGraw-hill Book Co., Toronto
- Reyes, J. C., Borja, M. A., Cordero, R. L. and Agudo, A. L., Influence of Phosphorus on the Structure and the Hydrodesulfurization and Hydrodenitrogenation Activity of W/Al₂O₃ Catalysts, *Appl. Catal.*, 1994, **120**, 147

- Rintijema, R. T., Hydrodesulfurization of Benzothiophene Emulsions Through In Situ Hydrogen Generation. MSc. Thesis, 1992, University of Waterloo
- Rollmann, L. D., Catalytic Hydrogenation of Model Nitrogen, Sulfur, and Oxygen Compounds, *J. Catal.*, 1977, **46**, 243
- Sapre, A. V. and Gates, B. C., Hydrogenation of Aromatic Hydrocarbons Catalyzed by Sulfided CoO-MoO₃/γ-Al₂O₃. Reactivities and Reaction Networks, *Ind. Eng. Chem. Proc. Res. Dev.*, 1981, **20**, 68
- Schmitz, A. D., Bowers, G. and Song, C., Shape-Selective Hydrogenation of Naphthalene over Zeolite-Supported Pt and Pd catalysts, *Catal. Today*, 1996, **31**, 45
- Shaheen, E. I., Catalytic Processing in Petroleum Refining, 1983, PennWell Co., Oklahoma, 5
- Shchibrya, G., Morozov, N. and Temkin, M., Kinetics and Mechanism of the Catalytic Reaction of the CO with Water vapor. II. Reaction of Zinc-Chromium -Copper Oxide Catalyst, *Kinet. Katal.*, 1965, **6**, 1010.
- Shi, L., Tin, K. C., Wong, N. B., Wu, X. Z. and Li, C. L., Kinetics and Mechanism of Benzothiophene Hydrodesulfurization over NiO-MoO/γ-Al₂O₃ Commercial Catalyst, *Fuel Science And Tech. Int'l*, 1996, **14**(6), 767
- Siewe, C. N. and Ng, F. T., Hydrodesulfurization of Cold Lake Diesel Fraction Using Disperesed Catalysts: Influence of Hydroprocessing Medium and Sources of H₂, *Energy & Fuels*, 1998, **12**, 598
- Song, C. and Schmitz, A., Zeolite-Supported Pd and Pt Catalysts for Low-Temperature Hydrogenation of Naphthalene in the Absence and Presence of Benzothiophene, *Energy & Fuels*, 1997, **11**, 656
- Speight, J.G., The chemistry and technology of petroleum, 1991, 2^{cd} edn, vol. 4. Ch 7 and Ch 12. Marcel Dekker Inc., New York
- Speight, J. G., The Desulfurizaation of Heavy Oils and Residua, 1981. Marcel Dekker, New York
- Stenberg, V. I., Raman, K., Srinivas, V. R., Baltisberger, R. J. and Woolsey, N. F., H₂S as Promoter for WGSR, *Angew. Chem. Int. Ed. Engl.*, 1982, **21**, 619

- Takemura, Y., Itoh, H. and Ouchi, K., Catalytic Hydrodesulfurization of Residual Oil by a Mixture of Carbon Monoxide and Water, *J. Japan Petrol. Inst.*, 1981, **24**(6), 357
- Van Parijs, I. A. and Froment, G. F., Kinetics of Hydrodesulfurization on a Co-Mo/ γ -Al₂O₃ Catalyst. 1. Kinetics of the Hydrogenolysis of Thiophene, *Ind. Eng. Chem. Prod. Res. Dev.*, 1986a, **25**, 431
- Van Parijs, I. A., Hosten, L. H. and Forment, G. F., Kinetics of Hydrodesulfurization on a Co-Mo/ γ -Al₂O₃ Catalyst. 2. Kinetics of the Hydrogenolysis of Benzothiophene, *Ind. Eng. Chem. Prod. Res. Dev.*, 1986b, **25**, 437
- Vrinat, M. L., The kinetics of the Hydrodesulfurization Process: A Review, *Appl. Catal.*, 1983, **6**, 137
- Welters, W. J. J., de Beer, V. H. J. and van Santen, R. A., Influence of Zeolite on Thiophene Hydrodesulfurization Activity, *Appl. Catal.*, 1994, **119**, 253
- Wilson, M. A., Foster, N. R., Vaughan, J., Quezada, R. and Cosstick, R., *Fuel Proc. Technol.*, 1982, **5**, 267
- Xue, E., O'Keefe, M. and Ross, J. R. H., Water gas Shift Conversion using with a Low Steam to Carbon Monoxide Ratio and Containing Sulfur, *Catal. Today*, 1996, **30**, 107
- Yoshida, T., Matsuda, T., Okano, T. Kitani, T. and Otsuka, S., Activation of Water Molecule 2. Generation of Strong Hydroxo Bases by the Reaction of Water with Platinum(0) Phosphine Complexes and the Application as Catalysts for H-D Exchange and Hydration Reaction, *J. Am. Chem. Soc.*, 1979, **101**, 2027.
- Yue, Y., Sun, Y. and Gao, Z., Disordered Mesoporous KIT-1 as a Support for Hydrodesulfurization catalysts, *Catal. Letters*, 1997, **47**, 167
- Yumoto, M., Kukes, S. G., Klein, M. T. and Gates, B. C., Hydrodesulfurization and Hydrogenation of Aromatic Compounds Catalyzed by Ni-Mo/ γ -Al₂O₃: Effects of Nickel Sulfide and Vanadium Sulfide Deposits, *Catal. Letters*, 1994, **26**, 1
- Yumoto, M., Kukes, S.G., Klein, K. T. and Gates, B.C., Catalytic Hydroprocessing of Aromatic Compounds: Effects of Nickel and Vanadium Sulfide Deposits on Reactivities and Reaction Networks, *Ind. Eng. Chem. Res.*, 1996, **35**, 3203
- Zhan, X. and Guin, J. A., High-Pressure Hydrogenation of Naphthalene Using a Reduced Iron Catalyst, *Energy & Fuels*, 1994, **8**, 1384

Appendix A

Experimental Methods and Preparation Procedures

A.1 Steps of Loading, Sealing and Leak testing the Reactor

- 1- After the AE batch reactor was cleaned with toluene reagent the feed was prepared and charged into the reactor.
- 2- The main nut of the closure assembly was sprayed with molycot lubricant to ensure good performance.
- 3- The closure was assembled by tightening the main nut into position so that the gland retaining ring locks over the three holes above the locknut.
- 4- The eight screws were tightened by hand with a hex key, and then the screws were sealed with a torque wrench to 32 ft-lbs, torque in a 10 ft-lbs, increments.
- 5- The nitrogen gas was introduced into the line to purge any gases from previous runs, and to eliminate any traces of oxygen.
- 6- Then the reactor pressurized with nitrogen to 1500 - 2000 psi, leak was tested with a SNOOP solution. If a leak was detected the reactor was depressurized, and the problem rectified.

Appendix A.2 Catalyst Solution Preparation

To prepare the different concentrations of the catalyst solutions (e. g., PMA catalyst), the

molecular formula is as follows: $12 \text{ MoO}_3 \cdot \text{H}_3\text{PO}_4 \cdot \text{XH}_2\text{O}$

M wt = 1825.24 g/gmol

Weight of PMA catalyst = 8 g

Weight of deionized H_2O = 142 g

Total weight of the catalyst solution = 150 g

The weight of Mo in the prepared catalyst solution is:

8 g PMA	1 mol PMA	12 mol Mo	95.94 g Mo
150 g catalyst solution	1825.24 g PMA	1 mol PMA	1 mol Mo

\therefore 1 g catalyst solution = 0.0322 g Mo

\therefore 1 g catalyst solution = 0.0533 g PMA

Therefore,

$$\text{Mo, ppm} = \frac{\text{Weight of Mo in catalyst solution (g)}}{\text{Total weight of loaded solution in reactor system (g)}}$$

The calculations were carried out by the use of the Excel worksheet; the results are listed in Table A.2.1. The same procedure was done for the MA, and the AMT catalysis results are listed in Table A.2.2 and Table A.2.3.

Table A.2.1: The different values of the Mo concentration for the PMA catalyst

.0533 g (PMA)/ g(sol)		8 g PMA			
(BTH+NAPH) Mix		150 g sol			
PMA cat sol (g)	g (PMA)	H₂O g	H₂O Loaded g	g (Mo)	ppm [Mo]
1.00	0.0533	0.9467	69.0533	0.0336	111.9572
2.00	0.1066	1.8934	68.1066	0.0673	223.8746
3.00	0.1599	2.8401	67.1599	0.1009	335.7523
4.00	0.2132	3.7868	66.2132	0.1345	447.5904
4.30	0.2292	4.0708	65.9292	0.1446	481.1341
4.35	0.2319	4.1181	65.8819	0.1463	486.7243
4.40	0.2345	4.1655	65.8345	0.1480	492.3145
4.45	0.2372	4.2129	65.7872	0.1497	497.9047
4.50	0.2398	4.2602	65.7399	0.1513	503.4945
4.60	0.2452	4.3548	65.6452	0.1547	514.6742
5.00	0.2665	4.7335	65.2665	0.1682	559.3888
6.00	0.3198	5.6802	64.3198	0.2018	671.1476
7.00	0.3731	6.6269	63.3731	0.2354	782.8667
8.00	0.4264	7.5736	62.4264	0.2691	894.5462
8.50	0.4531	8.0469	61.9531	0.2859	950.3712
8.90	0.4744	8.4256	61.5744	0.2993	995.0240
8.95	0.4771	8.4730	61.5271	0.3010	1000.6142
8.99	0.4792	8.5108	61.4892	0.3024	1005.0700
9.00	0.4797	8.5203	61.4797	0.3027	1006.1860
10.00	0.5330	9.4670	60.5330	0.3363	1117.7870
11.00	0.5863	10.4137	59.5863	0.3699	1229.3480
12.00	0.6396	11.3604	58.6396	0.4036	1340.8690
13.00	0.6929	12.3071	57.6929	0.4372	1452.3510
13.30	0.7089	12.5911	57.4089	0.4473	1485.7880
13.40	0.7143	12.6385	57.3615	0.4490	1491.3782
13.50	0.7196	12.7804	57.2196	0.4540	1508.0770
13.60	0.7249	12.8751	57.1249	0.4574	1519.2210
22.00	1.1726	20.8274	49.1726	0.7399	2453.9140
23.00	1.2259	21.7741	48.2259	0.7735	2565.0020
24.00	1.2792	22.7208	47.2792	0.8072	2676.0510
25.00	1.3325	23.6675	46.3325	0.8408	2787.0610
26.00	1.3858	24.6142	45.3858	0.8744	2898.0310
26.92	1.4391	25.5609	44.4391	0.9081	3008.9630
27.00	1.4391	25.5609	44.4391	0.9081	3008.9630

Table A.2.2: The different values of the Mo concentrations for the MA catalyst

0.02667	g(MA)/g(sol)		4 g MA		
			150.01 g sol		
(BTH+NAPH) MIX					
MA cat sol (g)	g (MA)	H ₂ O g	H ₂ O Loaded g	g (Mo)	ppm [Mo]
1.00	0.0267	0.9733	69.0267	0.0151	50.2987
2.00	0.0533	1.9467	68.0533	0.0302	100.5885
8.00	0.2134	7.7866	62.2134	0.1209	402.1396
9.00	0.2400	8.7510	61.2400	0.1360	452.3669
10.00	0.2667	9.7333	60.2667	0.1511	502.5854
11.00	0.2934	10.7066	59.2934	0.1662	552.7948
12.00	0.3200	11.6710	58.3200	0.1813	602.9954
14.00	0.3734	13.6266	56.3734	0.2115	703.3610
14.10	0.3760	13.7239	56.2760	0.2130	708.3877
14.20	0.3787	13.8213	56.1787	0.2145	713.4054
15.00	0.4001	14.5999	55.4001	0.2266	753.5438
15.10	0.4027	14.6973	55.3027	0.2281	758.5607
15.20	0.4054	14.7946	55.2054	0.2296	763.5775
15.30	0.4081	14.8919	55.1080	0.2312	768.5942
15.60	0.4161	15.1839	54.8160	0.2357	783.6438
16.00	0.4267	15.5733	54.4267	0.2417	803.7087
17.00	0.4534	16.5466	53.4534	0.2568	853.8648
18.00	0.4801	17.5199	52.4801	0.2719	904.0120
19.00	0.5067	18.4933	51.5067	0.2871	954.1503
20.00	0.5334	19.4666	50.5334	0.3022	1004.2797
21.00	0.5601	20.4399	49.5601	0.3173	1054.4003
22.00	0.5867	21.4133	48.5867	0.3324	1104.5119
23.00	0.6134	22.3866	47.6134	0.3475	1154.6147
24.00	0.6401	23.3599	46.6401	0.3626	1204.7085
25.00	0.6668	24.3333	45.6667	0.3777	1254.7936
25.50	0.6801	24.8199	45.1801	0.3853	1279.8327
25.91	0.7077	25.1955	44.6923	0.3929	1304.8718
45.00	1.2002	43.7998	26.2001	0.6799	2254.6332
46.00	1.2268	44.7732	25.2268	0.6950	2304.5323
47.00	1.2535	45.7465	24.2535	0.7101	2354.4226
48.00	1.2802	46.7198	23.2802	0.7252	2404.3041
49.00	1.3068	47.6932	22.3068	0.7403	2454.1768
50.00	1.3335	48.6665	21.3335	0.7554	2504.0407

Table A.2.3: The different values of the Mo concentrations for the AMT catalyst

0.01346 g(AMT)/g(Sol)		2.02 g AMT			
		50.04 g Sol			
MIX (BTH+NAPH)					
AMT cat sol(g)	g (AMT)	H ₂ O g	H ₂ O Loaded g	g (Mo)	ppm [Mo]
1.00	0.01346	0.9865	69.0135	0.0073	24.3510
2.00	0.02692	1.9731	68.0269	0.0146	48.6999
3.00	0.04038	2.9596	67.0404	0.0219	73.0466
4.00	0.05384	3.9462	66.0538	0.0293	97.3911
5.00	0.0673	4.9327	65.0673	0.0366	121.7334
6.00	0.08076	5.9192	64.0808	0.0439	146.0735
7.00	0.09422	6.9058	63.0942	0.0512	170.4115
8.00	0.10768	7.8923	62.1077	0.0585	194.7473
9.00	0.12114	8.8789	61.1211	0.0658	219.0809
10.00	0.1346	9.8654	60.1346	0.0731	243.4123
45.00	0.6057	44.3943	25.6057	0.3291	1093.6406
46.00	0.61916	45.3808	24.6192	0.3365	1117.8938
47.00	0.63262	46.3674	23.6326	0.3438	1142.1447
52.00	0.69992	51.3001	18.6999	0.3803	1263.3670
53.00	0.71338	52.2866	17.7134	0.3877	1287.6049
54.00	0.72684	53.2732	16.7268	0.3950	1311.8407
55.00	0.7403	54.2597	15.7403	0.4023	1336.0743
56.00	0.75376	55.2462	14.7537	0.4096	1360.3058
57.00	0.76722	56.2328	13.7672	0.4169	1384.5351
58.00	0.78068	57.2193	12.7807	0.4242	1408.7622
59.00	0.79414	58.2059	11.7941	0.4315	1432.9871
60.00	0.8076	59.1924	10.8076	0.4389	1457.2099
61.00	0.82106	60.1789	9.8211	0.4462	1481.4305
61.70	0.83452	61.1655	8.8345	0.4535	1505.6490
62.00	0.83452	61.1655	8.8345	0.4535	1505.6490
70.00	0.9422	69.0578	0.9422	0.5120	1699.3187

Because the ATTM catalyst is insoluble in water, the following calculation was carried out to obtain the 1500 ppm Mo concentration as shown in Table A.2.4. The molecular formula is as follows: $(\text{NH}_4)_2\text{MoS}_4$.

Table A.2.4: The different values of the Mo concentrations for the ATTM catalyst

ATTM purity =	99.97%	
M Wt.=	260.27	g / gmol
1 g of ATTM =	0.3685	g Mo/ g ATTM
Wt ATTM (g)	g Mo	ppm [Mo]
1.80	0.6633	2195.31
1.50	0.5527	1831.24
1.40	0.5159	1709.72
1.30	0.4791	1588.13
1.23	0.4544	1500.00
1.00	0.3685	1222.85
0.90	0.3317	1100.93
0.85	0.3132	1039.94
0.80	0.2948	978.93
0.79	0.2911	966.73
0.70	0.2579	856.85
0.60	0.2211	734.69

Appendix A.3 DCP- Calibration Curve

The Direct Current Plasma Emission Spectrometer (DCP) is a system used to quantify most metals in solutions. In this thesis the metal Mo was used. To establish a calibration curve, different concentrations of Mo-metal were prepared from 10,000 ppm Mo stock solution obtained from BDH Inc., as listed in Table A.3.1 and shown in Figure A.3.1.

Table A.3.1: Calibration data for a standard solution

Sample Sol	DCP-Reading	% Error
0	0	
200	200.4726	-0.2363
400	399.0219	0.2445
600	606.1648	-1.0275
800	784.3603	1.9549
1000	1009.9804	-0.9980

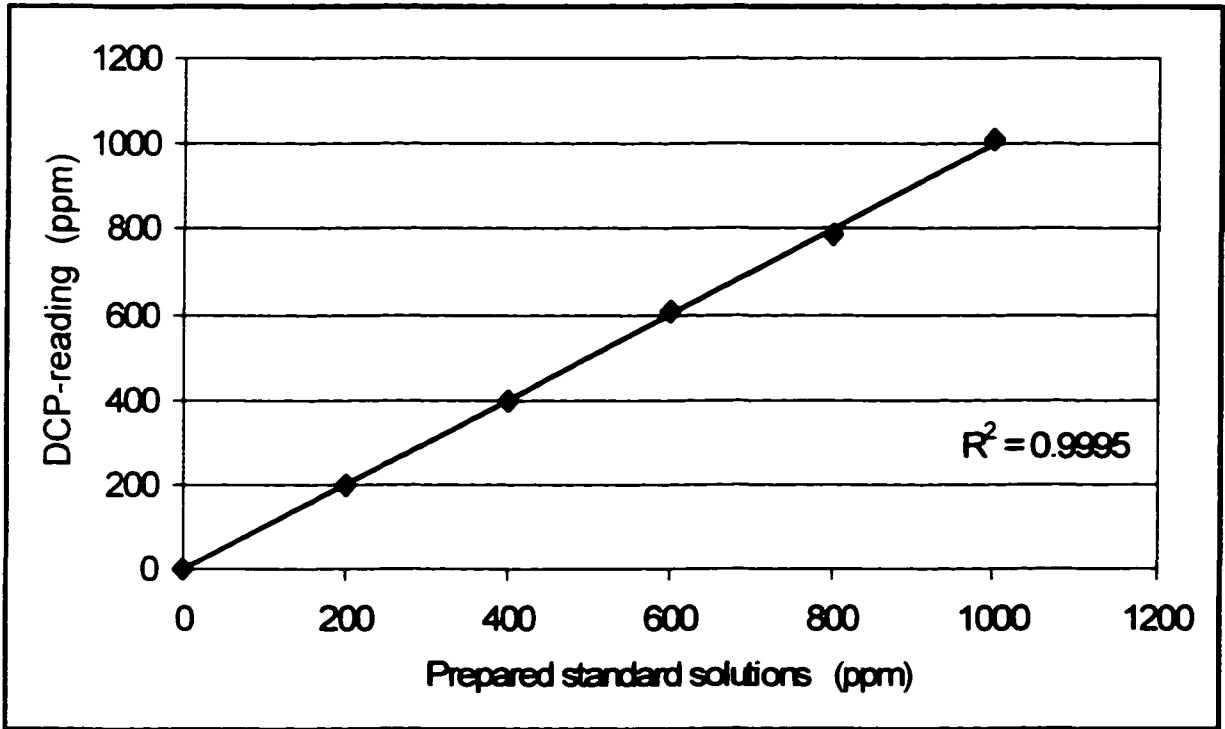


Figure A.3.1: DCP- Calibration curve

Appendix A.4

Amount of NAPH and BTH feed to the reactor

The NAPH was calculated to equal that in diesel fuel, which has 20 % aromatics.

$$\text{Wt of Toluene} = 200 \text{ ml} \times 0.865 \text{ g / ml} = 173 \text{ g}$$

$$\text{Wt of NAPH} = X \text{ g}$$

$$\text{Total wt of solution} = 173 + X$$

$$\frac{X}{173 + X} = 0.2$$

$$\therefore X = 43.25 \text{ g NAPH} \quad (0.3374 \text{ mol})$$

The BTH was calculated to equal in diesel fuel, which has 1.8 % sulfur.

$$\text{Wt of Toluene} = 173 \text{ g}$$

$$\text{Wt of BTH} = X \text{ g}$$

$$0.018 = \frac{\frac{32.064 \text{ g / mol}}{134.20 \text{ g / mol}} \times X \text{ g BTH}}{173 \text{ g} + X \text{ g BTH}}$$

$$\therefore X = 14.1 \text{ g BTH} \quad (0.1051 \text{ mol})$$

Therefore, the NAPH/ BTH ratio is 3.2 mol/mol in all of the experimental runs in this study.

Appendix A.5

GC Method for Gas Analysis

Section 1	GC Control			
		1	2	3
Oven Temp (oC)		35.0	75.0	100.0
Iso Time (min)		2.0	2.0	3.0
Ramp Rate (oC/min)		20.0	25.0	

HWD 1 Range Low

HWD 1 Polarity B-A

FID 2 SENS Low

Det Zero On

Initial Det 1

Inj 2 Temp 120

Det 1 Temp 180

Det 2 Temp 180

Pressure 1 40.0 psig

Equilib Time 0.4 min

Total Run Time 10.0 min

Section 2	Timed Events	
TIME	EVENT	
-0.5	Relay 3	On
-0.4	Relay 3	Off
-0.3	Integ	Off
0.00	Attn	64
0.05	Relay 2	On
0.10	Relay 2	Off
0.55	Set Zero	
0.56	Attn	8
0.58	Integ	On
0.75	Integ	Off
0.76	Attn	1024
0.77	HWD Pol	A-B
0.78	Set Zero	
0.79	Set Zero	
0.80	Attn	64
0.82	Integ	On
1.65	Integ	Off
1.67	Relay 3	On
1.77	Relay 3	Off
1.80	Set Zero	

1.81	Attn	32
1.92	Integ	On
1.94	Width	-7
3.00	Set Zero	
3.20	Set Zero	
3.50	Set Zero	
3.51	Integ	On
5.19	Integ	Off
5.20	Set Zero	
5.49	Integ	Off
5.70	Integ	On
5.72	Integ	-7

Section 3 **Data Handling**

Data Acquisition		Report	
Start Time	0.00 min	Calc Type	Ext Std
End Time	10.00 min	Area/HT Calc	Area
Width	4.00	Output	
Skim Sens	0.00	Screen	Yes
Base Line Cor	B-B	Printer	No
Det 1 Area Sens	100.00		
Det 2 Area Sens	50.00		

Det 1 Base Sens 200.00

Det 2 Base Sens 4.00

Peak Identification Quantitation (Calib Avg of 6)

Unretd Peak Time 0.00 min Scaling factor 1.0000

Area/HT reject 0.100 min RF for unknowns 1.0000

Ref pk time 0.67 min SMP amount 1.0000

Compnt:

Tol ABS 0.02

Tol % 2.00

Component List

RT	RF	STD AMT	Name	GRP
0.67	21.6300	90.000	H ₂	1
0.98	0.8700	78.084	O ₂	1
1.44	0.8740	20.946	N ₂	1
2.20	1.0000	100.000	CH ₄	1
2.88	0.7346	100.000	CO ₂	1
4.70	0.7556	100.000	CO	1
6.79	1.2152	10.000	H ₂ S	1
7.74	1.0000	100.000	COS	1

Appendix A.6

GC- Methods for Liquid Analysis

A.6.1 BTH –HDS Method

Section 1 GC control

	1	2
Oven Temp (oC)	50.0	220.0
Iso Time (min)	2.0	0.0
Ramp Rate (oC/min)	20.0	
HWD 1 Range	off	
HWD 1 Polarity	A-B	
FID 2 Sens	low	
Det Zero	on	
Initial Det	2	
Inj 2 Temp	300	
Det 2 Temp	300	
Det 2 Temp	300	
Pressure 1	40 psig	
Equilibrium Time	1.0 min	
Total Run Time	10.5 min	

Section 2 Timed Events

Time	Event	
-0.20	Relay 1	on
-0.10	Attn	8
0.02	Set Zero	

Section 3 Data handling

Data Acquisition		Report	
Start Time	0.00 min	Calc Type	Ext Std
End time	10.50 min	Area/HT Calc	Area
		Print Tol	0.0000
Width	-3	Output	
Skim Sens	0	Screen	Yes
Baseline Corr	B-B	Printer	no
Det 1 Area Sens	100		
Det 2 Area Sens	750		
Det 1 Base Sens	200		
Det 2 Base Sens	7		
Peak Identification		Quantitation (Calib Avg of 6)	
Unretd Peak Time	0.00 min	Scaling Factor	1.0000
Area/HT Reject	0.00 min	RF for Unknown	0.0000
Ref pk: Time	2.38 min		
Time Tol	0.05 min	SMP Amount	1.0000

Comnt: Tol ABS 0.02
Tol% 0.50

Component List

RT	RF	STD AMT	NAME	GRP
2.36	5.5547	217.3000	Toluene	1
3.53	4.8728	94.2000	ETHBZ	1
7.54	5.0668	22.4000	BTH	1

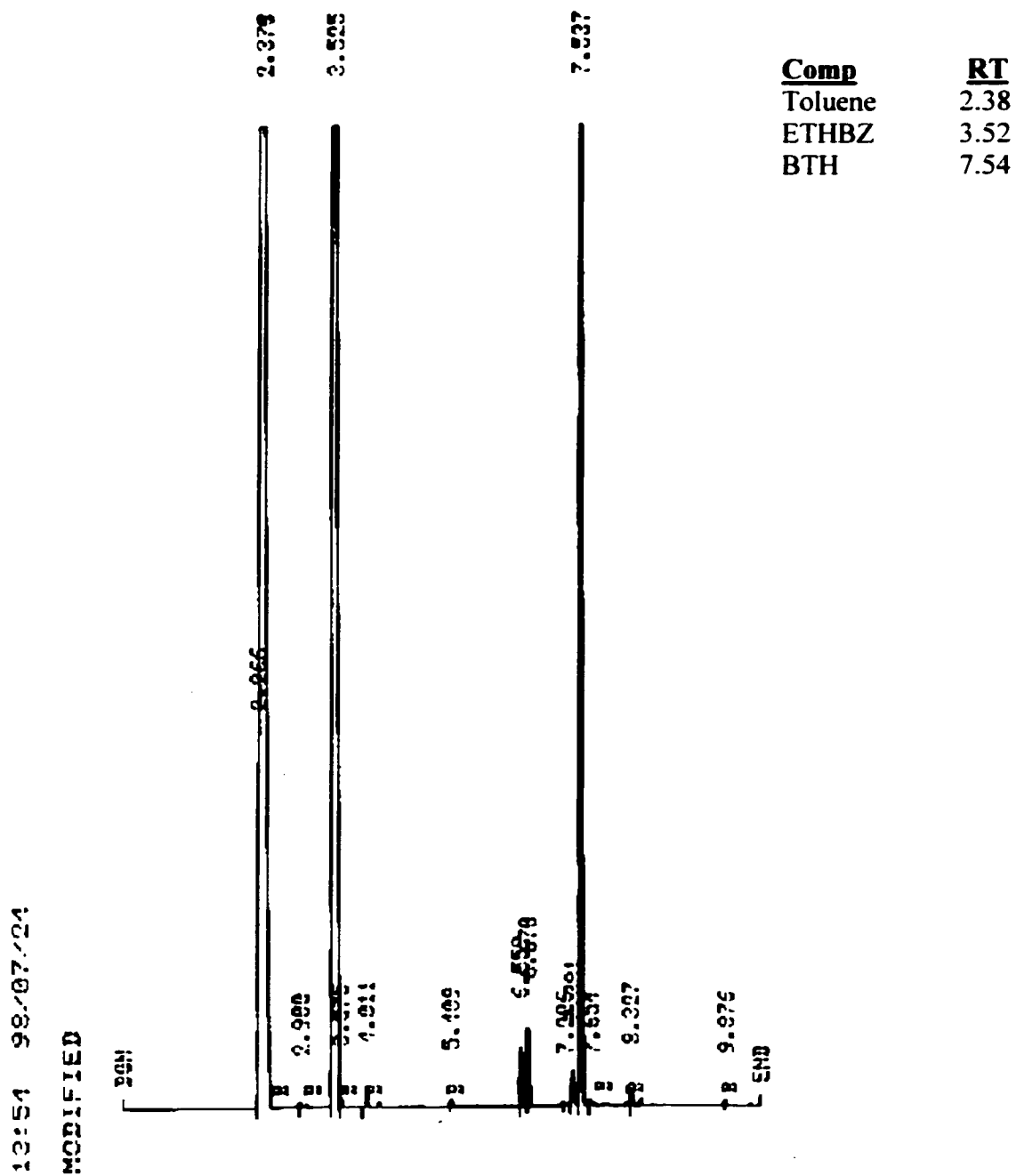


Figure A.6.1.1: The calibration chromatograph for the BTH reaction network

A.6.2 NAPH- AHYD Method

Section 1 GC control

	1	2
Oven Temp (°C)	50.0	250.0
Iso time (min)	2.0	0.0
Ramp rate (°C/min)	20.0	

HWD 1 Range off

HWD 1 Polarity A-B

FID 2 Sens low

Det Zero on

Initial Det 2

Inj 2 Temp 325

Det 2 Temp 325

Det 2 Temp 325

Pressure 1 39 psig

Equilibrium Time 1.5 min

Total Run Time 10.5 min

Section 2 Timed Events

Time	Event	
-0.20	Relay 1	on
-0.10	Attn	8
0.02	Set Zero	

Section 3 Data handling**Data Acquisition**

Start Time 0.00 min

End Time 12.00 min

Width -3

Skim Sens 0

Baseline Corr B-B

Det 1 Area Sens 100

Det 2 Area Sens 750

Det 1 Base Sens 200

Det 2 Base Sens 7

Peak Identification

Unretd Peak Time 0.00 min

Area/HT Reject 0.00 min

Ref pk: Time 2.48 min

Time Tol 0.50 min

Comnt: Tol ABS 0.01

Tol% 0.50

Report

Calc Type Ext std

Area/HT Calc Area

Print Tol 0.0000

Output

Screen Yes

Printer no

Quantitation (Calib Avg of 5)

Scaling Factor 1.0000

RF for Unknown 0.000

SMP Amount 1.0000

Component List

RT	RF	STD AMT	NAME	GRP
2.38	7.1459	228.1300	Toluene	1
5.38	3.5466	11.1400	trans-DEC	1
5.89	3.5863	18.4400	cis-DEC	1
6.91	3.6511	37.8900	TET	1
7.41	4.9640	78.4100	NAPH	1

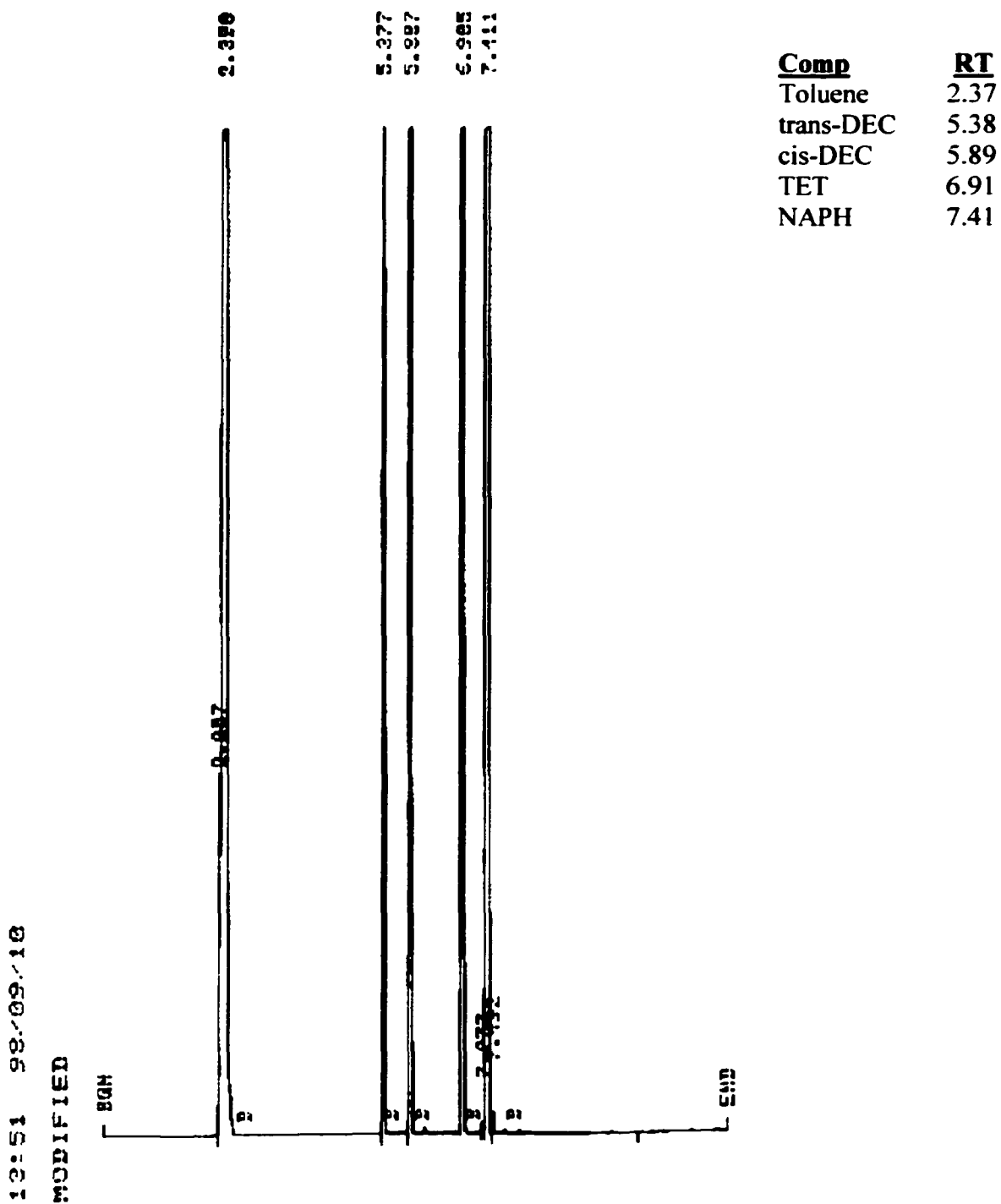


Figure A.6.2.1: The calibration chromatograph for the NAPH reaction network

A.6.3 Mixture of (NAPH + BTH) Method

Section 1 GC Control

	1	2
Oven Temp (°C)	50.0	180.0
Iso time (min)	2.0	0.0
Ramp rate (°C/min)	12.0	
HWD 1 Range off		
HWD 1 Polarity A-B		
FID 2 Sens	low	
Det Zero	on	
Initial Det	2	
Inj 2 Temp	300	
Det 2 Temp	300	
Det 2 Temp	300	
Pressure 1	40 psig	
Equilibrium Time	0.7 min	
Total Run Time	12.8 min	

Section 2 Timed Events

Time	Event	
-0.20	Relay 1	on

-0.10 Attn 8

0.02 Set Zero

Section 3 Data handling

Data Acquisition

Start Time 0.00 min

End time 12.83 min

Width -3

Skim Sens 0

Baseline Corr B-B

Det 1 Area Sens 100

Det 2 Area Sens 1000

Det 1 Base Sens 200

Det 2 Base Sens 7

Peak Identification

Unretd Peak Time 0.00 min

Area/HT Reject 0.00 min

Ref pk: Time 2.46 min

Time tol 0.5 min

Comnt: Tol ABS 0.01

Tol% 0.50

Report

Calc Type Ext std

Area/HT Calc Area

Print Tol 0.000

Output

Screen Yes

Printer no

Quantitation (calib Avg of 11)

Scaling Factor 1.000

RF for unknown 1.000

SMP amount 1.000

Component List

RT	RF	STD AMT	NAME	GRP
1.99	9.3835	257.9770	Toluene	1
3.07	6.7559	42.3848	ETHBZ	0
5.68	5.2433	7.4500	trans-DEC	1
6.52	5.3089	14.5389	cis-DEC	1
8.31	5.3661	19.1362	TET	1
9.18	5.2261	23.4840	NAPH	0
9.43	6.6396	23.6960	BTH	1

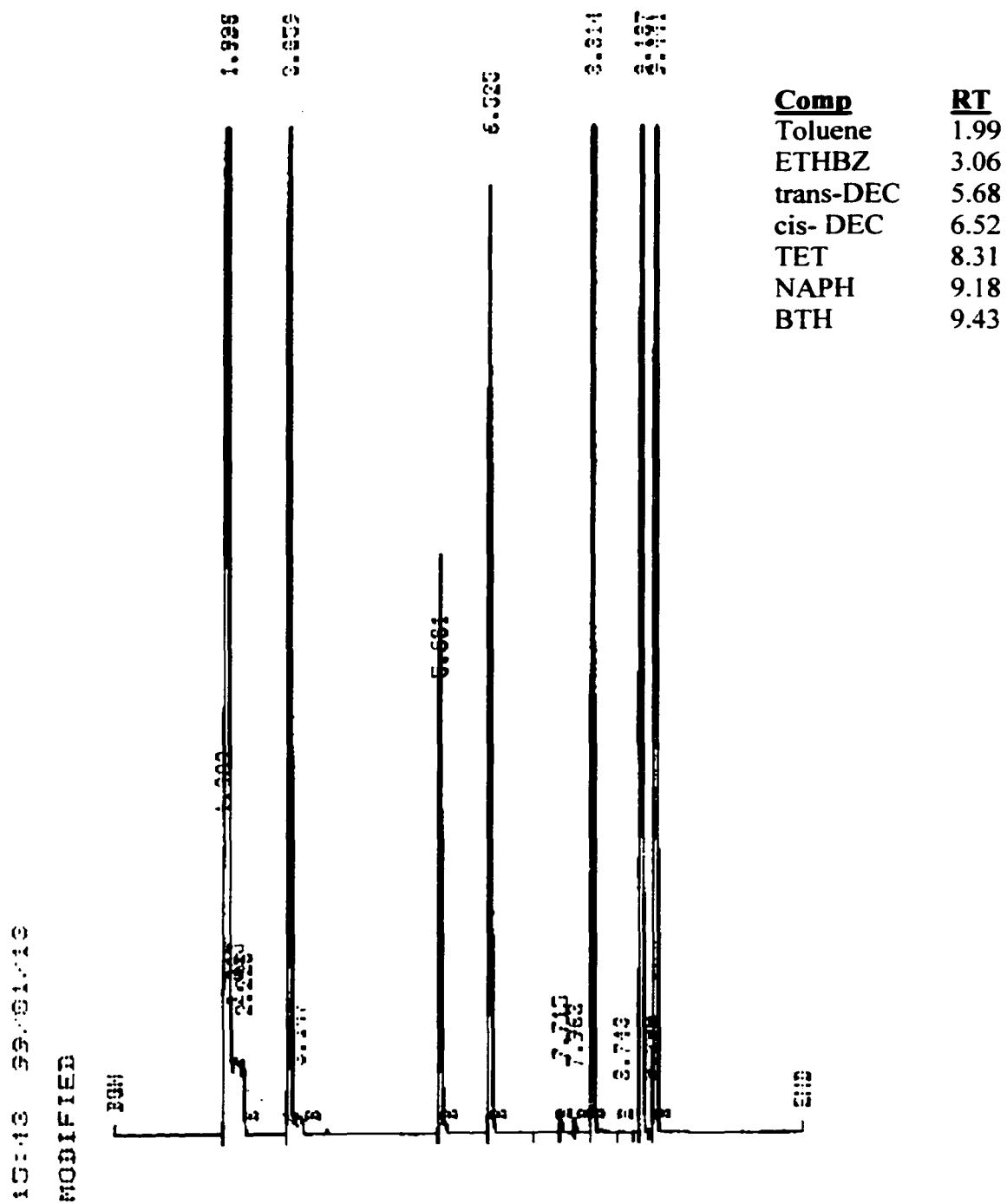


Figure A.6.3.1: The calibration chromatograph for the mixture of BTH and NAPH reaction networks

Appendix A.7 X-Ray Diffraction (XRD)

This instrument is located in the Chemistry Department at University of Waterloo. (Siemens D500 X-ray diffractometer). The essential components of the XRD instrument are the X-ray source, a monochromator (restricts the wave length rage applied), a sample holder mounted on a goniometr (rotatable table which is precisely defined θ), a radiation detector (mounted on a second rotatable table), and a signal processor.

Software Used:

EDM	Edit method
DCM	Execution file to download results
EVA	Compute and quantify results

Program Setting:

FN:	Fatima.CMD
Start:	2.00
End:	80.00
Step:	0.050
Time:	0.50
Psi:	0.0
Mode:	Step
Type:	Std
Plot:	Yes
Peak:	Yes
Width:	0.100
Yscale:	200

Appendix A.8

Thermogravimetric/ Differential Thermal Analyzer (TGA/DTA)

This instrument is available from the analytical chemistry services in the Department of Chemical Engineering at the University of Waterloo. The (TA Instruments 2100 thermal analysis) is used to characterize any material that shows a weight change and to detect phase changes due to decomposition, oxidation or, dehydration. The method used for analyzing the spent catalyst samples of the current study is through oxidation in 5 % O₂ in He atmosphere. The calibration of the TGA/DTA established before the sample analysis, as shown in Figure A.8.1.

Operating Parameters

Temperature Range (°C)	50 - 600
Control Thermocouple	Platinum-Platinum/13% Rhodium
Sample and Reference Thermocouple	Platinum-Platinum/13% Rhodium
Heating Rate (°C/min)	10
Cooling Time	10 min: 600 to 50 °C
O ₂ /He pressure (psi)	14
He flow rate (mL/min)	110
Sampling System	
Sample Cups	
Type	Platinum
Volume capacity	110 µL

Sample of calculation, for % weight loss of spent PMA catalyst solids, is based on the analysis of Run#23, as follows:

$$\% \text{ of weight loss} = \frac{w_1 - w_2}{w_1} \times 100$$

where,

w_1 = Initial weight at $T = 50^\circ \text{C}$ (mg)

w_2 = Final weight at $T = 600^\circ \text{C}$ (mg)

\therefore

$$\% \text{ of weight loss} = \frac{19.2860 - 12.7005}{19.2860} \times 100 = 34.15$$

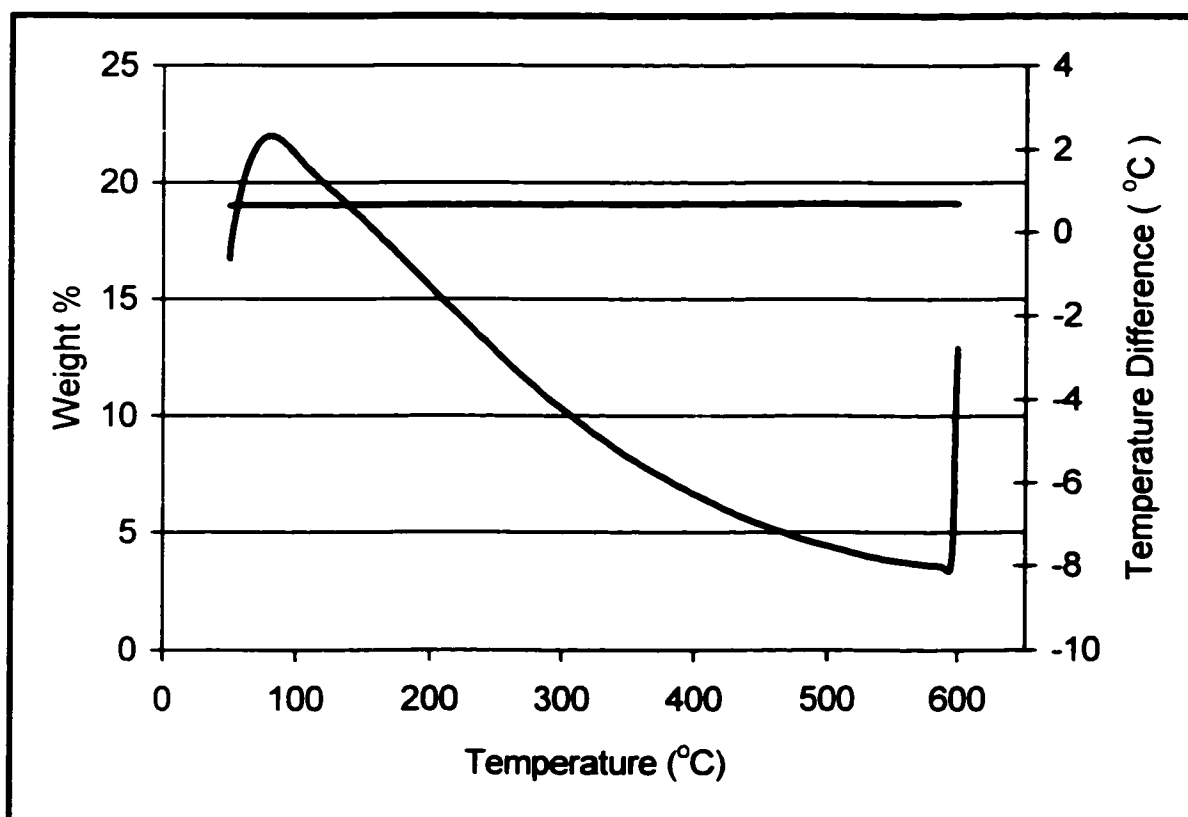


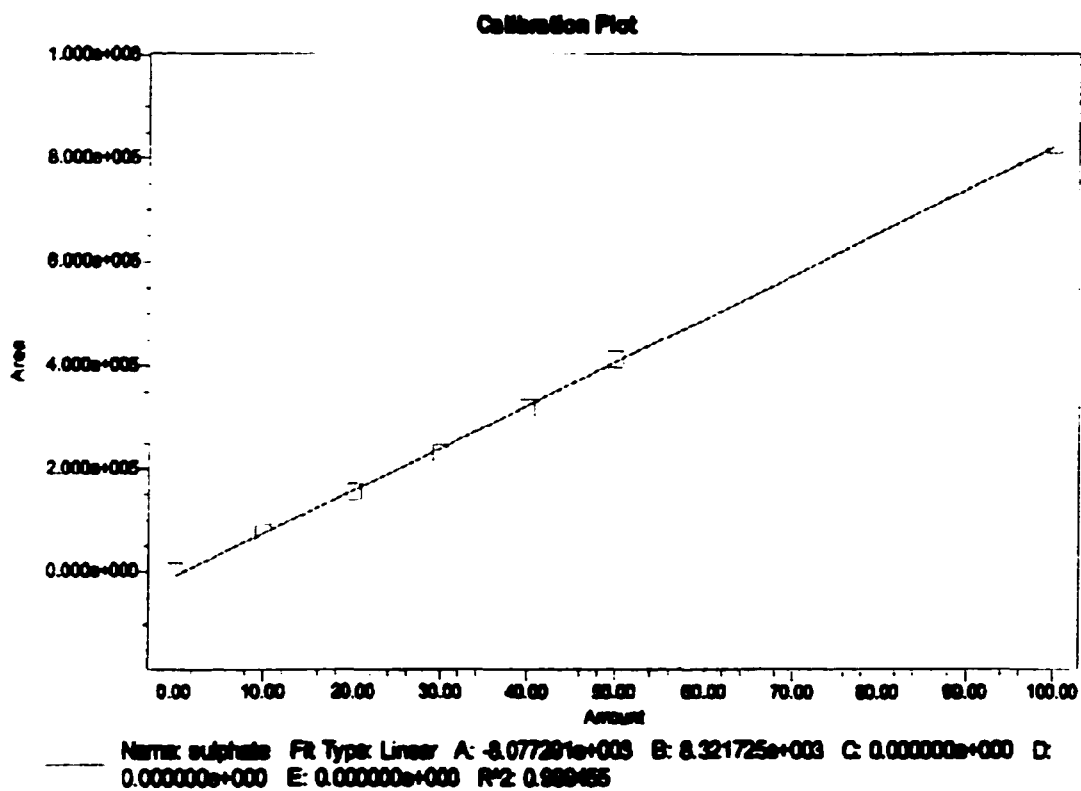
Figure A.8.1: The calibration curve for the TGA/DTA instrument

Appendix A.9 Ion Chromatograph (IC)

The Dionex DX 500, chromatograph system is located in the analytical chemistry services at the Department of Chemical Engineering at the University of Waterloo. The system is typically used to separate and quantify anions in solutions. The system is integrated into software called Water Millenium 32 for data handling. The current study measures the sulfate ions (SO_4^-) in the aqueous layer after the reaction is completed. Figure A.9.1 and Figure A.9.2 shows the calibration curve, and the sulfate peak value as obtained during calibration. In addition Figures A.9.3, A.9.4, A.9.5, A.9.6 and A.9.7 are representing the sulfate peaks for Runs # 23, Run #26, Run #27, Run#29 and Run #30 respectively.

Program Setting:

Column:	Dionex AS11-4 mm
Eluent:	20 mH NaOH (isocratic) at 1 ml/min
Detector:	Conductivity
Injection volume:	25 ul
Dilution factor:	100 ml



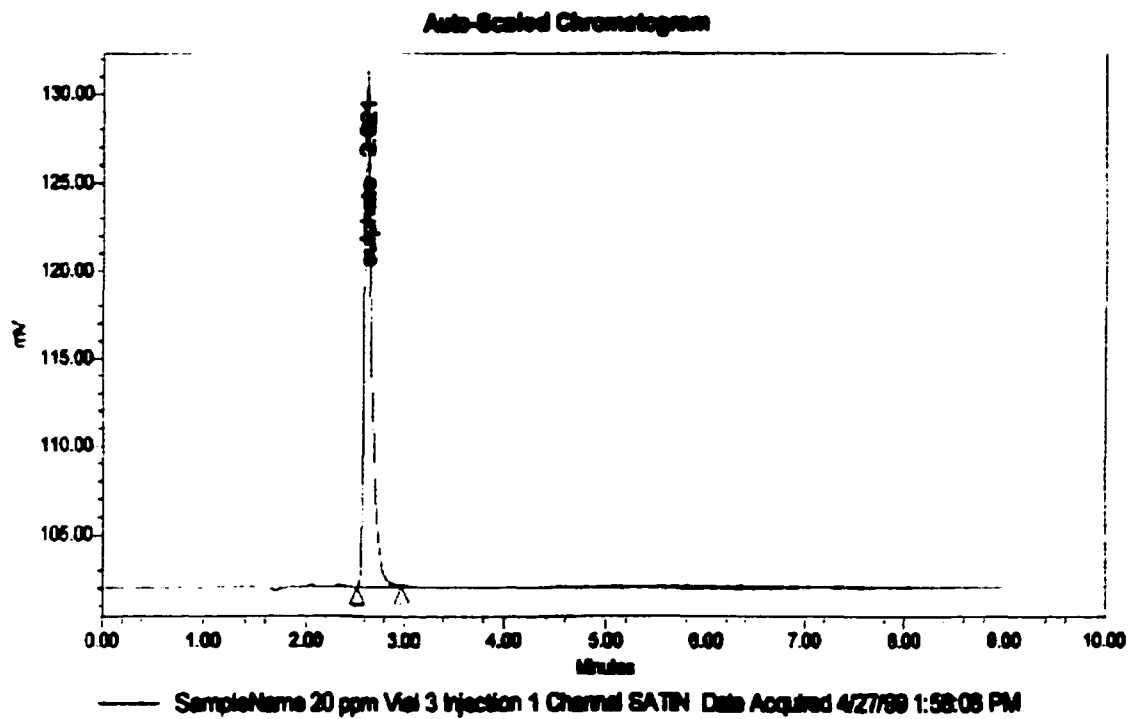
Peak: sulphate

	Name	Level	X Value	Response	Calc. Value	% Deviation	Manual	Ignore
1	sulphate	1	0.000000	1401.000000	1.138882		No	No
2	sulphate	2	10.000000	73024.800000	8.889162	-0.138	No	No
3	sulphate	3	20.000000	146013.100000	18.870346	-1.648	No	No
4	sulphate	4	30.000000	232891.800000	28.889484	-3.788	No	No
5	sulphate	5	40.000000	318882.000000	38.882376	-1.544	No	No
6	sulphate	6	50.000000	413888.800000	48.811808	1.222	No	No
7	sulphate	7	100.000000	827013.800000	100.380732	0.361	No	No

Figure A.9.1: The calibration curve for sulfate ion on IC

Current Date 4/28/99

4 of 2

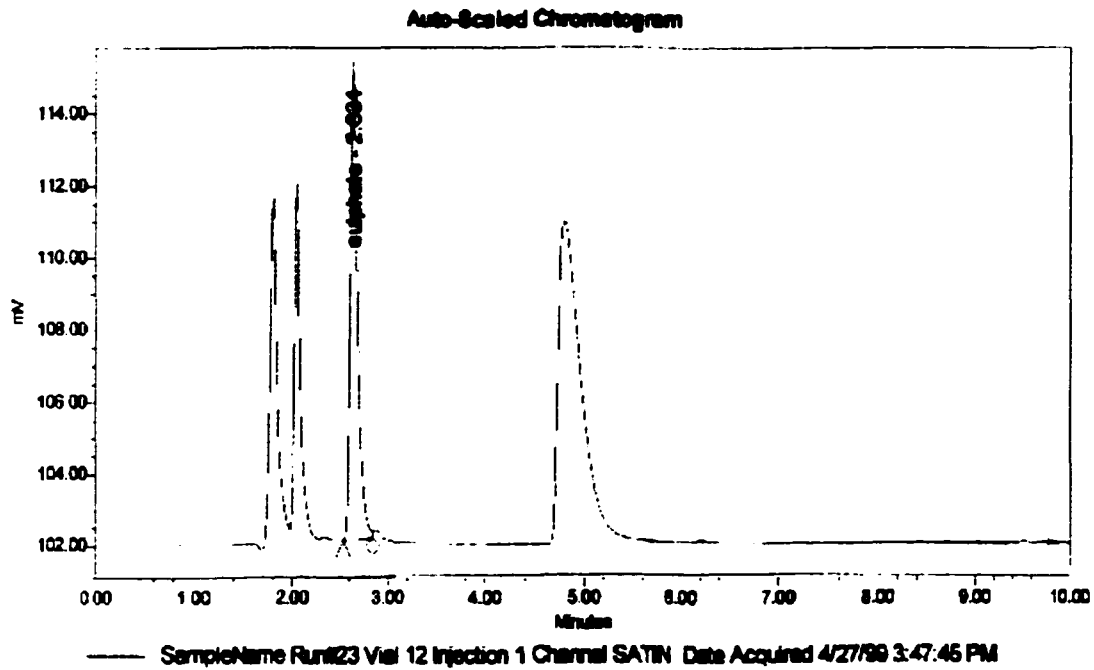
**Peak Results**

	Name	RT	Area	Height	Amount	Units
1	sulfate	2.621	198813	28781	20.000	mg/L

Figure A.9.2: The Ion chromatogram for the sulfate peak

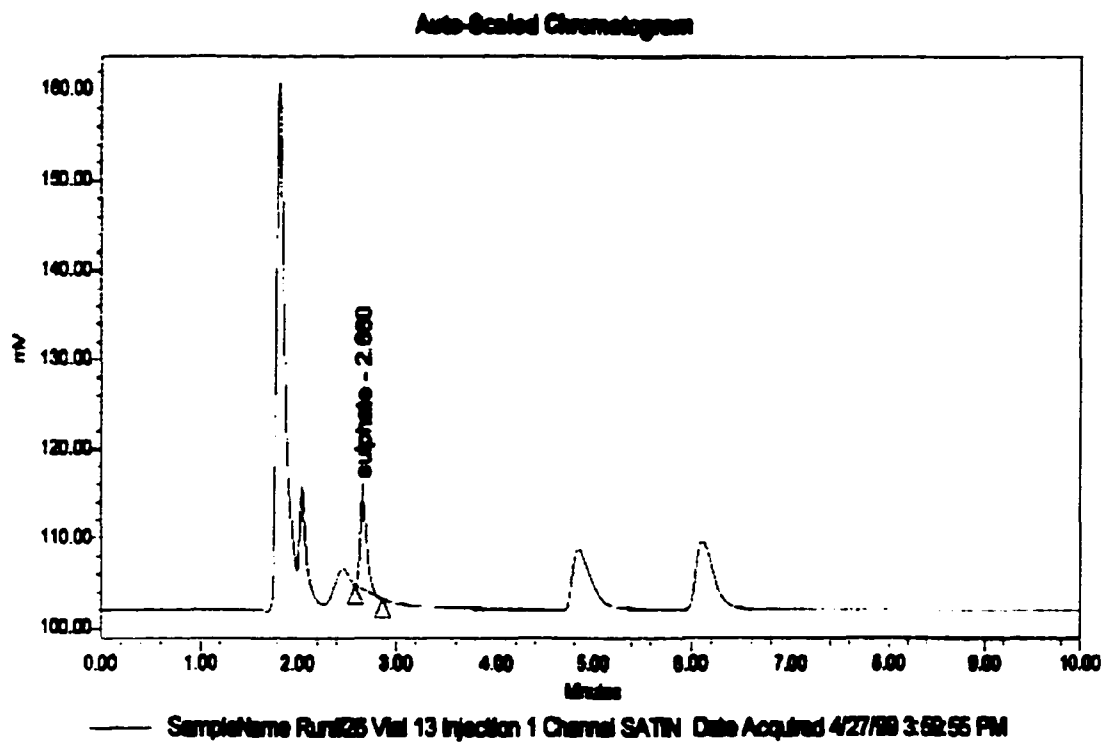
Current Date 4/28/99

13 of 2

**Peak Results**

	Name	RT	Area	Height	Amount	Units
1	sulphate	2.834	68982	13018	82.600	mg/L

Figure A.9.3: IC chromatogram of the sulfate peak of Run #23



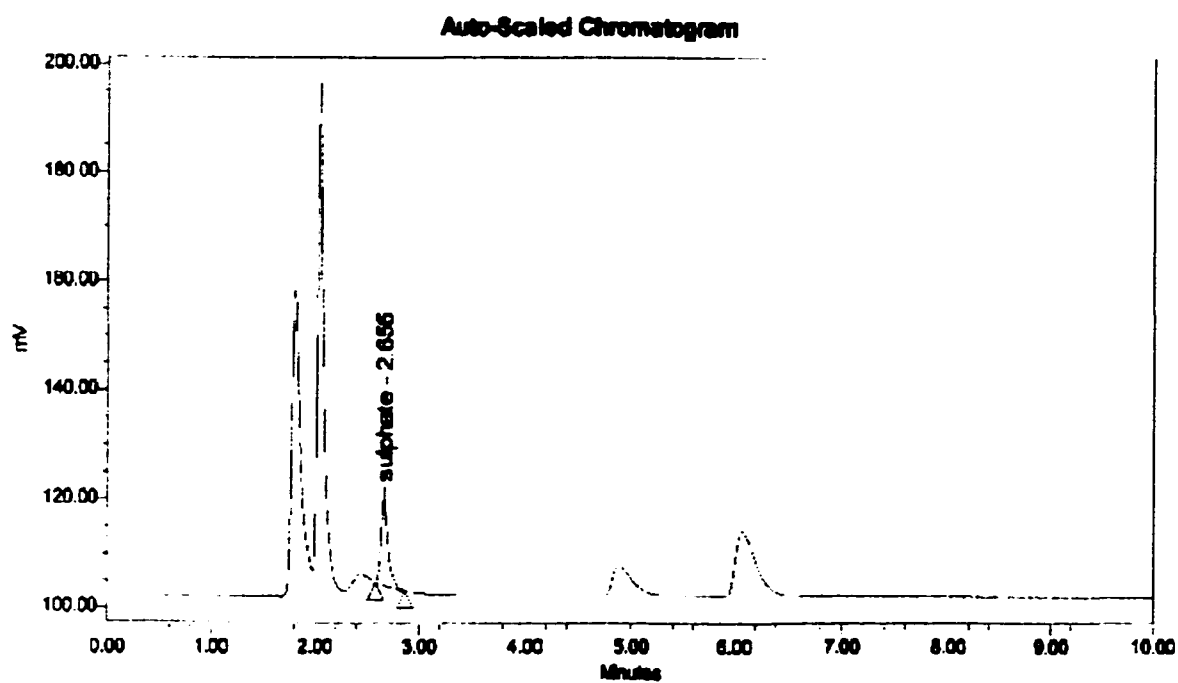
Peak Results

	Name	RT	Area	Height	Amount	Units
1	sulfate	2.860	48218	10336	67.848	mg/L

Figure A.9.4: IC chromatogram of the sulfate peak of Run #26

Current Date 4/28/99

15 of 2



SampleName Run#27 Vial 14 Injection 1 Channel SATIN Date Acquired 4/27/99 4:12:07 PM

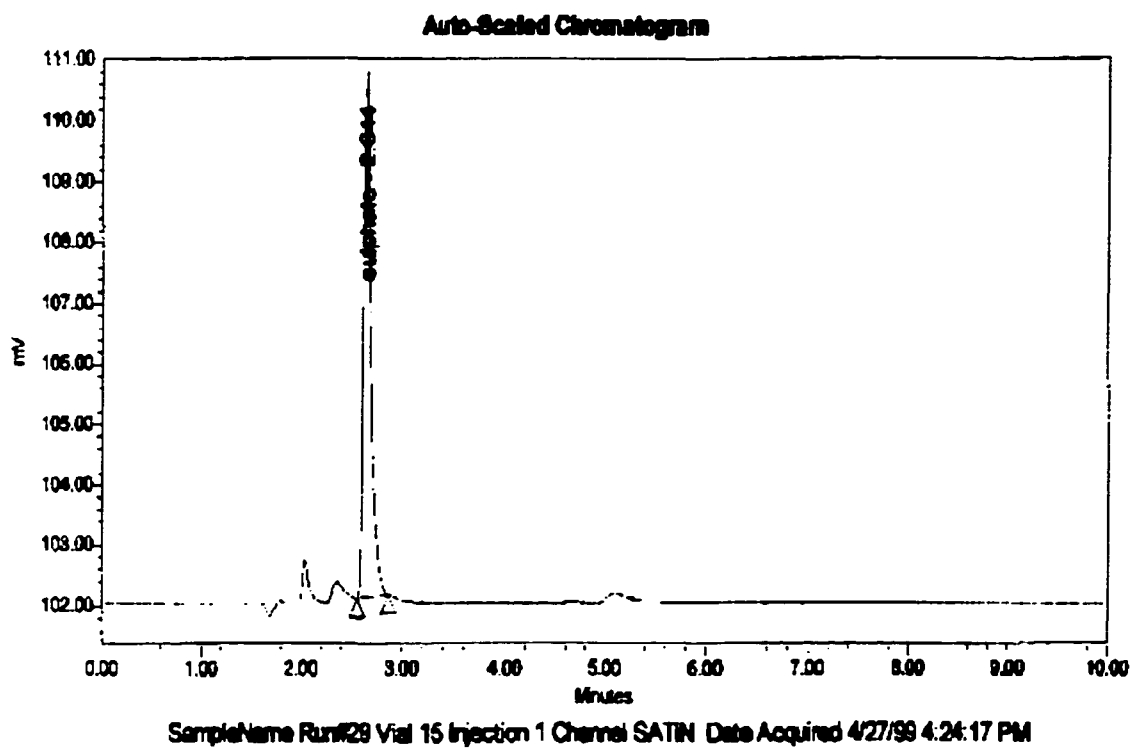
Peak Results

	Name	RT	Area	Height	Amount	Units
1	sulphate	2.666	76737	19881	101.919	mg/L

Figure A.9.5: IC chromatogram of the sulfate peak of Run #27

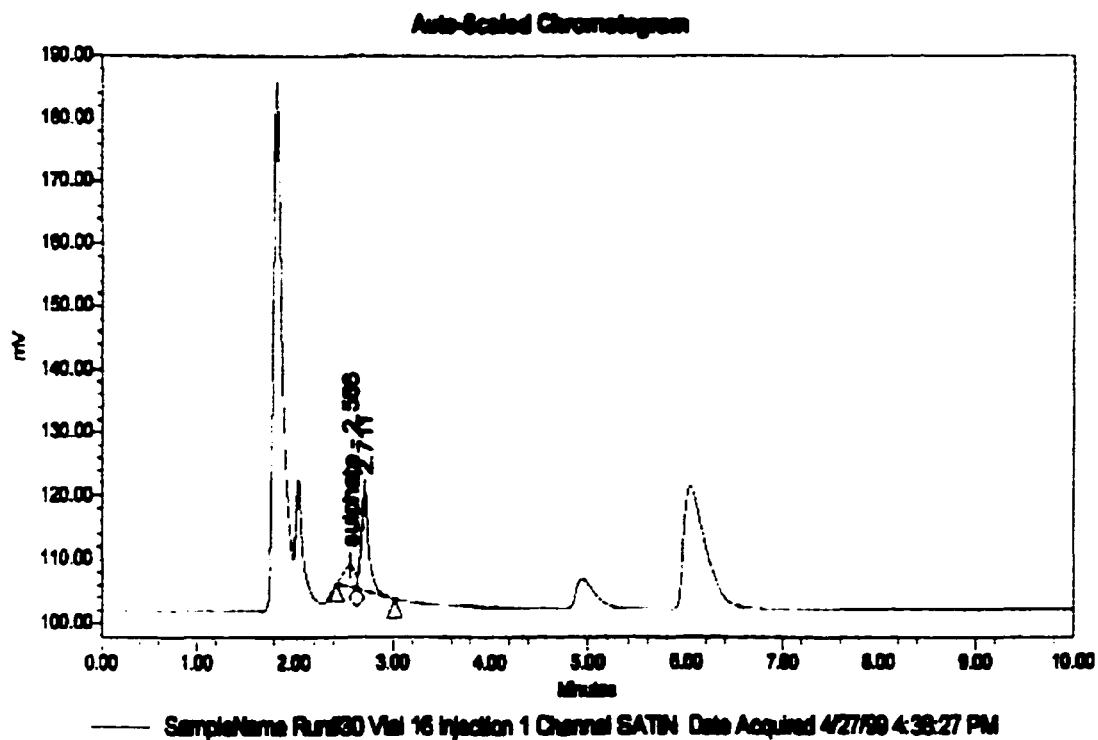
Current Date 4/28/99

16 of 2

**Peak Results**

	Name	RT	Area	Height	Amount	Units
1	sulfate	2.644	44405	8442	630.866	mg/L

Figure A.9.6: IC chromatogram of the sulfate peak of Run #29



Peak Results

	Name	RT	Area	Height	Amount	Units
1	sulfate	2.885	27236	3043	42.436	ng/L
2		2.711	79150	16987		

Figure A.9.7: IC chromatogram of the sulfate peak of Run #30

For the sulfur content in the final aqueous liquid product, the calculation is based on the data of Run # 23, # 26 , # 27, and #29.

The total amount of sulfur initially fed to the system:

➤ **Via H₂S**

$$\text{Initial mmol (H}_2\text{S)} = \frac{(1.021 \text{ atm} \times 0.725 \text{ L})}{(0.082061 \text{ atm/L mol K} \times (20 + 273) \text{ K})} \times 1000 = 30.79 \text{ mmol}$$

$$\text{Initial amount of (H}_2\text{S) available} = 0.03079 \text{ mol} \times 34.078 \text{ g/mol} = 1.049 \text{ g}$$

$$\begin{aligned} \therefore \text{Initial amount of (S) available} &= \frac{1.049 \text{ g (H}_2\text{S)} \times 32.064 \text{ g/mol} \times 1 \text{ mol (S)}}{34.078 \text{ g/mol} \times 1 \text{ mol (H}_2\text{S)}} \\ &= 0.987 \text{ g (S)} \cong (987.0 \text{ mg}) \end{aligned}$$

➤ **Via BTH**

$$\text{Initial amount of (BTH) available} = 14.1 \text{ g}$$

$$\begin{aligned} \therefore \text{Initial amount of (S) available} &= \frac{14.1 \text{ g (BTH)} \times 32.064 \text{ g/mol} \times 1 \text{ mol (S)}}{134.2 \text{ g/mol} \times 1 \text{ mol (BTH)}} \\ &= 3.36887 \text{ g (S)} \cong (3368.87 \text{ mg}) \end{aligned}$$

$$\text{Total amount of (S) available in the feed} = 987 + 3368.87 = 4355.87 \text{ mg}$$

The concentration of sulfate ion (SO_4^{2-}), as measured on the IC for Run # 26 was shown in Figure A.9.4. This enables to calculate the final amount of sulfur in aqueous liquid product as follows:

$$\therefore 67.649 \text{ mg / L } (\text{SO}_4^{2-}) \times \frac{100}{1000} \text{ L} \times \frac{32.064 \text{ g / mol } (S) \times 1 \text{ mol } (S)}{96.064 \text{ g / mol } (\text{SO}_4^{2-}) \times 1 \text{ mol } (\text{SO}_4^{2-})} = 2.26 \text{ mg}$$

\therefore Final aqueous product contains = 2.26 mg (S)

The same calculation was carried out for Run #23 , Run #27, Run#29

For Run # 30 the initial amount of sulfur in the system is as follows:

$$\therefore 1.23 \text{ g } (ATTM) \times \frac{32.064 \text{ g / mol } (S) \times 1 \text{ mol} \times 4 (S)}{260.27 \text{ g / mol } (ATTM) \times 1 \text{ mol } (ATTM)} = 0.6061 \text{ g } \quad (606.1 \text{ mg})$$

\therefore Total amount of (S) available in feed = 336887 + 606.1 = 397497 mg

Appendix B

Sample of Calculations for Individual Model compounds

B.1 Gas Analysis

This sample calculation is based on Run # 10 using the PMA catalyst. Assuming ideal gas law:

$$PV = nRT$$

$$\therefore \text{Total number of mols} = \frac{P V_{\text{gas}}}{R T}$$

Initial reading for loading CO, Run # 10

Temperature (°C) = 29.7 (302.7 K)

Pressure (psi) = 585 (39.80925 atm)

Volume of liquid feed (ml) = 270 (0.270 L)

$V_{\text{gas Feed}} = 0.725 \text{ L}$

Initial reading for loading H₂S, Run # 10

Temperature (°C) = 21.3 (294.3 K)

Pressure (psi) = 15 (1.02075 atm)

Volume of liquid feed (ml) = 270 (0.270 L)

$V_{\text{gas Feed}} = 0.725 \text{ L}$

Final reading for the gas product, Run # 10

Temperature (°C) = 34 (307 K)

Pressure (psi) = 519.2 (35.33156 atm)

Total working reactor volume (ml) = 995 (0.995 L)

Volume of liquid product (ml) = 164 (0.164 L)

R gas constant = 0.082061 atm L / mol K

$$V_{\text{gas pro}} = V_{\text{reactor}} - V_{\text{liquid}}$$

$$\therefore V_{\text{gas pro}} = 0.831 \text{ L}$$

$$N(\text{CO})_i = \frac{39.80925 \text{ atm} \times 0.725 \text{ L}}{(0.082061 \text{ atm L / mol K}) \times (302.7 \text{ K})}$$

$$= 0.116191 \text{ mol}$$

$$= 1161.91 \text{ mmol}$$

$$N(\text{H}_2\text{S})_i = \frac{1.02075 \text{ atm} \times 0.725 \text{ L}}{(0.082061 \text{ atm L / mol K}) \times (294.3 \text{ K})}$$

$$= 0.0306429 \text{ mol}$$

$$= 30.6429 \text{ mmol}$$

$$\begin{aligned} \therefore \text{Total number of mols in gas product} &= \frac{35.3316 \text{ atm} \times 0.831 \text{ L}}{(0.082061 \text{ atm L / mol K}) \times (307 \text{ K})} \\ &= 1.165437 \text{ mol} \\ &= 1165.437 \text{ mmol} \end{aligned}$$

Table B.1.1: GC analysis for final gas product and its total mmol

Gas Products	Mol %	mmol
H ₂	20.017	233.2855
CO ₂	65.703	765.7307
CO	6.124	71.3727
H ₂ S	8.156	95.0477

For CO conversion equation (3-1) is applied:

$$\begin{aligned} X_{CO} (\%) &= \frac{N_{CO_i} - N_{CO_f}}{N_{CO_i}} \times 100 \\ &= \frac{1161.91 - 71.3727}{1161.91} \times 100 \\ &= 94 \% \end{aligned}$$

Equations, (3-4), (3-5) and (3-6) are used to calculate the following:

$$H_2 \text{ Consumed} = 765.73 - 233.28 = 532.45 \text{ mmol}$$

$$H_2 \text{ Generated} = 1161.91 - 71.37 = 1090.54 \text{ mmol}$$

$$H_2S \text{ Generated} = 95.05 - 30.64 = 64.41 \text{ mmol}$$

B.2 WGSR Kinetics

To calculate k_1 CO rate constant, data from Run # 23 is used to illustrate the method of calculation.

Table B.2.1: GC analysis during the reaction time (mol %)

Batch	Mol%				
Time (min)	H ₂	CO ₂	CO	H ₂ S	Total
0	18.8034	37.1308	40.470	3.594	100
20	18.1023	50.7385	24.540	6.617	100
40	18.3076	57.7040	15.320	8.664	100
60	18.8872	61.5880	9.536	9.989	100
80	20.8228	63.7928	7.087	8.297	100
100	21.4829	64.7364	5.088	8.693	100
120	21.7199	65.8608	3.299	9.121	100
140	20.9737	66.0254	2.965	10.040	100
160	21.5373	66.2298	2.395	9.838	100
180	21.2203	66.9360	2.041	9.803	100
210	19.9513	67.4149	1.708	10.930	100
240	20.9993	67.3003	1.676	10.020	100

To calculate the partial pressures of CO, first the vapour pressure of H₂O at the reaction temperatures should be determined by the use of Forst Kalkwarf- Thodos equation (Reid, et al., 1987).

$$\ln\left(\frac{P_{vp}}{P_c}\right) = (1-x)^{-1}(Ax + Bx^{1.5} + Cx^3 + Dx^6)$$

where,

$$x = 1 - \frac{T}{T_c}$$

Where, P_{vp} = Vapour pressure (bars)

P_c = Critical pressure (bars)

T = Temperature (K)

T_c = Critical temperature (K)

A,B,C and D= Constants

For H₂O, the values of the constants are as follows:

$$A = -7.76451$$

$$B = 1.45838$$

$$C = -2.77580$$

$$D = -1.23303$$

This procedure was carried out on a spreadsheet from Excel software to enable the correction of the total pressure in the system, as shown in Table B.2.2.

Table B.2.2: Corrected pressures in the system, Run # 10

Batch Time (min)	Press. (psi)	Temp. (°C)	"x"	VP H ₂ O (psi)	Corrected Press (psi)
0	3090.50	340.39	0.052387	2155.34	935.1639
20	2995.90	340.00	0.052989	2144.81	851.0923
40	3022.30	342.10	0.049745	2201.99	820.3098
60	2957.40	341.39	0.050842	2182.52	774.8784
80	2895.80	341.70	0.050363	2191.00	704.7951
100	2826.50	341.89	0.050070	2196.22	630.2826
120	2752.70	342.00	0.049900	2199.24	553.4602
140	2676.80	341.79	0.050224	2193.47	483.3272
160	2606.40	342.10	0.049745	2201.99	404.4098
180	2527.20	341.40	0.050827	2182.79	344.4051
210	2455.70	341.60	0.050518	2188.27	267.4345
240	2394.10	340.29	0.052541	2152.63	241.4675

The partial pressure of each component was calculated using an Excel spread sheet as shown in Table B.2.3,

Where,

$$\text{Partial pressure} = \text{number of mols} \times \text{corrected total pressure}$$

Table B.2.3: The partial pressure for each component (psi)

Batch Time (min)	H ₂	CO ₂	CO	H ₂ S
0	175.84	347.23	378.48	33.61
20	154.07	431.83	208.88	56.31
40	150.18	473.35	125.70	71.07
60	146.35	477.23	73.89	77.40
80	146.76	449.61	49.95	58.48
100	135.40	408.02	32.07	54.79
120	120.21	364.51	18.26	50.48
140	101.37	319.12	14.33	48.50
160	87.10	267.84	9.68	39.79
180	73.08	230.53	7.03	33.76
210	53.36	180.29	4.57	29.22
240	50.71	162.51	4.05	24.21

Assuming the WGSR is an irreversible reaction, and from the ideal gas law, CO concentration was calculated as shown in Table B.2.4.

Table B.2.4: The CO concentration during the reaction time

Batch Time (min)	[CO] (mmol/L)	Ln [CO ₀ /CO _t]
0	511.511	0.0000
20	282.480	0.5938
40	169.416	1.1050
60	99.702	1.6352
80	67.364	2.0273
100	43.232	2.4708
120	24.609	3.0342
140	19.327	3.2759
160	13.052	3.6684
180	9.484	3.9877
210	6.163	4.4189
240	5.471	4.5378

Plotting the time vs $\ln [CO_0/CO_t]$ giving a straight line passing through the origin with a slope k_1 as shown in Figure B.2.1.

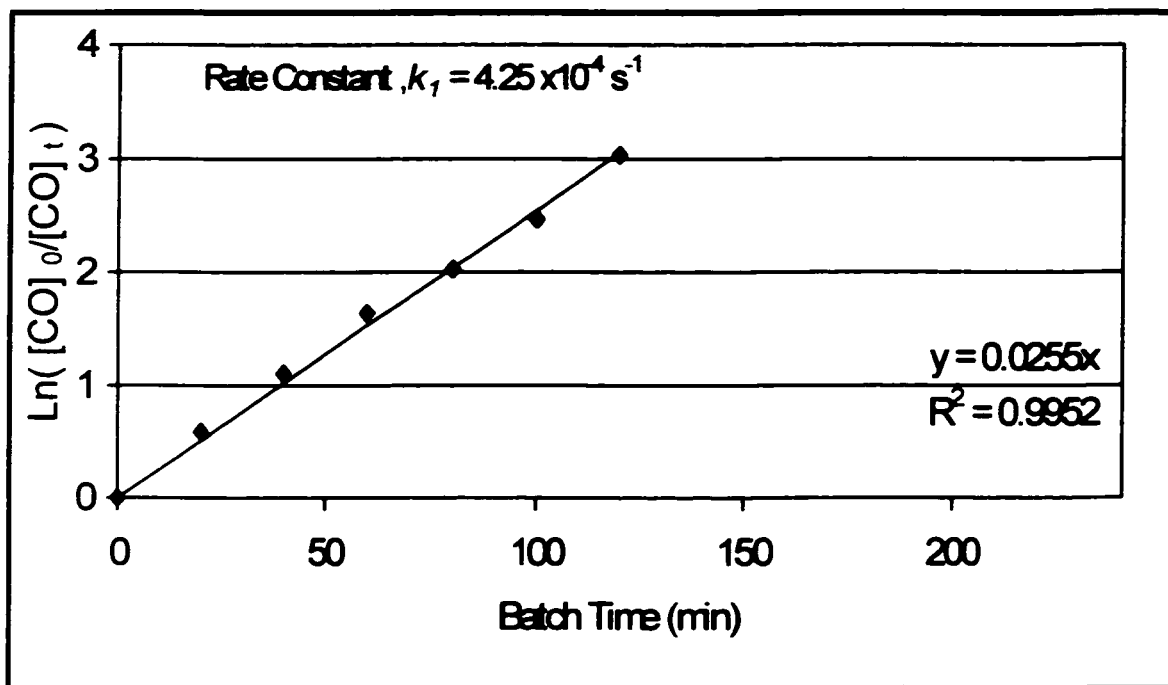


Figure B.2.1: The pseudo first order rate constant for CO conversion, Run # 10

B.3 Liquid Analysis of HDS of BTH

This calculation is based on the calculations of Run # 10 using the PMA catalyst (1500 ppm Mo). Table B.3.1 shows the raw data on a spreadsheet for the liquid analysis on GC.

Table B.3.1: GC- liquid analysis for BTH reaction network during reaction time, Run#10

Batch Time (min)	Toluene	ETHBZ	BTH	DHBTH	N _{Total}
	Mol				
Feed	355.5578		21.7624		377.3202
0	418.6503	2.6715	11.5364	10.2294	443.0876
20	334.3022	9.1827	2.8734	6.1364	352.4947
40	371.8900	16.0736	1.0469	2.5399	391.5504
60	502.2827	25.2293	0.2208	0.6070	528.3398
80	498.6527	25.6592	0	0.0647	524.3768
100	499.6566	25.9128	0	0.1429	525.7123
120	459.5031	23.8810	0	0	483.3841
140	484.1386	25.6486	0	0	509.7872
160	513.1689	26.6360	0	0	539.8049
180	476.3292	24.5033	0	0	500.8325
210	489.5299	25.6351	0	0	515.1650
240	472.0110	24.4835	0	0	496.4945
Liquid Product	357.8132	18.7009	0.1586	0	376.6727

Equations 3-14, 3-15 and 3-16, were used to calculate each component mole fraction % as shown in Table B.3.2.

➤ For BTH mole fraction, equation (3-15) applied at time, $t = 0.0$ min:

$$\text{mol \% BTH} = \frac{11.5364}{443.0876} \times 100 = 0.8152$$

➤ For ETHBZ mole fraction equation (3-16) applied at time, $t = 0.0$ min

$$\text{mol \% ETHBZ} = \frac{2.6715}{443.0876} \times 100 = 0.6029$$

➤ For DHBTH mole fraction equation (3-17) applied at time, $t = 0.0$ min

$$\text{mol \% DHBTH} = \frac{10.2294}{443.0876} \times 100 = 2.3087$$

Table B.3.2: Mole fraction % for each component, Run#10

Batch Time (min)	Toluene	ETHBZ	BTH	DHBTH	Total
	Mol %				
Feed (N_{BTH})_i	94.2324		5.7676		100
0	94.4848	0.6029	2.6036	2.3087	100
20	94.8389	2.6051	0.8152	1.7409	100
40	94.9788	4.1051	0.2674	0.6487	100
60	95.0681	4.7752	0.0418	0.1149	100
80	95.0944	4.8933	0	0.0124	100
100	95.0437	4.9291	0	0.0272	100
120	95.0596	4.9404	0	0	100
140	94.9688	5.0312	0	0	100
160	95.0656	4.9344	0	0	100
180	95.1075	4.8925	0	0	100
210	95.0239	4.9761	0	0	100
240	95.0687	4.9313	0	0	100
Final Product (N)_f	94.9931	4.9648	0.0421	0	100

The mole fraction obtained will enable the following calculations:

(1) BTH conversion, equation (3-18) used:

$$X_{BTH} = \frac{5.7676 - 0.0421}{5.7676} \times 100 = 99.27 \%$$

(2) Sulfur removal, equation (3-19) applied for the final product:

$$\% S \text{ Re } m = \frac{4.9648}{(4.9648 + 0 + 0.0421)} = 99.16 \%$$

(3) ETHBZ yield, equation (3-20) applied for the final product:

$$\% \text{ yield} = \frac{4.9648}{5.7676} \times 100 = 86.08 \%$$

(4) ETHBZ selectivity, equation (3-21) applied for the final product:

$$ETHBZ \text{ Sel} = \frac{4.9648}{4.9648 + 0} = 1$$

B.4 HDS Kinetics

The calculation of BTH rate constant (k_2) based on equation (3-23). Plotting $\ln(N_0/N_t)_{\text{BTH}}$ vs time, t , resulted in a straight line passing through the origin with a slope equal to k_2 , the data shown in Table B.4.1.

Table B.4.1: The calculated data for pseudo first order plot, Run#10

Batch Time (min)	Mol % BTH	$\ln(N_0/N_t)_{\text{BTH}}$
0	2.6036	0
20	0.8152	1.1613
40	0.2674	2.2760
60	0.0418	4.1320
80	0	#DIV/0!
100	0	#DIV/0!
120	0	#DIV/0!
140	0	#DIV/0!
160	0	#DIV/0!
180	0	#DIV/0!
210	0	#DIV/0!
240	0	#DIV/0!

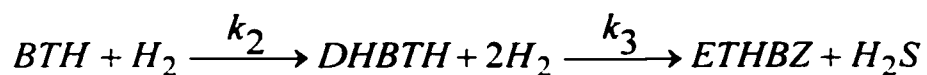
B.5 Availability of H₂ during the HDS of BTH

From the calculation in Appendix B.1, the amount of H₂ generated in the system is 1091 mmol.

Initial weight of BTH = 14.1 g

$$\text{Amount of S in (14.1 g) BTH} = \frac{14.1 \times 32.06}{134.2} = 3.368 \text{ g} \quad (105.1 \text{ mmol})$$

For the BTH reaction network to completely hydrogenate BTH to ETHBZ 3 atom of H₂ is needed. Therefore, 315.2 mmol of H₂ is enough for the complete desulfurization of BTH.



∴

$$\text{Number of mols of } H_2 \text{ in excess} = 1091 - 315.2 = 775.8 \text{ mmol}$$

B.6 Liquid Analysis of AHYD of NAPH

This calculation is based on the data of Run # 8 using PMA catalyst (1500 ppm Mo). As shown in section 4.2 the GC results of liquid analysis for NAPH reaction network were based on the data analyzed by the GC for each liquid sample, during the course of the reaction, see Table B.6.1.

Table B.6.1: GC- liquid analysis for NAPH reaction network during reaction time, Run#8

Batch Time (min)	Toluene	trans-DEC	cis-DEC	TET	NAPH	N _{Total}
	Mol					
Feed	465.6937	0	0		89.1934	554.8871
0	185.0347	0	0	0.5491	45.0331	230.6169
30	246.0972	0	0	3.8399	44.7658	294.7029
60	238.2940	0	0	7.1863	39.8808	285.3611
90	408.8552	0	0	18.4322	56.5653	483.8527
120	289.0877	0.0862	0	16.9908	33.9700	340.1347
150	400.9875	0	0	30.2487	43.6740	474.9102
180	374.7870	0.1071	0.3605	30.3214	33.3196	438.8956
210	315.9856	0.0792	0	28.5058	25.2867	369.8573
240	400.6369	0.2541	0.1329	38.0592	28.1610	467.2441
Liquid Product	389.6886	0.36345	0.2673	41.8780	24.6624	456.8597

The calculation of the % mole fraction for each component as the following:

$$\% \text{ mol fraction of component} = \frac{\text{mols of component}}{\text{Total mols of all components}} \times 100$$

The calculation was carried out on Excel spreadsheet, results shown in Table B.6.2.

Table B.6.2: Mole fraction % for each components, Run#8

Batch Time (min)	Toluene	trans-DEC	cis-DEC	TET	NAPH	Total
	Mol %					
Feed (N_{NAPH})_i	83.9258	0	0	0	16.0742	100
0	80.2347	0	0	0.2381	19.5272	
30	83.5069	0	0	1.3030	15.1901	100
60	83.5062	0	0	2.5184	13.9756	100
90	84.4999	0	0	3.8095	11.6906	100
120	84.9921	0.0253	0	4.9953	9.9872	100
150	84.4344	0	0	6.3693	9.1963	100
180	85.3932	0.0244	0.0821	6.9086	7.5917	100
210	85.4345	0.0214	0	7.7072	6.8369	100
240	85.7447	0.0544	0.0284	8.1455	6.0270	100
Final Product(N)_f	85.2972	0.079554	0.0585	9.1665	5.3983	100

The result facilitates the following calculation:

(1) NAPH conversion, equation (3-24) used:

$$X_{NAPH} \% = \frac{16.0742 - 5.3983}{16.0742} \times 100 = 66.42 \%$$

(2) Aromatic removal, equation (3-25) used for the final product:

$$\% A_{rem} = \frac{9.1665 + 0.0585 + 0.0796}{5.3983 + 9.1665 + 0.0585 + 0.0796} \times 100 = 63.28 \%$$

(3) TET yield, equation (3-26) used for the final product:

$$\% \text{ yield} = \frac{9.1665}{16.0741} \times 100 = 57.026 \%$$

(4) Tetralin selectivity, equation (3-27) used for the final product:

$$TET \text{ Sel} = \frac{9.1665}{9.1665 + 0.07955 + 0.0585} = 0.985$$

(5) Hydrogenation Activity A_H

Equation (3-28) is used to calculate the hydrogenation activity as follows:

$$A_H = \frac{2(9.1665) + 5(0.0585 + 0.0796)}{5(5.3982 + 9.1665 + 0.0585 + 0.0796)} = 0.259$$

The same calculation for A_H was carried out for Run#26, #27, #29, and #30, for raw data refer to Appendix F.

B.7 AHYD kinetics

The calculation of the rate constant of the NAPH conversion (k_4) is based on the pseudo first order reaction plot, equation (3-32). Table B.7.1. shows calculated data of Run #8.

Table B.7.1: The data for the pseudo first order plot, Run#8

Batch Time (min)	Mol % NAPH	$\ln(N_0/N_t)_{\text{NAPH}}$
0	19.5272	0
30	15.1901	0.2512
60	13.9756	0.3345
90	11.6906	0.5130
120	9.9872	0.6705
150	9.1963	0.7530
180	7.5917	0.9448
210	6.8369	1.0495
240	6.0270	1.1756

Plotting time, t , versus $\ln(N_0/N_t)$ resulted a straight line passing through the origin, as shown previously in Figure 4.2.5, with a slope equal to k_4 .

B.8 Availability of H₂ during the HYD of NAPH

Initial reading for loading CO, Run # 8

Temperature (°C) = 29.3 (302.3 K)

Pressure (psi) = 585 (39.80925 atm)

Volume of liquid feed (ml) = 270 (0.270 L)

$V_{\text{gas Feed}} = 0.725 \text{ L}$

Final gas product reading for Run # 8

Temperature (°C) = 35.2 (308.2 K)

Pressure (psi) = 532.4 (36.22982 atm)

Total working reactor volume (ml) = 995 (0.995 L)

Volume of liquid product (ml) = 208 (0.208 L)

R gas constant = 0.082061 atm L/ mol K

$$V_{\text{gas}} = V_{\text{reactor}} - V_{\text{Liquid}}$$

$$\therefore V_{\text{gas Pro}} = 0.787 \text{ L}$$

$$H_2 \text{ Consumed} = 758.6297 - 257.9388 = 500.6909 \text{ mmol}$$

$$H_2 \text{ Generated} = 1163.4482 - 96.1496 = 1067.2980 \text{ mmol}$$

The raw data for the gas analysis of Run # 8 can be found in Appendix F.

For the hydrogenation of NAPH, 2 atoms of H₂ is needed to hydrogenate the first ring,

whereas 3 atoms of H₂ are required to hydrogenate the second ring as shown below:



Therefore.

Initial weight of NAPH = 43.25 g

$$\text{Amount of aromatics in 43.25g NAPH} = \frac{43.25}{128.17} = 0.33744 \text{ mol} \quad (337.44 \text{ mmol})$$

Therefore. 674.88 mmol of H₂ is required to hydrogenate the first ring

∴

$$\text{Number of mols of } H_2 \text{ in excess} = 1067.298 - 674.88 = 392.418 \text{ mmol}$$

Appendix C

Sample of Calculations for Binary Mixture

C.1 Gas Analysis

Initial reading for CO loading, Run # 23

Temperature ($^{\circ}\text{C}$) = 27.8 (300.8 K)

Pressure (psi) = 585 (39.80925 atm)

Volume of liquid feed (ml) = 270 (0.270 L)

$V_{\text{gas Feed}} = 0.725 \text{ L}$

Initial reading for H₂S loading, Run # 23

Temperature ($^{\circ}\text{C}$) = 20 (293 K)

Pressure (psi) = 15 (1.02075 atm)

Volume of liquid feed (ml) = 270 (0.270 L)

$V_{\text{gas Feed}} = 0.725 \text{ L}$

Final reading for the gas product, Run # 23

Temperature ($^{\circ}\text{C}$) = 32.6 (305.6K)

Pressure (psi) = 446.6 (30.3911 atm)

Total working reactor volume (ml) = 995 (0.995 L)

Volume of liquid product (ml) = 224 (0.224 L)

R gas constant = 0.082061 atm L/ mol K

The same calculation used in Appendix B.1, resulted the following:

$$N(CO)_i = 1169.2499 \text{ mmol}$$

$$N(CO)_f = 30.77889 \text{ mmol}$$

$$H_2S \text{ generated} = 78.19769 - 30.77889 = 47.4188 \text{ mmol}$$

$$H_2 \text{ consumed} = 598.4214 \text{ mmol}$$

$$H_2 \text{ generated} = 1105.32 \text{ mmol}$$

$$X_{CO} (\%) = 94.53$$

The raw data, for the GC gas analysis of Run # 23 is available in Appendix F.

C.2 Liquid Analysis

The calculation are based on Run # 23 for using a mixture of model compounds (BTH+NAPH) under the same operating conditions and Table C.2.1 indicates the GC analysis for the feed and liquid samples during the course of the reaction.

Table C.2.1: GC- Liquid analysis for binary mixture of BTH+NAPH during reaction time. Run#23

Batch Time (min)	Toluene	ETHBZ	trans-DEC	cis-DEC	TET	NAPH	BTH	DHBTH	N _{Total}
	Mol								
Feed	489.2236					72.0237	22.7779		584.0252
0	552.8164	3.5542	0	0	2.7476	75.2608	9.9831	9.9955	654.3576
30	498.3674	12.8861	0	0	10.0666	66.2645	2.5638	6.4079	596.5563
60	507.7524	19.5112	0	0	19.6567	57.1613	0.5055	1.6284	606.2155
90	690.3661	29.4127	0.3022	0	39.6754	64.6732	0	0.3421	824.4296
120	453.8987	19.3355	0	0	32.6974	36.0567	0	0	541.9882
150	435.2254	18.6215	0.0715	0	35.6593	30.0628	0	0	519.6405
180	429.2230	18.1857	0.1854	0.1543	38.4606	26.2710	0	0	512.4800
210	483.9977	20.4172	0.2496	0.1408	46.2840	26.6663	0	0	577.7556
240	434.3126	18.6054	0.3206	0.1459	43.3899	22.0799	0	0	518.8543
Liquid Product	439.2428	18.971	0.5185	0.1779	45.6778	21.0207	0	0	525.6087

Calculating the % mol fraction for each component as follows:

$$\% \text{ mol fraction of component} = \frac{\text{mols of component}}{\text{Total mols of all components}} \times 100$$

Table C.2.2: Mole fraction % for each component, Run#23

Batch Time(min)	Toluene	ETHBZ	trans-DEC	cis-DEC	TET	NAPH	BTH	DHBTH	Total
	Mol%								
Feed (N)_i	83.76755					12.3323	3.9001		100
0	84.4823	0.5432	0	0	0.4199	11.50149	1.5256	1.5275	100
30	83.5407	2.1601	0	0	1.6874	11.10784	0.4298	1.0741	100
60	83.7577	3.2185	0	0	3.2425	9.42920	0.0834	0.2686	100
90	83.7386	3.5676	0.0367	0	4.8125	7.84460	0	0.0415	100
120	83.7469	3.5675	0	0	6.0329	6.65266	0	0	100
150	83.7551	3.5835	0.0138	0	6.8623	5.78531	0	0	100
180	83.7541	3.5486	0.0362	0.0301	7.5048	5.12625	0	0	100
210	83.7721	3.5339	0.0432	0.0244	8.0101	4.61550	0	0	100
240	83.7061	3.5859	0.0618	0.0281	8.3626	4.25551	0	0	100
Final Product (N)_f	83.5684	3.6093	0.0987	0.0338	8.6905	3.9993	0	0	100

These results enable to calculate the following, using equations (3-18)-(3-21) and equations (3-24)-(3-28):

$$X_{BTH} = 100 \%$$

$$S_{rem} = 100 \%$$

$$ETHBZ \text{ yield} = 92.54 \%$$

$$ETHBZ \text{ Sel} = 1$$

$$X_{NAPH} = 67.57 \%$$

$$A_{rem} = 68.81 \%$$

$$TET \text{ yield} = 70.50 \%$$

$$TET \text{ Sel} = 0.985$$

$$A_H = 0.281$$

Table C.2.3 illustrates the kinetic calculation by using the pseudo first order reaction equations (3-23) and (3-32) to calculate the rate constants for both BTH and NAPH respectively.

Table C.2.3: The kinetic data

	NAPH	BTH
Batch Time (min)	$\ln(N_0/N_t)$	$\ln(N_0/N_t)$
0	0	0
30	0.034825	1.266923
60	0.198664	2.906682
90	0.38265	#DIV/0!
120	0.547458	#DIV/0!
150	0.687154	#DIV/0!
180	0.808101	#DIV/0!
210	0.913056	#DIV/0!
240	0.994261	#DIV/0!

Refer to section 4.3 for the pseudo first order plots.

C.3 Availability of H₂ during the HYD of Binary Mixture

This calculation is based on the data obtained from Run#23:

H₂ generated = 1105.32 mmol

Completely S removal = 315.2 mmol of H₂ are needed

HYD of NAPH to TET = 674.88 mmol of H₂ are needed

Total mmol of H₂ needed = 990.08 mmol

Number of mol of H₂ in excess = 1105.32 – 990.08 = 115.24 mmol

H₂ in gas products (GC – analysis) = 96.90 mmol

$$\% \text{ Error} = \frac{115.24 - 96.90}{115.24} \times 100 = 16 \%$$

C.4 Calculation of H₂O/CO ratio

C.4.1 Via CO loading

This calculation is based on the data obtained from Run # 23 and Run # 25

➤ For 600 psi CO loading, Run # 23:

$$\text{Weight of H}_2\text{O used} = 70 \text{ g} \quad (3.889 \text{ mol})$$

$$\text{Initial number of mols of CO} = 1.1692 \text{ mol}$$

$$\therefore H_2O/CO = \frac{3.889}{1.1692} = 3.33 \text{ mol/mol}$$

➤ For 300 psi CO loading, Run # 25 for experimental raw data check Appendix F:

$$\text{Weight of H}_2\text{O used} = 70 \text{ g} \quad (3.889 \text{ mol})$$

$$\text{Initial number of mols of CO} = 0.5729 \text{ mol}$$

$$\therefore H_2O/CO = \frac{3.889}{0.5729} = 6.788 \text{ mol/mol}$$

$$H_2 \text{ generate} = 572.87 - 41.34 = 531.53 \text{ mmol}$$

$$H_2 \text{ in excess} = 531.53 - 990.80 = -459.27 \text{ mmol}$$

Therefore, there is a lack of 456.27 mmol of H₂ when 300 psi CO loading is used.

C.4.2 Via H₂O amount

This calculation is based on the data obtained from Run # 23 and Run # 18

- For Run # 23 refer to Appendix C.4.1.

- For Run # 18 check Appendix F for experimental raw data,

Weight of H₂O used = 35 g (1.944 mol)

Initial number of mols of CO = 1.1696 mol

$$\therefore H_2O/CO = \frac{1.944}{1.1696} = 1.662 \text{ mol/mol}$$

$$H_2 \text{ generated} = 1169.639 - 89.136 = 1080.5 \text{ mmol}$$

$$H_2 \text{ in excess} = 1080.50 - 990.80 = 89.70 \text{ mmol}$$

$$H_2 \text{ in gas product (GC - analysis)} = 85.88 \text{ mmol}$$

Appendix D

Mass balance

D.1 Overall Mass Balance

This calculation was based on the liquid phase of the recorded weights for each liquid sample collected, and the flushing between samples, during the course of the reaction neglecting the gas phase for Run # 8 as follows:

$$\text{Total weight of feed (Input)} = 280.17 \text{ g}$$

$$\text{Weight of flushed samples (Output)} = 13.94 \text{ g}$$

$$\text{Total weight of samples (Output)} = 29.78 \text{ g}$$

$$\text{Weight of cold Liquid product (Output)} = 184 \text{ g}$$

$$\text{Total Input} = 280.17 \text{ g}$$

$$\text{Total Output} = 227.72 \text{ g}$$

$$\begin{aligned} \% \text{Losses} &= \frac{\text{Input} - \text{Output}}{\text{Input}} \times 100 \\ &= \frac{280.17 - 227.72}{280.17} \times 100 = 18.72 \% \end{aligned}$$

$$\text{Overall Mass balance} = \frac{227.72}{280.17} \times 100 = 81.28 \%$$

D.2 Component Balance

This calculation is based on the amount of the model compound in the feed, and the amount of the product obtained according to its reaction network. The data from Run # 23 are used to illustrate this calculation, see Table D.2.1 and Table D.2.2.

➤ For BTH reaction network, ETHBZ is the primary product.

Table D.2.1: BTH mass balance

BTH Balance (GC-Liquid analysis)			
Input	mol%	Output	mol%
BTH	3.90	BTH	0.00
		ETHBZ	3.61
		DHBTH	0.00
Total	3.9	Total	3.61

$$\% \text{ losses} = \frac{3.90 - 3.61}{3.90} \times 100 = 7.44\%$$

$$\therefore \text{mol balance} = 92.56 \%$$

These losses may have occurred because some of the BTH available in the vapour phase or because of some of the BTH deposited on the catalysts.

- For the NAPH reaction network, TET is the primary product with negligible quantities of decalins.

Table D.2.2: NAPH mass balance

NAPH Balance (GC-Liquid analysis)			
Input	mol%	Output	mol%
NAPH	12.330	NAPH	3.990
		TET	8.690
		cis-DEC	0.034
		trans-DEC	0.098
Total	12.33	Total	12.812

$$\% \text{ losses} = \frac{12.33 - 12.812}{12.33} \times 100 = -0.039\%$$

$$\therefore \text{mol balance} = 103.91\%$$

- For the gas components, the mass balance was based on Run # 23 as shown in Table D.2.3.

Table D.2.3: Gas mass balance

Gas balance (GC-gas analysis)			
Input	mmol	Output	mmol
CO	1169.25	H ₂	96.900
H ₂ S	30.78	CO ₂	695.322
		CO	63.932
		H ₂ S	78.197
Total	1200.03	Total	934.351

$$\% \text{ losses} = \frac{1200.03 - 934.351}{1200.03} \times 100 = 22.14\%$$

$$\therefore \text{mol balance} = 77.86 \%$$

These losses are due to the following:

- The losses of H_2 during sampling and flushing.
- The ability of CO_2 and H_2S gases to dissolve in liquid phase.

Appendix E

Reproducibility

Run #:13 and Run # 17

Using H₂, 585 psi, H₂S 15 psi

Operating Conditions :

200 ml Tol

13.45g PMA catalyst solution + 57.27g water, PH_i=1.92

43.25g NAPH

14.11g BTH

Table E.1: Reproducibility of Run #13 and Run #17

Run #	13	17	S	S_E
GC- Liquid Analysis				
BTH_{Initial} (mol%)	3.69	3.980	0.20506	0.145
NAPH_{Initial} (mol%)	11.60	12.518	0.64912	0.459
X_{CO} (%)	NA	NA	*****	*****
X_{BTH} (%)	100.00	100	0	0
S removal (%)	100.00	100	0	0
ETHBZ yield (%)	99.1	99.16	0.04243	0.030
X_{NAPH} (%)	57.88	59.57	1.19501	0.845
A removal (%)	58.63	60.14	1.06773	0.755
TET yield (%)	60.22	61.31	0.77075	0.545

S= Standard deviation, S_E= Standard Error, *Based on NAPH conversion

Run #:20 and Run # 25Using CO, 285 psi, H₂S 15 psi

Operating Conditions :

200 ml Tol

13.45g PMA catalyst solution + 57.28g water, PH_i =1.93

43.25g NAPH

14.1g BTH

Table E.2: Reproducibility of Run #20 and Run #25

Run #	20	25	S	S _E
GC- Liquid Analysis				
BTH_{Initial} (mol%)	3.75	3.88	0.09192	0.065
NAPH_{Initial} (mol%)	11.95	12.19	0.16971	0.120
X_{CO} (%)	93.32	92.78	0.38184	0.270
X_{BTH} (%)	99.03	96.74	1.61927	1.145
S removal (%)	98.33	93.91	3.12541	2.210
ETHBZ yield (%)	88.38	89.57	0.84146	0.595
X_{NAPH} (%)	24.88	24.65	0.16263	0.115
A removal (%)	25.81	27.89	1.47078	1.040
TET yield* (%)	26.14	29.14	2.12132	1.500

S= Standard deviation, S_E= Standard Error, *Based on NAPH conversion

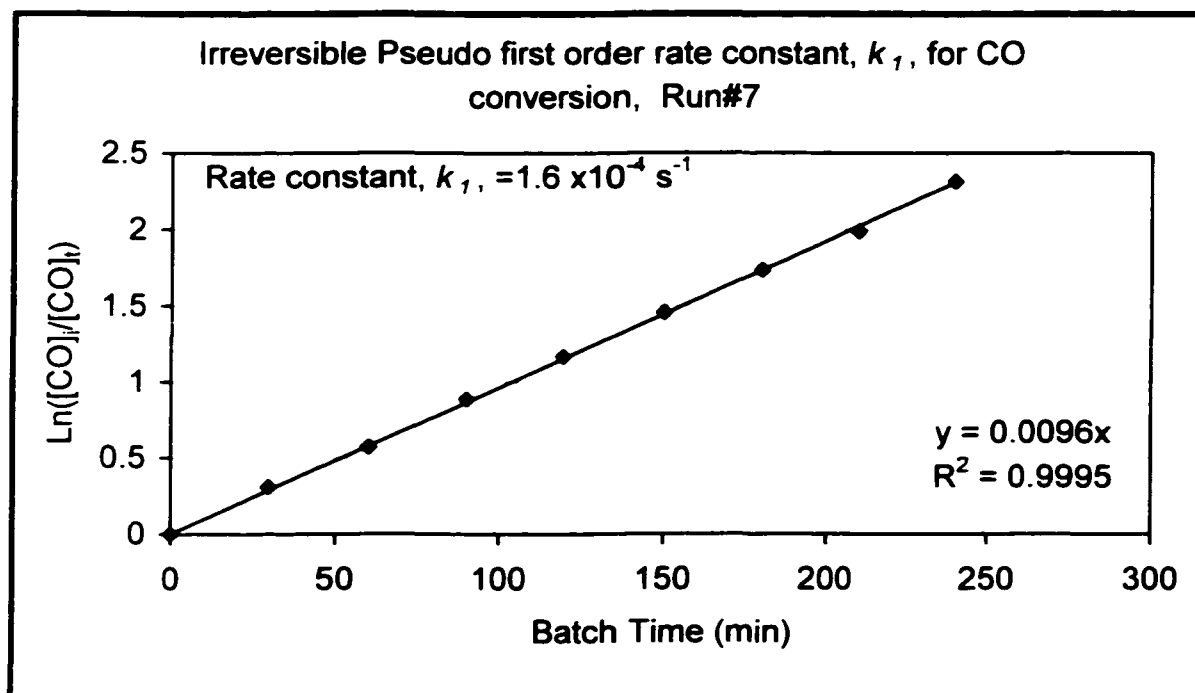
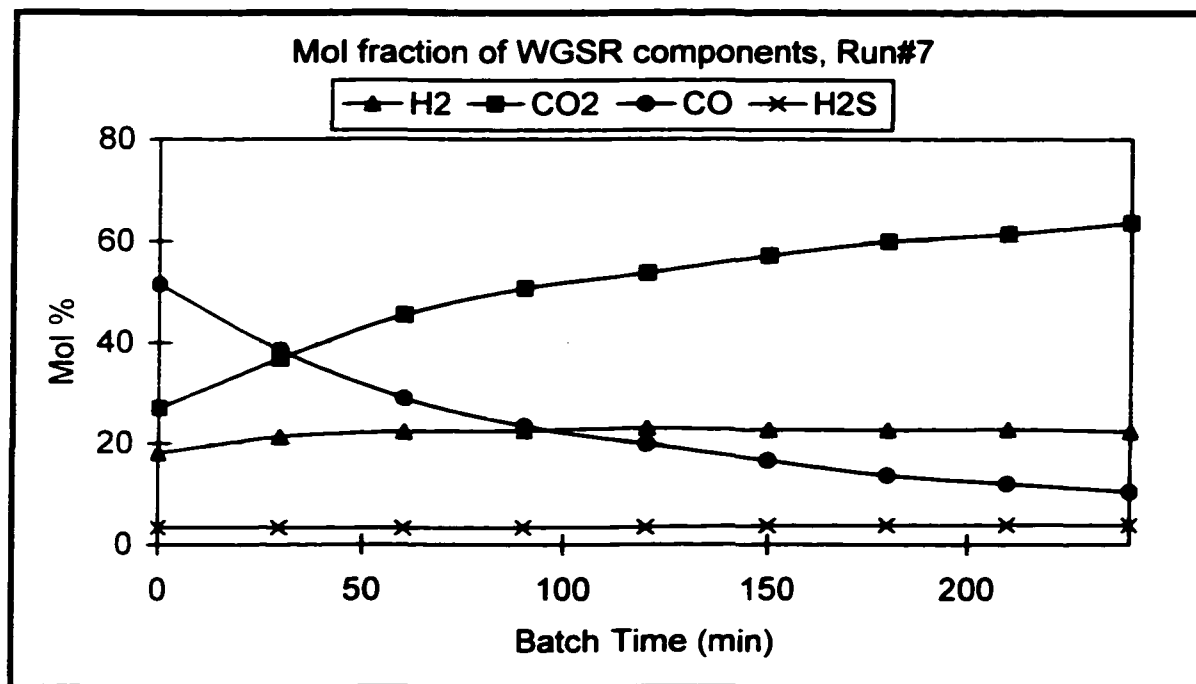
Appendix F
Raw Data and Figures for Selected Runs

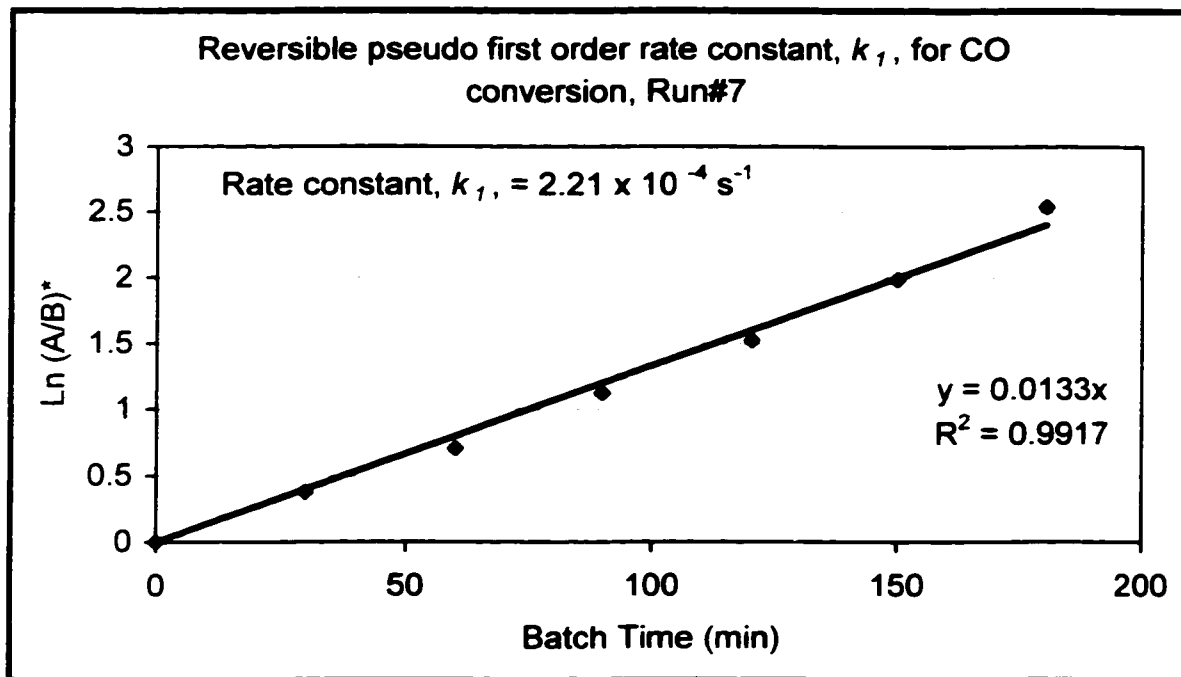
➤ Gas analysis, Run #7

Using CO, 585 psi, H₂S 15 psi,
 Operating Condition :
 200 ml Tol,
 4.5g PMA catalyst (500 ppm Mo) + 65.73g water, pH_i= 2.31
 43.25g Naphthalene

GC analysis Gas Product						
	1	2	3	AVR	mol %	mmol
H ₂	19.8066	19.8087	20.5679	20.0611	27.1060	331.3232
CO ₂	41.4012	41.1364	41.9721	41.5032	56.0781	685.4563
CO	11.0997	11.0750	11.1117	11.0955	14.9919	183.2498
H ₂ S	1.3528	1.3107	1.3864	1.3500	1.8240	22.2957
Totals	73.6603	73.3308	75.0381	74.0097	100.0000	

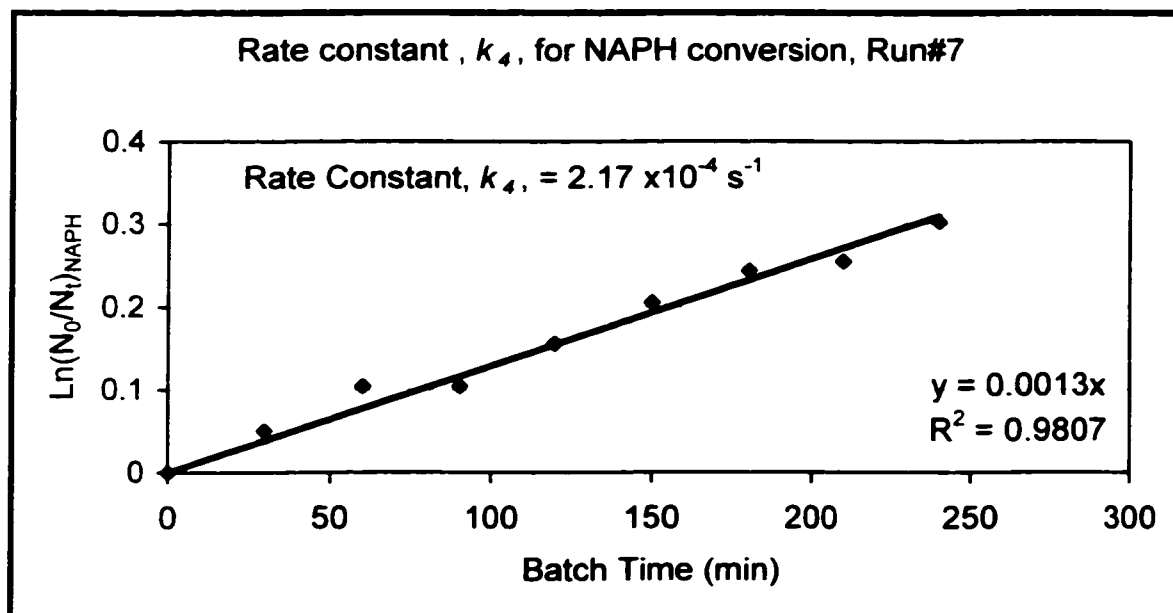
GC- Gas analysis during reaction					
Batch	Mol%				
Time(min)	H ₂	CO ₂	CO	H ₂ S	Total
0	18.0455	27.1033	51.4627	3.3885	100
30	21.2903	36.8382	38.4897	3.3818	100
60	22.2803	45.4357	29.0017	3.2823	100
90	22.4839	50.6346	23.4546	3.4269	100
120	22.9912	53.6467	19.8693	3.4929	100
150	22.6123	57.0822	16.5991	3.7064	100
180	22.5998	59.9374	13.6474	3.8154	100
210	22.7635	61.3734	11.9675	3.8956	100
240	22.2394	63.5255	10.3780	3.8570	100





*For calculation, refer to Rintjema (1992)

➤ Liquid analysis, Run #7



➤ Gas analysis, Run # 8

Using CO, 585 psi, H₂S 15 psi

Operating Conditions :

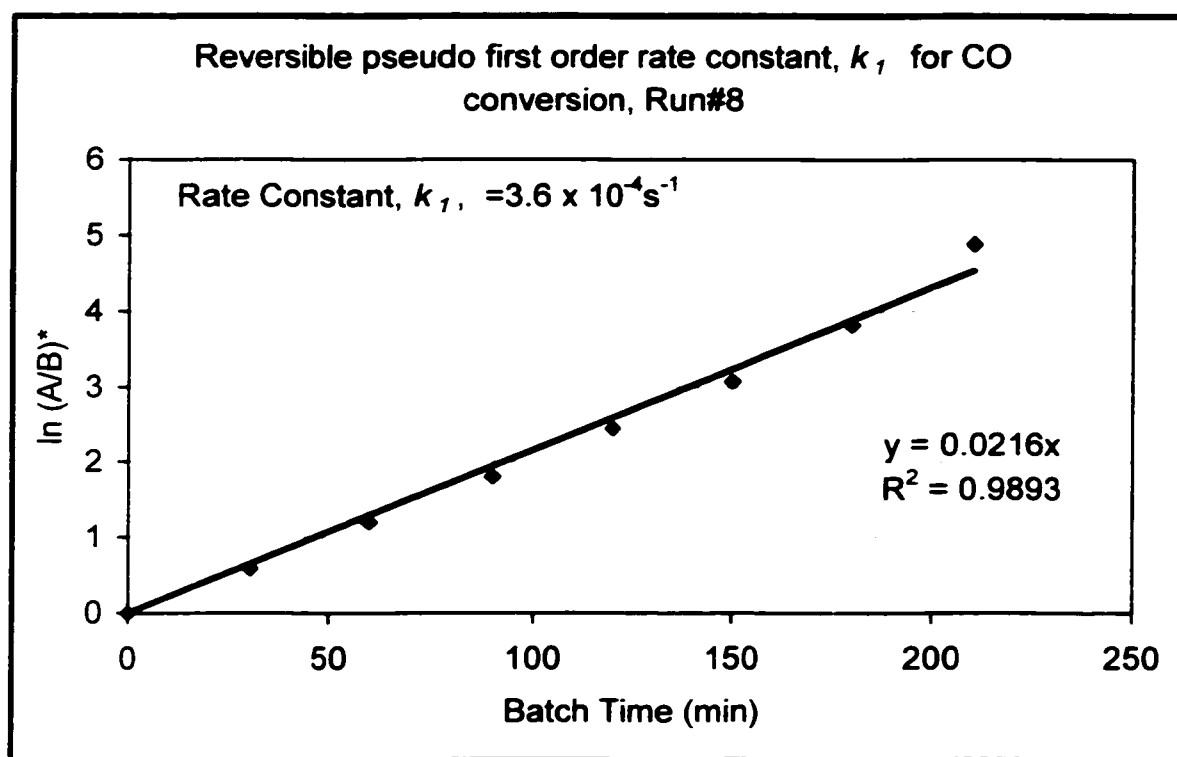
200 ml Tol

13.4g PMA catalyst solution + 57.29g water, PH₁=1.92

43.25g NAPH

GC analysis Gas Product						
	1	2	3	AVR (3)	mol %	mmol
H ₂	17.0664	17.5065	17.3456	17.3062	22.8794	257.9388
CO ₂	51.3303	50.7902	50.5782	50.8996	67.2912	758.6297
CO	6.5211	6.4478	6.3843	6.4511	8.5286	96.1496
H ₂ S	0.9465	0.7810	1.2243	0.9839	1.3008	14.6650
Totals	75.8643	75.5255	75.5324	75.6407	100	

GC- Gas analysis during reaction						
Batch	Mol%					
Time(min)	H ₂	CO ₂	CO	H ₂ S	Total	
0	20.7333	35.5745	41.390	2.303	100	
30	23.4908	50.1271	24.320	2.061	100	
60	23.3683	60.5316	13.650	2.447	100	
90	22.7561	65.6543	8.941	2.649	100	
120	22.3971	69.1297	5.851	2.622	100	
150	22.2740	71.1082	4.100	2.517	100	
180	22.0066	72.6506	2.906	2.437	100	
210	21.3196	73.6958	2.339	2.646	100	
240	19.8806	75.2934	2.068	2.758	100	



*For calculation, refer to Rintjema (1992)

➤ Gas analysis, Run # 18

Using CO, 585 psi, H₂S 15 psi

Operating Conditions :

235 ml Tol

13.25g PMA catalyst solution + 21.75g water= 35.00 ml H₂O PH₁=1.65

43.25g NAPH

14.11g BTH

GC analysis Gas Product						
	1	2	3	AVR (3)	mol %	mmol
H ₂	8.5802	8.6083	8.4305	8.5397	9.6211	85.8845
CO ₂	63.6652	63.9289	63.6779	63.7573	71.8312	641.2154
CO	8.7816	8.9414	8.8660	8.8630	9.9854	89.1363
H ₂ S	7.2205	7.6760	7.9034	7.5999	8.5624	76.4338
Totals	88.2475	89.1546	88.8778	88.75996667	100	

GC- Gas analysis during reaction						
Batch	Mol%					
Time(min)	H ₂	CO ₂	CO	H ₂ S	Total	
0	15.9892	27.8493	55.300	0.861	100	
30	15.1231	42.4185	40.350	2.109	100	
60	13.4385	54.1155	27.630	4.811	100	
90	12.8237	59.8035	21.290	6.081	100	
120	12.2206	64.4211	16.420	6.940	100	
150	11.3282	67.9390	13.220	7.515	100	
180	10.8832	70.2814	10.990	7.844	100	
240	8.8006	73.9328	7.281	9.986	100	

➤ Liquid analysis, Run #18

GC- Liquid analysis

Batch Time	Tol	ETHBZ	trans-DEC	cis-DEC	TET	NAPH	BTH	DHBTH	Total
min	Mol%								
Feed (N₀)	83.807					12.3031	3.89002		100
0	85.031	0.7427	0	0	1.0561	10.7541	1.0212	1.3944	100
30	85.096	1.6113	0	0	1.9741	9.9316	0.4631	0.9237	100
60	85.363	2.4087	0	0.0040	2.9728	8.7370	0.1788	0.3359	100
90	85.149	2.7738	0	0	3.9068	7.9790	0.0774	0.1139	100
120	85.544	2.8492	0.0209	0.0124	4.5956	6.9396	0.0185	0.0202	100
150	85.223	2.9139	0.0251	0	5.4270	6.4113	0	0	100
180	85.151	2.9709	0.0818	0.0234	5.9514	5.8215	0	0	100
210	85.390	2.9611	0.0341	0.0348	6.3254	5.2548	0	0	100
240	84.974	2.9887	0.0505	0.0286	6.9307	5.0093	0.0185	0	100
Cold product (N_r)	85.505	2.9586	0.0489	0.0470	6.97025	4.47036	0	0	100

$$X_{BTH} = 100 \%$$

$$S_{rem} = 100 \%$$

$$ETHBZ \text{ yield} = 76.06 \%$$

$$ETHBZ \text{ Sel} = 1.0$$

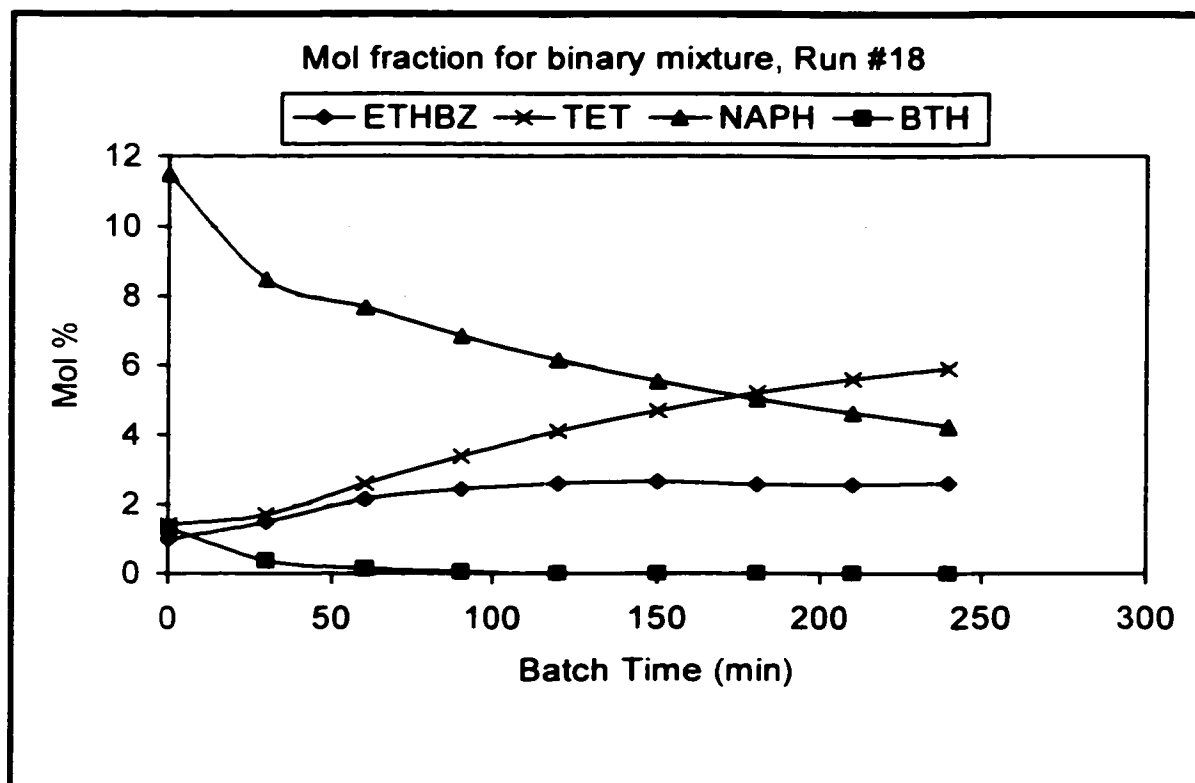
$$X_{NAPH} = 63.66 \%$$

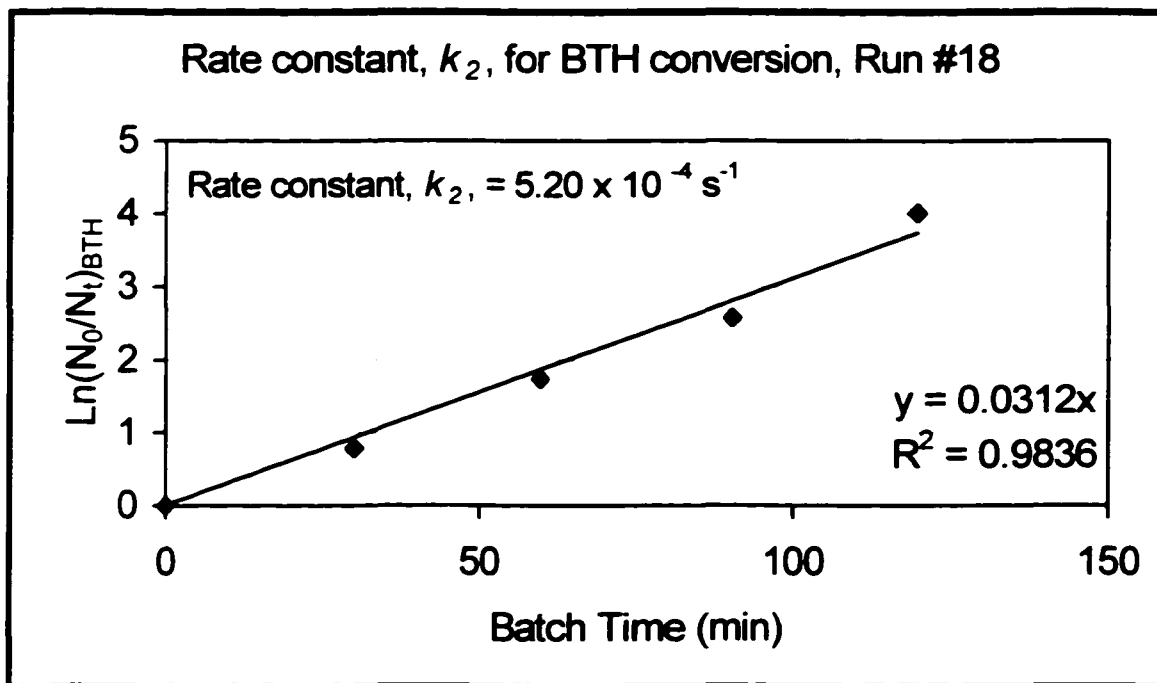
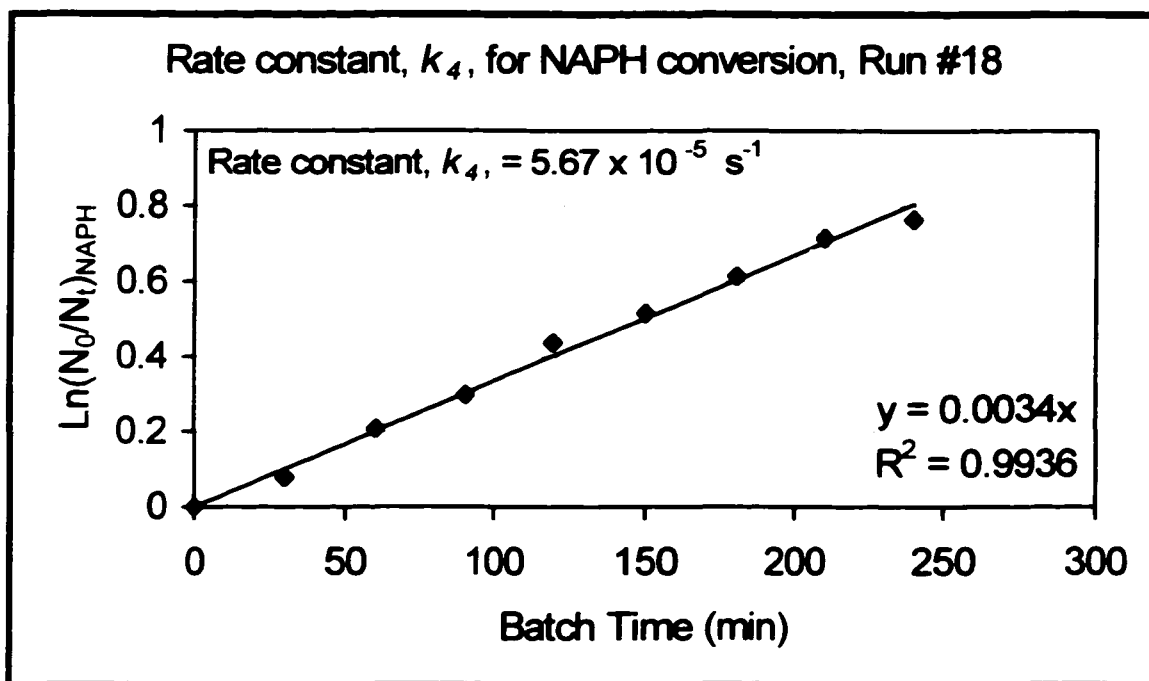
$$A_{rem} = 61.25 \%$$

$$TET \text{ yield} = 56.65 \%$$

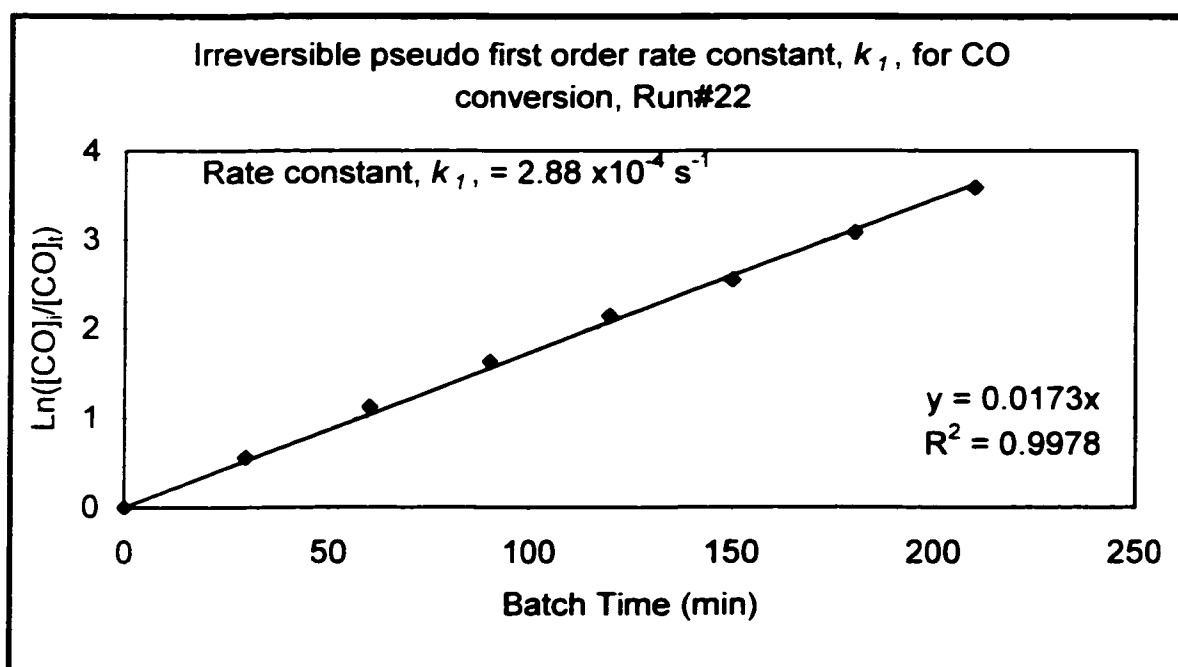
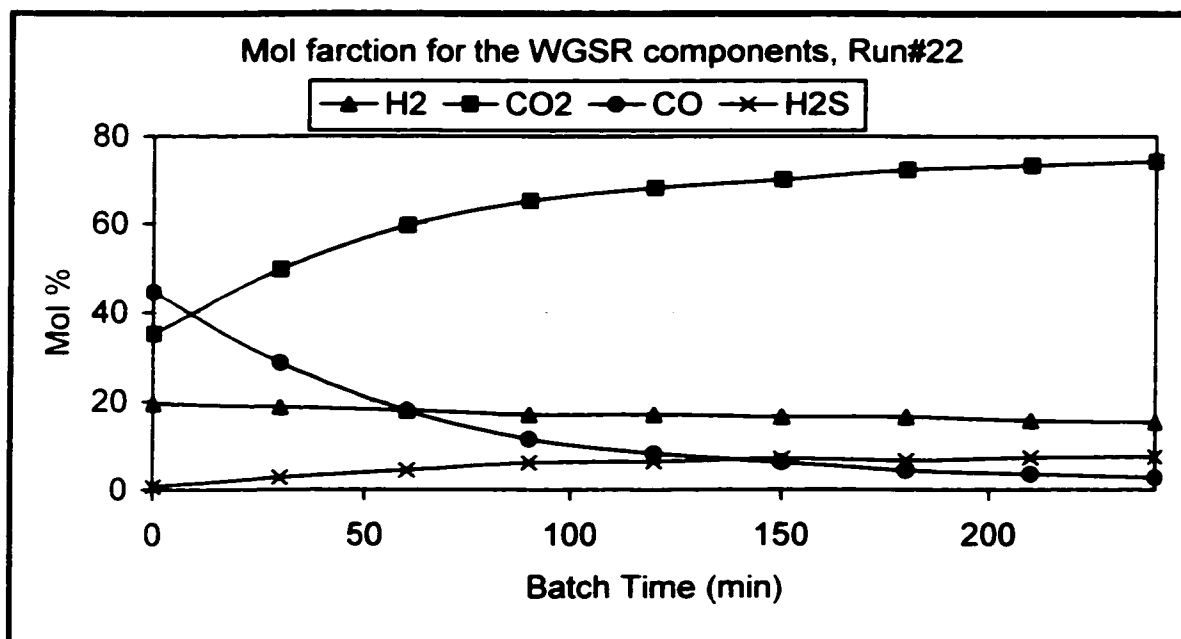
$$TET \text{ Sel} = 0.986$$

$$A_H = 0.25$$

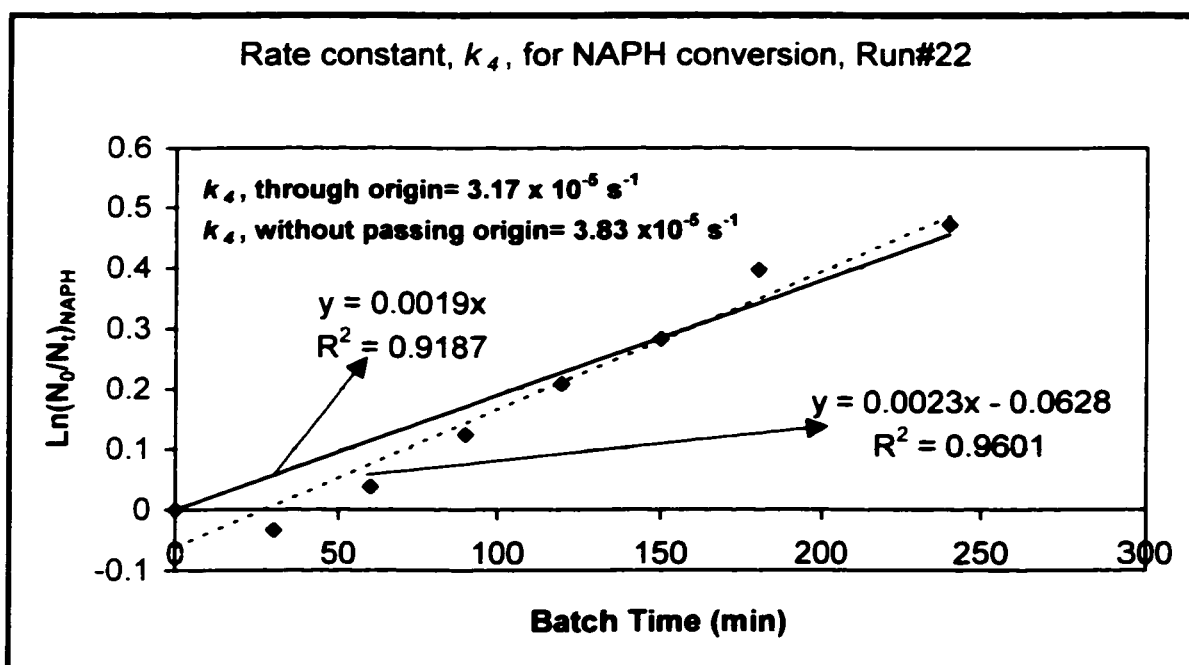
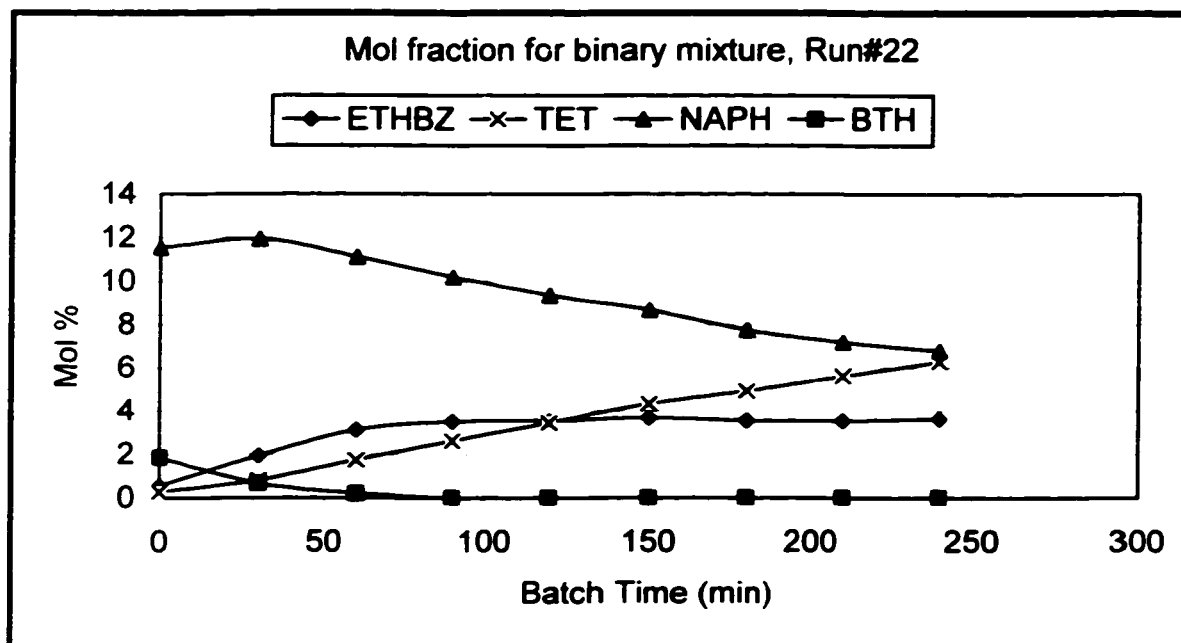


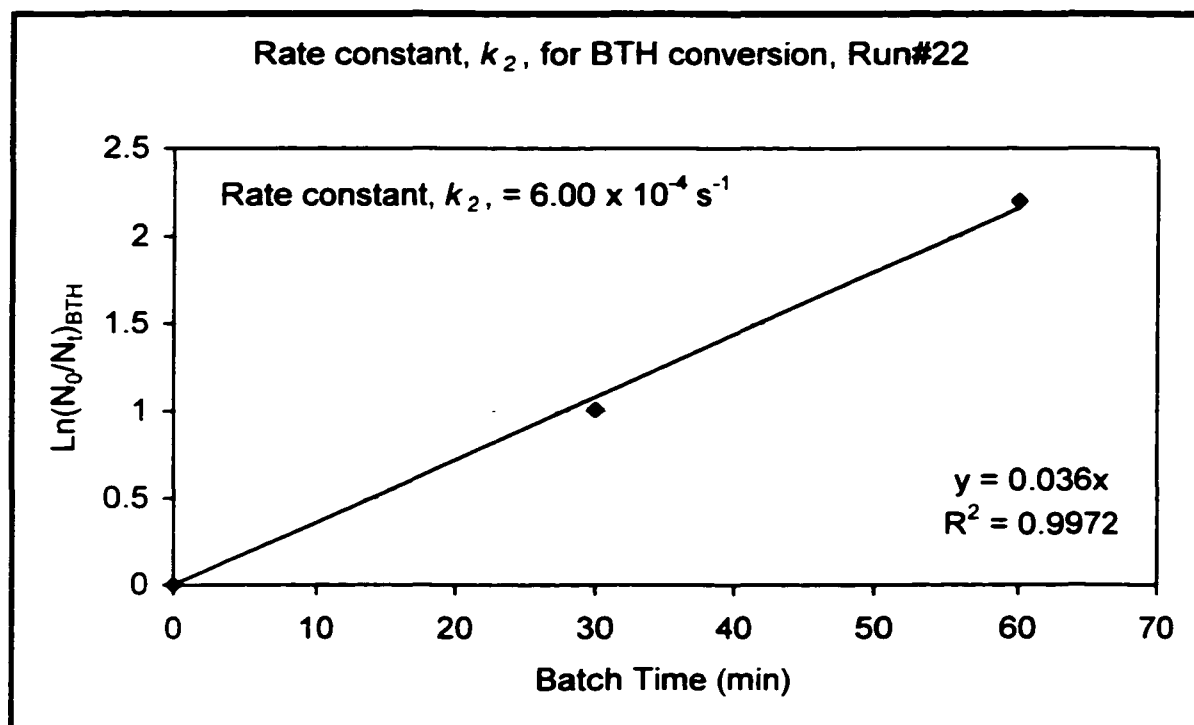


➤ Gas analysis, Run # 22



➤ Liquid analysis, Run # 22





➤ Gas analysis, Run # 23

Using CO, 585 psi, H₂S 15 psi

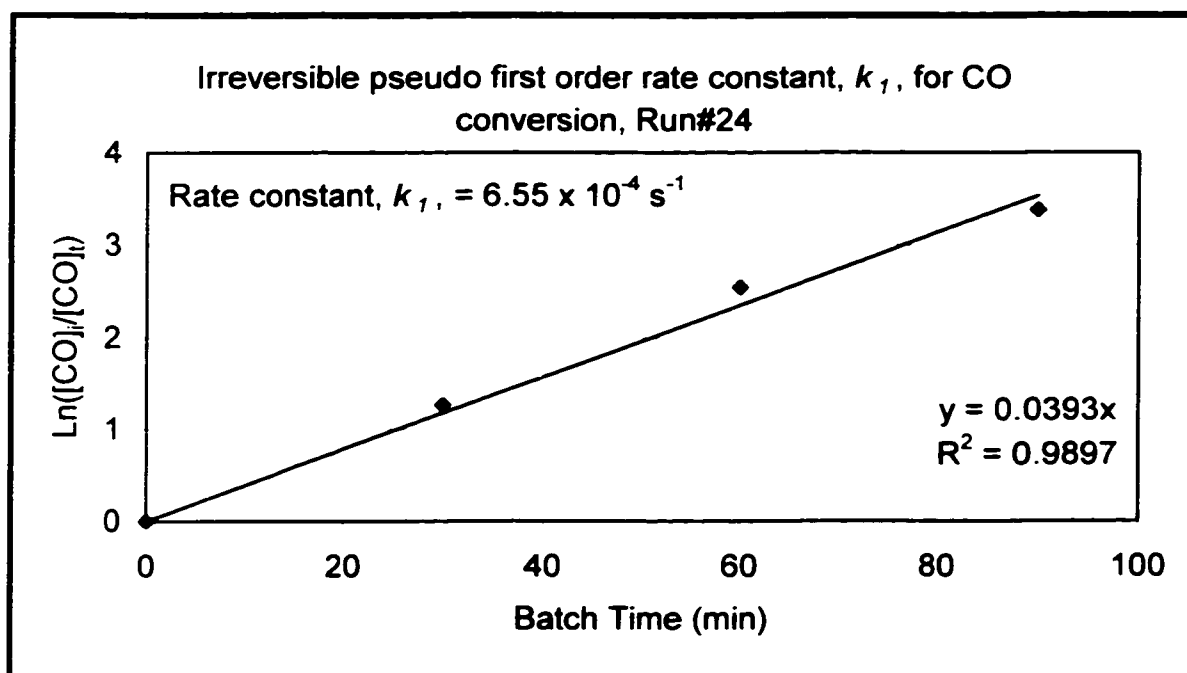
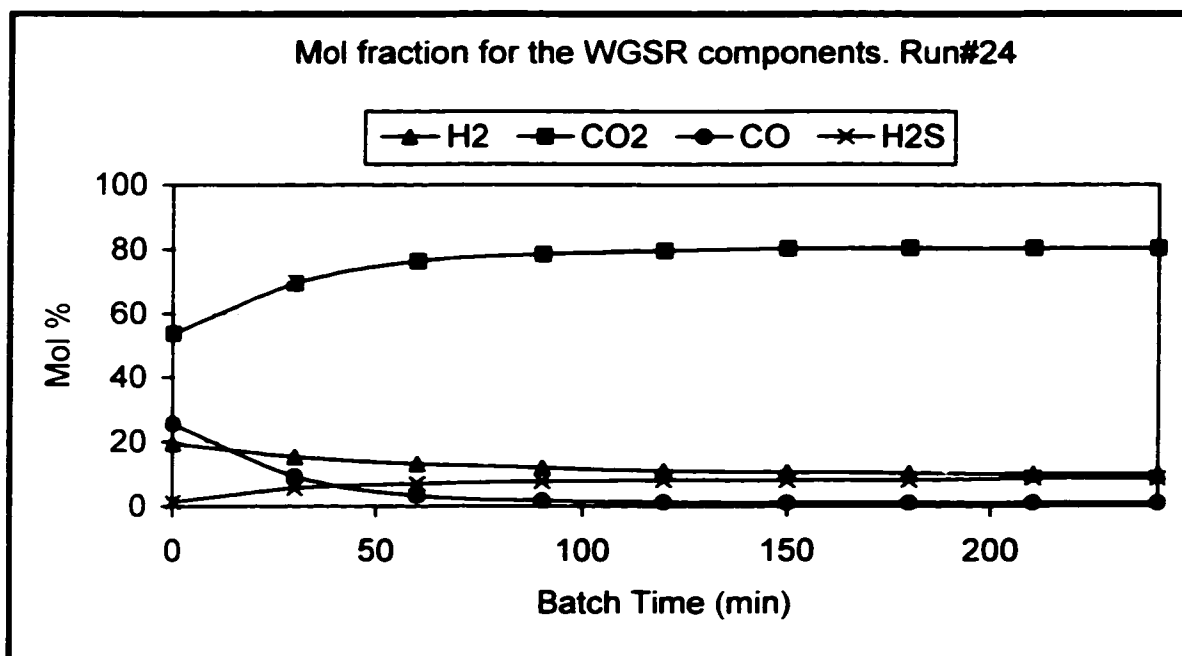
Operating Conditions :

200 ml Tol,
13.45g PMA catalyst solution + 57.27g water, PH_i=1.9
43.25g NAPH
14.1g BTH

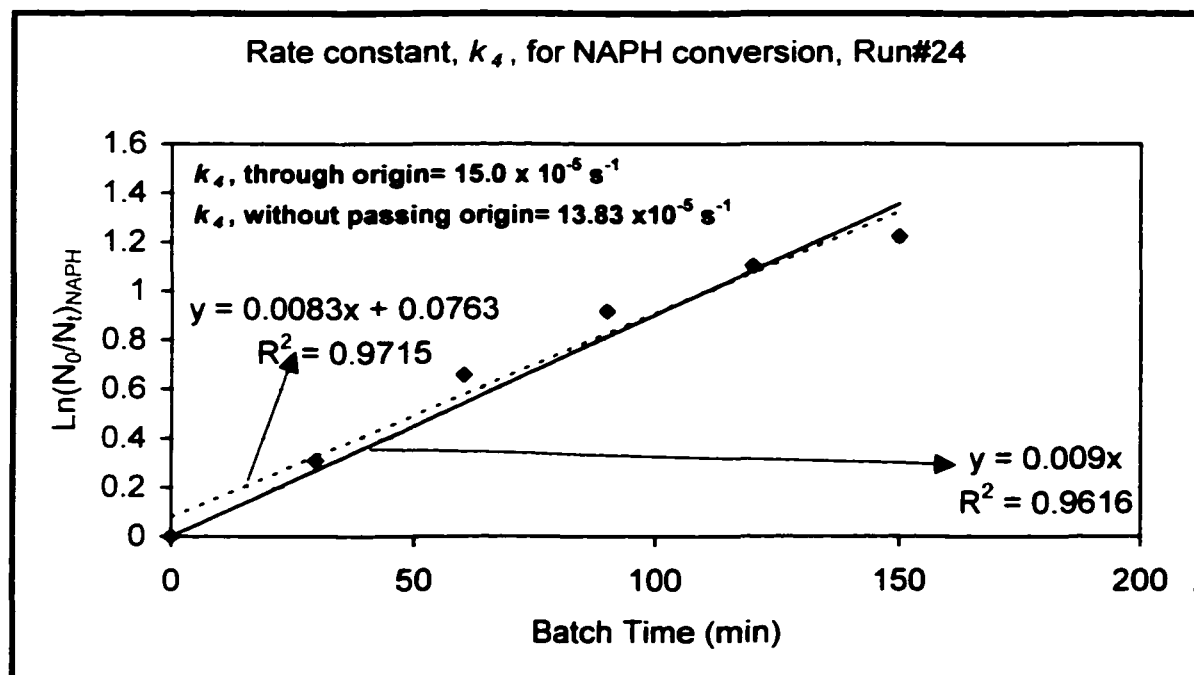
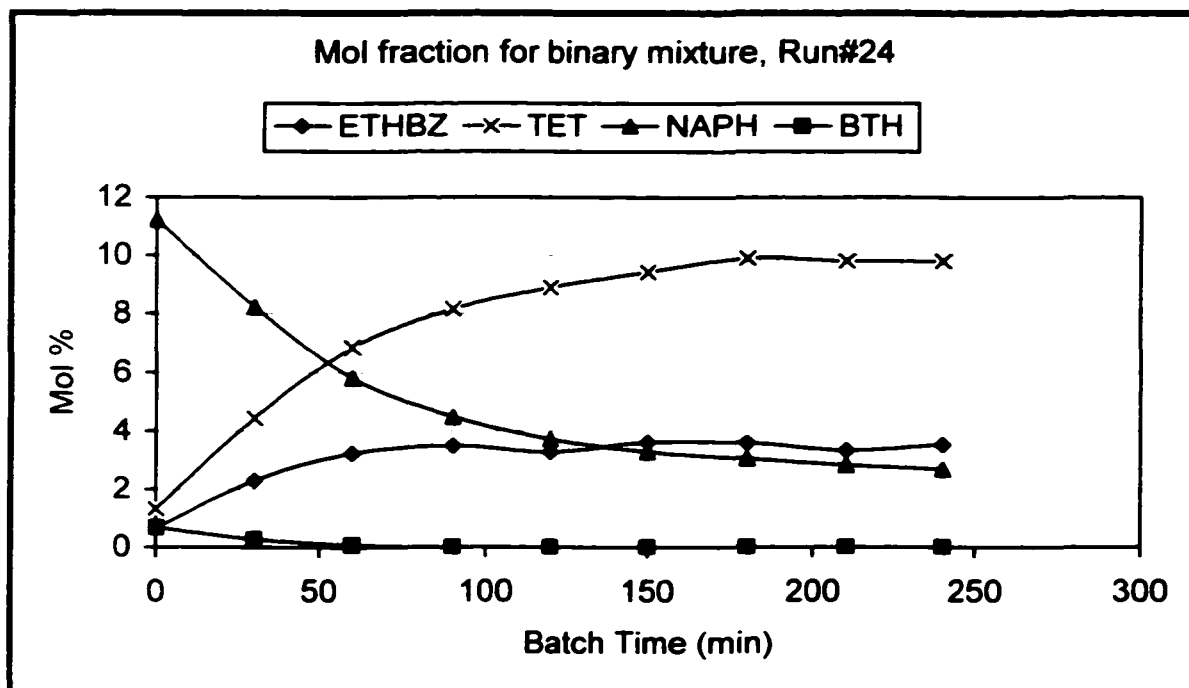
GC analysis Gas Product						
	1	2	3	AVR (3)	mol %	mmol
H ₂	9.1258	9.2873	9.2571	9.2234	10.3709	96.9008
CO ₂	66.0427	65.9728	66.5351	66.1835	74.4175	695.3222
CO	6.0444	6.0987	6.1129	6.0853	6.8424	63.9325
H ₂ S	7.2217	7.3998	7.708	7.4432	8.3692	78.1977
Totals	88.4346	88.7586	89.6131	88.9354	100	

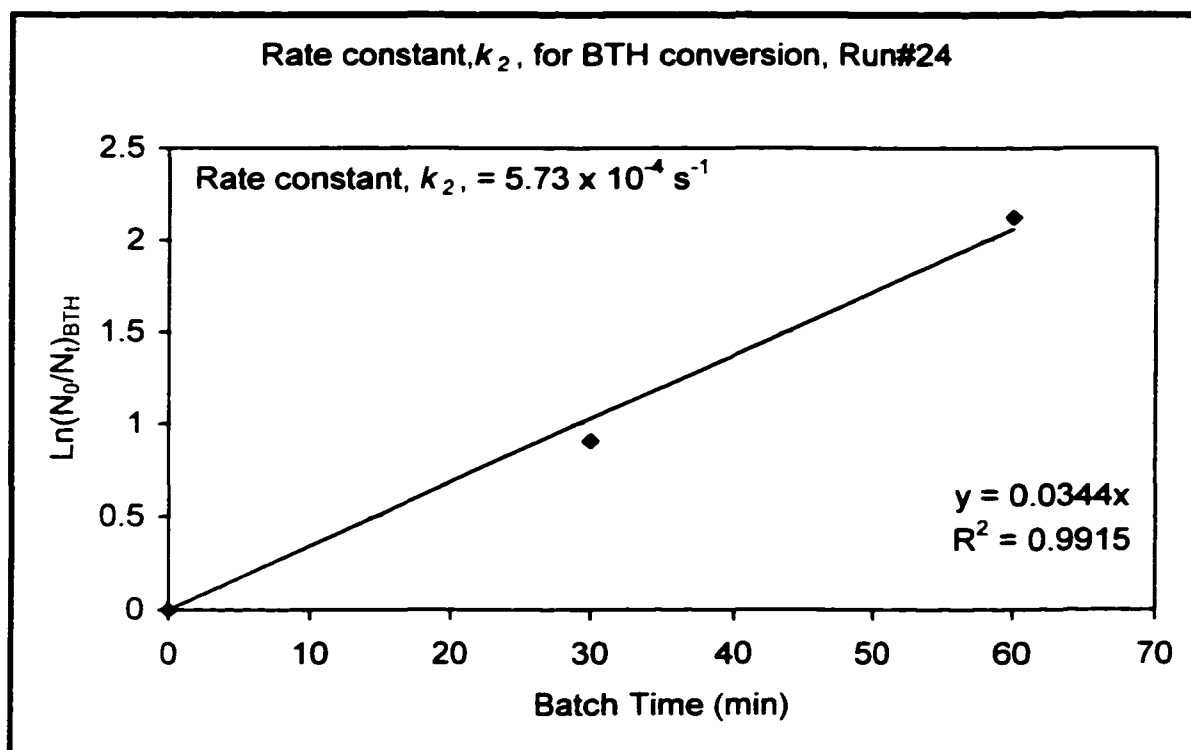
GC- Gas analysis during reaction					
Batch	Mol%				
Time(min)	H ₂	CO ₂	CO	H ₂ S	Total
0	20.5662	38.6880	39.700	1.043	100
30	18.8689	57.6374	18.270	5.227	100
60	17.8732	67.8394	8.309	5.978	100
90	16.1635	72.2263	4.130	7.480	100
120	15.0535	74.8032	2.157	7.986	100
150	14.3638	75.9965	1.592	8.048	100
180	13.4473	76.7094	1.387	8.457	100
210	12.3799	77.5631	1.295	8.762	100
240	11.8275	78.1801	1.079	8.913	100

➤ Gas analysis, Run # 24



➤ **Liquid analysis, Run # 24**





➤ Gas analysis, Run # 25

Using CO, 285 psi, H₂S 15 psi

Operating Conditions :

200 ml Tol

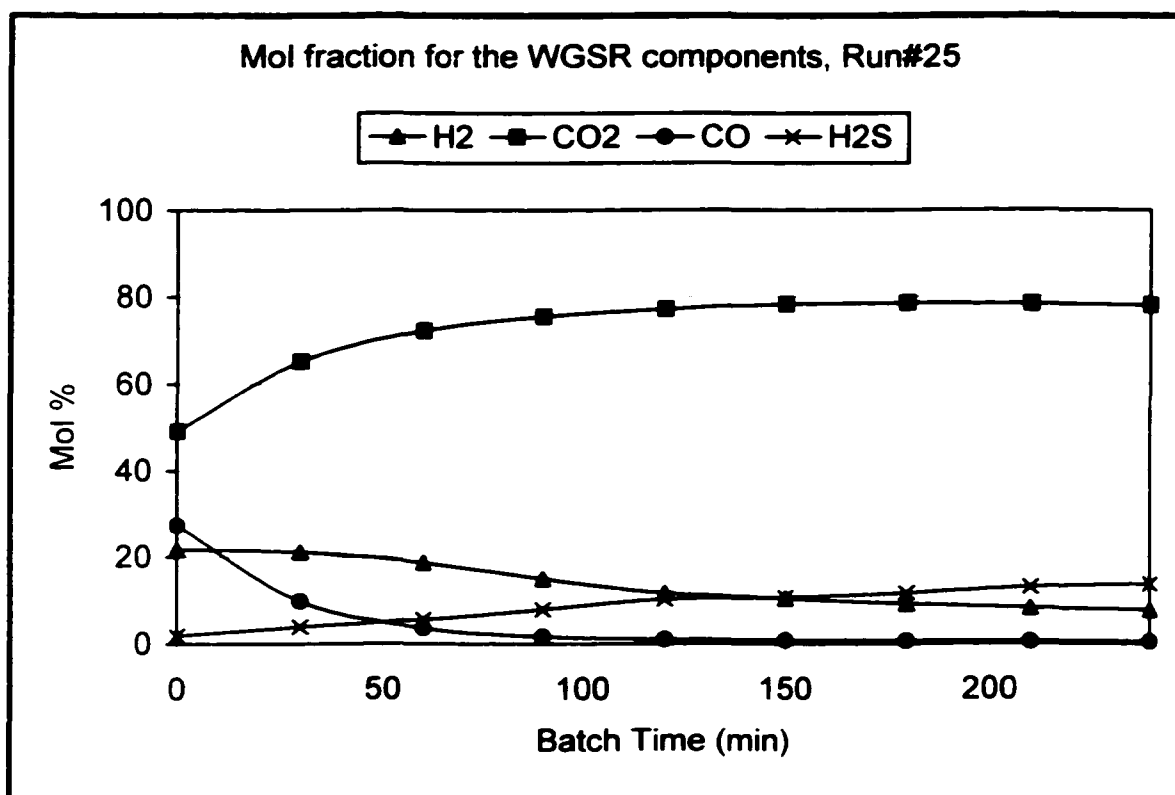
13.45g PMA catalyst solution + 57.28g water, PH_i=1.93

43.25g NAPH

14.1g BTH

GC analysis Gas Product						
	1	2	3	AVR	mol %	mmol
H ₂	6.8846	6.9505	6.8250	6.8867	7.5440	35.6568
CO ₂	63.3758	63.5585	63.7381	63.5575	69.6234	329.0771
CO	7.9627	8.1395	7.8513	7.9845	8.7465	41.3408
H ₂ S	12.5967	12.8074	13.1726	12.8589	14.0862	66.5786
Totals	90.8198	91.4559	91.5870	91.28756667	100	

GC- Gas analysis during reaction					
Batch	Mol%				
Time(min)	H ₂	CO ₂	CO	H ₂ S	Total
0	21.7091	49.1089	27.310	1.874	100
30	21.0785	65.1809	9.799	3.942	100
60	18.6198	72.2167	3.597	5.567	100
90	14.9287	75.4918	1.673	7.906	100
120	11.5886	77.1836	1.007	10.220	100
150	10.3705	78.2382	0.824	10.570	100
180	9.1533	78.5313	0.686	11.630	100
210	8.1591	78.3079	0.540	12.990	100
240	7.7596	78.0451	0.478	13.720	100



➤ Liquid analysis, Run #25

GC- Liquid analysis

Batch Time (min)	Toluene	ETHBZ	trans-DEC	cis-DEC	TET	NAPH	BTH	DHBTH	Total
	Mol%								
Feed (N)_i	83.919					12.196	3.8845		100
0	84.57	0.3541	0	0	0.3945	11.4210	1.5720	1.6880	100
30	83.655	1.0995	0	0	1.1175	11.4470	0.9448	1.7369	100
60	83.916	1.8438	0	0	1.7699	10.6190	0.6746	1.1766	100
90	83.860	2.3399	0	0	2.2849	10.1980	0.5410	0.7756	100
120	83.856	2.7444	0	0	2.6964	9.7853	0.4136	0.5043	100
150	84.001	2.7990	0	0	3.0352	9.5361	0.3143	0.3143	100
180	83.726	3.2052	0	0	3.1869	9.4111	0.2726	0.1986	100
210	83.777	3.3208	0	0	3.3215	9.2404	0.1965	0.1437	100
240	83.568	3.4408	0	0	3.4676	9.2650	0.1550	0.1029	100
Cold Product (N)_r	83.551	3.4794	0	0	3.5542	9.1895	0.1266	0.0989	100

$$X_{BTH} = 96.74 \%$$

$$S_{rem} = 93.91 \%$$

$$ETHBZ \text{ yield} = 89.43 \%$$

$$ETHBZ \text{ Sel} = 0.972$$

$$X_{NAPH} = 24.65 \%$$

$$A_{rem} = 27.89 \%$$

$$TET \text{ yield} = 29.12 \%$$

$$TET \text{ Sel} = 1.0$$

$$A_H = 0.11$$

➤ Gas analysis, Run # 26

Using CO, 585 psi, H₂S 15 psi,

Operating Condition :

200 ml Tol,

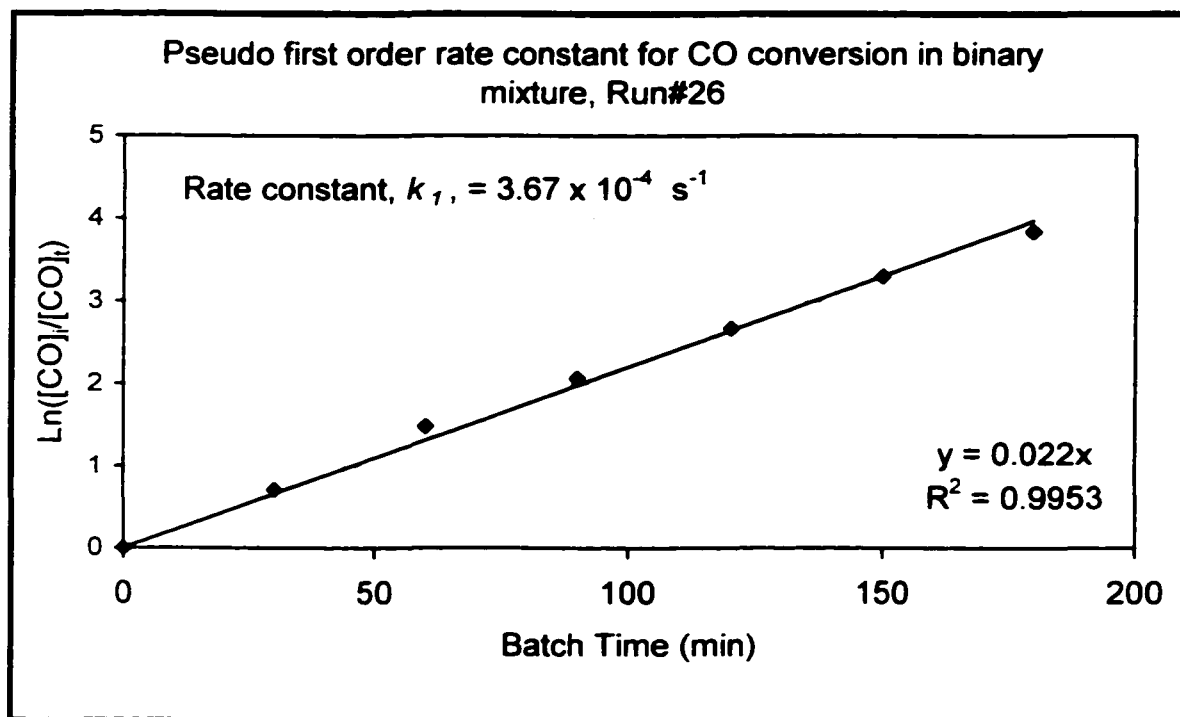
29.91 MA catalyst solution +,40.8 water pH_i=5.36

43.25g NAPH

14.1g BTH

GC analysis Gas Product						
	1	2	3	AVR	mol %	mmol
H ₂	8.6939	8.5804	8.6234	8.6326	10.1583	94.6238
CO ₂	63.7622	63.9612	64.252	63.9918	75.3017	701.4304
CO	5.6278	5.7486	5.8096	5.7287	6.7412	62.7934
H ₂ S	6.1264	6.8156	6.9404	6.6275	7.7988	72.6453
Totals	84.2103	85.1058	85.6254	84.9805	100	

GC Gas analysis during reaction					
Batch	Mol%				
Time(min)	H ₂	CO ₂	CO	H ₂ S	Total
0	23.4126	48.2728	27.2126	1.1019	100
30	19.6213	62.4760	14.2449	3.6579	100
60	17.9659	68.5828	8.1983	5.2530	100
90	16.9230	71.8992	4.9241	6.2537	100
120	15.7031	74.4539	3.5079	6.3351	100
150	14.0087	76.2299	2.0368	7.7246	100
180	14.0852	76.9727	1.5530	7.3891	100
210	13.3608	77.7229	1.3556	7.5606	100
240	12.4222	78.0982	1.3916	8.0881	100



➤ Liquid analysis, Run # 26

GC- Liquid analysis

Batch Time	Toluene	ETHBZ	trans-DEC	cis-DEC	TET	NAPH	BTH	DHBTH	Total
min	Mole%								
Feed (N)_i	83.3366					12.6658	3.9976		100
0	85.0893	1.3975	0.0000	0.0000	0.5811	10.8218	0.8580	1.2523	100
30	83.5764	2.9421	0.0000	0.0000	1.6073	10.9251	0.2754	0.6737	100
60	83.1327	3.6366	0.0000	0.0000	2.8943	10.0393	0.0880	0.2090	100
90	83.2717	3.8374	0.0000	0.0000	3.9284	8.9625	0.0000	0.0473	100
120	83.2532	3.8955	0.0207	0.0000	4.9209	7.9096	0.0000	0.0000	100
150	83.2441	3.8886	0.0000	0.0000	5.7623	7.1051	0.0000	0.0000	100
180	83.2432	3.8870	0.0311	0.0217	6.5064	6.3105	0.0000	0.0000	100
210	82.9297	3.9490	0.0000	0.0000	7.2794	5.8419	0.0000	0.0000	100
240	83.2707	3.9128	0.0385	0.0276	7.6000	5.1504	0.0000	0.0000	100
Final Product (N)_r	83.1115	3.9152	0.0588	0.0000	8.0350	4.8794	0.0000	0.0000	100

$$X_{BTH} = 100 \%$$

$$S_{rem} = 100 \%$$

$$ETHBZ \text{ yield} = 100 \%$$

$$ETHBZ \text{ Sel} = 1$$

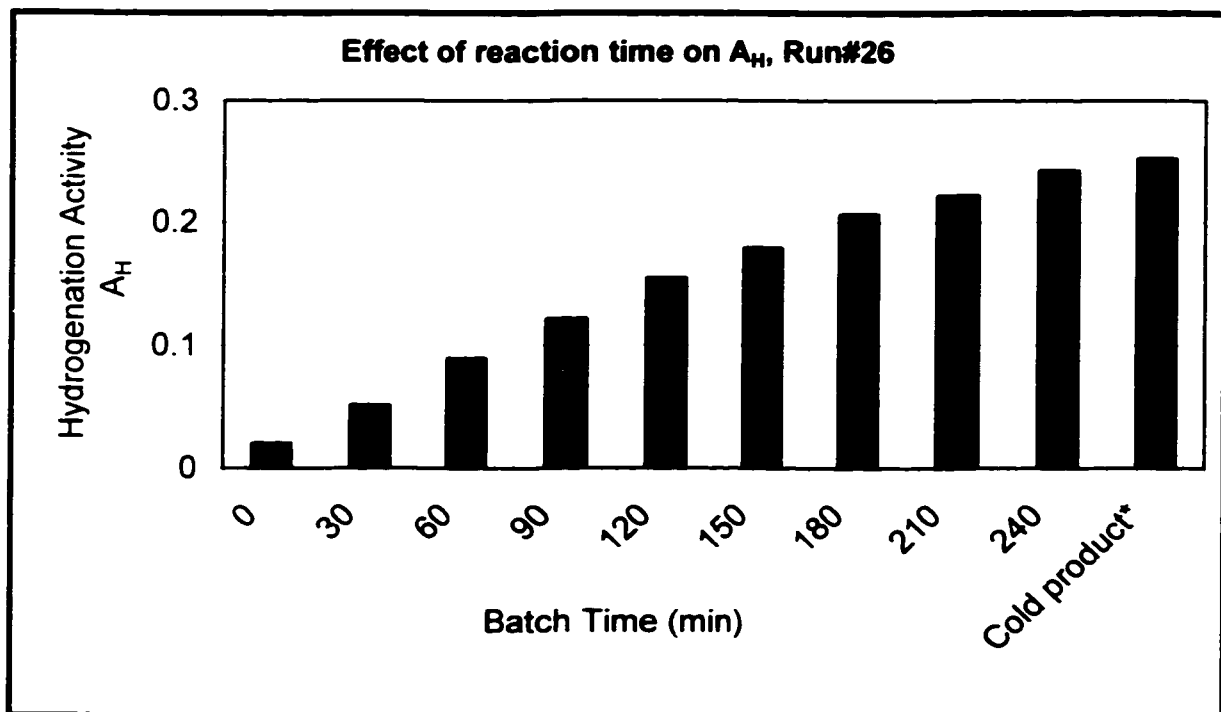
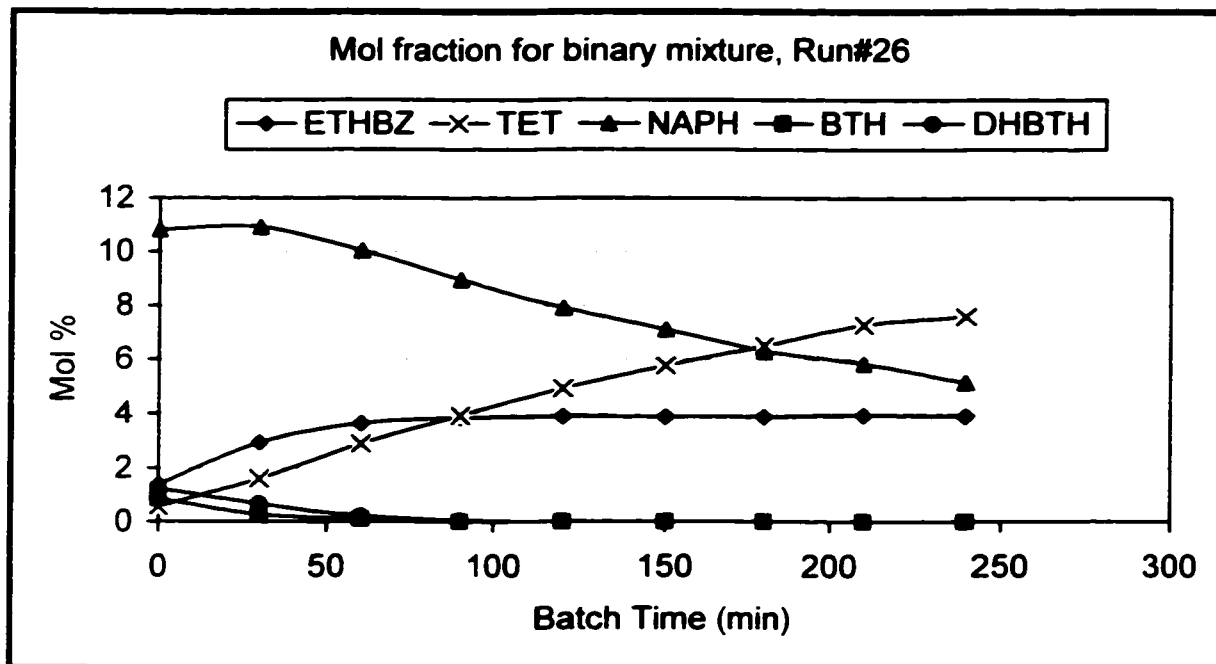
$$X_{NAPH} = 61.47 \%$$

$$A_{rem} = 62.39 \%$$

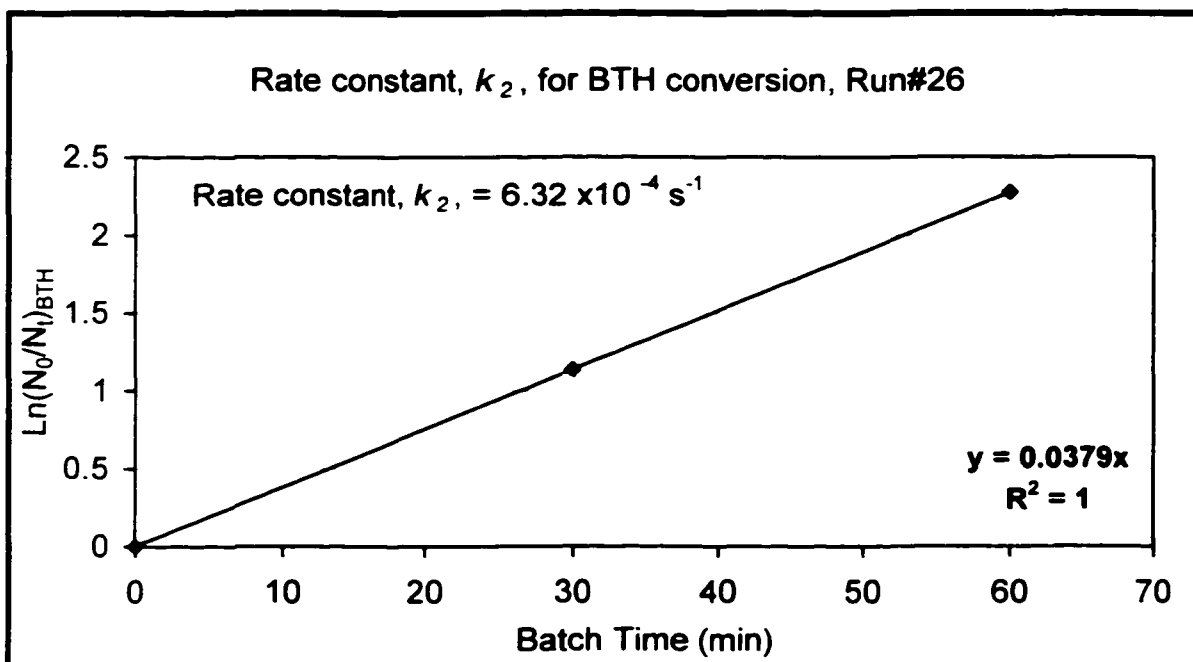
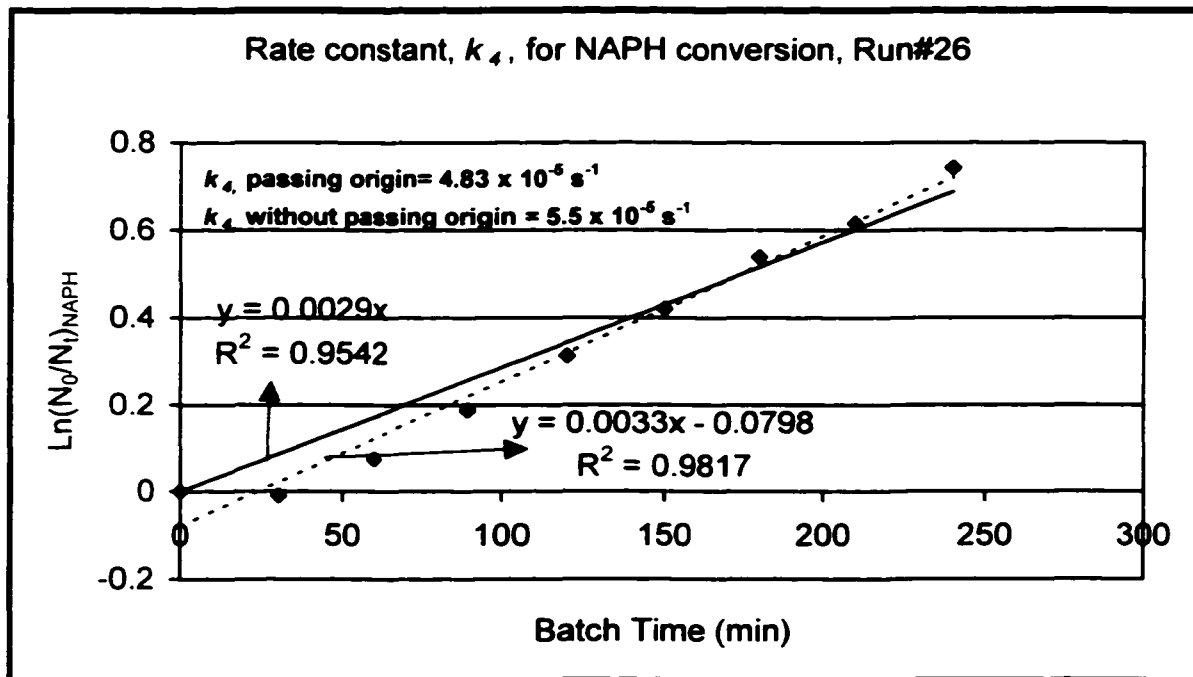
$$TET \text{ yield} = 61.93 \%$$

$$TET \text{ Sel} = 0.993$$

$$A_H = 0.25$$



*Product collected at the end of reaction after the reactor has cooled down



➤ Gas analysis, Run # 27

Using CO, 585 psi, H₂S 15 psi,

Operating Condition :

200 ml Tol

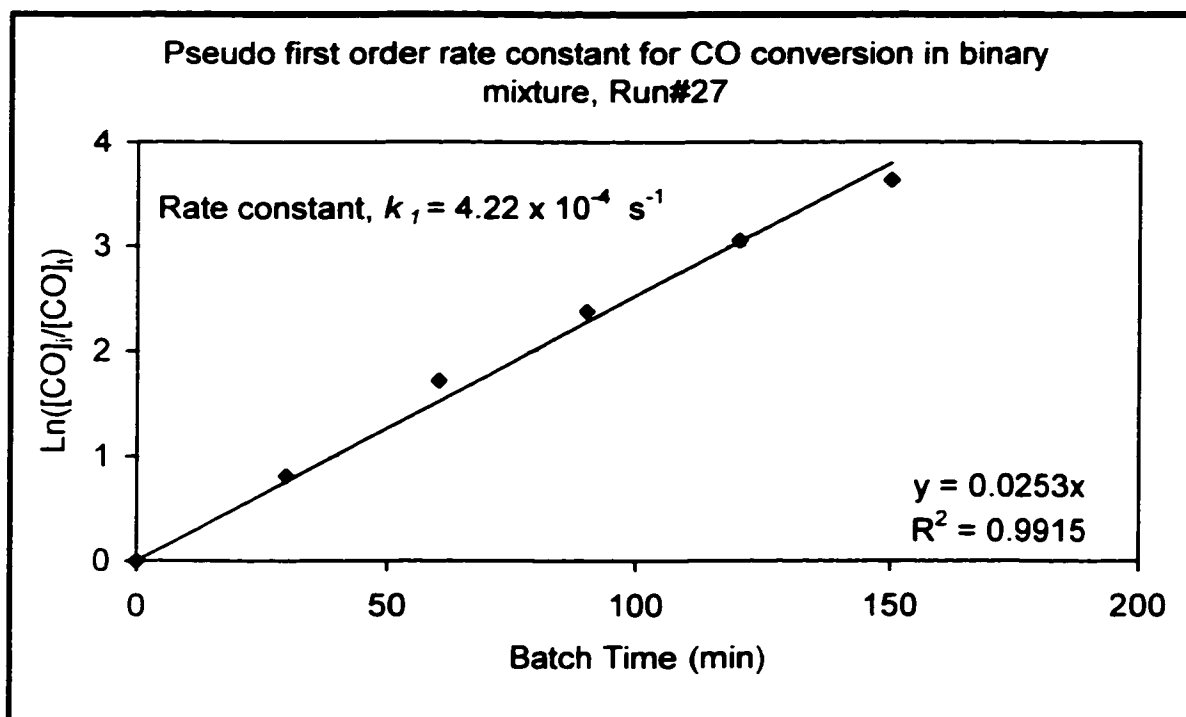
61.79 AMT catalyst, 9.04 water, PH=5.1

43.25g NAPH

14.1g BTH

GC analysis Gas Product						
	1	2	3	AVR	mol %	mmol
H ₂	8.4780	8.5011	8.2004	8.3932	10.1845	95.4398
CO ₂	62.6916	61.9109	60.8361	61.8129	75.0056	702.8824
CO	5.3970	5.4156	5.3645	5.3924	6.5433	61.3173
H ₂ S	6.8679	6.9494	6.6206	6.8126	8.2667	77.4674
Totals	83.4345	82.7770	81.0216	82.4110	100.0000	

GC Gas analysis during reaction					
Batch	Mol%				
Time(min)	H ₂	CO ₂	CO	H ₂ S	Total
0	18.1163	51.7849	25.3944	4.704	100
30	16.5976	64.1205	11.8198	7.462	100
60	15.4414	69.5464	5.8715	9.141	100
90	14.5397	72.4721	3.5325	9.456	100
120	13.9268	74.2423	2.1955	9.635	100
150	12.7681	76.0739	1.4720	9.686	100
180	11.7287	76.6245	1.3944	10.25	100
210	11.1977	77.2085	1.2247	10.37	100
240	10.5758	78.2776	1.0234	10.12	100



➤ Liquid analysis, Run # 27

GC- Liquid analysis

Batch Time	TOL	ETHBZ	trans- DEC	cis- DEC	TET	NAPH	BTH	DHBTH	Total
min	Mole%								
Feed (N) _i	83.3054					12.7053	3.9893		100
0	84.6377	1.8872	0.0000	0.0000	0.5702	11.1916	0.8781	0.8352	100
30	82.9210	3.5791	0.0000	0.0000	1.6445	11.2175	0.2661	0.3718	100
60	83.3151	3.8989	0.0000	0.0000	2.7909	9.9951	0.0000	0.0000	100
90	83.1700	3.9741	0.0000	0.0000	3.9830	8.8729	0.0000	0.0000	100
120	83.2937	3.9110	0.0000	0.0000	5.0140	7.7812	0.0000	0.0000	100
150	83.1547	3.8922	0.0366	0.0000	5.9433	6.9732	0.0000	0.0000	100
180	83.1953	3.9395	0.0491	0.0000	6.6224	6.1936	0.0000	0.0000	100
210	83.2797	3.9317	0.0000	0.0000	7.2572	5.5314	0.0000	0.0000	100
240	83.1000	3.9543	0.0472	0.0245	7.7813	5.0927	0.0000	0.0000	100
Cold Product (N) _f	83.2486	3.9102	0.0877	0.0000	8.0809	4.6726	0.0000	0.0000	100

$$X_{BTH} = 100 \%$$

$$S_{rem} = 100 \%$$

$$ETHBZ \text{ yield} = 100 \%$$

$$ETHBZ \text{ Sel} = 1$$

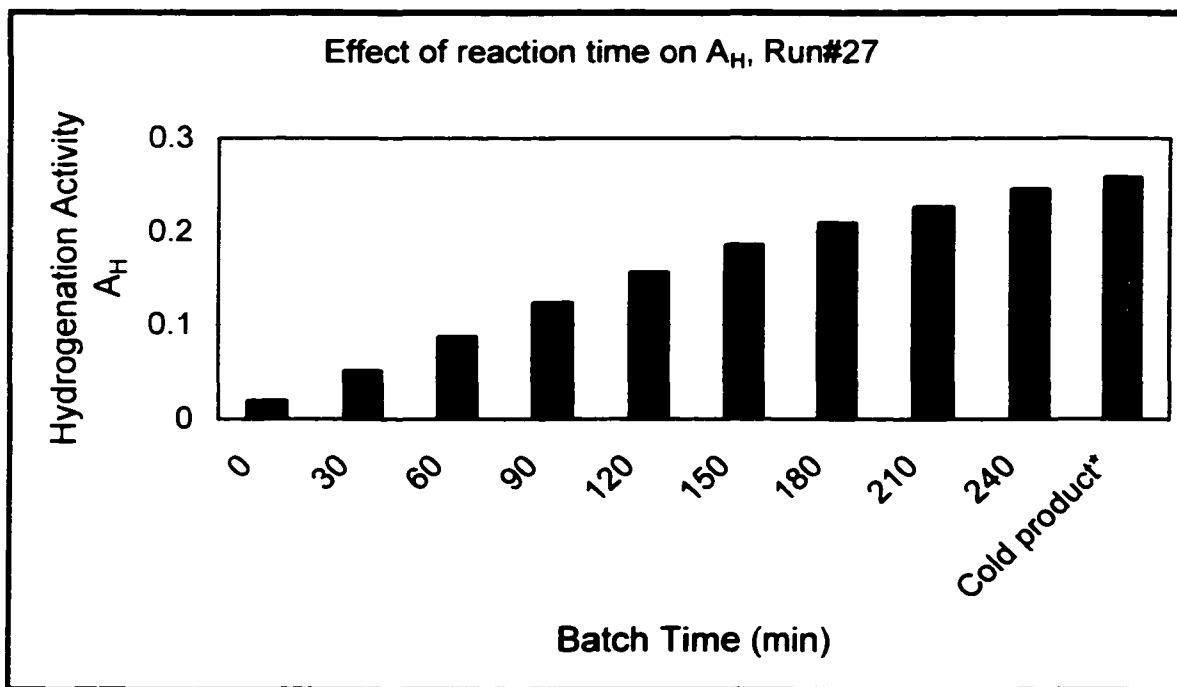
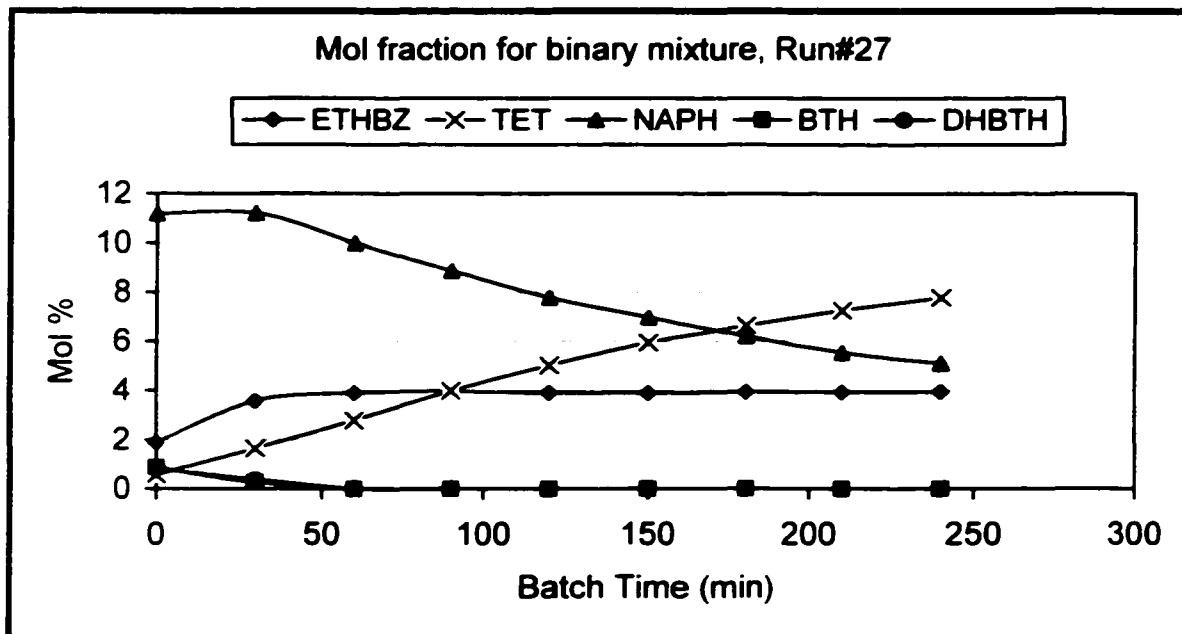
$$X_{NAPH} = 63.22 \%$$

$$A_{rem} = 63.61 \%$$

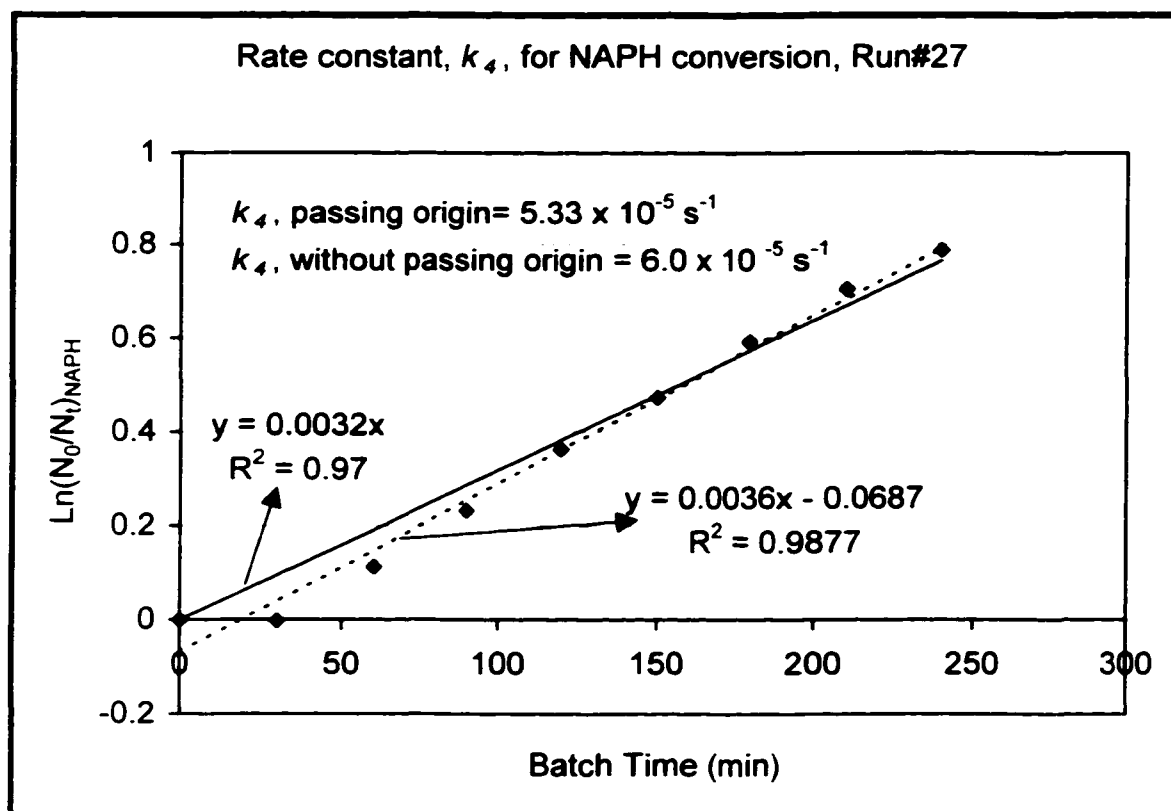
$$TET \text{ yield} = 62.93 \%$$

$$TET \text{ Sel} = 0.989$$

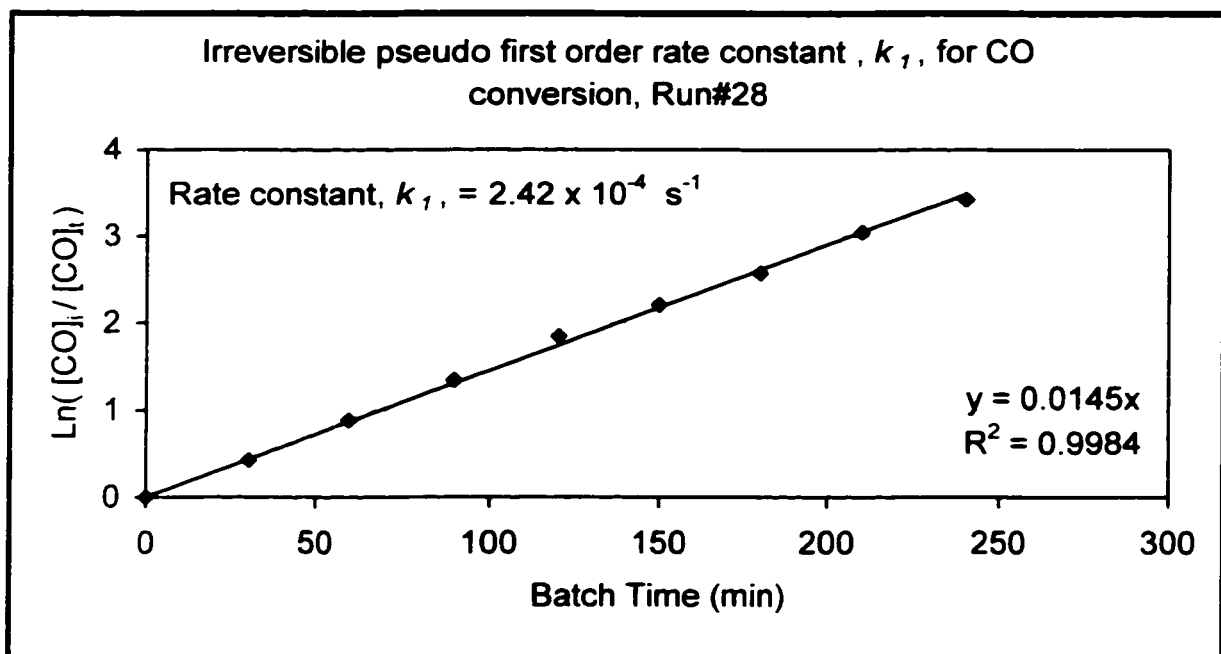
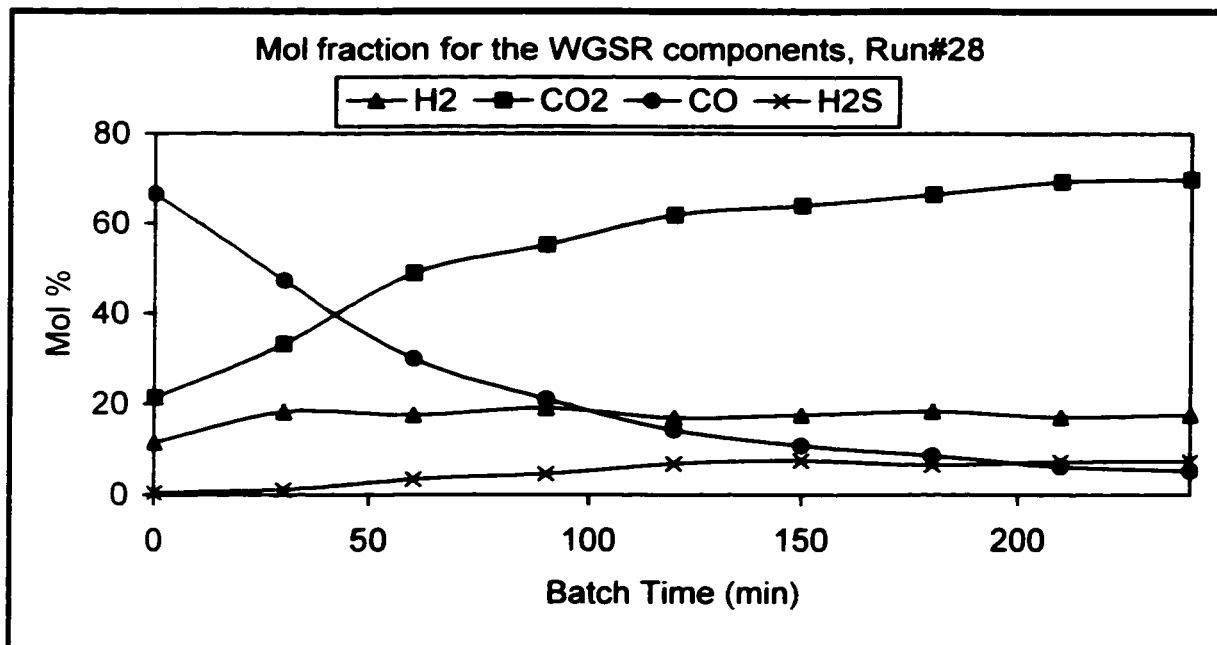
$$A_H = 0.26$$



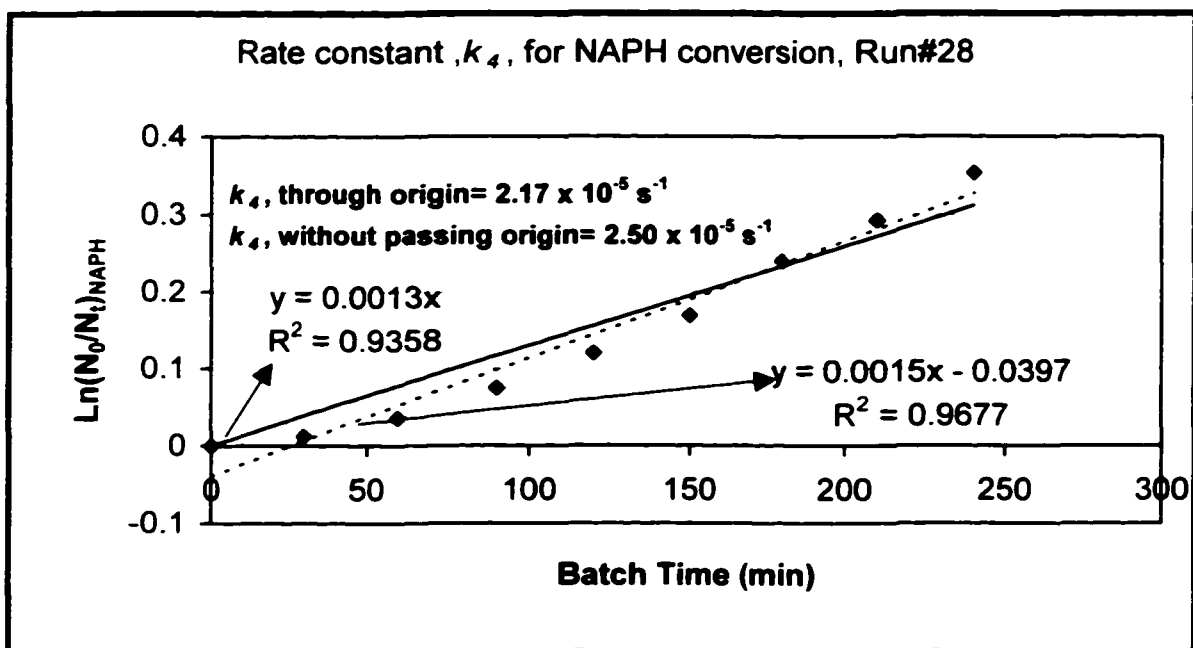
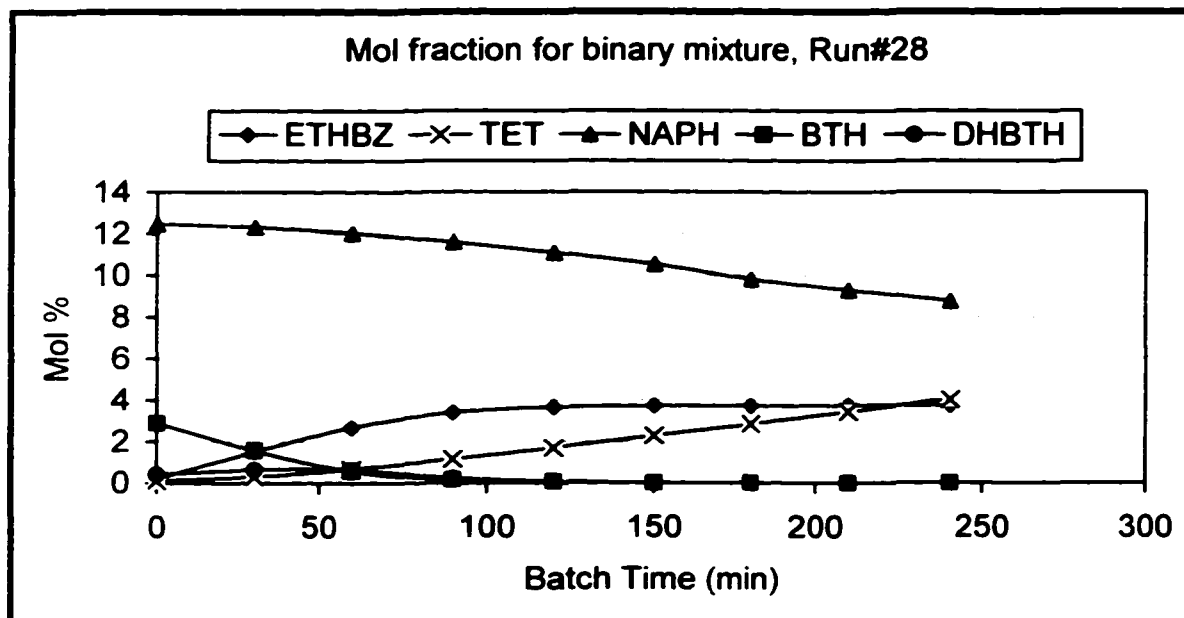
* Product collected at the end of reaction after the reactor has cooled down

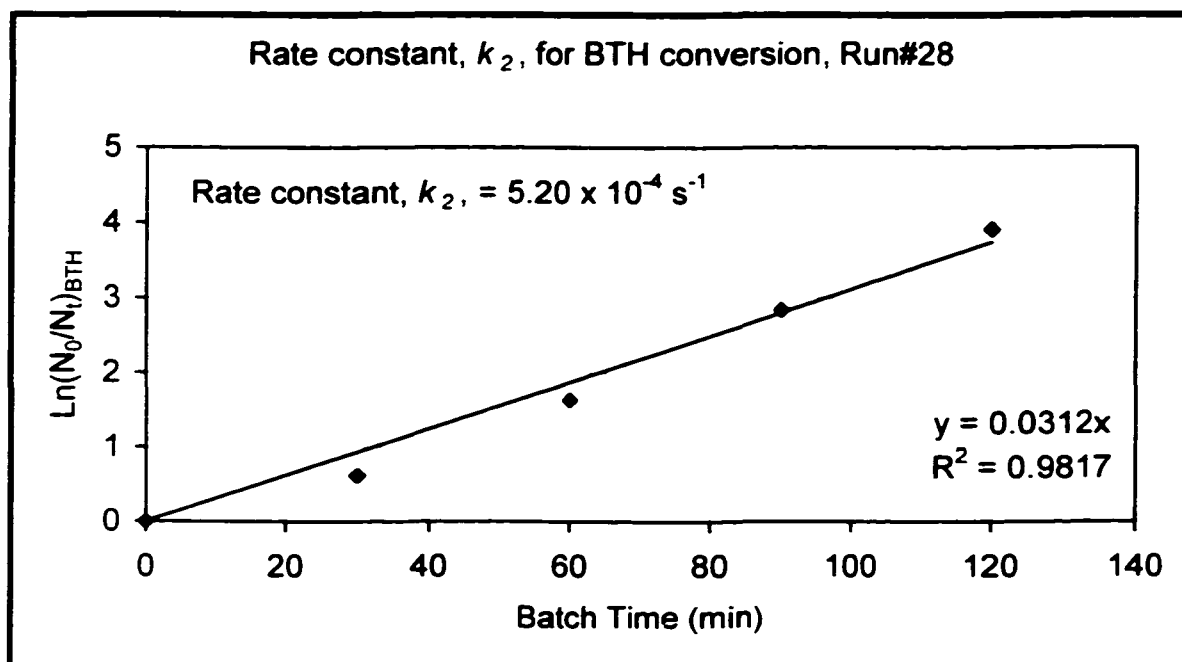


➤ Gas analysis, Run # 28



➤ **Liquid analysis, Run # 28**





➤ Gas analysis, Run # 29

Using CO, 585 psi, H₂S 15 psi

Operating Condition :

200 ml Tol

Catalyst: Balnk

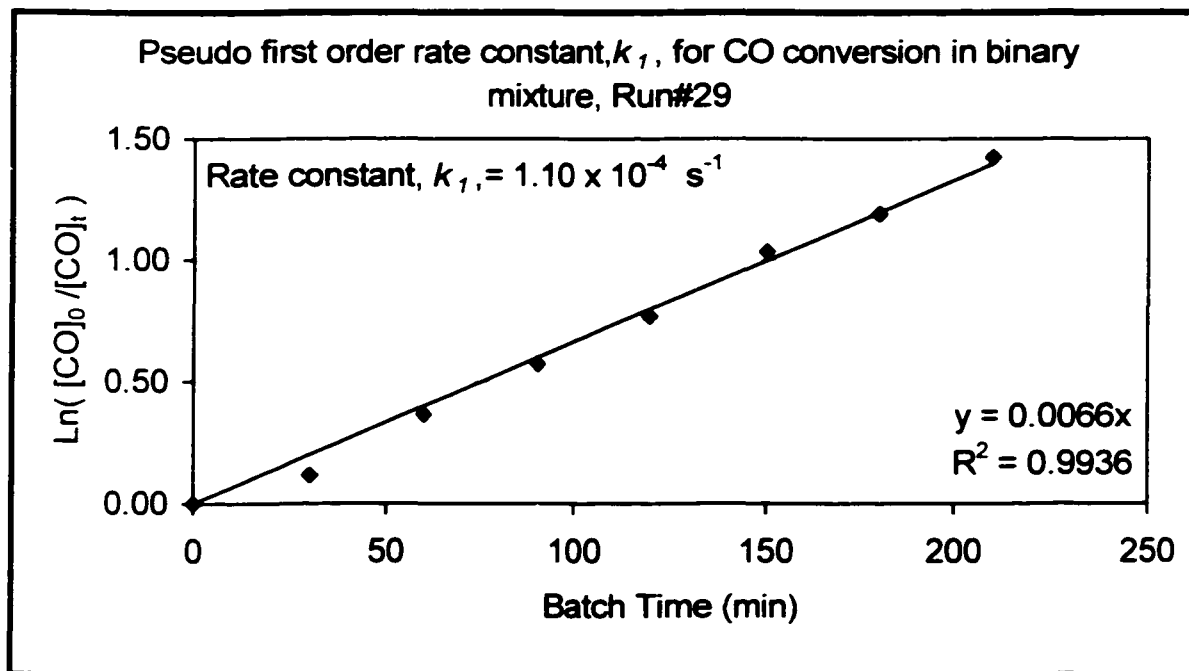
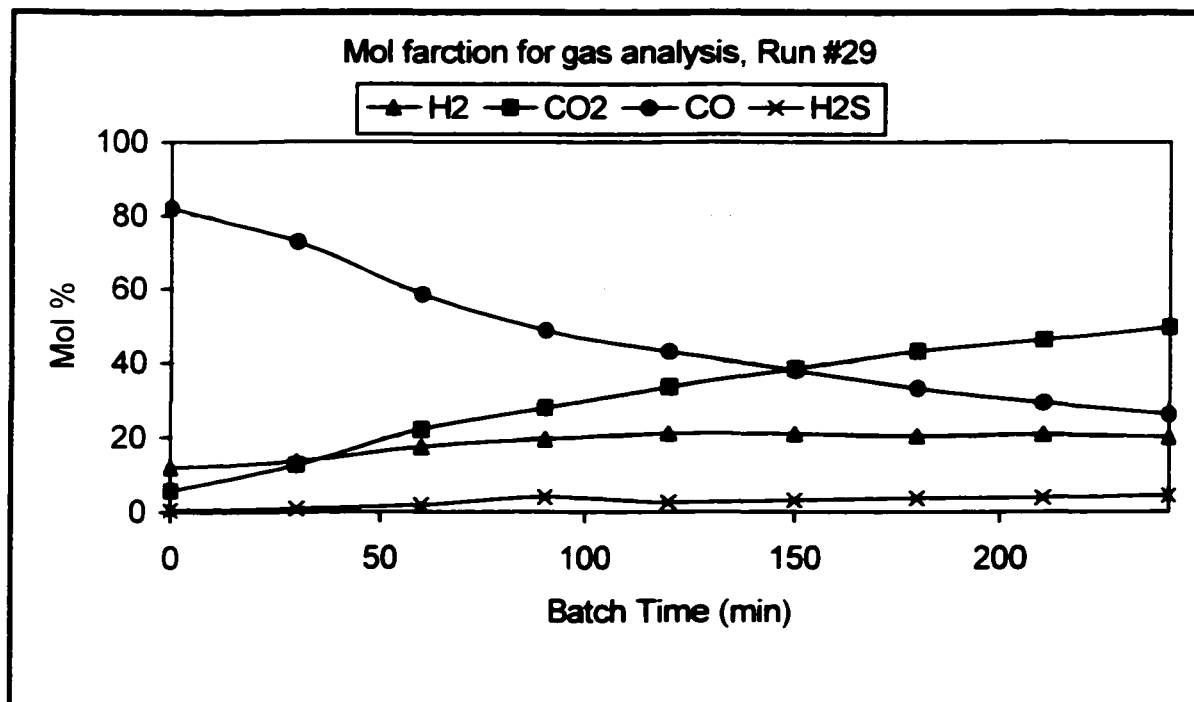
70 ml water PH_i = 5.65

43.25g NAPH

14.1g BTH

GC analysis Gas Product						
	1	2	3	AVR	mol %	mmol
H ₂	14.3022	13.9996	13.8872	14.0630	17.5574	209.6578
CO ₂	42.4208	41.7845	41.5347	41.9133	52.3280	624.8638
CO	20.6761	20.4038	20.3763	20.4854	25.5756	305.4060
H ₂ S	3.4363	3.7100	3.7605	3.6356	4.5390	54.2012
Totals	80.8354	79.8979	79.5587	80.0973	100.0000	

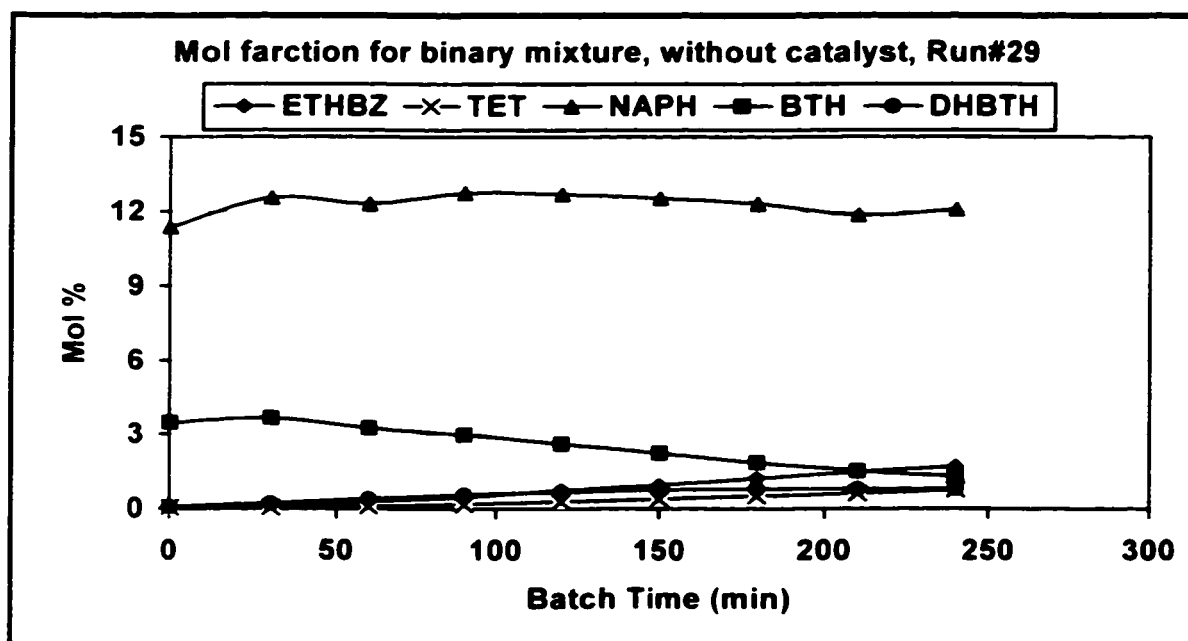
GC Gas analysis during reaction					
Batch	Mol%				
Time(min)	H ₂	CO ₂	CO	H ₂ S	Total
0	11.8956	5.6249	81.9906	0.4889	100
30	13.6378	12.6271	72.9018	0.8333	100
60	17.5048	22.1577	58.4293	1.9083	100
90	19.4867	27.8989	48.6075	4.0070	100
120	21.0559	33.4509	42.8878	2.6053	100
150	20.9176	38.2746	37.7157	3.0921	100
180	20.3780	42.9614	33.0199	3.6407	100
210	20.8021	46.0197	29.3158	3.8623	100
240	19.9687	49.5006	26.1252	4.4054	100



➤ Liquid analysis, Run # 29

GC-Liquid analysis

Batch Time min	Toluene	ETHBZ	tranc- DEC	cis- DEC	TET	NAPH	BTH	DHBTH	Total
	Mol%								
Feed (N)_i	83.6479					12.4231	3.9290		100
0	85.0173	0.0265	0	0	0.0519	11.3557	3.4818	0.0669	100
30	83.5255	0.0149	0	0	0.0406	12.5597	3.6555	0.2039	100
60	83.6900	0.2755	0	0	0.0858	12.3235	3.2527	0.3725	100
90	86.6039	0.4652	0	0	0.1744	12.7565	2.9823	0.5597	100
120	86.2905	0.7258	0	0	0.2824	12.7012	2.6154	0.6738	100
150	86.1381	0.9410	0	0	0.3825	12.5384	2.2335	0.7661	100
180	85.9460	1.2205	0	0	0.5167	12.3168	1.8631	0.7995	100
210	83.7562	1.4697	0	0	0.6194	11.8492	1.5216	0.7839	100
240	85.4736	1.6845	0	0	0.7531	12.0789	1.3053	0.7919	100
Final Product (N)_f	83.7842	2.0621	0.0000	0.0000	0.9149	11.5296	0.9600	0.7492	100



Resulted the following calculation:

$$X_{BTH} = 75.56 \%$$

$$S_{rem} = 54.68 \%$$

$$ETHBZ \text{ yield} = 52.48 \%$$

$$ETHBZ \text{ Sel} = 0.73$$

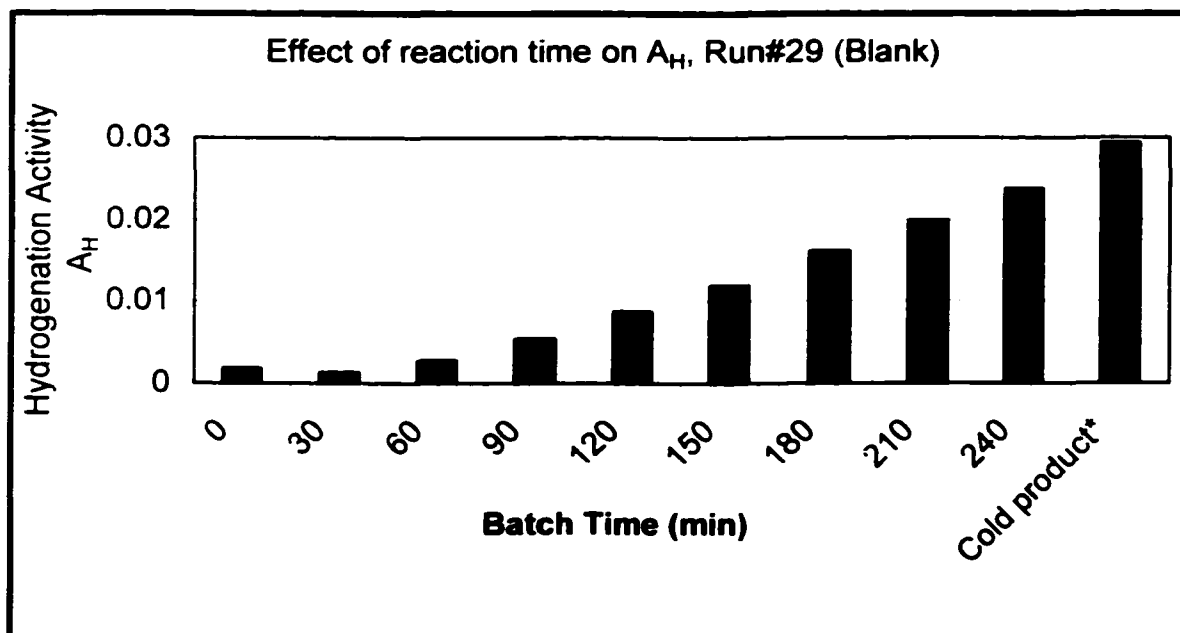
$$X_{NAPH} = 7.19 \%$$

$$A_{rem} = 7.36 \%$$

$$TET \text{ yield} = 7.36 \%$$

$$TET \text{ Sel} = 1.0$$

$$A_H = 0.029$$



➤ Gas analysis, Run # 30

Using CO, 600 psi,

Operating Condition:

200 ml Tol

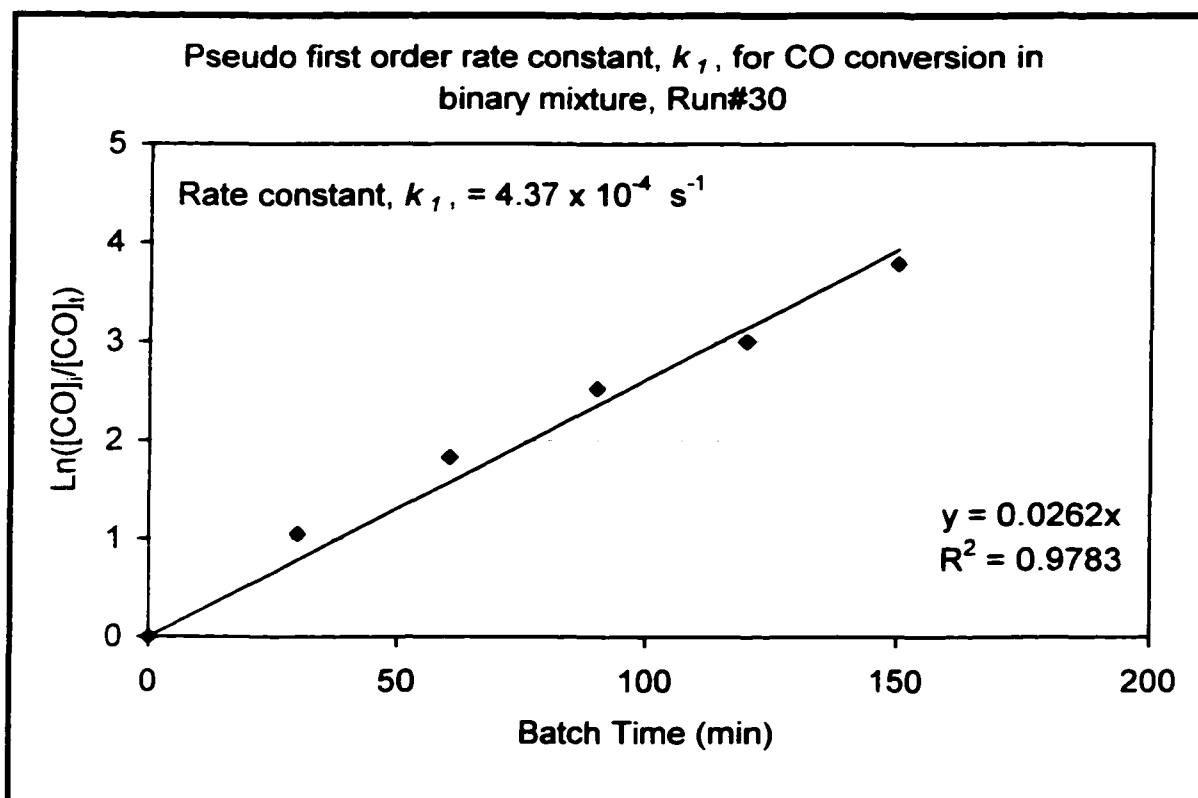
70 ml water, 1.23 gm ATTM Catalyst., PH= 9.8

43.25g NAPH

14.1g BTH

GC analysis Gas Product						
	1	2	3	AVR	mol %	mmol
H2	10.2561	10.3691	10.2953	10.3068	12.3304	123.1476
CO2	61.3559	62.4619	62.0697	61.9625	74.1278	740.3374
CO	5.9661	6.0572	6.1698	6.0644	7.2550	72.4580
H2S	4.9748	5.3268	5.4634	5.2550	6.2867	62.7875
Totals	82.5529	84.2150	83.9982	83.5887	100.0000	

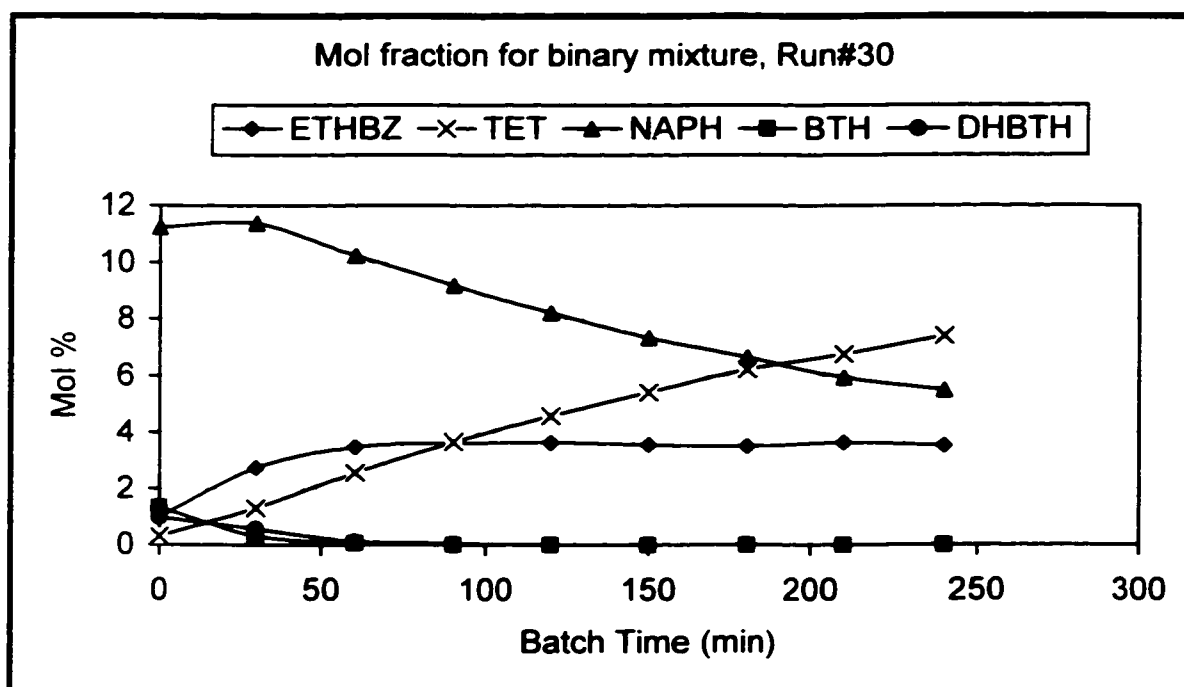
GC Gas analysis during reaction					
Batch	Mol%				
Time(min)	H ₂	CO ₂	CO	H ₂ S	Total
0	23.1865	39.5989	36.9166	0.2980	100
30	22.6264	60.6562	14.1080	2.6093	100
60	21.6976	67.6076	7.0954	3.5994	100
90	19.2013	71.6717	4.0839	5.0431	100
120	18.2335	72.7199	3.0612	5.9853	100
150	17.2444	75.1311	1.6605	5.9640	100
180	16.5365	76.0515	1.4822	5.9298	100
210	14.8870	77.3095	1.4649	6.3386	100
240	14.7742	77.2714	1.4545	6.5000	100



➤ Liquid analysis, Run # 30

GC- Liquid analysis

Batch Time min	Toluene Mole%	ETHBZ	trans- DEC	cis- DEC	TET	NAPH	BTH	DHBTH	Total
Feed (N) _i	83.5524					12.8058	3.6418		100
0	85.1317	0.9825	0.0000	0.0000	0.3053	11.2511	1.3462	0.9832	100
30	83.6813	2.7391	0.0000	0.0000	1.3055	11.3835	0.3266	0.5640	100
60	83.5499	3.4829	0.0000	0.0000	2.5650	10.2338	0.0536	0.1149	100
90	83.5357	3.6286	0.0000	0.0000	3.6560	9.1798	0.0000	0.0467	100
120	83.5571	3.6500	0.0000	0.0000	4.5831	8.2099	0.0000	0.0000	100
150	83.6465	3.5705	0.0150	0.0157	5.4204	7.3320	0.0000	0.0000	100
180	83.6020	3.5120	0.0328	0.0000	6.2167	6.6364	0.0000	0.0000	100
210	83.5702	3.6457	0.0327	0.0427	6.7643	5.9444	0.0000	0.0000	100
240	83.5051	3.5357	0.0440	0.0246	7.4029	5.4877	0.0000	0.0000	100
Final Product (N) _f	83.2265	3.6514	0.0607	0.0264	7.9269	5.1081	0.0000	0.0000	100



$$X_{BTH} = 100 \%$$

$$S_{rem} = 100 \%$$

$$ETHBZ_{yield} = 100 \%$$

$$ETHBZ_{Sel} = 1.0$$

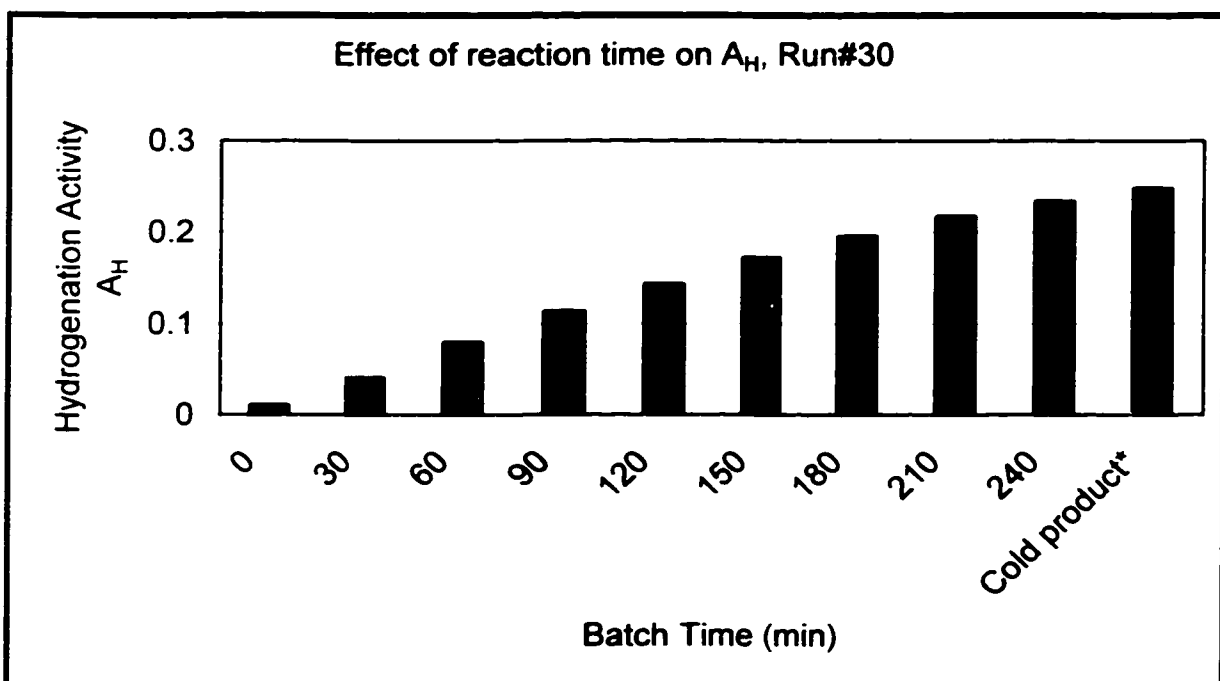
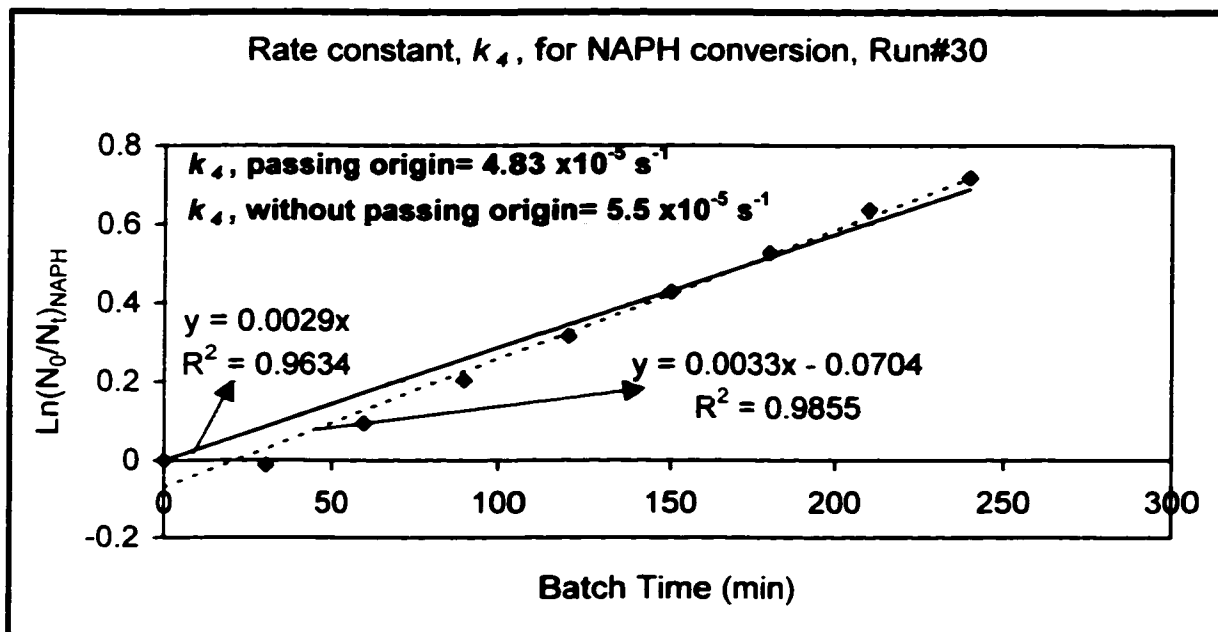
$$X_{NAPH} = 60.11 \%$$

$$A_{rem} = 61.07 \%$$

$$TET_{yield} = 60.81 \%$$

$$TET_{Sel} = 0.989$$

$$A_H = 0.25$$



* Product collected at the end of reaction after the reactor has cooled down

Appendix G
Summary of Experimental Runs

Summary G.1

Run#	Medium	X _{CO} (%)	k ₁ (s ⁻¹ x10 ⁴)	X _{BTH} (%)	k ₂ (s ⁻¹ x10 ⁴)	S Rem (%)	X _{NAPH} (%)	k ₄ (s ⁻¹ x10 ⁵)	A Rem (%)
6	CO/H ₂ S/H ₂ O PMA (500 ppm Mo) BTH	80.96	2.20	97.72	3.95	92.79	NA	NA	NA
7	CO/H ₂ S/H ₂ O PMA (500 ppm Mo) NAPH	84.21	(2.21) ¹	NA	NA	NA	28.76	2.17	21.83
8	CO/H ₂ S/H ₂ O PMA (1500 ppm Mo) NAPH	91.73	(3.60) ¹	NA	NA	NA	66.42	8.50	63.28
9	CO/H ₂ S/H ₂ O PMA (1500 ppm Mo) NAPH+BTH	95.33	4.85	100	7.55	100	65.76	8.33	66.27
10	CO/H ₂ S/H ₂ O PMA (1500 ppm Mo) BTH	93.86	4.25	99.27	10.78	99.16	NA	NA	NA
12	CO/H ₂ S/H ₂ O PMA (1500 ppm Mo) NAPH+BTH	94.47	5.02	99.56	15.37	99.53	63.23	7.33	65.56
13	H ₂ /H ₂ S/H ₂ O PMA (1500 ppm Mo) NAPH+BTH	NA	NA	100	5.38	100	57.88	5.50	58.63
14	H ₂ /H ₂ S/H ₂ O PMA (1500 ppm Mo) NAPH	NA	NA	NA	NA	NA	52.96	4.67	43.36

¹k₁, value calculated from a reversible first order kinetics, refer to Rintjema (1992)

Summary G.2

Run#	Medium	X _{CO} (%)	k ₁ (s ⁻¹ x10 ⁴)	X _{BTH} (%)	k ₂ (s ⁻¹ x10 ⁴)	S Rem (%)	X _{NAPH} (%)	k ₄ (s ⁻¹ x10 ⁵)	A Rem (%)
15	H ₂ /H ₂ S/H ₂ O PMA (1500 ppm Mo) BTH	NA	NA	98.86	6.00	96.87	NA	NA	NA
16	300 H ₂ /H ₂ S/H ₂ O PMA (1500 ppm Mo) NAPH+BTH	NA	NA	99.04	3.28	98.99	19.87	NA	22.46
17	H ₂ /H ₂ S/H ₂ O PMA (1500 ppm Mo) NAPH+BTH	NA	NA	100	4.57	100	59.57	5.00 (5.33) ²	60.14
18	CO/H ₂ S/H ₂ O PMA (1500 ppm Mo) NAPH+BTH	92.38	1.82	100	5.20	100	63.66	5.67	61.25
19	CO/H ₂ S/H ₂ O PMA (1500 ppm Mo) TET	92.24	3.57	NA	NA	NA	X _{TET} 4.77	NA	3.01
20	300 CO/H ₂ S/H ₂ O PMA (1500 ppm Mo) NAPH+BTH	93.32	NA	99.03	2.63	98.33	24.88	2.0	25.81
21	CO/H ₂ S/H ₂ O PMA (1500 ppm Mo) NAPH+BTH	94.59	4.05	99.03	2.63	99.01	20.54	1.67	25.72
22	CO/H ₂ S/H ₂ O PMA (1000 ppm Mo) NAPH+BTH	93.98	2.88	100	6.0	100	49.31	3.17 (3.83) ²	47.98

² k_i, value calculated when intercept ≠ 0.0

Summary G.3

Run#	Medium	X _{CO} (%)	k ₁ (s ⁻¹ x10 ⁴)	X _{BTH} (%)	k ₂ (s ⁻¹ x10 ⁴)	S Rem (%)	X _{NAPH} (%)	k ₄ (s ⁻¹ x10 ⁶)	A Rem (%)
23	CO/H ₂ S/H ₂ O PMA (1500 ppm Mo) NAPH+BTH	94.5	4.88	100	7.87	100	67.57	7.33 (8.33) ²	68.81
24	CO/H ₂ S/H ₂ O PMA (3000 ppm Mo) NAPH+BTH	95.46	6.55	100	5.73	100	78.67	15.0 (13.83) ²	79.58
25	300 CO/H ₂ S/H ₂ O PMA (1500 ppm Mo) NAPH+BTH	92.78	NA	96.74	1.7	93.71	24.65	2.0 (2.17) ²	27.89
26	CO/H ₂ S/H ₂ O MA (1500 ppm Mo) NAPH+BTH	94.63	3.67	100	6.32	100	61.47	4.83 (5.50) ²	62.39
27	CO/H ₂ S/H ₂ O AMT (1500 ppm Mo) NAPH+BTH	94.77	4.22	100	6.63	100	63.22	5.33 (6.00) ²	63.61
28	CO/H ₂ S/H ₂ O PMA (500 ppm Mo) NAPH+BTH	92.06	2.42	100	5.20	100	34.72	2.17 (2.50) ²	35.50
29	CO/H ₂ S/H ₂ O Blank NAPH+BTH	74.02	1.10	75.56	0.58	54.68	7.19	NA	7.35
30	CO/H ₂ S/H ₂ O ATTM (1500 ppm Mo) NAPH+BTH	94.01	4.37	100	8.73	100	60.11	4.83 (5.50) ²	61.07

² k₄, value calculated when intercept ≠ 0.0